UNIVERSITY OF NAPLES "FEDERICO II"

DOCTORATE SCHOOL OF PHYSICAL SCIENCES

SEISMIC RESPONSE OF SOIL EMBANKMENTS IN *NEAR-SOURCE* CONDITIONS

Angelo Dello Russo

A Dissertation Submitted in Partial Fulfillment of the Requirements for
the Degree of PHILOSOPHIAE DOCTOR in
SEISMIC RISK
XXVII Cycle

TUTOR
Prof. Stefania Sica

COORDINATOR
Prof. Aldo Zollo

UNIVERSITY OF NAPLES “FEDERICO II”

DOCTORATE SCHOOL OF PHYSICAL SCIENCES

Date: March 2015

Author: Angelo Dello Russo

Title: Seismic response of soil embankments in *near-source* conditions

Department: Department of Physics
Department of Engineering

Degree: Philosophiae Doctor

Signature of Author

Table of contents

Abstract

The research activity carried out in PhD period focused on numerical modelling of the seismic response of soil embankments in near-source conditions. The interest on such a topic comes from the fact that in Italy and worldwide there are many large earth dams placed very close to active faults. In such conditions the seismic response of the structure could be affected by near-source phenomena. Worth mentioning are the case-histories of Conza Dam during the Irpinia 1980 earthquake and Campotosto reservoir during the 2009 Abruzzo earthquake. In the first case, the embankment was partially jeopardized by the seismic event, being the dam site very close to the source (≈ 10 km). In the latter case, the epicenters of several aftershocks following the April 6, 2009 main event migrated in the NW direction, just below the 315-million-m^3 Campotosto reservoir. In those days, the authorities in charge of the dam safety acted completely unprepared to face the emergency, due to the lack of pre-arranged predictive/interpretative tools.

The investigated research theme is quite new in the geotechnical field. It requires a detailed knowledge of basic seismological aspects to properly simulate the seismic source and wave propagation pattern to get the input motion exciting the site and the embankment.

As regards the implications in the field of civil engineering, an important feature of near-source phenomena is ground-motion asynchronism. This means that two points placed not very far each other, i.e. at a distance comparable to the dimensions of strategic infrastructures - as dams, road embankments, or bridges - may undergo quite different motion at their base (even not accounting for site effects). In such a context, the proper characterization of the motion at the bedrock level may provide a better prediction of the structure response to seismic loadings. This issue is crucial for large earth-dams or embankments. If the points placed at the base of these structures experience very different seismic motions (as expected in near-source conditions) significant differential settlements and fractures of the embankment may occur, with the consequent reduction of structure safety.

In the *first chapter* the peculiarities of the near source seismic propagation will be illustrated referring to a detailed literature review on such an issue. At the end of the chapter some preliminary numerical results will be provided on typical embankments and simplified source models.

In the *second chapter*, the mathematical formulation of the DRM approach, will be provided. According to DRM it is possible to divide the problem at the site scale from the problem of seismic motion generation which consists in the simulation of the source and the seismic propagation until the site of interest. Once known the nodal displacements, it is possible to determine the effective nodal forces (Bielak et al., 2003) which represent in the second model (model 2) the

actions due to the seismic source. In this research project it was developed a novel algorithm to export the stiffness matrix to be used for calculating the effective nodal forces at the interface of the detail model at the site scale. This procedure has been implemented in a commercial software based on finite difference method.

In the *third chapter* the methodology to simulate the reference source mechanism (1980 Irpinia earthquake) and the propagating media on a "regional scale" will be illustrated. A quasi-deteministic approach will be used, in which the determination of the seismic motion generated by the fault will be reproduced by the use of the empirical Green's functions in the frequency domain (Discrete Wave Number Method, by Cotton & Coutant, 1997). The source model was reconstructed from numerous publications on 1980 Irpinia source mechanism (Westaway & Jackson, 1984; Westaway & Jackson, 1987; Bernard & Zollo, 1988; Bernard & Zollo, 1989; Cocco & Pacor, 1993).

In the *fourth chapter*, the mathematical formulation necessary to solve the boundary value problem in the geotechnical field will be presented. Some constitutive models suitable to represent soil behaviour under cyclic loads will be briefly described.

In the *fifth chapter*, the model at the "site scale" of DRM approach will be described. It includes an interesting case history of an earth dam that in the 1980 Irpinia earthquake suffered huge damage, probably just due to the near-source seismic propagation. With the input motion provided by the large DRM model (step I), the seismic response of Conza dam will be evaluated.

Comparisons will be provided between the predicted response of the dam by the DRM procedure and the measured one, as interpreted by Brigante (2010).

Finally, the main differences between the DRM approach developed during the PhD activity, and a more traditional one (where a unique input motion is adopted) will be highlighted and the engineering implications discussed.

Acknowledgements

I would like to express my sincere thanks to my tutor Prof. Stefania Sica who believed in my ability, giving me the opportunity to study a very challenging geotechnical topic and who, in particular, guided me through this work with precious suggestions, motivations and support.

Special thanks are due to Prof. Aldo Zollo, Prof. Raffaella De Matteis and Ph.D. Sergio Del Gaudio for giving me precious suggestions on the geophysical aspects of my research work.

I am grateful to Prof. Luca Pagano to have kindly allowed the use of the Conza dam as reference case history to validate the proposed procedure.

I would like also to thank Prof. Francesco Silvestri for his helpfulness during the Ph.D. courses.

I want to thank the Department of Engineering of the University of Sannio, especially Prof. Armando Lucio Simonelli and Dr. Augusto Penna, and all my colleagues for sharing with me the good and bad moments that I had during the last three years.

Finally, I am grateful to my family and girlfriend, for their constant support and encouragement.

1. Near-Source Propagation

1.1. Introduction

The first part of the research activity was concentrated on the seismologic aspects of the problem, starting from the proper use of the terms “near-field” and “near-source” (or “near-fault”), according to the seismological viewpoint:

(i) the “near-field” term refers to one of the three mathematical contributes providing the motion of a point; it is called “near” because it extinguishes at small distance from the source;

(ii) the “near-source” term is a more general expression referring to all those factors making the surface ground motion dependent on source features.

From the engineering point of view will be so important to properly study the effects related to the latter term.

Many literature study has been synthesized on near-source phenomena caused by strong earthquakes. It is worth noting that on such an issue many aspects are still unclear (for example, directivity effects observed in normal or inverse focal mechanisms). Accelerometric and velocimetric recordings acquired in different sites located at short distance from seismic sources, during several earthquakes worldwide have shown the variability of seismic motion characteristics in near-source conditions. In particular, in the vicinity of the seismic source the presence of a bimodal spectral shape on at least one of the components of motion was observed (Somerville 2005). A significant energy content at high frequencies is observed, due to minor dissipation occurred during the short wave path form the seismic source and the site. The spectral peak at low frequencies, however, is probably caused by the presence of an impulsive component induced by the phenomenon of “forward directivity” (Somerville 2005). Other typical characteristics of the near-source motion are: the presence of residual displacements at the ground level, or evidence of the fault on the surface (“fling-step”); high PGA, PGV and PGD values compared to those recorded far from the source (far-field conditions) for earthquakes with the same magnitude; the presence of a not-negligible vertical motion, with reference to the horizontal components; the almost simultaneous arrival of S and P waves due to the short source-site distance; further P and S waves contribute to both horizontal and vertical motions because the wave-fronts approach the surface with an inclination which can be very different from the sub-vertical (as it happens for sites far from the focal mechanism). Finally, the frequency content of the signal depends on the focal mechanism, i.e. geometry and direction of fracture propagation, slip map and source-site relative position.

In geotechnical earthquake engineering, it is particularly important to characterize both the frequency content of the seismic signal and its asynchronism at the bedrock. In this context, the seismic response of structures characterised by predominant longitudinal development (such as dams, road embankments, tunnels, bridges, pipelines) can be significantly influenced by kinematic and dynamic effects due to the near-source wave propagation. The asynchronism of the seismic motion at the base of an earth embankment, for example, may induce unsafe stresses and deformations: in the case of strategic constructions, such as dams and large embankments, the risk associated to the failure is very high.

At the end of chapter, it is illustrated a study on the seismic motion induced in near source conditions at the base of embankments (for simplicity, reference is made to a typical section), for different positions of the structure with respect to the location and size of the rupture zone.

1.2. Near-Source evidences

Ground motion close to a ruptured fault can be significantly different from ground motion observed far away from the seismic source. Whereas significant differences in acceleration-time histories may not be evident, examination of the velocity and displacement time histories in the near-source conditions reveals the special nature of the pulse-like motion due to forward-directivity (Figure 1.1).

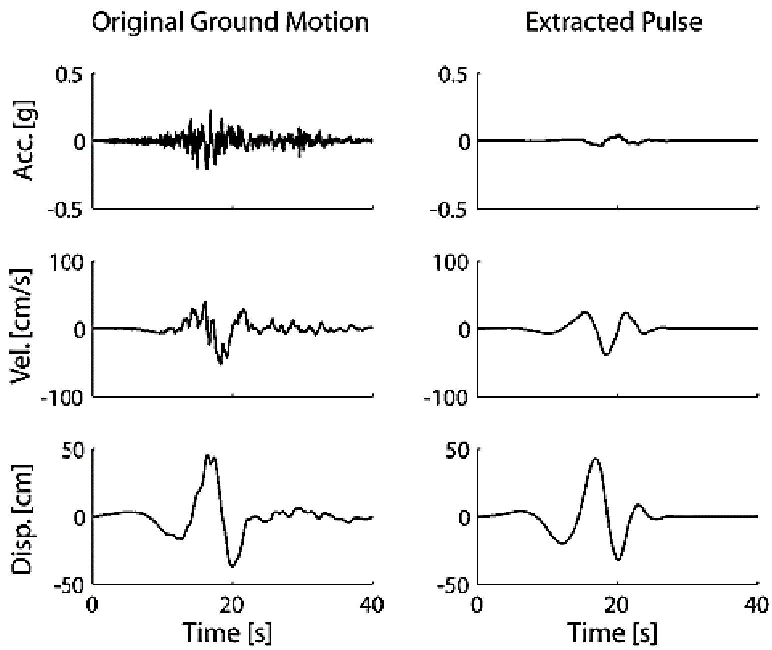

Figure 1.1 From top to bottom: acceleration, velocity and displacement time histories recorded at Yermo Fire Station during the 1992 Landers earthquake (California) and the extracted pulse associated with this ground motion (Baker, 2007).

The near-fault zone is typically assumed to be restricted within a distance of about 20 km from the ruptured fault. In the near-fault zone, ground motions are significantly influenced by the rupture mechanism and slip direction (relative to the site) and by permanent ground displacements deriving from tectonic movement (‘fling-step’). The propagation of fault rupture toward a site at a velocity close to the shear wave velocity of the rock, causes most of the seismic energy generated at the source to arrive in a single large pulse of motion, which occurs at the beginning of the record, as reported in Somerville et al. (1997).

This pulse represents the cumulative effect of almost all seismic radiation from the fault. The radiation pattern of the shear dislocation on the fault causes this large pulse of motion to be oriented in the direction perpendicular to the fault plane, causing the strike-normal component of the ground motion to be larger than the strike-parallel component (see Figure 1.2). To accurately characterize near-fault ground motions, it is therefore necessary to specify separate time histories and response spectra for the strike-normal and strike-parallel components of the ground motion. Ground motions in the near-fault zone can exhibit the dynamic consequences of “forward-directivity”, “neutral-directivity”, or “backward-directivity”.

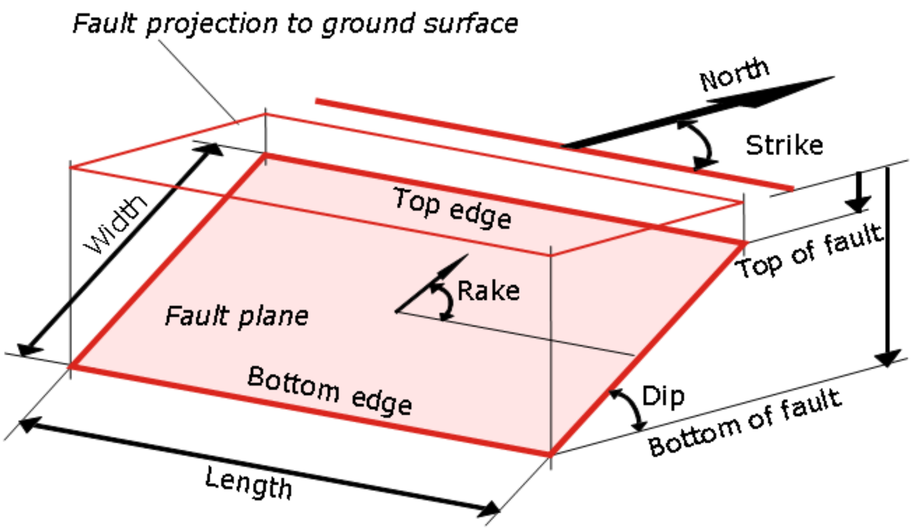

Figure 1.2 Representation of fault geometry (length, width) and spatial orientation (dip, strike, rake).

Forward-directivity effects occur when two conditions are met: the rupture front propagates toward the site and the direction of slip on the fault is aligned with the site. This conditions can be present for both strike-slip and dip-slip events. In strike-slip events, forward-directivity conditions are typically larger for sites near the end of the fault when the rupture front is moving towards the site. In dip-slip events, forward-directivity conditions occur for sites located in the up-dip projection of the fault plane. The radiation pattern of the shear dislocation on the fault causes this single large pulse of motion to be oriented in a direction perpendicular to the fault plane.

- Forward-directivity produces ground motions that have large amplitudes and short durations (*constructive interference* of elastic waves). In particular, the rupture directivity pulse can be very strong at the end of a strike-slip fault, where there is little or no permanent displacement (Loma Prieta and Northridge earthquakes). Some near-fault velocity time-histories for the fault-normal and fault parallel components of motion are shown in Figure 1.3. These time histories refer to L'Aquila earthquake of April 6, 2009 (Chiocchiarelli & Iervolino, 2010).

- Backward-directivity effects, which occur when the rupture propagates away from the site, give rise to the opposite effect: long duration motions having low amplitudes at long periods (with possibility of *destructive interference* between waves). The conditions required for forward directivity are also met in dip-slip faulting. The alignment of both the rupture direction and the slip direction up-dip on the fault plane produces rupture directivity effects at sites located around the surface evidence of the fault (or its up-dip projection if it does not break the surface).

- Neutral-directivity occurs for sites located off the fault surface when the rupture is neither predominantly towards nor away from the site.

The estimation of ground motions for a site close to an active fault should account for these special aspects of near-fault ground motions.

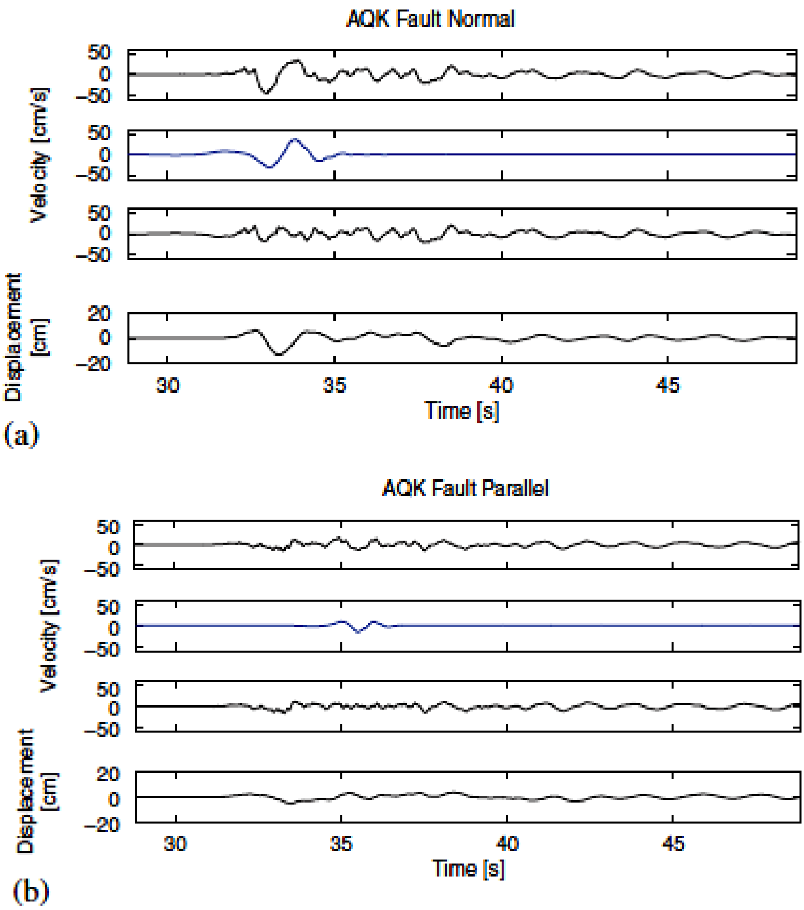

Figure 1.3 From the top to the bottom: velocity time history, extracted pulse, residual velocity, and displacement signal for FN (a) and FP (b) components of AQK recording at L'Aquila (IT) during the April 6, 2009 earthquake (Chiocchiarelli & Iervolino, 2010).

The strike-slip case is shown in Figure 1.4, where the fault defines the strike direction. The rupture directivity pulse is oriented in the strike-normal direction and the permanent ground displacement ("fling step") is oriented parallel to the fault strike. The dip-slip case is shown in vertical cross section, where the fault defines the dip direction; the strike direction is orthogonal to the page. The rupture directivity pulse is oriented in the direction normal to the fault dip, and has components in both vertical direction and horizontal (strike normal) direction. The permanent ground displacement is oriented in the direction parallel to the fault dip, and has components in both vertical direction and horizontal (strike normal) direction (Figure 1.4a).

Figures 1.4 (b)-(c) show instead, the partition of near fault ground motions into the dynamic ground motion, which is dominated by the rupture directivity pulse, and the permanent ground displacement. For a strike-slip earthquake, the rupture directivity pulse is partitioned mainly on the strike-normal component, and the permanent ground displacement is partitioned on the strike-parallel component. If the permanent ground displacement is removed from the strike-parallel component, the dynamic motion is almost negligible.

For a dip-slip earthquake (Figure 1.4b), the dynamic and permanent displacements occur together on the strike-normal component, and both motions are negligible on the strike-parallel component. If the permanent ground displacement is removed from the strike-normal component, a large directivity pulse remains.

The dynamic and permanent components occur on orthogonal components in strike-slip faulting, but on the same component in dip-slip faulting. This indicates that separate models are needed for predicting the dynamic and permanent components of near-fault ground displacements at a site. The separately estimated dynamic and permanent components of the ground motion can be combined to produce a unique time history containing both effects, peculiarity which will be considered in the approach presented in this thesis.

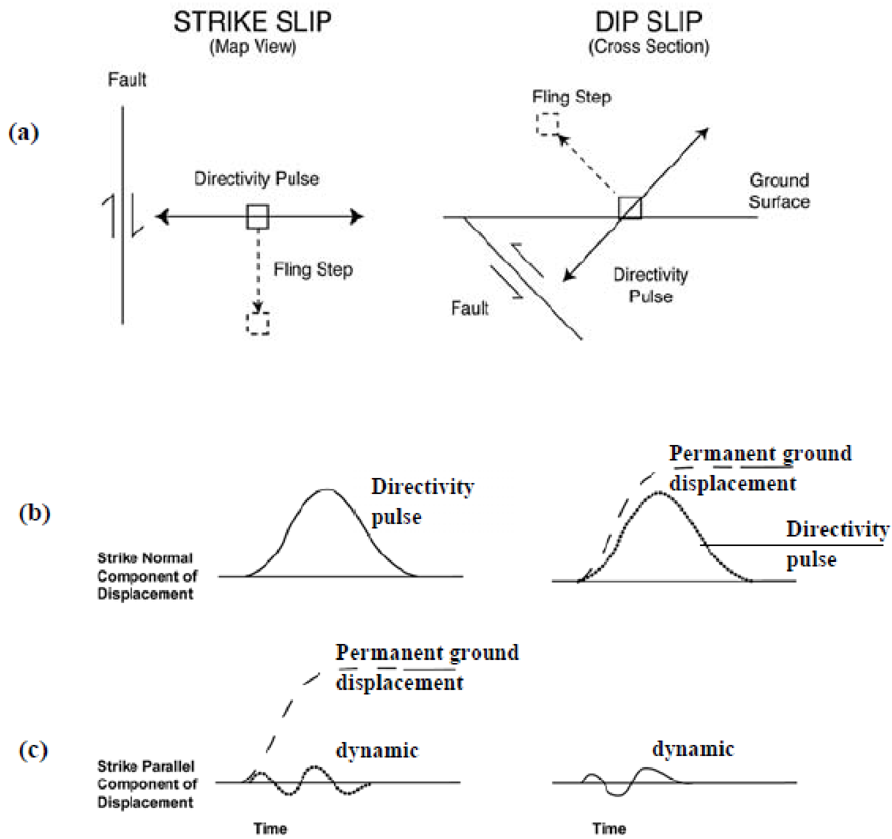

Figure 1.4 (a) Schematic orientation of the rupture directivity pulse and fault displacement ("fling step") for strike-slip (left) and dip-slip (right) faulting. Schematic partition of the rupture directivity pulse and fault displacement between the strike normal (b) and strike parallel (c) components of ground displacement (modified from Somerville, 2005).

With reference to strike-slip faults Hisada & Bielak (2004) carried out numerical simulations in the frequency domain, using synthetic Green's functions. Their study enhanced significant differences between surface and buried faults when considering the dynamic and static components of the seismic motion in near-source stations (Figure 1.15a).

It was noted that:

- the dynamic terms excite the directivity pulses in the fault normal components for both fault models, especially in the forward rupture direction (Figure 1.15a);
- the static terms of the surface fault generate large fling steps, *i.e.* large amplitudes in the fault parallel components close to the fault. In the buried fault the presence of the continuous medium above the fault prevents slip dislocation of the fault which cannot reach the ground.

As the site gets further from the fault, the static terms are quickly attenuated, whereas the dynamic terms are not. This is because the static terms consist of the static traction Green's function (with order of attenuation of $1/r^2$). As demonstrated in Hisada & Bielak (2004), the dynamic terms consist of body and surface waves (with order of attenuation of $1/r$ to $1/\sqrt{r}$). Therefore, for emerging faults the directions of the maximum velocities of the total waves are inclined with respect to the fault plane in the vicinity of the surface fault (Figure 1.15b), while the fling steps disappear and the directivity pulses are dominant for the buried fault (Figure 1.15c). In addition, Hisada & Bielak (2004) showed that directivity pulses, crossing sedimentary layer, assumes higher wavelengths. Practically, the frequency content is spread over lower periods. Conversely, no big differences can be seen in the fling step (i.e., the static term).

From experimental observations, the main effect of forward directivity on the response spectra consists in amplification of the spectral accelerations in the range of periods between 0.5 and 2.5 seconds, with different dominant periods in the fault-normal and fault-parallel direction. For example, the spectra, obtained numerically by Lai et al. (2009) (Figure 1.6), show that the effects of directivity occur with a bi-modal shape and with a narrow band for the spectral acceleration peak. Usually, the directivity pulses, as seen in the 1994 Northridge and 1995 Kobe earthquakes, have destructive effects on short- to medium-period structures, whereas the fling steps, as seen in the 1992 Landers and 1999 Chi-Chi earthquakes, may have destructive effects on long-period structures, such as high-rise and base-isolated structures.

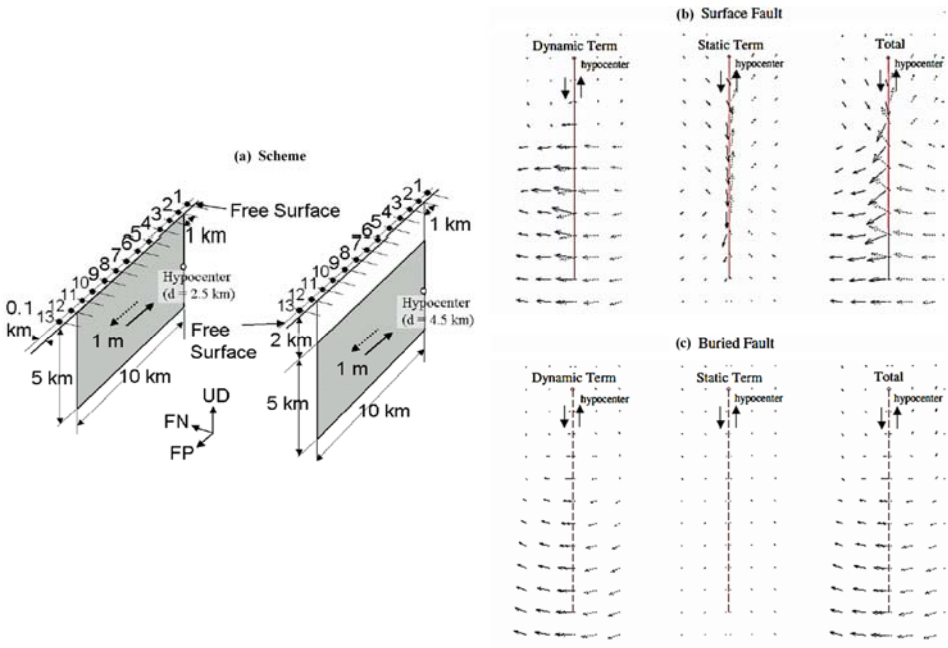

Figure 1.5 (a) Scheme of surface fault (left) and buried fault (right). Vectors of maximum velocities along the free surface for surface (b) and buried (c) fault (Hisada & Bielak, 2004).

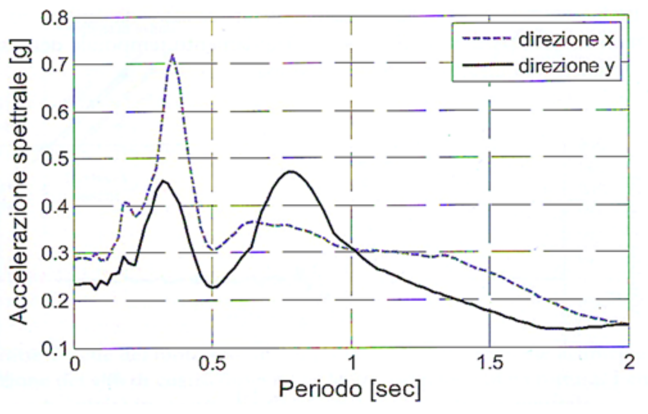

Figure 1.6 Response spectra highlighting the effects of forward directivity (Lai et al. 2009). Both components have a peak around 0.3 s, while only the fault-normal (y) has a second peak at higher frequencies due to the pulse.

1.2.1. Probability of occurrence of pulselike records

The geometric parameters used to estimate the probability of occurrence of pulselike records are the angle between the direction of rupture propagation and the wave direction from the fault to the site, and the part of the rupture surface that lies between the hypocenter and the site. Important effects of forward-directivity may result from smaller angles between the site and the fault and for larger fractions of the ruptured fault between the site and hypocenter (Somerville et al., 1997).

Different models have been developed for the prediction of pulse occurrence, mainly for Probabilistic Seismic Hazard Analysis (PSHA). Iervolino & Cornell (2008), following the pioneering work of Somerville et al. (1997), analyzed the time histories of the L'Aquila earthquake to assess if pulses occurred. In general, pulse identification is based on geometric parameters (mainly, source-site configuration).

In the case of dip or oblique slip mechanisms (see Figure 1.7), the following variables may be defined:

- the closest distance of the site to fault rupture (R);
- the fraction of the rupture surface that lies between the hypocenter and the site (d);
- the angle between the direction of rupture propagation and the direction between the hypocenter and the site (ϕ).

Depending on the angle ϕ between *dip* and hypocenter-site direction (Figure 1.7 and Figure 1.8) there are three cases:

- *case 0* ($\phi > 90°$): zero pulse probability;
- *case 1* ($0° \leq \phi \leq 90°$): pulse probability increasing with the decrease of ϕ (maximum pulse likelihood is obtained at the point where the direction of the *dip* reaches the surface, $\phi = 0°$);
- *case 2* ($\phi < 0°$): pulse probability exponentially decreasing with the increase of R.

With reference to the above defined *cases 1* and *2*, the function of pulse occurrence, P [pulse], takes the following form:

$$P[pulse|R, d, \phi] = \frac{e^{\alpha+\beta\cdot R+\gamma\cdot d+\delta\cdot\phi}}{1 + e^{\alpha+\beta\cdot R+\gamma\cdot d+\delta\cdot\phi}}$$

with α (generally positive), β, γ and δ (generally negative) representing empirical coefficients.

It should be noted that even when the geometric conditions for forward-directivity are satisfied, the effects of forward-directivity might not occur. This could happen if a station is placed at the end of a fault and rupture occurs towards the station, but slip is concentrated near the end of the fault. Conversely, forward-directivity may also occur when the geometric conditions are not satisfied, such as for a strike-slip event where the hypocenter is at high depth and the rupture progresses up-dip towards a site near the epicenter of the event.

In the same way, many velocity pulses may not be caused by directivity effects, but by other phenomena. For example, if a site is located near an asperity in the fault rupture, the waves caused by that asperity may produce a pulse at the site. Alternatively, constructive interference of seismic waves passing through a complicated earth structure, such as the edge of a geologic basin, might also result in velocity pulses. Although directivity effects are the presumed cause of many near-fault pulses, not always the signal-processing approach is able to distinguish between the potential causal mechanisms.

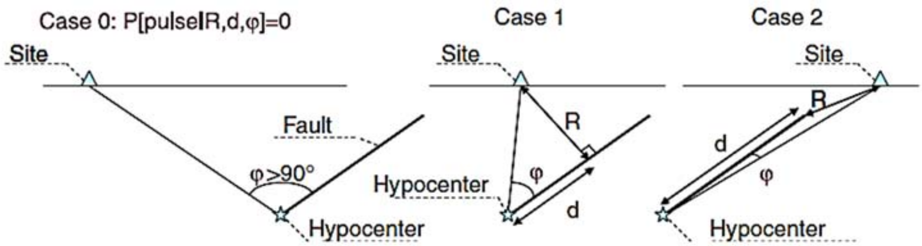

Figure 1.7 Different cases of pulse occurrence and geometrical features regulating the phenomenon (Chioccarelli & Iervolino, 2010).

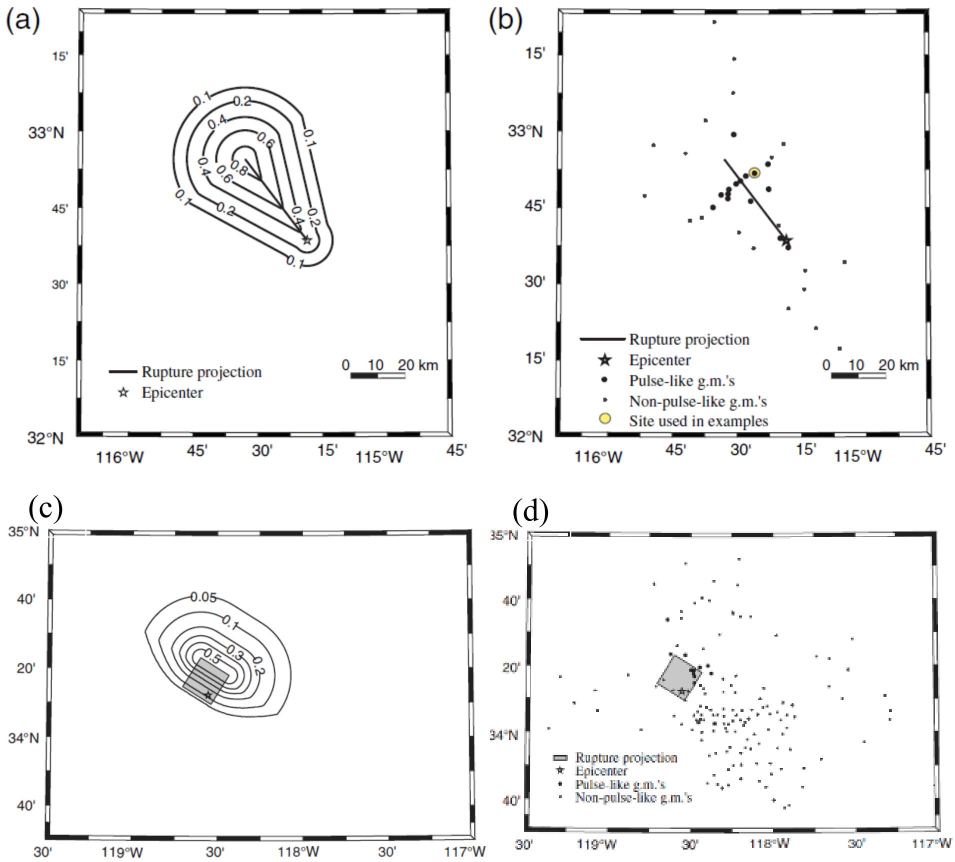

Figure 1.8 Map of the transverse fault mechanism (Imperial Valley earthquake): (a) contours of probability of pulse occurrence for the given rupture; (b) sites where pulselike ground motion was observed. With reference to oblique-slip and dip-slip categories of fault mechanism, the Northridge earthquake is considered: (c) contours of probability of pulse occurrence for the given rupture; (d) sites where pulselike ground motion was observed (Shahi & Baker, 2011).

Recent research on the response of structures in near-fault regions has found the time-domain representation of ground motion to be preferable to classical response spectrum representation in the frequency domain, since the latter implies a process with a relatively uniform distribution of energy throughout the whole duration of the motion.

When the energy is concentrated in a single pulse of motion, the resonance phenomenon (easily detectable by response spectrum) has insufficient time to build-up.

Whereas the fault-normal component of velocity is generally well characterized by simple pulses, the fault-parallel pulse sometimes shows more irregular velocity-time histories. Nonetheless, a clearly defined pulse in the fault-parallel direction exists in many cases.

A simplified representation of pulse motions using sine pulses is shown in Figure 1.9. The ground motions in fault-normal and fault-parallel direction are defined by the number of equivalent half-cycles of pulse motions (N), the period of each half-cycle ($T_{v;i}$) and their corresponding amplitude (A_i).

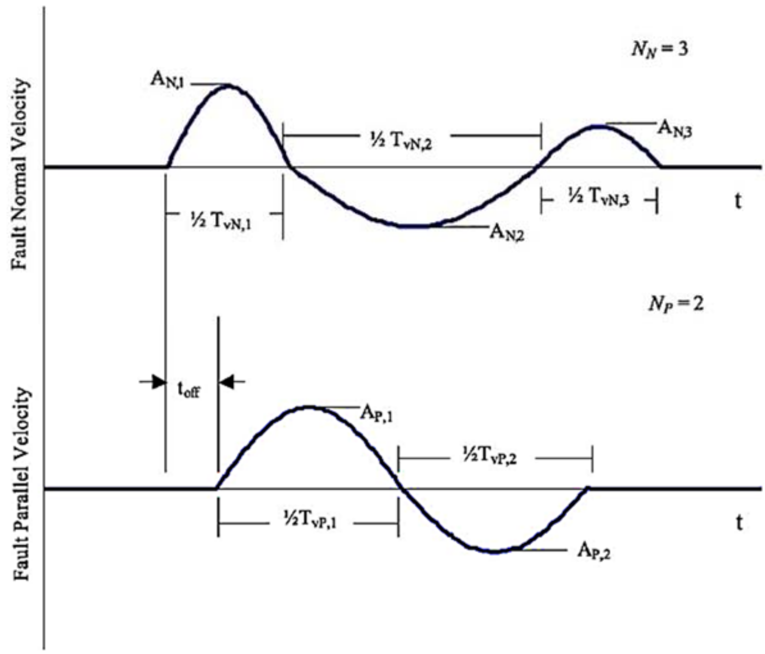

Figure 1.9 Parameters required to define the fault-normal and fault-parallel components of simplified velocity pulses (Bray & Rodriguez-Marek, 2004).

In addition, the time lag between the initiation of the fault-normal and fault-parallel component (t_{off}) must also be defined to fully represent bi-directional horizontal shaking. Two near-fault motions with significantly time shift between the fault-normal (FN) and fault-parallel (FP) motions are shown in Figure 1.10. The differences can be found on the instantaneous values of the two components as shown using a horizontal velocity trace plot Figure 1.10.

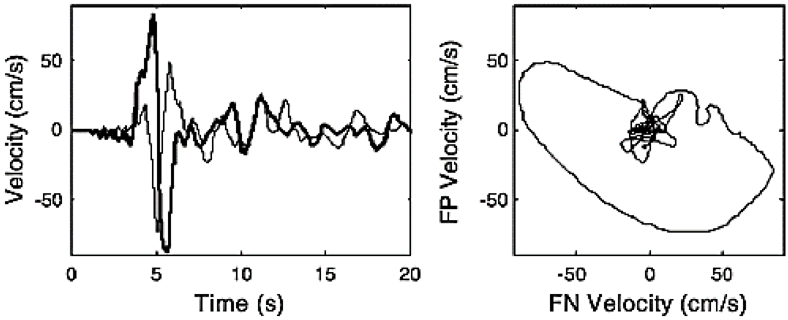

Figure 1.10 FN and FP velocity-time histories and horizontal velocity-traces for two near-fault records (Bray & Rodriguez-Marek, 2004).

When the time history of a near-source ground motion is used for the analysis of a structure, the strike-normal and strike-parallel components need to be oriented with respect to the strike of the fault that dominates the seismic hazard at the site. Indeed, both the horizontal component of motion may be important in evaluating the seismic response of soil deposits, because they are sensitive to bi-directional shaking. Nonlinear analyses of the seismic response of soil deposits to bi-directional shaking demonstrate that local soil conditions can affect the peak velocity and pulse period in the fault-normal and fault-parallel direction. In fact, soil stiffness degradation induced by a large fault-normal component of the motion influence soil response in the fault-parallel direction too. Accordingly, soil response to bi-directional shaking affects the characteristics of the ground motion at the surface of a soil deposit, which in turn can affect structural performance.

The number of significant cycles in the velocity-time history (due to subsequent replication of forward-directivity pulses or to the arrive of wave-fronts from other asperities) is an important parameter of ground motion, in particular, for soil response. It is important to note that, in general, each earthquake has a well-defined pulse sequence associated to all possible asperities. This might be expected for faults that have a relatively uniform slip distribution or concentrated over a single zone.

For stations in the near-fault region path effects are minimized. For an earthquake with highly non-uniform slip, such as the 1994 Northridge earthquake, the observed pulse sequence depends on the relative distance from the asperities. In fact, Somerville (2005) suggests that the number of half-sine pulses in the velocity time-history might be associated to the number of asperities in a fault. From the point of view of ground motion prediction, this implies that the number of significant velocity pulses for a given earthquake is associated to the determination of slip distribution in the causative fault. This is, of course, difficult to estimate a priori.

Finally, the vertical motions in the near-fault zone are important for the possible consequences on structural performance. Therefore also the vertical motions need to be estimated, because in near-source conditions the wave-front arrives at the surface not vertically. In these conditions, the P and S waves arriving almost simultaneously, produce a significant vertical motion.

1.2.1.1. Wavelet Analysis

A type of signal processing known as “wavelet analysis” is well suited for velocity pulse identification and extraction. The pulse wavelet can be subtracted from the ground motion to obtain the residual ground motion. The basic concepts of the method derive from the Fourier analysis. Fourier analysis represents a signal using a linear combination of sine waves, each one characterized by infinite time length and a single frequency. In contrast, wavelet analysis decomposes a signal into wavelets localized in time and covering a narrow range of frequencies. For non-stationary signals such as earthquake ground motions, it can be advantageous to represent the signal as a summation of wavelets rather than of stationary sine waves.

Wavelets are basis functions that satisfy a certain set of mathematical requirements. Many wavelet prototypes can be used to decompose a signal (Figure 1.11). The prototype function is referred to as a “mother” wavelet, and this function is scaled and translated in time to form a set of basis functions. The wavelet basis function at time *t* is mathematically defined as:

$$\Phi_{s,l}(t) = \frac{1}{\sqrt{s}} \Phi\left(\frac{t-l}{s}\right) \tag{1.1}$$

where Φ is the mother wavelet function, *s* is the scale parameter that dilates the wavelet, and *l* is the location parameter that translates the wavelet in time. Any signal *f(t)* can be represented as a linear combination of basis functions, and the corresponding coefficients are determined by the convolution integral (1.2), which is conceptually identical to the Fourier transform calculation.

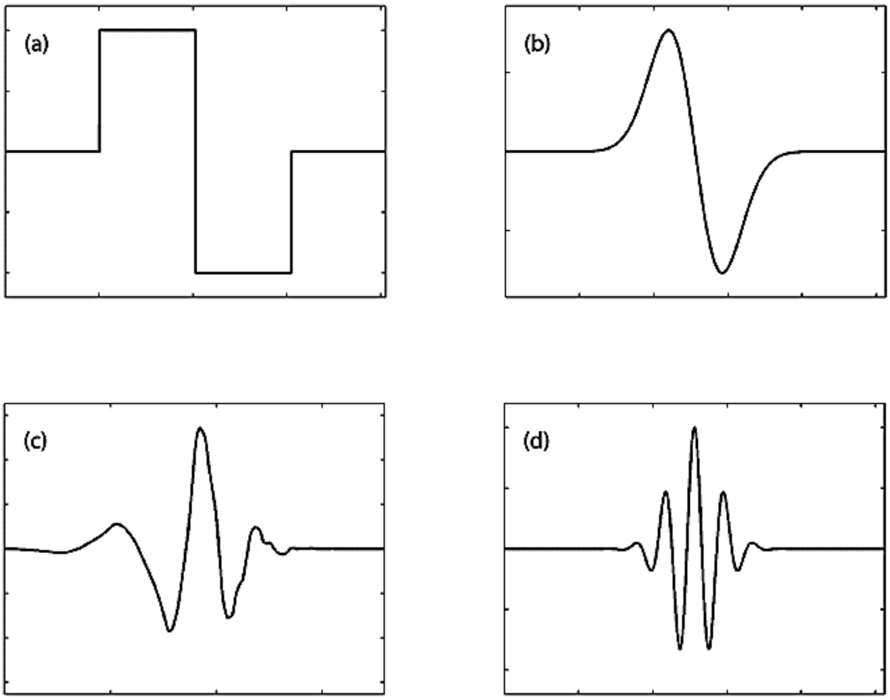

Figure 1.11 Typical mother wavelets used in wavelet analysis: (a) Haar wavelet, (b) Gaussian wavelet of order 1, (c) Daubechies wavelet of order 4, and (d) Morlet wavelet. (Baker, 2007).

The coefficient associated with the wavelet having scale *s* and position *l* is given by:

$$C_{s,l} = \int_{-\infty}^{\infty} f\,(t)\Phi_{s,l}(t)dt = \int_{-\infty}^{\infty} f\,(t)\frac{1}{\sqrt{s}}\Phi\left(\frac{t-l}{s}\right)dt \tag{1.2}$$

If the wavelets are orthogonal, then only *n* wavelets are needed to completely describe any discrete time signal of length *n*. The wavelet transform (discrete algorithm) provides the *n* coefficients describing the amplitude of the *n* wavelets at various scales and locations. If *n* is a power of 2, then an extremely efficient algorithm exists to perform the calculations (analogous to the fast Fourier transform). Further, if the mother wavelet closely represents the shape of the signal, then even fewer than *n* coefficients are needed to closely represent the signal. A few coefficients will be large and their associated wavelets will represent the main features of the signal. The other coefficients will be close to zero because the associated wavelet represents relatively small features.

If a significant portion of ground-motion time history is described by one or a few wavelets with large coefficients, then this will indicate the presence of a pulse (Figure 1.12).

For non-pulselike records, however, the extracted pulse is typically a minor feature of the ground motion and the residual ground motion is nearly identical to the original motion.

The correct identification of the pulse in the signal allows a large part of energy content to be associated to it (see cumulative squared velocity plot in Figure 1.13). Differently from filtering of signals, the pulse extraction does not cause any time-shift between the original signal and extracted impulse (Figure 1.13).

(a)

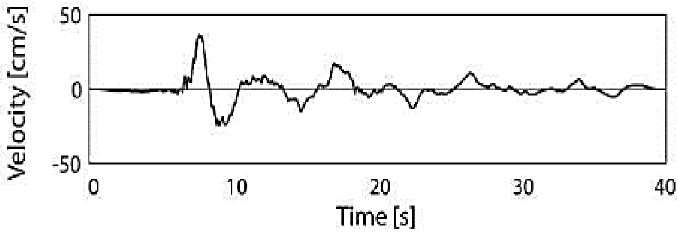

(b)

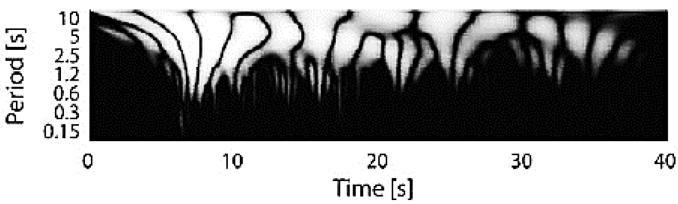

Figure 1.12 Ground-motion velocity time history of the fault-normal component recorded at Brawley Airport during the 1979 Imperial Valley earthquake (a). Wavelet transform coefficients: light shading indicates a large absolute value of the coefficient as function of the fixed period and time location (b) (Baker, 2007).

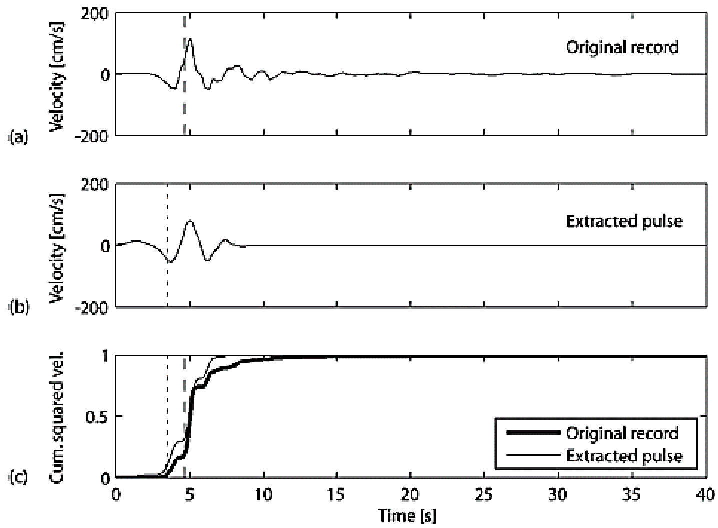

Figure 1.13 An early-arriving pulse (1979 Imperial Valley earthquake recorded at EC Meloland Overpass FF location). (a) Original ground motion. (b) Extracted pulse. (c) Cumulative squared velocities (Baker, 2007).

In near-source conditions the forward-directivity and the number of pulses contained in a record are strongly related to slip distributions and consequently they are difficult to predict.

Two checks can be done to identify if pulse-like ground motions are related to directivity effects:

- the identified pulse arrives early in the ground motion (indicating that it is likely due to directivity effects);
- the ground motion has a high peak velocity (small earthquakes might appear pulselike only because their time-history is simple but they are not affected by directivity).

1.2.1.2. Identification of Pulse Period

The period of the velocity pulse is an important parameter in the geotechnical field, as the ratio of the pulse period to the fundamental period of the soil deposit can greatly affect ground response. The most widely used approach to identify pulse period considers as pseudo-period the reciprocal of the dominant frequency of the wavelet used to identify the ground motion velocity pulse (i.e. the largest wavelet coefficient). It is straightforward to compute a pulse period in this way.

However, no well-defined concept of period exists for wavelets such as, instead, occurs for sine waves in the Fourier analysis. Also the period associated with the maximum Fourier amplitude of the wavelet can be used to identify the pseudo-period.

Sometimes, it is better not to correlate the pulse period to a single value of the wavelet coefficients (although the highest). After a wavelet analysis the period of the pulse can be identified by using the wavelet with the highest coefficient and those located within ± one-half of its length.

The methods based on wavelet analysis provide accurate pulse periods, but have the slight disadvantage of requiring user judgment.

The primary alternative to wavelet analysis is to select the period associated to the peak of velocity response spectrum of the original ground motion.

In cases where the periods obtained from the wavelet analysis and the velocity spectrum methods differ significantly, the wavelet period appears to be the more robust estimation of pulse period. In these cases, the period with maximum spectral velocity is associated to the higher frequencies of the ground motion, whereas the wavelet pulse period is associated to the visible velocity pulse. Therefore, combination of the two approaches is the ideal method for determining the period of velocity pulses and because it provides a more consistent identification of the pulse period. An example is shown in Figure 1.14, where the peak spectral velocity of the record occurs at a period of 1.4 s, whereas the wavelet pseudo-period of 7.5 s closely matches the period of the pulse identified visually.

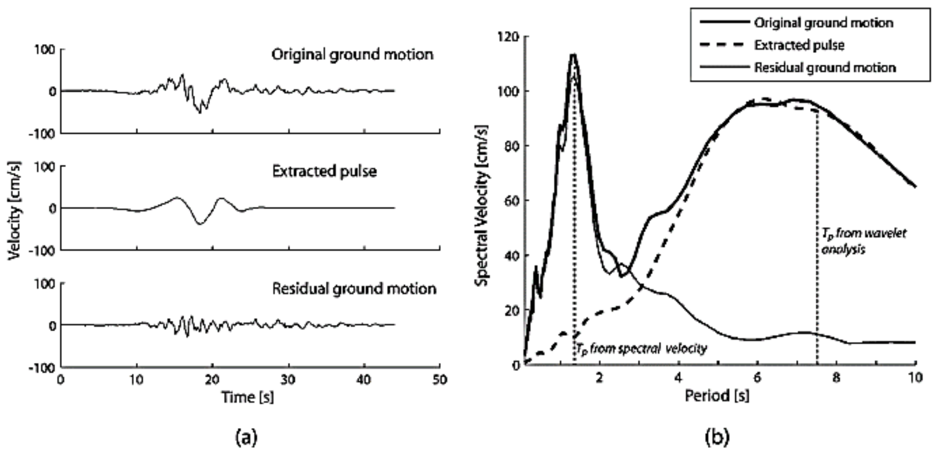

Figure 1.14 (a) Velocity time histories of the original ground motion, extracted pulse, and residual ground motion for the 1992 Landers earthquake, recorded at Yermo Fire Station; (b) velocity spectra, with T_p values determined using the spectral velocity and wavelet analysis criteria (Baker, 2007).

1.2.2. Attenuation law

The time-domain parameterization of pulse-type motions is used to develop attenuation relationships for ground motion parameters in cases of forward-directivity typical of the near-fault propagation. These relationships are necessary for the selection or generation of ground motions in the time domain to carry out seismic site response analyses or dynamic analyses of buildings. As previously indicated, the response of soil deposits and structural systems to bi-directional shaking may be important and in same case, the fault-parallel component of the near-fault ground motion may also be required.

The structure of the attenuation relationship is of the type:

$$ln(PGV) = a + bM_w + cln(R^2 + d^2) + S \tag{1.3}$$

where R is the planar site-source distance; M_W is the moment magnitude; a, b, c and d are model parameters and S represents site effects.

Figure 1.15 shows that the median peak ground velocities for soils are larger than for rocks with the difference increasing as the distance increases.

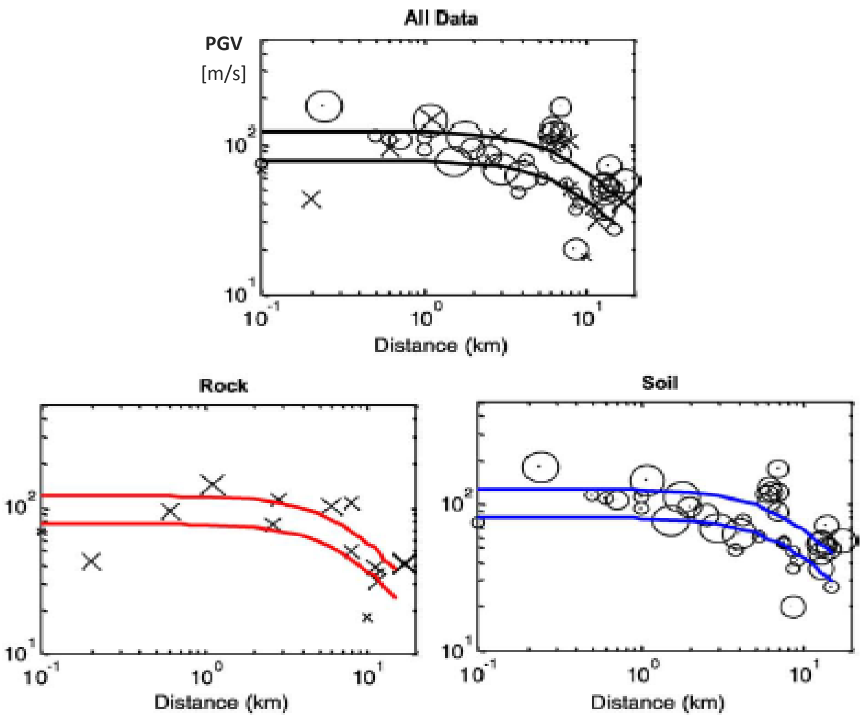

Figure 1.15 Attenuation relationship for PGV in near-fault region. From left to right: all recordings, only records on soil and only records on rock (Bray & Rodriguez-Marek, 2004).

1.2.3. Pulse period estimation

To estimate the pulse period, the use of a linear relationship between logarithm of rise time and magnitude is justified, being the logarithm of the rise time a linear function of the moment magnitude. Thus, the relationship for pulse period becomes:

$$ln(T_V) = a + bM_w + S \tag{1.4}$$

where T_v is the pulse period, M_W is the moment magnitude, a and b are model parameters and S represents the site effects.

This scaling relationship (1.4) generally provides pulse period about two times larger than the slip rise time, which measures the duration of the slip at a single point of the fault. In fact, from considerations of the physics of fault rupture, the rise time can be seen as a lower bound of pulse period (Somerville, 1998).

From the point of view of ground motion prediction, Figure 1.16 illustrates the importance of considering local site effects in the evaluation of near-fault ground motions. The results shown in Figure 1.16 show that for lower magnitude events there are longer periods at soil sites than at rock sites for events with magnitude lower than about 7. This difference diminishes as magnitude increases so that for events with $7 < M_w < 7.5$, the pulse periods at rock and soil sites are approximately the same. This makes very often difficult to identify with certainty if the pulse extracted from a recorded signal is due to directivity effect or simple to a site effect.

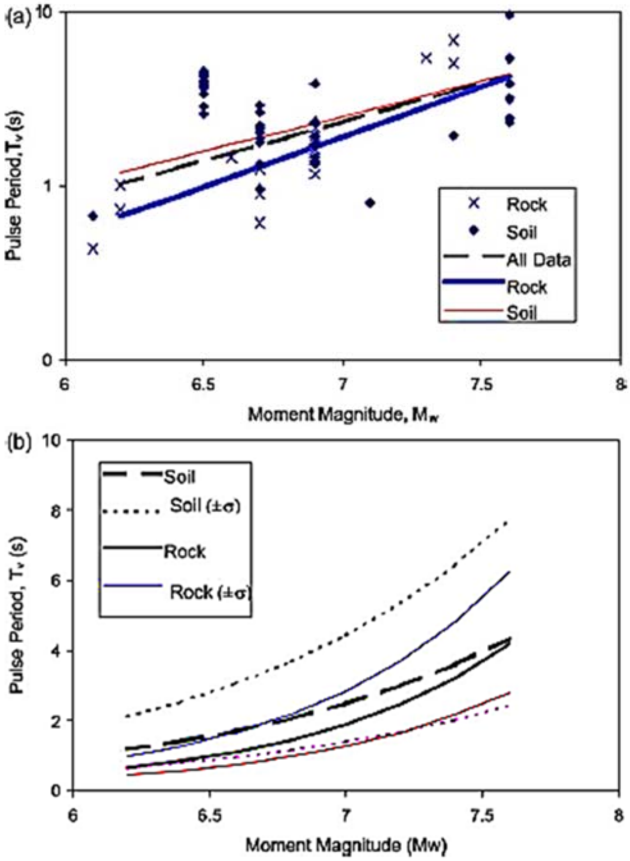

Figure 1.16 Relationship for pulse period (T_V) vs M_W: (a) Logarithmic scale. (b) Arithmetic scale with a one standard deviation band superimposed (Bray & Rodriguez-Marek, 2004).

Figure 1.17 shows FN velocity-time histories and pseudo-velocity response spectra for ground motions recorded at different rupture distances during the 1989 Loma Prieta earthquake. With reference to Gilroy registration it is possible to observe that the fault-normal pulse sequence has the same characteristics both on rock and on soil, with an initial half-cycle pulse followed by two full cycles of motion. The corresponding pulse periods, however, vary significantly depending on site conditions, as indicated in Figure 1.17b, with soil sites having larger velocity pulse periods than rock sites. This difference highlights the need to account for site effects in the evaluation of near-fault ground motions. The longer pulse period of soil sites can lead to an increase in seismic demand for structures of considerable extension (i.e. dams, large embankments, etc).

Therefore, ground motions recorded at near-fault sites for large magnitude earthquakes should be assumed as the *worst-case scenarios* for the design of large structures. On the contrary, lower magnitude earthquakes may result in velocity pulses with periods closer to the natural period of smaller systems. In this case, the lower magnitude earthquake may result in larger levels of damage associated with the velocity pulse.

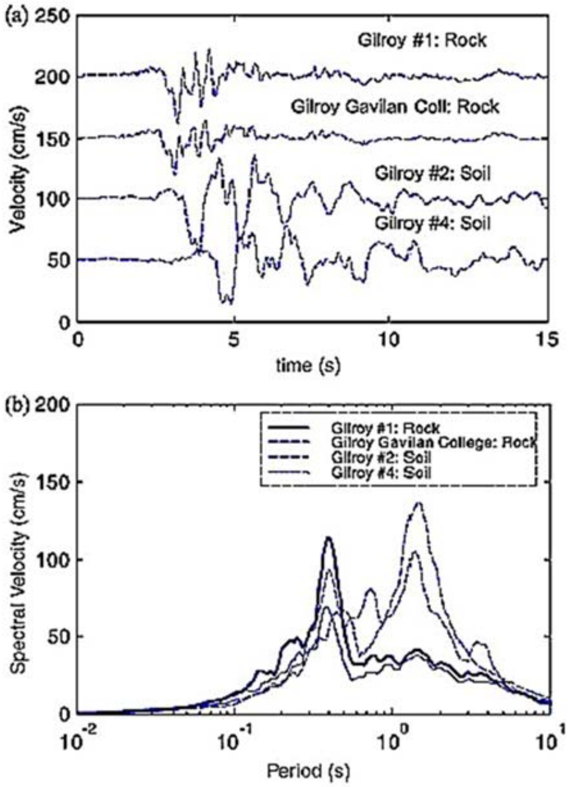

Figure 1.17 FN ground velocities recorded in the Gilroy area during the 1989 Loma Prieta earthquake: (a) velocity-time histories, and (b) pseudo-velocity spectra. Gilroy #1, Gavilan College, Gilroy #2 and #4 have rupture distances of 11, 12, 13 and 16 km, respectively (Bray & Rodriguez-Marek, 2004).

To study the effects of magnitude scaling, Somerville (2005) schematized the pulse signals through a simple bi-triangular form having different amplitude and duration (Figure 1.8a), with amplitude and pulse period provided by relations (1.3) and (1.4) for any magnitude. In the elastic response spectra it is underlined the presence of peaks related to the pulse period (Figure 1.18b-c). For spectral acceleration (b), the period of the peak is about 0.7÷0.8 times the period of the velocity pulse, and for spectral velocity (c), the peak is at about 0.8÷0.9 times the period of the velocity pulse. Because the peak of the pulse does not increase very rapidly with magnitude, response spectra do not increase monotonically with magnitude at all periods, as it is the case in conventional ground motion interpretation (i.e. *far-source* conditions). Conversely, in some period ranges the response spectra for smaller earthquakes are stronger than the response spectra of larger earthquakes (Figure 1.18).

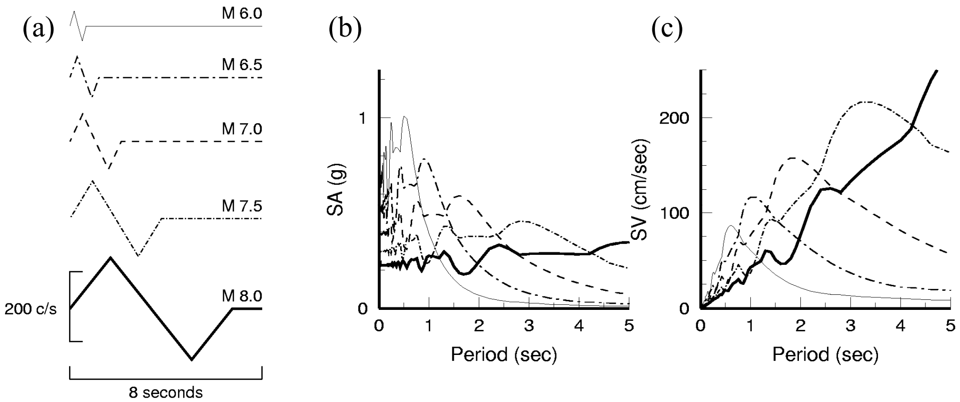

Figure 1.18 Magnitude scaling of simple velocity pulses representing near-fault ground motions (a) with associated acceleration (b) and velocity (c) response spectra (Somerville, 2005).

1.3. Near-source effects on large embankments

In modelling geotechnical earthquake engineering problems, the subsoil border generally coincides with the bedrock, which is excited by a single seismic input motion. In this study, for taking into account the peculiarities of near-source wave propagation, the geometric model is considerably wider, as it includes the seismic source, and requires the simulation of the focal mechanism and the subsequent wave propagation.

1.3.1. Numerical modelling

The analysed problem consists of a physical domain of 200x200 km in plain and of a depth of 20 km (200x20 kilometres for 2D analyses). The domain is subdivided into two layers: the first, from the ground level down to a depth of 250m, is made up of silt and clay of medium consistency; the second is a rigid substratum. Above the ground surface a trapezoidal element is placed, which represents the cross section of an earth dam. All the materials are characterised by a linear visco-elastic behaviour, with the exception of the area around the rupture zone along the fault; an elastic perfectly plastic mechanical model has been adopted at the interface between the two tectonic plates. As regards the damping parameters, the formulation with one-frequency control proposed by Raylegh has been used; in particular a damping, ξ, equal to 0.5% at the dominant frequency of about 0.025 Hz, was assigned at the bedrock, while a damping equal to 5% at the frequency of 0.40 Hz has been adopted for the soil and the earth dam layers. Table 1.1 and Table 1.2 show the values of some mechanical parameters of the constitutive models adopted for the different materials.

Zone	Density, ρ (kg/m^3)	Poisson coeff., ν (-)	S wave velocity, V_S (m/s)	Damping, ξ (%)
Embankment	2000	0.30	430	5
Soil	1900	0.30	410	5
Rock	2750	0.20	2000	0.5

Table 1.1 Mechanical parameters characterising the visco-elastic behaviour of the different materials.

Zone	ρ (kg/m³)	ν (-)	V_S (m/s)	ξ (%)	Cohesion, c (MPa)
Fault	2600	0.20	635	0.5	150

Table 1.2 Mechanical parameters of the material around the fault.

The system boundary conditions consist of absorbent surfaces according to the treatment proposed by Lysmer and Kuhlemeyer (1969). Finally, the size of the mesh elements has been calibrated as a function of the shear wave velocity of each material, in order to be able to study the development of body waves with a frequency up to 7.5 Hz. Around the fault area a condensation of the mesh has been used. Since the propagation of the rupture is not controlled from the outside, it is simulated in real time, in dependence of equilibrium and congruence equations, failure criterion and constitutive model assigned to the region of the fault. This allowed us to correctly estimate the generation of an additional energy content at high frequencies during the propagation of the rupture at the source.

Source model

Three different geometries of the fault have been adopted (see Figure 1.19b), which reproduce typical active faults present in Central and Southern Italy:

- *Case 1*: fault extension ("width") equal to 5 km, positioned at a distance varying between 2 and 7 km from ground level;
- *Case 2*: fault with extension of 10 km, positioned at a distance varying between 2 and 12 km from the ground surface;
- *Case 3*: Fault with extension of 15 km, positioned at a distance varying between 3 and 18 km from the ground level.

The angle of immersion of the faults ("dip") has been varied between 25° and 75°; the midpoint of all the faults is located on the axis of the geometric model (Figure 1.19a). Being the plan dimension of the source increasing with depth (from case 1 to case 3) also the expected magnitude value will be different. In particular, as proposed by Wells & Coppersmith (1994), were generated magnitude of 5.5, 6.25 and 6.5 respectively for the cases 1, 2 and 3. The starting point of the rupture is the deepest point of the fault and the propagation occurs from left to right in Figure 1.19b. The failure is a "second mode" mechanism, because the rupture occurs by sliding along the fault plane, with the rake (slip direction) parallel to the interface and the direction equal to the propagation of the rupture.

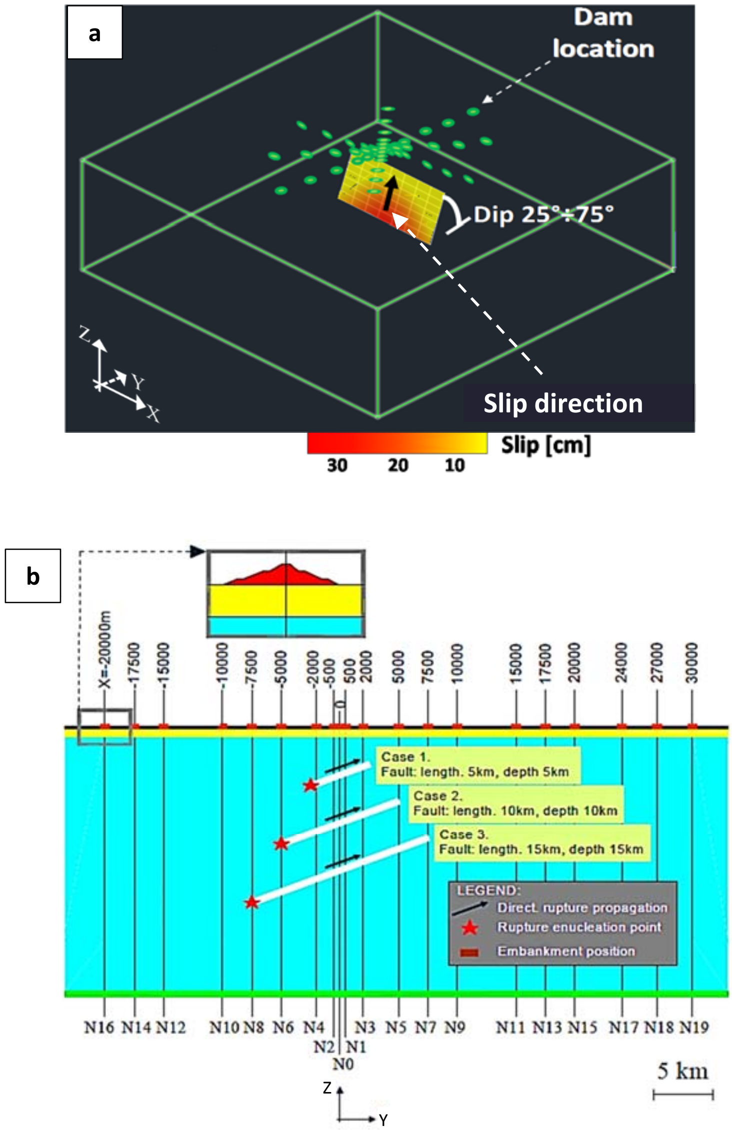

Figure 1.19 Physical model with the different positions of the embankment, relative to the three different sources examined: (a) 3D representation; (b) model scheme.

To properly simulate the rupture process at the interface, for each node of the source a delay between the rupture initiation at the point of nucleation and the start of motion in the considered node was imposed. For the estimation of the delay-time, a speed of rupture propagation (V_{Rup}) equal to 80% of the speed of propagation of shear waves in the rock was considered (Aki & Richards 2002).

In the performed analyses four different time histories (Figure 1.20) of the velocity vector of the upper zone of the interface (fault) were hypothesized. The results here shown refer to the triangular function of slip (1.5), which produces the higher content of high frequencies at the source.

$$f_{(t)} = \begin{cases} \dfrac{2}{\alpha \cdot \tau^2} \cdot t & [0 \le t \le \alpha\tau] \text{ and } [0 \le \alpha \le 1] \\ \dfrac{2}{(1-\alpha) \cdot \tau^2} \cdot (\tau - t) & [\alpha\tau < t \le \tau] \text{ and } [0 \le \alpha \le 1] \\ 0 & [t < 0 \cup t > \tau] \end{cases} \tag{1.5}$$

In (1.5), τ is the duration of the process of rupture to a single node (rise time).

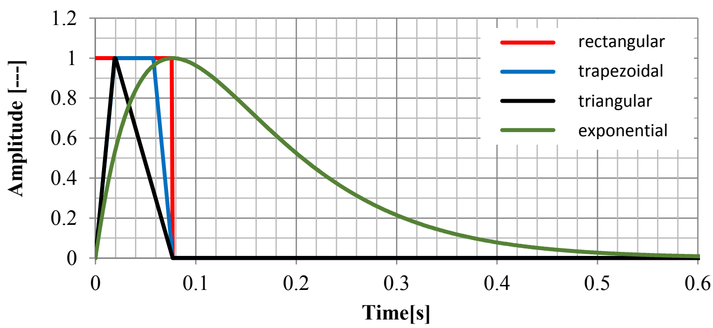

Figure 1.20 Time-histories of the slip-velocity used to simulate the rupture in the single nodes on fault. The functions are dimensionless in area (modified from Hisada e Bielak, 2003).

Each input node is also differentiated in terms of amplitude and duration of the rupture (Madariaga 1976), allowing a more realistic slip distribution on the extended source (decreasing slip-map, Figure 1.21).

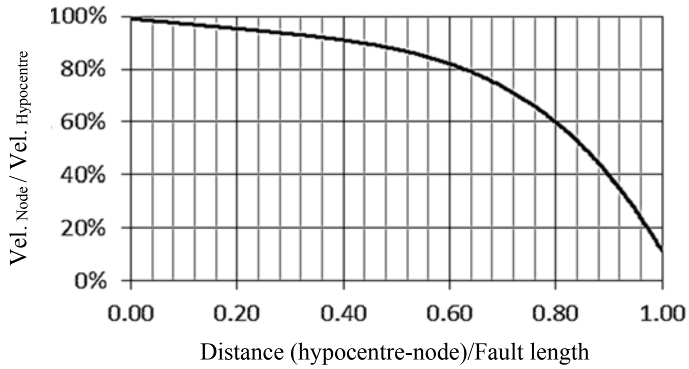

Figure 1.21 Scale factor applied to the nodal velocity to simulate the different distribution of the rupture along the fault segment. The values are expressed in function of the distance from the point of nucleation.

The generation of the seismic wave source was simulated by a kinematic model. The kinematic approach consists of inserting a velocity function at each of the individual nodes included in the mesh of the source (Haskell 1964). In each element, the failure conditions are governed by the Tresca resistance criterion assigned to the interface material, a criterion that is suitable to reproduce the mechanisms of rupture of second mode (crisis for slipping plane). The assumption of an elasto-plastic behaviour for the interface material has allowed to simulate the permanent deformations and especially to generate a content of higher frequencies, through the generation (local and temporary) of single plastic zones in the source volume. During the rupture propagation the foot-wall of the fault is fixed, by further internal constraints. These constraints are then removed during the subsequent stages of propagation of the wave front, avoiding abnormal reflections from the interface fault.

Embankment model

Embankments with different heights (40, 60, 80 and 100 meters for 2D model; 20, 50 and 100m for 3D model) and having a ratio between the maximum horizontal extent of the cross section and the height of about 6:1 have been analysed. For 3D analyses, the longitudinal extension of the plant is 1km for all types of embankments. Hereinafter, only the analyses relating to embankments with a height of 100 m for 2D analyses, and 50 m for 3D analyses, will be discussed, where the effects are more marked. In order to study the effect of the relative distance between the site (embankment) and source (fault), the embankment location has been progressively moved in the analyses, with the fault in a fixed position. The cross section of the embankment is typical of a zoned dam, with a clay core inside lateral coarse-grained materials, properly compacted. In these parametric analyses the presence of water within the dam body, which has a very important role in the dynamic response of the system, has not been considered. Nevertheless, this assumption does not significantly affects the proper determination of the variability of the seismic motion at the embankment base, which is the real object of this study. As shown in Table 1.1, for both the dam body and the base formations a linear visco-elastic behaviour was considered; the stiffness parameters have been properly reduced, in order to consider, in a simplified way, non-linear effects induced by the seismic excitation. In fact, in epicentral areas, even for earthquakes of moderate magnitude, it is possible to have high acceleration values and consequently significant effects of soil non-linearity. The above simplified assumptions do not compromise the primary purpose of the study, which is the assessment of the seismic motion variability at the base of the structure, and not the assessment of the real dynamic response of the embankment. Further improvements of the response are possible using advanced constitutive models, able to reproduce the complex aspects of the response of soils under cyclic stresses (Sica et al. 2008).

1.3.2. Parametrical analysis results

As well known, geotechnical earthquake engineering problems are traditionally studied simulating the upward propagation of seismic waves from the bedrock, which moves simultaneously according to an applied input motion. The results of the present study show that this approach is ineffective when the site is close to the seismic source. As a matter of fact, the motion at the bedrock level is not the same, but differs on the bedrock surface, due to the influence of the focal mechanism and the travel path in the rock formation. Consequently, the motion at the ground surface can vary even more significantly. Hence a structure quite large in one or both the horizontal directions, is subjected to a non-uniform input motion at its base. A traditional approach generally uses only the horizontal components of the motion, assuming that the P waves energy contribute and the vertical component of the motion are negligible and therefore it is possible to consider the whole seismic signal as a only contribution of the waves S (that scheme is showed in Figure 1.22). This hypothesis is possible in conditions far from the source, but is decidedly forced and inappropriate for faults close to the analysed site.

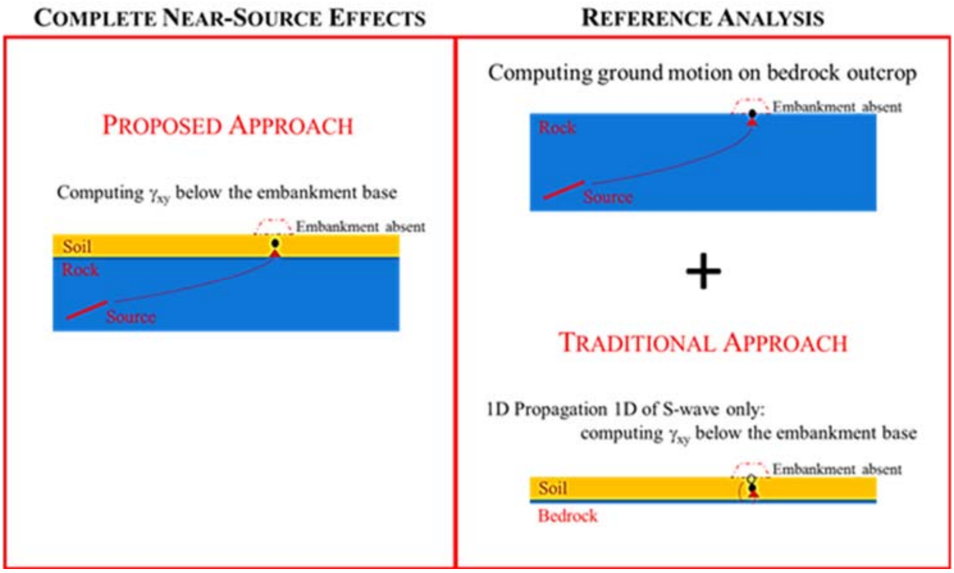

Figure 1.22 Logical scheme of the two different approaches of analysis.

Near-source propagation

In Figure 1.23, with reference to the free-field conditions for each of the three source models of Figure 1.19b, the acceleration Fourier amplitudes calculated along the ground level are shown (an epicentral area between the coordinates –15 and +15 km from the vertical axis of any faults). It is possible to observe as that the higher frequencies (>3Hz), typical of the near-source conditions are attenuated with increasing fault depth (i.e. moving from Figure 1.23a to Figure 1.23c). Moreover, the greater extension of the source produces a transfer of the energy content to the lower frequencies (0.5-1.5 Hz).

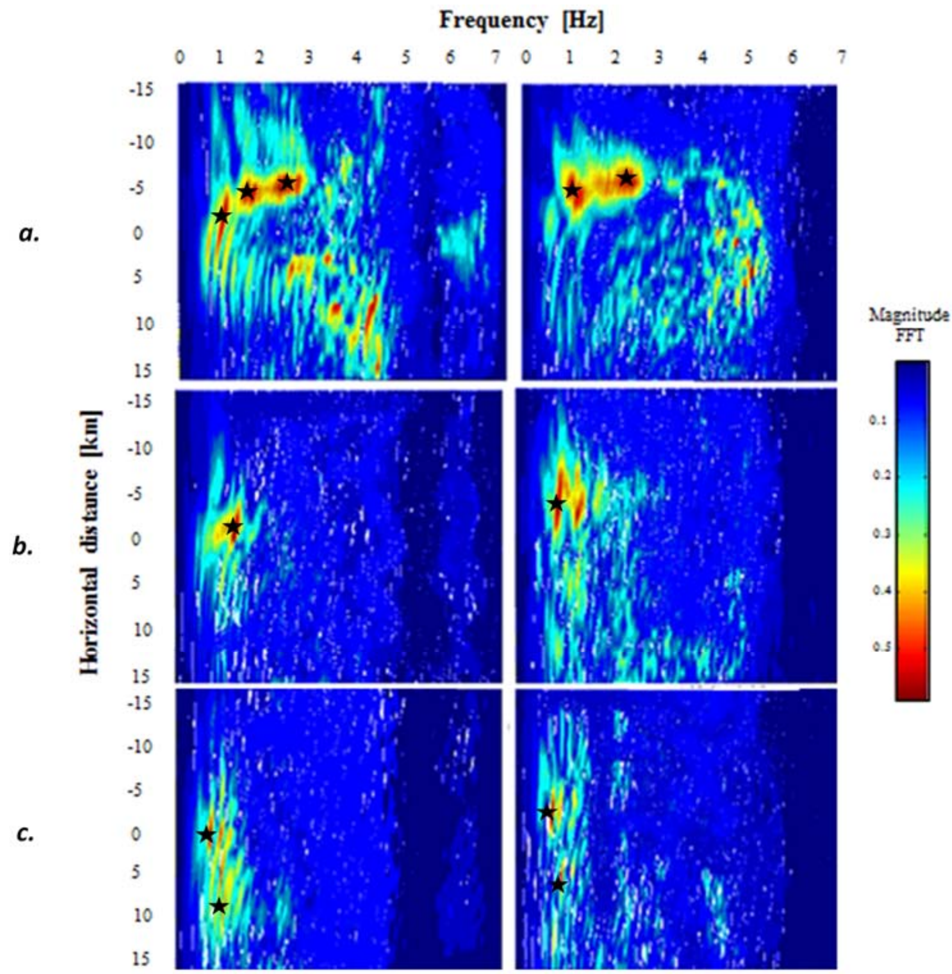

Figure 1.23 Fourier spectra of the horizontal (left) and vertical (right) accelerograms calculated on the ground level between fault distances of -15 and 15 kilometres for all three source models. Figures a, b and c represent case 1, 2 and 3 of Figure 1.19. The star symbols indicate the position of FFT picks.

A potentiality of investigating the near-source propagation, is to assess the differentiation of the input along horizontal planes at fixed depth below the ground level. As reference was used the distortional deformation, γ, computed from an analysis of the traditional type, i.e. by propagating from the bedrock to the surface a single signal (suitably deconvoluted).

Figure 1.24 shows the distortional increases in a fixed element of the subsoil (at depth 50m below the ground level) with respect to the distortion obtained from a traditional approach. The increases are calculated as the difference between the deformations resulting from the analyses carried out considering the propagation in near-source conditions and those deriving from the traditional procedure (Figure 1.22). As is possible to observe, the difference between the two approaches is maximum for the locations closer to the fault and decreases with increasing the distance from the fault (Figure 1.24). That is in line with expectations, because at large distances from the source the hypothesis of the traditional approach are more consistent.

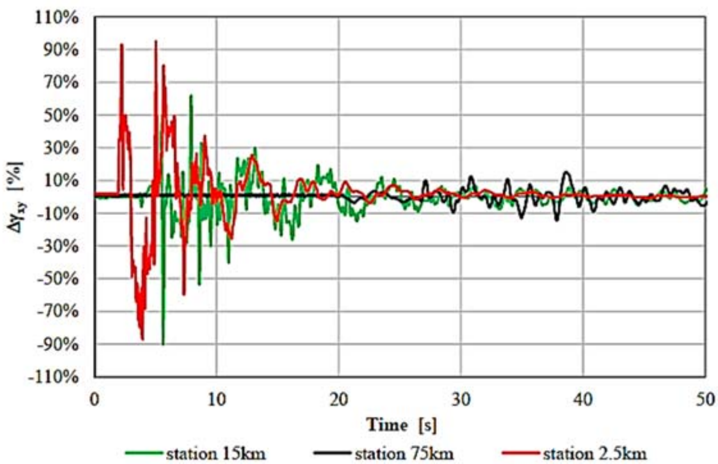

Figure 1.24 2D Model. Distortional increments in elements of the subsoil placed at a fixed depth of 50m below the ground level and at a distance of 2.5 (red), 15 (green) and 75 (black) km from the fault axis; the increments are reported in percentage of the value provided by traditional approach results.

Finally, the ratio between the maximum increments Δγ, and the maximum reference value in the same elements of the subsoil, are reported in Figure 1.25. It clearly appears that the strain increments tend to significantly decrease as the depth of the source increases (from Case 1, grey markers, to Case 3, blue markers).

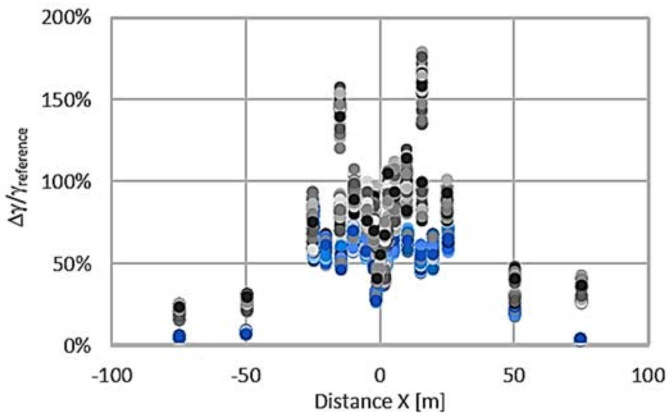

Figure 1.25 Maximum distortional increments in percentage of the maximum deformations calculated using a traditional approach, computed at different distances from the fault axis (2D model) and at a fixed depth of 50m below the ground level; grey markers are relative to the shallower source (Case 1), blue markers refer to deeper one (Case 3).

Effects of near-source propagation on earth-embankments

Now will be discussed some results of the performed analyses with including the embankments. In particular the comparison among accelerograms computed at different points of the embankment base, for different location of the structure (2D model), is illustrated in Figure 1.26. In particular Figure 1.26a and Figure 1.26b respectively refer to two embankments placed at distances of 5 and 10 km from the central point of a fault segment 5 km in length. For each embankment three accelerograms are plotted, computed along the base at the upstream, axis and downstream points. The magnitude of the acceleration values slightly varies moving from the upstream to the downstream points of the base; the main difference among the three accelerograms is the significant “time delay” in their occurrence along the base of the embankment (going from closer up to farthest point of the source). Consequently, the maximum values of the three signals are clearly asynchronous, sometimes with considerable time delay along the base of the structure, especially if compared to the wave travel time in the subsoil. This shift of seismic accelerations at the base of the embankment implies that, at the same instant, the structure can undergo significantly different stresses, and even stresses of opposite sign (see Figure 1.26b).

The difference among the seismic input motions exciting the base of the embankment is evident in the Fourier spectra plotted in Figure 1.26c, relative to the three accelerograms of Figure 1.26b (embankment located at a distance of 5 km). The shapes of the diagrams are quite similar, and the spectral content of the three signals is practically the same up to a frequency of about 0.6 Hz; for higher frequencies, the differences in amplitude of the Fourier spectra are relevant.

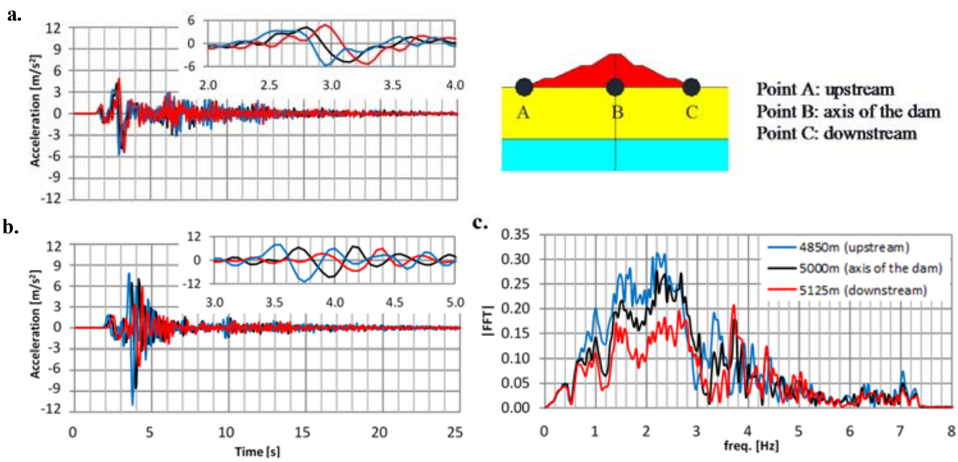

Figure 1.26 Horizontal accelerograms along the base, for embankments at distances of 5 and 10 km (figure *a* and *b* respectively) from the axis of the fault (whose extension is 5km). (*c*) Fourier Spectra of the three signals.

In the Figure 1.27, it is shown, instead, the horizontal and vertical accelerograms calculated at the base of the embankment (located at 0, 5 and 10 km from the axis of the fault) for a fault of 10 km. It is possible to make similar considerations to those previously made on the diagrams of Figure 1.26; from these further results also it may be noted that the vertical accelerations are high and comparable to the horizontal ones. In addition, from Figure 1.27c, it emerges that the peak horizontal accelerations in the upstream and central location of the embankment base (t = 7.4 s) are simultaneous, while in the point placed downstream the maximum acceleration is attained in the opposite direction (t = 8 s).

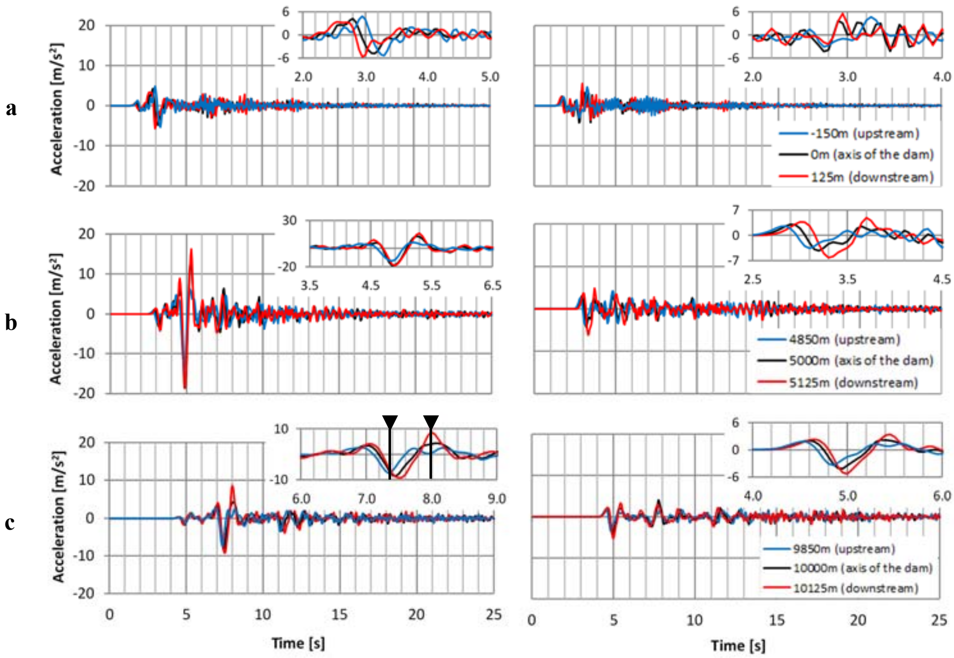

Figure 1.27 Horizontal (left) and vertical (right) accelerograms obtained at the embankment base for three their different positions: (a) 0 km, (b) 5 km and (c) 10 km from fault axis. The results are referred to the second case (10 km fault length).

Further parametric analyses

The same study discussed above has been solved also with a 3D model where the source is simulated as a finite fault (differently from 2D case) in the transverse direction (x) as shown in Figure 1.29. For each embankment the time-histories relative to the points indicated in Figure 1.28 were analysed. With the letters are represented points on the ground level sufficiently far from the embankments to consider free-field motion. With the numbers are indicated, instead, monitoring points on the external boundaries of the embankment (top and shells) for two embankments of the same height (h = 50m), one located in the vicinity of the fault (near-source, Figure 1.29a) and another far enough from it (far-source, Figure 1.29b). As can be seen in Figure 1.30, the accelerations in far-fault conditions (figure *b*) are well below those computed in near-fault condition (figure *a*). Furthermore, the embankment displacements for sites closer to the source are highly diversified along the longitudinal axis. This differentiation is induced by the variability of the motion at the dam base.

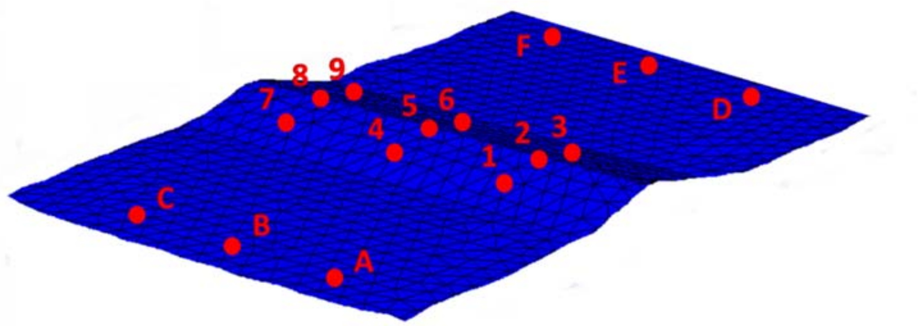

Figure 1.28 Scheme of dam where are reported the position of monitoring points on free surface (letters from A to F) and dam surface (numbers from 1 to 9).

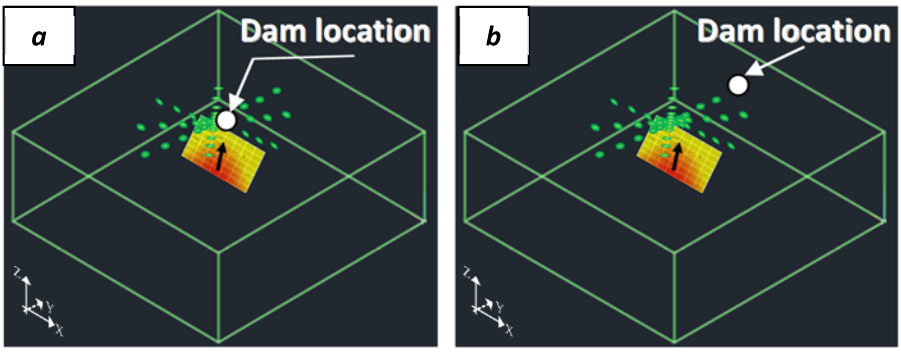

Figure 1.29 Localization of study sites: (a) embankment in near-source conditions; (b) embankment in far-source conditions.

In Figure 1.31 the contours of the vertical displacements at a fixed time (the time of maximum acceleration in point 5) are provided. As it is possible to observe, for the embankment placed near the fault (Figure 1.31a), the spatial distribution of the vertical displacements is less uniform than that obtained in the other case (Figure 1.31b). This implies higher differential displacements to which cracking phenomena may be related.

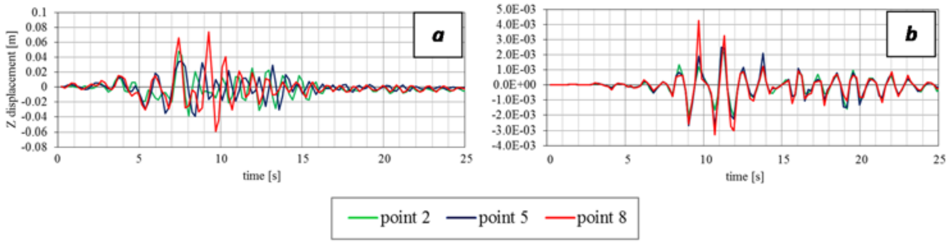

Figure 1.30 Time histories of vertical displacements for points 2, 5 and 8 of Figure 1.28c for an embankment in near-source conditions (a) and in far-source conditions (b).

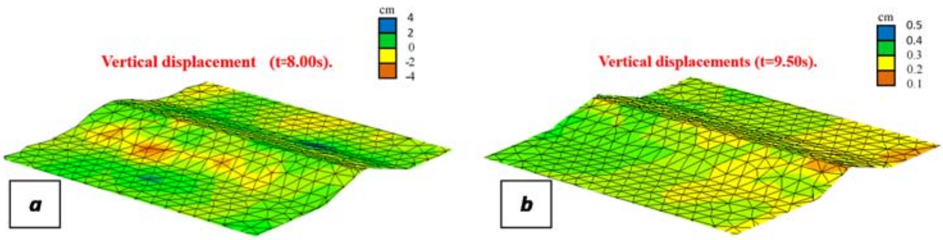

Figure 1.31 Contour of vertical displacements for embankments near (a) and far (b) from the fault mechanism.

Concluding remarks

The performed parametric analyses evidence that in near-source conditions it is not correct assuming a unique seismic motion at the base (as it is usually assumed in the case of structures placed at considerable distances from the source). Accelerograms calculated at the base of the embankment clearly show a phenomenon of asynchronism ("delay" of the signal with the distance from the source): this phenomenon is of particular relevance in the case of earth dams of considerable spatial extension. Equally important are the effects of directivity and frequency content in the base signals when near-source propagation occurs. The specific features of the seismic motion in near-source conditions should be properly studied for dams placed in the vicinity of seismogenic zones, considered the high risk associated to these structures.

2. Domain Reduction Method

2.1. Introduction

Following some recent catastrophic earthquakes the scientific community is devoting particular attention to the seismic response of sites placed close to seismogenic faults (near-source). Indeed, the phenomena of dislocation and directivity, as peculiar aspects of the seismic motion in near-source conditions, are worth of consideration. The correct approach should account for source mechanism, the location of the site relative to the source and the properties of the solid medium interposed. The use of a global formulation can be advantageous even in situations in which the causative fault is not far from the region of interest.

Despite the recent advances in the simulation of seismic boundary value problems and the development of physics-based 3D models for simulating earthquake ground motion, nowadays there are still restrictive simplifications and approximations in 3D simulations. A limitation is the maximum frequency that can be considered in media with low wave velocities (as soils).

Many analysis methods have been proposed over the years:

- Boundary Element and Discrete WaveNumber Methods (e.g., Mossessian and Dravinski, 1987; Kawase and Aki, 1990; Hisada *et al.*, 1993; Sánchez-Sesma and Luzón, 1995; Bouchon and Barker, 1996).
- Finite Differences Methods (e.g., Frankel and Vidale, 1992; Frankel, 1993; Graves, 1993, 1996; Olsen *et al.*, 1995; Pitarka, 1999; Stidham *et al.*, 1999; Sato *et al.*, 1999)
- Finite Elements Methods (e.g., Zienkiewicz at al., 1967; Lysmer and Drake, 1971; Zienkiewicz at al., 1973; Toshinawa and Ohmachi, 1992; Bao, 1998; Bao *et al.*, 1998; Aagaard *et al.*, 2001).

BEM and DWN approach are popular for moderate-sized problems with relatively simple geometry and geological conditions. The last two methods, due to their flexibility and simplicity, are better suited for larger domains that include realistic basin models with highly inhomogeneous materials, near-source ground motion, basin structure and directivity effects. Conversely they require high computational time with increasing the refinement of the mesh, because the grid size is proportional to the lowest shear wave velocity in the model and inversely proportional to the maximum frequency of interest.

Rather than analysing simultaneously the entire domain, which includes both the fault and the structure, the response of a smaller region close to the structure at hand is worth of consideration. This is the basic principle of the Domain Reduction Method (Loukakis, 1988, Loukakis & Bielak, 1994, Bielak et al. 2003, Yoshimura et al., 2003, Scandella, 2007), which is capable of efficiently modelling 3D wave fields for an arbitrary earthquake source, in highly heterogeneous geological systems with large impedance contrasts among layers and arbitrary shapes, also accounting for complexity of the geological structures, such as sedimentary basins and ridges.

2.2. Formulation of the method

The main advantage of the Domain Reduction Method (**DRM**) is the possibility of substructuring the original problem (Figure 2.1a) into two numerical sub-models characterized by different scale dimensions and solved in two different steps (Figure 2.2). The methodology is illustrated in Yoshimura et al. (2003) and Bielak et al. (2003) for 3D problems of increasing physical and computational complexity.

<u>Step 1</u>. The first model, which may span thousands of meters (Figure 2.1b), is an auxiliary one and represents a simplification of the *real external domain*. In this step the earthquake source and propagation path are simulated. As proposed by Bielak et al. (2003), a stratigraphic system (flat-layer scheme), solved by means of 3D Green's function, is simulated.

<u>Step 2</u>. The second model (Figure 2.1c) contains the domain of interest with reduced spatial dimensions (*internal domain*), including the structure and the surrounding soil. The seismic source and most of the propagation path from the source to the site are now excluded. The input is given as a set of equivalent nodal forces applied to interface elements and able to reproduce the seismic source modelled in the first step.

In the following, the method proposed by Bielak et al. (2003) is recalled.

The problem of a semi-infinite seismic region that contains localized geological features such as sedimentary valleys and ridges as well as seismically active faults is considered Figure 2.1a. The geometry is arbitrary, the material is linearly elastic and the earthquake excitation is prescribed as a kinematic source, defined by the jump of the tangential displacements across the fault, while the normal displacements and tractions remain continuous. Such transfer, of course, needs to be performed in a way that the resulting ground motion within the region of interest is identical to that due to the original source (Figure 2.1c), where $\boldsymbol{P_b}$ are the nodal forces transmitted by Ω^+ onto Ω.

These forces are localized on the fictitious surface Γ, which, as anticipated, divides the entire domain in the two regions Ω and Ω^+, containing respectively the geological features of interest and the semi-infinite exterior subdomain, which includes the fault (Figure 2.1b).

Whereas the methodology is applicable to elastic and inelastic problems, in this paragraph only the elastic case is considered. With reference to Figure 2.1b, the vector field of nodal displacements defined in the interior domain Ω, the exterior domain Ω^+ and the boundary between them, Γ, will be denoted, , by u_i (interior), u_e (exterior), and u_b (boundary) respectively. In the same figure Γ^+ is the outer boundary that truncates the original semi-infinite region and where the absorbing boundary conditions are applied.

The equations of elasto-dynamics, spatially discretized by finite or spectral elements, can be expressed for the internal and external domain of Figure 2.1c respectively as follows:

$$\begin{bmatrix} \underline{M}_{ii}^{\Omega} & \underline{M}_{ib}^{\Omega} \\ \underline{M}_{bi}^{\Omega} & \underline{M}_{bb}^{\Omega} \end{bmatrix} \begin{Bmatrix} \ddot{\boldsymbol{u}}_i \\ \ddot{\boldsymbol{u}}_b \end{Bmatrix} + \begin{bmatrix} \underline{K}_{ii}^{\Omega} & \underline{K}_{ib}^{\Omega} \\ \underline{K}_{bi}^{\Omega} & \underline{K}_{bb}^{\Omega} \end{bmatrix} \begin{Bmatrix} \boldsymbol{u}_i \\ \boldsymbol{u}_b \end{Bmatrix} = \begin{Bmatrix} 0 \\ -\boldsymbol{P}_b \end{Bmatrix} \quad in\ \Omega$$

$$\begin{bmatrix} \underline{M}_{bb}^{\Omega^+} & \underline{M}_{be}^{\Omega^+} \\ \underline{M}_{eb}^{\Omega^+} & \underline{M}_{ee}^{\Omega^+} \end{bmatrix} \begin{Bmatrix} \ddot{\boldsymbol{u}}_b \\ \ddot{\boldsymbol{u}}_e \end{Bmatrix} + \begin{bmatrix} \underline{K}_{ii}^{\Omega^+} & \underline{K}_{ib}^{\Omega^+} \\ \underline{K}_{bi}^{\Omega^+} & \underline{K}_{bb}^{\Omega^+} \end{bmatrix} \begin{Bmatrix} \boldsymbol{u}_b \\ \boldsymbol{u}_e \end{Bmatrix} = \begin{Bmatrix} \boldsymbol{P}_b \\ \boldsymbol{P}_e \end{Bmatrix} \quad in\ \Omega^+ \tag{2.1}$$

In these equations, the matrices M and K denote the mass and stiffness matrices, the subscripts *i* and *e* denote the interior and exterior domain, respectively, *b* the boundary Γ.

The summation of the previous systems yields to the traditional form of the equation of motion in the original domain:

$$\begin{bmatrix} \underline{M}_{ii}^{\Omega} & \underline{M}_{ib}^{\Omega} & 0 \\ \underline{M}_{bi}^{\Omega} & \underline{M}_{bb}^{\Omega} + \underline{M}_{bb}^{\Omega^+} & \underline{M}_{be}^{\Omega^+} \\ 0 & \underline{M}_{eb}^{\Omega^+} & \underline{M}_{ee}^{\Omega^+} \end{bmatrix} \begin{Bmatrix} \ddot{\boldsymbol{u}}_i \\ \ddot{\boldsymbol{u}}_b \\ \ddot{\boldsymbol{u}}_e \end{Bmatrix} + \begin{bmatrix} \underline{K}_{ii}^{\Omega} & \underline{K}_{ib}^{\Omega} & 0 \\ \underline{K}_{bi}^{\Omega} & \underline{K}_{bb}^{\Omega} + \underline{K}_{bb}^{\Omega^+} & \underline{K}_{be}^{\Omega^+} \\ 0 & \underline{K}_{eb}^{\Omega^+} & \underline{K}_{ee}^{\Omega^+} \end{bmatrix} \begin{Bmatrix} \boldsymbol{u}_i \\ \boldsymbol{u}_b \\ \boldsymbol{u}_e \end{Bmatrix} = \tag{2.2}$$

$$= \begin{Bmatrix} 0 \\ 0 \\ \boldsymbol{P}_e \end{Bmatrix} \quad in\ \Omega \cup \Omega^+$$

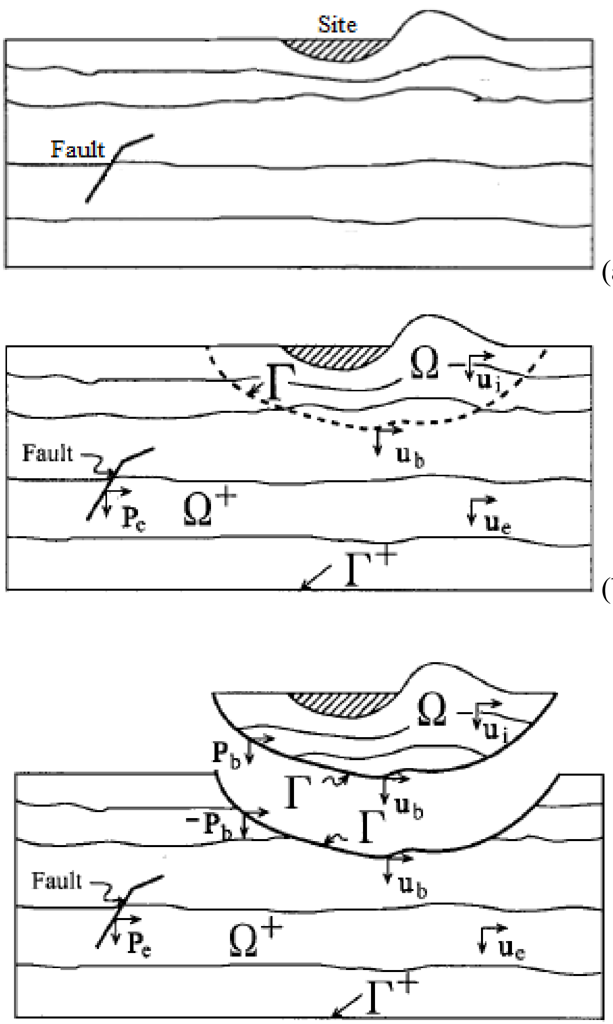

Figure 2.1 Real seismic region. (a) Scheme of the semi-infinite seismic region, including the causative fault, geological structure and local features. (b) Outer boundary Γ^+ restricts computation to a finite domain; fictitious interface Γ divides region into two subdomains: Ω^+ which includes the seismic source, represented by nodal forces $\boldsymbol{P_e}$ and Ω containing the geological features in the domain of interest. (c) Scheme of the region partitioned in two subdomains across the interface Γ with the nodal forces $\boldsymbol{P_b}$ transmitted from Ω^+ onto Ω^+ (Bielak et al.,2003).

To transfer the seismic excitation from the fault to Γ, an auxiliary problem is considered, in which the exterior region and the material therein, as well as the causative fault, are identical to those of the original problem. The new interior domain, indicated as Ω_0, is equivalent to the domain Ω^+, except for geological heterogeneities (replaced by the same material as the surrounding soil), background structure, local topographic features, etc. The problem thus defined over the total domain $\Omega_0 \cup \Omega^+$ is easier to solve than the original problem (**Figure 2.2**a). We denote by $\boldsymbol{u_i^0}$, $\boldsymbol{u_b^0}$, $\boldsymbol{u_e^0}$ and $\boldsymbol{P_b^0}$ the corresponding nodal displacements and interface forces, as shown in **Figure 2.2**b. Is worth emphasizing that the *auxiliary model* requires a mesh that is only as fine as dictated by the stiffness of the material of the background model. Therefore it will contain much less elements than the mesh including simultaneously both the external and the internal domain.

After spatial discretization, the equation of motion in Ω^+ for the auxiliary problem can be expressed as

$$\begin{bmatrix} \underline{M}_{bb}^{\Omega^+} & \underline{M}_{be}^{\Omega^+} \\ \underline{M}_{eb}^{\Omega^+} & \underline{M}_{ee}^{\Omega^+} \end{bmatrix} \begin{Bmatrix} \boldsymbol{\ddot{u}_b^0} \\ \boldsymbol{\ddot{u}_e^0} \end{Bmatrix} + \begin{bmatrix} \underline{K}_{bb}^{\Omega^+} & \underline{K}_{ib}^{\Omega^+} \\ \underline{K}_{be}^{\Omega^+} & \underline{K}_{ee}^{\Omega^+} \end{bmatrix} \begin{Bmatrix} \boldsymbol{u_b^0} \\ \boldsymbol{u_e^0} \end{Bmatrix} = \begin{Bmatrix} -\boldsymbol{P_b^0} \\ \boldsymbol{P_e} \end{Bmatrix} \quad in\ \Omega^+ \qquad \textbf{(2.3)}$$

The partitioned mass and stiffness matrices, as well as $\boldsymbol{P}_e$, are the same as in (2.1) because the material properties in Ω^+ and the earthquake source are identical in both cases. From the second equation in (2.3), we can now express the nodal forces $\boldsymbol{P}_e$ in terms of the free field motion, as follows:

$$P_e = \underline{M}_{eb}^{\Omega^+} \cdot \boldsymbol{\ddot{u}}_b^o + \underline{M}_{ee}^{\Omega^+} \cdot \boldsymbol{\ddot{u}}_e^o + \underline{K}_{eb}^{\Omega^+} \cdot \boldsymbol{u_b^0} + \underline{K}_{ee}^{\Omega^+} \cdot\cdot\, \boldsymbol{u_b^0} \qquad \textbf{(2.4)}$$

Then, by substituting (2.4) into (2.2), we can solve for the displacements u_i, u_b and u_e for the complete domain. This formulation offers no advantage over the traditional approach because (2.4) includes the terms $M_{ee}^{\Omega^+}\ \ddot{u}_e^0$ and $K_{ee}^{\Omega^+}\ \ddot{u}_e^0$, which require that the free field u_e^0 be stored throughout the domain Ω^+.

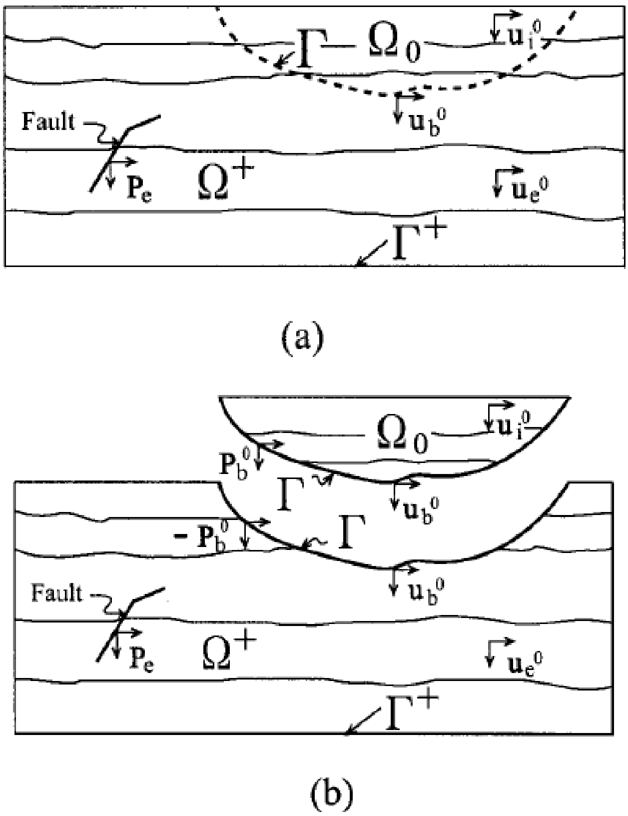

Figure 2.2 Auxiliary seismic region. (a) Entire scheme, (b) partitioned scheme into two substructures. The details, localized in Ω, have been replaced by a simpler structure (domain Ω_0). From Bielak et al. (2003).

To simplify the analysis, a variable transformation is introduced, expressing the total displacement in the external domain $\boldsymbol{u_e}$ as the sum of the free field $\boldsymbol{u_e^o}$ and the residual field $\boldsymbol{w_e}$ due to refraction within the inside region:

$$\boldsymbol{u_e} = \boldsymbol{u_e^o} + \boldsymbol{w_e} \qquad \textbf{(2.5)}$$

Then, substituting (2.5) into (2.2), and writing the terms that contain the free field on the right side, results in:

$$\begin{bmatrix} \underline{M}_{ii}^{\Omega} & \underline{M}_{ib}^{\Omega} & 0 \\ \underline{M}_{bi}^{\Omega} & \underline{M}_{bb}^{\Omega} + \underline{M}_{bb}^{\Omega^+} & \underline{M}_{be}^{\Omega^+} \\ 0 & \underline{M}_{eb}^{\Omega^+} & \underline{M}_{ee}^{\Omega^+} \end{bmatrix} \begin{Bmatrix} \ddot{\boldsymbol{u}}_{\boldsymbol{i}} \\ \ddot{\boldsymbol{u}}_{\boldsymbol{b}} \\ \ddot{\boldsymbol{u}}_{\boldsymbol{e}} \end{Bmatrix} + \begin{bmatrix} \underline{K}_{ii}^{\Omega} & \underline{K}_{ib}^{\Omega} & 0 \\ \underline{K}_{bi}^{\Omega} & \underline{K}_{bb}^{\Omega} + \underline{K}_{bb}^{\Omega^+} & \underline{K}_{be}^{\Omega^+} \\ 0 & \underline{K}_{eb}^{\Omega^+} & \underline{K}_{ee}^{\Omega^+} \end{bmatrix} \begin{Bmatrix} \boldsymbol{u}_{\boldsymbol{i}} \\ \boldsymbol{u}_{\boldsymbol{b}} \\ \boldsymbol{w}_{\boldsymbol{e}} \end{Bmatrix} = \begin{Bmatrix} 0 \\ -\underline{M}_{be}^{\Omega^+} \ddot{\boldsymbol{u}}_e^o \quad -\underline{K}_{be}^{\Omega^+} \boldsymbol{u}_e^o \\ \boldsymbol{P}_{\boldsymbol{e}} \quad -\underline{M}_{ee}^{\Omega^+} \ddot{\boldsymbol{u}}_e^o \quad -\underline{K}_{ee}^{\Omega^+} \boldsymbol{u}_e^o \end{Bmatrix} in\ \Omega \cup \Omega^+ \qquad \textbf{(2.6)}$$

Finally, substituting for $\boldsymbol{P_e}$ from the expression (2.4) into (2.6) the following system is obtained:

$$\begin{bmatrix} \underline{M}_{ii}^{\Omega} & \underline{M}_{ib}^{\Omega} & 0 \\ \underline{M}_{bi}^{\Omega} & \underline{M}_{bb}^{\Omega} + \underline{M}_{bb}^{\Omega^+} & \underline{M}_{be}^{\Omega^+} \\ 0 & \underline{M}_{eb}^{\Omega^+} & \underline{M}_{ee}^{\Omega^+} \end{bmatrix} \begin{Bmatrix} \ddot{\boldsymbol{u}}_{\boldsymbol{i}} \\ \ddot{\boldsymbol{u}}_{\boldsymbol{b}} \\ \ddot{\boldsymbol{u}}_{\boldsymbol{e}} \end{Bmatrix} + \begin{bmatrix} \underline{K}_{ii}^{\Omega} & \underline{K}_{ib}^{\Omega} & 0 \\ \underline{K}_{bi}^{\Omega} & \underline{K}_{bb}^{\Omega} + \underline{K}_{bb}^{\Omega^+} & \underline{K}_{be}^{\Omega^+} \\ 0 & \underline{K}_{eb}^{\Omega^+} & \underline{K}_{ee}^{\Omega^+} \end{bmatrix} \begin{Bmatrix} \boldsymbol{u}_{\boldsymbol{i}} \\ \boldsymbol{u}_{\boldsymbol{b}} \\ \boldsymbol{w}_{\boldsymbol{e}} \end{Bmatrix} = \begin{Bmatrix} 0 \\ -\underline{M}_{be}^{\Omega^+} \ddot{\boldsymbol{u}}_{\boldsymbol{e}}^{\boldsymbol{o}} \quad -\underline{K}_{be}^{\Omega^+} \boldsymbol{u}_{\boldsymbol{e}}^{\boldsymbol{o}} \\ \underline{M}_{eb}^{\Omega^+} \ddot{\boldsymbol{u}}_{\boldsymbol{b}}^{\boldsymbol{o}} \quad \underline{K}_{eb}^{\Omega^+} \boldsymbol{u}_{\boldsymbol{b}}^{\boldsymbol{o}} \end{Bmatrix} \quad \Omega \cup \Omega^+ \qquad \textbf{(2.7)}$$

The mass and stiffness matrices at the left side of the system are identical to those of the original problem (Figure **2.4**), and the seismic forces $\boldsymbol{P_e}$ which simulate the fault have been replaced by the following effective nodal forces $\boldsymbol{P^{eff}}$:

$$\boldsymbol{P}^{\boldsymbol{eff}} = \begin{Bmatrix} \boldsymbol{P}_{\boldsymbol{i}}^{\boldsymbol{eff}} \\ \boldsymbol{P}_{\boldsymbol{b}}^{\boldsymbol{eff}} \\ \boldsymbol{P}_{\boldsymbol{e}}^{\boldsymbol{eff}} \end{Bmatrix} = \begin{Bmatrix} 0 \\ -\underline{M}_{be}^{\Omega^+} \ddot{\boldsymbol{u}}_{\boldsymbol{e}}^{\boldsymbol{o}} \quad -\underline{K}_{be}^{\Omega^+} \boldsymbol{u}_{\boldsymbol{e}}^{\boldsymbol{o}} \\ \underline{M}_{be}^{\Omega^+} \ddot{\boldsymbol{u}}_{\boldsymbol{b}}^{\boldsymbol{o}} \quad \underline{K}_{be}^{\Omega^+} \boldsymbol{u}_{\boldsymbol{b}}^{\boldsymbol{o}} \end{Bmatrix} \qquad \textbf{(2.8)}$$

These forces have the key property that they involve only the submatrices $\underline{M}_{be}$, $\underline{K}_{be}$, $\underline{M}_{eb}$, and $\underline{K}_{eb}$, which vanish everywhere except in a single layer of finite elements in Ω^+adjacent to Γ. This small domain lies between Γ and its adjacent surface Γ_e, as shown in Figure 2.3.

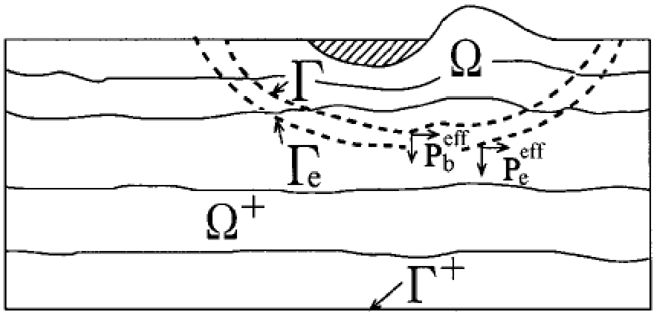

Figure 2.3 Seismic region with two neighbouring surfaces $\boldsymbol{\Gamma}$ and $\boldsymbol{\Gamma_e}$ on which effective nodal forces ($\boldsymbol{P_b^{eff}}$ and $\boldsymbol{P_e^{eff}}$) are applied. These forces are equivalent to and replace the original seismic forces P_e, which act in the vicinity of the causative fault (Jacobo Bielak et al., 2003).

Another important consequence of (2.8) is that all the waves in the exterior region Ω^+will be outgoing. This suggests that for solving (2.7), the size of the region Ω^+can be drastically reduced if one is interested only in the ground motion near the localized features. In numerical modelling spurious reflections from the external boundaries are generally unavoidable, and can lead to inaccuracies in the numerical results. Although these problems are reduced by the use of the Domain Reduction Method, it is possible to use suitable absorbing boundaries to further limit spurious waves. The first results of the method were derived in the context of a half-space and plane wave excitation in a slightly different form (Bielak and Christiano, 1984; Loukakis, 1988; Loukakis and Bielak, 1994a). The approach proposed in the present thesis is more rigorous and concise and incorporates explicitly the effect of an extended source on a finite fault. An approach similar to the original procedure (Loukakis, 1988) was developed subsequently by Aydinŏglu (1993), in the context of soil-structure interaction without explicit treatment of the earthquake source. Instead of using a finite-element formulation as former researchers, Aydinŏglu (1993) used a boundary integral representation for the tractions at the interface between the interior and exterior domains; to make the equations local at the interface, the traction was approximated in the form of a mass-dashpot-spring and the material outside the interface Γ was excluded from the computations.

In this thesis the approach proposed by Bielak et al. (2003), will be followed in combination with the finite difference method to solve the field equations.

Although the auxiliary problem (Figure 2.2) needs to be solved an additional advantage of substructuring the problem is to model just once the area of interest (which all details) and use the same refined mesh for different configurations of the source. Conversely, if we want to study more sites for a more defined source, the auxiliary problem remains unchanged (Yoshimura et al., 2003).

For simplicity in the analytical formulation previously recalled, the terms related to damping attenuation have not been reported. The addition of linear viscous damping would involve new terms in (2.8), proportional to velocity and displacement:

$$\boldsymbol{P}^{eff} = \begin{Bmatrix} \boldsymbol{P}_{\boldsymbol{i}}^{eff} \\ \boldsymbol{P}_{\boldsymbol{b}}^{eff} \\ \boldsymbol{P}_{\boldsymbol{e}}^{eff} \end{Bmatrix} = \begin{Bmatrix} & 0 & \\ -\underline{M}_{be}^{\Omega^+}\ddot{\boldsymbol{u}}_e^o & -\underline{C}_{be}^{\Omega^+}\dot{\boldsymbol{u}}_e^o & -\underline{K}_{be}^{\Omega^+}\boldsymbol{u}_e^o \\ \underline{M}_{eb}^{\Omega^+}\ddot{\boldsymbol{u}}_b^o & +\underline{C}_{eb}^{\Omega^+}\dot{\boldsymbol{u}}_b^o & +\underline{K}_{eb}^{\Omega^+}\boldsymbol{u}_b^o \end{Bmatrix} \tag{2.9}$$

where the terms $\underline{C}_{be}^{\Omega^+}$ and $\underline{C}_{eb}^{\Omega^+}$ represent the damping matrix.

If the formulation proposed by Rayleigh for linear visco-elastic material is adopted the damping matrix can be written as a linear combination of the mass and stiffness matrices:

$$\underline{C}_{eb}^{\Omega^+} = \alpha\underline{M}_{eb}^{\Omega^+} + \beta\underline{K}_{eb}^{\Omega^+} \tag{2.10}$$

and

$$\underline{C}_{be}^{\Omega^+} = \alpha\underline{M}_{be}^{\Omega^+} + \beta\underline{K}_{be}^{\Omega^+} \tag{2.11}$$

where coefficients α and β can be determined from specific damping ratios ξ_i and ξ_j for two representative i-th and j-th modes, respectively:

$$\frac{1}{2}\begin{bmatrix} 1/\omega_i & \omega_i \\ 1/\omega_j & \omega_j \end{bmatrix}\begin{Bmatrix} \alpha \\ \beta \end{Bmatrix} = \begin{Bmatrix} \xi_i \\ \xi_j \end{Bmatrix} \tag{2.12}$$

If both modes are assumed to have the same damping ratio ξ, as it is generally assumed in dynamic analysis, the coefficients become:

$$\alpha = \xi\frac{2\omega_i\omega_j}{\omega_i + \omega_j} \quad \text{and} \quad \beta = \xi\frac{2}{\omega_i + \omega_j} \tag{2.13}$$

From (2.9) it is obtained:

$$\boldsymbol{P^{eff}} = \begin{Bmatrix} \boldsymbol{P_i^{eff}} \\ \boldsymbol{P_b^{eff}} \\ \boldsymbol{P_e^{eff}} \end{Bmatrix} = \begin{Bmatrix} 0 \\ -(1+\alpha)\underline{M}_{be}^{\Omega^+}\boldsymbol{\ddot{u}_e^o} \quad -(1+\beta)\underline{K}_{be}^{\Omega^+}\boldsymbol{u_e^o} \\ (1+\alpha)\underline{M}_{be}^{\Omega^+}\boldsymbol{\ddot{u}_b^o} \quad (1+\beta)\underline{K}_{be}^{\Omega^+}\boldsymbol{u_b^o} \end{Bmatrix} \tag{2.14}$$

It is important to emphasize that the DRM is exact in consideration of typical spatial and time discretization errors. In this thesis a finite differences spatial formulation with second-order central differences in time has been used (Itasca, 2012).

In Finite Differences Method (FDM), as well as in Spectral Elements formulation (Scandarella, 2007), the effective forces depend only on the stiffness matrix, since the mass matrix (Appendix B) is naturally diagonal (Itasca, 2012), so that:

$$\boldsymbol{P^{eff}} = \begin{Bmatrix} \boldsymbol{P_i^{eff}} \\ \boldsymbol{P_b^{eff}} \\ \boldsymbol{P_e^{eff}} \end{Bmatrix} = \begin{Bmatrix} 0 \\ -\underline{K}_{be}^{\Omega^+}\boldsymbol{u_e^o} \\ -\underline{K}_{eb}^{\Omega^+}\boldsymbol{u_b^o} \end{Bmatrix} \tag{2.15}$$

Recalling in Appendix B the expression (B.30) of the nodal forces for a single mesh element *k* (Figure B.1):

$$-f_i^{(l)} = \frac{T_i^{(l)}}{3} + \frac{\rho\ b_i\ V}{4} - m^{(l)}\left(\frac{dv_i}{dt}\right)^{(l)} \tag{2.16}$$

where *l* indicates the node label, *i* is the *i*-th component of motion, ***T*** is the stress tensor related to the *k*-th element, ***f*** nodal force, *V* element volume, ρ density, ***b*** gravity acceleration, *m* nodal mass, v nodal velocity and *t* time.

In equation (2.16) the stress vector components $\boldsymbol{T}^{(l)}$ are defined as:

$$T_i^{(l)} = \sigma_{ij}{}^{(l)}\ n_j{}^{(l)}\ S^{(l)} \tag{2.17}$$

with $\boldsymbol{n^{(l)}}$ is the external unit vector normal to the element surface *S* opposite to the node *l*.

Considering time-independent term of the body forces ($\rho\ b_i\ V/4$) and being the mass matrix diagonal, it follows that the nodal forces, to be applied to the internal model, are equal to the change of the stress tensor $\underline{\mathrm{T}}$ in the *k*-th mesh element:

$$-\Delta f_i^{(l)} = \frac{1}{3}\Delta T_i^{(l)} \tag{2.18}$$

The total stress is then obtained from the relation:

$$\sigma_{i,j}{}^{(new)} = \sigma_{i,j}{}^{(old)} + \Delta\sigma_{i,j} \qquad \textbf{(2.19)}$$

with *new* = current step and *old* = previous step.

In an elastic and isotropic material behaviour, strain increments generate stress increments according to the linear and reversible law of Hooke:

$$\Delta\sigma_{i,j} = 2G\ \Delta\varepsilon_{i,j} + \alpha_2\ \Delta\varepsilon_{i,j}\ \delta_{ij} \qquad \textbf{(2.20)}$$

where the Einstein summation convention applies, δ_{ij} is the Kroenecker delta symbol and α_2 is a material constant related to the bulk modulus, *K*, and shear modulus, *G*, as:

$$\alpha_2 = K - \frac{2}{3}G \qquad \textbf{(2.21)}$$

Finally, in terms of vector of nodal forces, for each element *k* can be written:

$$-\Delta\boldsymbol{F}^{(l)} = \frac{S^{(l)}}{3}\Delta\underline{\sigma}^{(l)}\boldsymbol{n}^{(l)} \qquad \textbf{(2.22)}$$

The incremental stress-strain relations may be expressed as

$$\Delta\underline{\sigma} = \underline{K}\ \Delta\underline{\varepsilon} \qquad \textbf{(2.23)}$$

The global stiffness matrix $\underline{K}$ is calculated by applying a transformation of the form:

$$\underline{K} = \underline{Q}^T\ \underline{K'}\ \ \underline{Q} \qquad \textbf{(2.24)}$$

where $\underline{Q}$ is a suitable 6 × 6 matrix involving direction cosines of local axes in global axes and $\underline{K'}$ is the local stiffness matrix.

In summary, the matrix $\underline{K}$ is equivalent to the following formulation (for an isotropic linear-elastic material):

$$\underline{K} = \begin{bmatrix} \lambda + 2\mu & \lambda & 0 \\ \lambda & \lambda + 2\mu & 0 \\ 0 & 0 & \mu \end{bmatrix} \quad \text{or} \quad \underline{K} = \begin{bmatrix} E_{oed} & k_0 E_{oed} & 0 \\ k_0 E_{oed} & E_{oed} & 0 \\ 0 & 0 & G \end{bmatrix} \qquad \textbf{(2.25)}$$

where λ and μ are the Lame constants, E_{oed} is the oedometric modulus an k_0 is the rest lateral earth pressure.

2.3. Implementation

To better understand the physical concept related to the effective forces $\boldsymbol{P}^{eff}$, consider the following example, reported by Scandella, (2007).

With reference to Figure 2.4, the physical interpretation of $\boldsymbol{P}^{eff}$ for an idealised simple case referring to a triangular finite element. Once the free field displacement has been calculated, the nodal forces are derived in two steps:

- fix the degrees of freedom at the interface nodes *b* (denoted by **1** in Figure 2.4); prescribe the free field displacements at the remaining nodes *e* of the interface elements (denoted by **2** and **3** in Figure 2.4) with opposite sign; calculate the reaction forces at the fixed node *b* (**1**);
- fix the degrees of freedom of all the nodes *e* not lying on the interface (**2** ,**3**); apply the free field displacements at the remaining nodes *b* (**1**); calculate the reaction forces at the fixed node *b* (**1**); calculate the reaction forces at the fixed node *e* (**2** ,**3**).

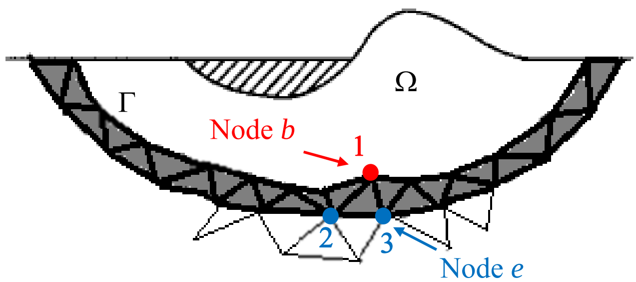

Figure 2.4 Idealised finite element simple case to show the physical meaning of the effective nodal forces at the highlighted nodes **1**, **2**, and **3**.

The resulting effective forces at the three nodes are:

$$\boldsymbol{P^{eff}} = \begin{Bmatrix} P_1^{eff} \\ P_2^{eff} \\ P_3^{eff} \end{Bmatrix} = \tag{2.26}$$

$$= \begin{Bmatrix} -(1+\alpha)\underline{M}_{12}\boldsymbol{u_2^o} & -(1+\beta)\underline{K}_{12}\boldsymbol{u_2^o} & -(1+\alpha)\underline{M}_{13}\boldsymbol{u_3^o} & -(1+\beta)\underline{K}_{13}\boldsymbol{u_3^o} \\ & -(1+\alpha)\underline{M}_{21}\boldsymbol{u_1^o} & -(1+\beta)\underline{K}_{21}\boldsymbol{u_1^o} & \\ & -(1+\alpha)\underline{M}_{31}\boldsymbol{u_1^o} & -(1+\beta)\underline{K}_{31}\boldsymbol{u_1^o} & \end{Bmatrix}$$

As anticipated (paragraph §2.2), in the case of diagonal mass matrices, the equation **(2.26)** becomes:

$$\boldsymbol{P^{eff}} = \begin{Bmatrix} P_1^{eff} \\ P_2^{eff} \\ P_3^{eff} \end{Bmatrix} = \begin{Bmatrix} -(1+\beta)\underline{K}_{12}\boldsymbol{u_2^o} \quad -(1+\beta)\underline{K}_{13}\boldsymbol{u_3^o} \\ -(1+\beta)\underline{K}_{21}\boldsymbol{u_1^o} \\ -(1+\beta)\underline{K}_{31}\boldsymbol{u_1^o} \end{Bmatrix} \tag{2.27}$$

As it is possible to see in this example, without the knowledge of the stiffness matrices, we can still get the effective forces imposing simply, to single node of the internal or external interface side, the single component of the motion resulting from the auxiliary problem and limiting the motion to the other nodes of the interface elements. Similarly, if you want to speed, to generalize and automate the process, you can fix at 1 the various components of the unit vectors $\boldsymbol{u_i^o}$ and to determine the individual ($\underline{K}_{ij}$) components of the stiffness matrix. In this way, a simple linear combination of the various contributions allow to get the $\boldsymbol{P^{eff}}$. It is important to highlight that, generalizing the process, we can perform only once the operation for the source mechanism and any site, granted that the nodal position of the interface elements (for congruence and also for the adjacent elements) is always the same.

This procedure may be easily implemented in any commercial software provided that it is permitted a minimum of user interaction with the code by external programming (see Diana, Abaqus, Flac, etc.).

In Figure 2.6 a simple flow chart of the algorithm developed during the thesis work is proposed, instead Figure 2.7 shows a schematization of its structure.

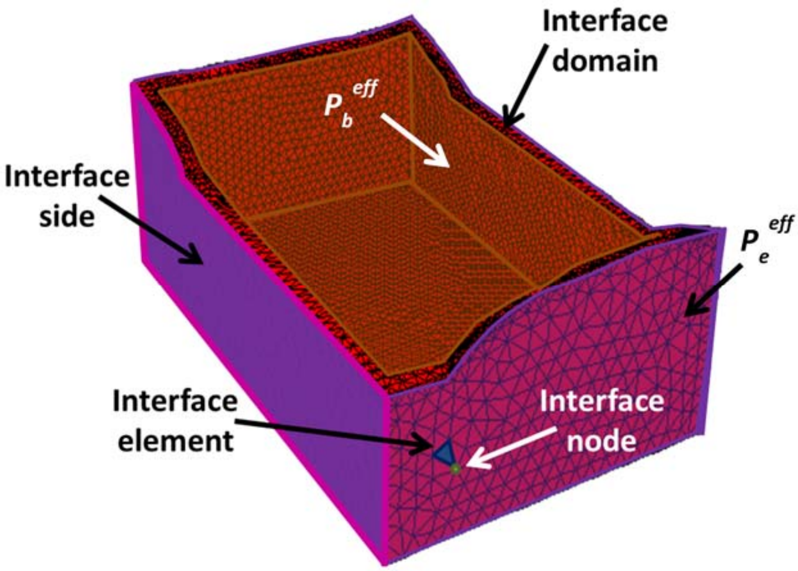

Figure 2.5 Interface zone between the internal and external domain, with representation of nodes, elements and sides.

Algoritmo

With reference to the diagram of Figure 2.6, the first step of the algorithm is the definition of the used variables to store the data. It is good practice to set to zero the initial variable values. Firstly, to calculate the stiffness matrix, we disregard the body forces and, therefore, it is necessary reset the gravity. Then we must automate, using a set of coordinates in input provided by user, the recognition of the sides belonging to the interface domain (Figure 2.5). The sides will be 10 in total, 5 of contact with the internal domain and 5 with the external domain. To each side of the interface, for each node belonging to it and for each spatial direction, the core of the algorithm must initialize automatically displacements and stresses to zero in the model, fix at 1 the displacement to the reference node, constrain the other nodes and launch the single analysis. The symmetry properties of stiffness matrices may be useful to optimize the algorithm. Finally, we need to save the variables, possibly already in a format recognizable by the code. We preferred to use a MATLAB SCRIPT for the linear combination of the different nodal reactions with nodal displacements resulting from the analysis on the auxiliary problem, so we do not have to re-launch the algorithm for each type of source examined, because for a mesh with many nodes running time could be of hours, depending also on the optimization degree of the algorithm.

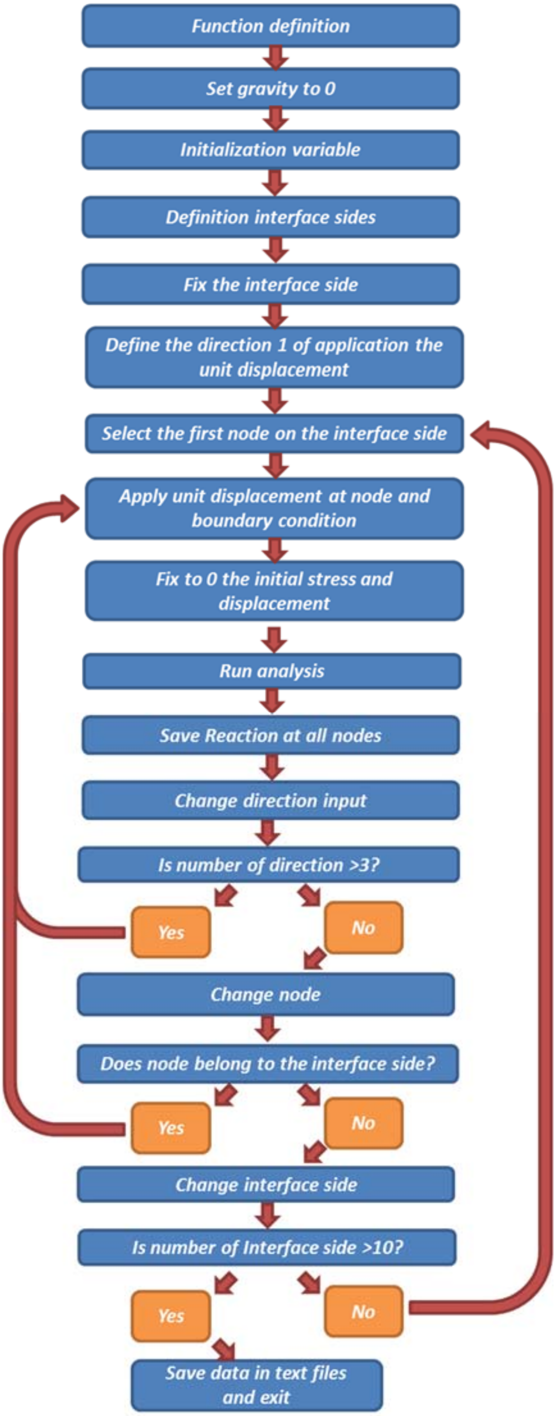

Figure 2.6 Flow chart of the algorithm to calculate the single components of the stiffness matrix.

```
function definition
 set gravity to 0
 initialization variables (reference_point_number and reaction_point_number)
 initialization arrays:
  X_reaction(1,max gp value) -> X or direction 1
  Y_reaction(1,max gp value) -> Y or direction 2
  Z_reaction(1,max gp value) -> Z or direction 3
 definition boundary side (case from 1 to 10)

 case 1
  while_loop reference_point_number .NE. (not equal) zero

   initialization variable: reference_point
   search point on side through coordinates (reference point)
   command
    initialization to 0 the displacements, velocities, stresses and body-forces
    fix motion to the nodes through constraints (except for the reference point)
    set to 1 the displacement (or velocity value) in direction 1 (or X) for reference point
    solve the analysis (for fixed step numbers if you set velocity value)
   end command
   initialization variables: reaction_point
   search point on side through coordinates (for reaction point)
   sum on reaction_point the nodal force in respective node
                                        (this operation can be
                                         made externally, for
                                            example with a
                                            'Octave-script')
   save the values of reactions on arrays
  end loop

  replay loop on reference_point for other direction (Y and Z or 2 and 3)

 replay for any case (boundary side: 2, ..., 10) the algorithm in case 1

 end case
 print on file the values of reactions saved in arrays

close function and return to the user interface
```

Initialization

Algorithm core

Figure 2.7 Schematic structure of the developed algorithm.

2.4. Literature examples

In literature the DRM approach has already been used for different problems. A validation study performed by Yoshimura et al. 2003 is shown below, along with some examples of the literature. These latter are cited relative to the vulnerability studies of underground structures, performed by Scandella in 2007 and Christchurch City, performed by Guidotti in 2012.

Studies on the seismic input definition for displacement-based analyses with the application of DRM were made by Smerzini in 2010 and later by the workgroup of the DPC-RELUIS Project 2 (2009-2012). In particular, the modelling of the Aterno valley response to the 2009 Abruzzo earthquake was performed (Figure 2.8).

Finally, in the DRM manual of GeoELSE code (Faccioli et al., 1997) an example, related the Aquasanta bridge (Genoa, Italy), is proposed too Figure 2.9.

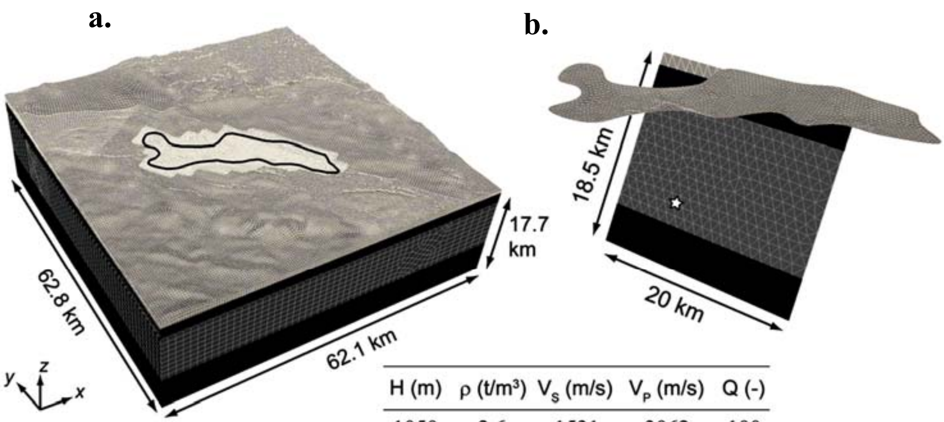

H (m)	ρ (t/m³)	V_S (m/s)	V_P (m/s)	Q (-)
1050	2.6	1531	3062	100
2750	2.6	2770	4709	200
9000	2.8	3797	7024	300
6650	2.8	3315	6000	300

Figure 2.8 3D numerical mesh by hexahedral spectral elements adopted for the numerical simulations by GeoELSE. (a) The map highlights the fault discretization (b), while the bottom table summarizes the main features of the deep crustal model (Paolucci & Smerzini, 2011).

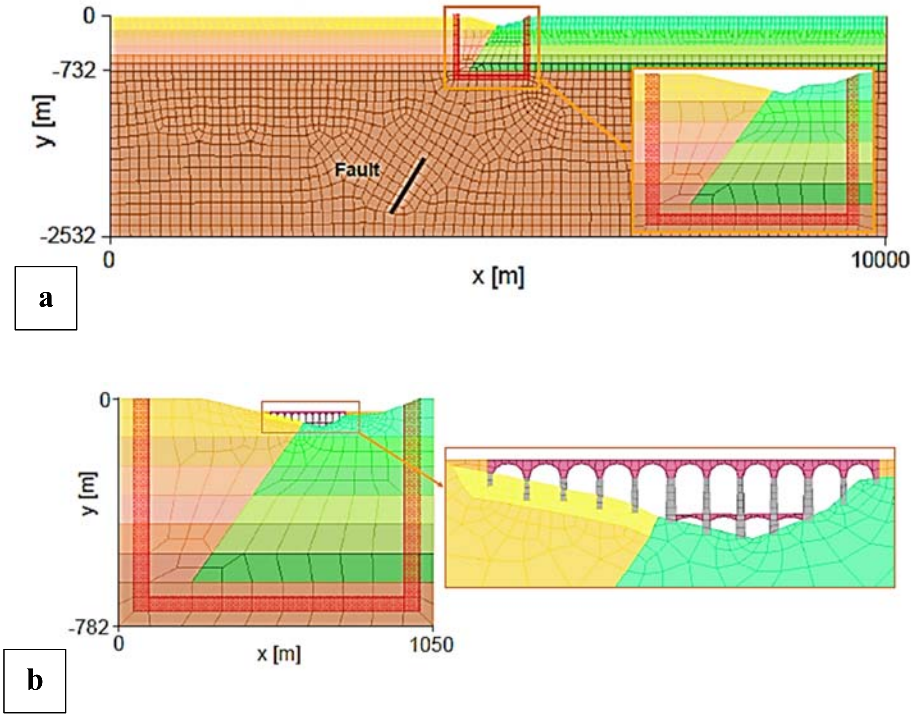

Figure 2.9 2D model of the auxiliary (a) and reduced (b) problem for the DRM analysis of the Acquasanta bridge (Genoa, Italy). The dark red strip represents the effective boundary where free field displacements are calculated (Scandelle & Vanini, 2007).

2.4.1. Free-field validation (Yoshimura et al., 2003)

To validate the method the authors realized a comparison between FEM analysis with Green function of a two-layer system underlain by an elastic half-space (Figure 2.10). The property of the layers are listed in Table 2.1 The seismic source is a dip-slip double couple buried at a point 1 km below the free surface. The strike, dip, and rake are 0°, 90°, and 90°, respectively, the seismic moment M_0 equal to 6×10^{15} N m (Figure 2.10). The boundary nodes were left unconstrained, thereby implying that the outer boundary is traction free.

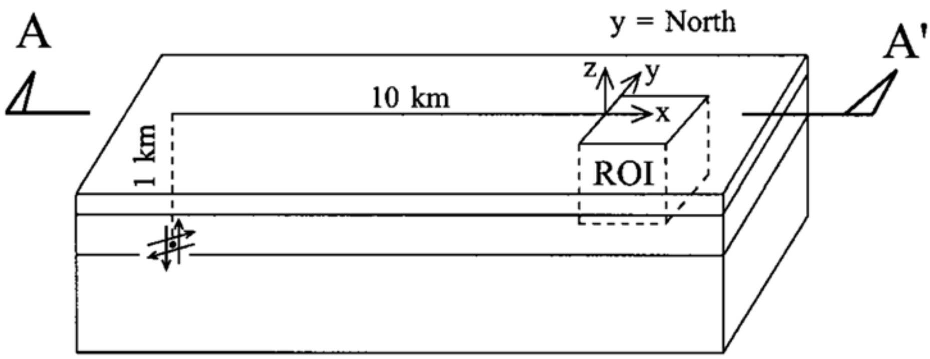

Figure 2.10 Flat-layered system used to verify the DRM, with seismic source and region of interest (Yoshimura et al, 2003).

Layer	Thickness	Vs	Vp	Density
	(m)	(m/s)	(m/s)	(kN/m^3)
1	200	250	500	20
2	400	500	500	20
3	∞	2000	500	20

Table 2.1 Soil parameters of the layered system.

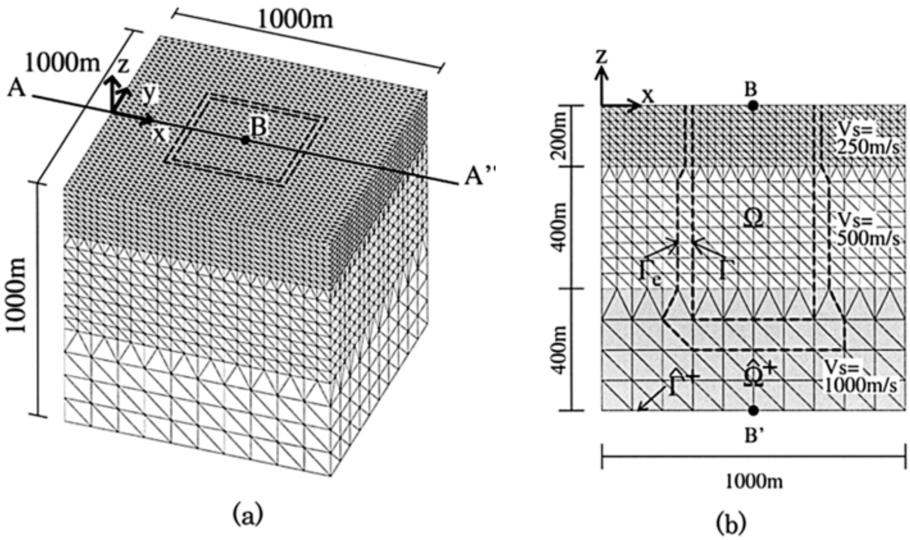

Figure 2.11 Layered system within region of interest. (a) Finite-element mesh tailored to shear-wave velocity of each layer and the half-space; (b) cross section on vertical plane through AA'. The bold dashed lines show surfaces $\boldsymbol{\Gamma}$ and $\boldsymbol{\Gamma_e}$ where effective forces P^{eff} are applied in step 2 (Yoshimura et al, 2003).

The solution obtained from the DRM for points on a fixed vertical that passes through points B and B' (Figure 2.11) is shown in

Figure **2.12**a depicts the x component of the displacement, and

Figure **2.12**b the vertical component, at various depths. The complete wave field, including body and surface waves, can be clearly observed in this figure. The corresponding results from the Green functions evaluations are also shown in

Figure **2.12**, for comparison. Peak values, with their signs, are listed on the right columns for both solutions next to the synthetic seismograms. The agreement between the two sets of waveforms is quite good, with maximum differences in amplitude on the order of 5%. This is consistent with the accuracy we can expect from a finite element approximation, which is tailored to 10 points per wavelength, according to the shear-wave velocity within each element and a maximum frequency of 1 Hz.

Notice that the agreement between the finite-element solutions and the corresponding Green functions remains quite close down to the interface Γ, at 700 m. Right below this point, the finite-element solution almost vanishes. The same behaviour is observed in Figure 2.16 for the seismograms on the free surface along AA' (Figure 2.11). The difference between the results from the DRM approach and the Green functions does not exceed 5% at these locations, and the displacements beyond Γ also essentially vanish. Recall that in the outer region $\widehat{\Omega}^{+}$, our formulation yields residual displacements; since the material is the same as that in the background structure for this example, w_e of the relation (2.5) must vanish. The fact that the numerical values of these residual displacements are close to zero provides a useful numerical check. An interesting consequence of the vanishing of w_e for this problem is that, theoretically, the outer boundary $\hat{\Gamma}^{+}$ must play no role in the solution, regardless of the absorbing boundary conditions one uses there. The boundary conditions (traction free) were used by the authors. The fact that residual displacements are $\widehat{\Omega}^{+}$ barely visible confirms that for the validation problem the boundary condition on $\hat{\Gamma}^{+}$ has an insignificant numerical effect. Moreover, since there are no waves leaving the region of interest Ω, one could modify the material in the exterior region beyond a single-element thick layer surrounding the surface Γ_e, and the results within Ω would not change.

Demonstrated the validity of the approach, Yoshimura et al. (2003) apply the methodology to two different examples below reported.

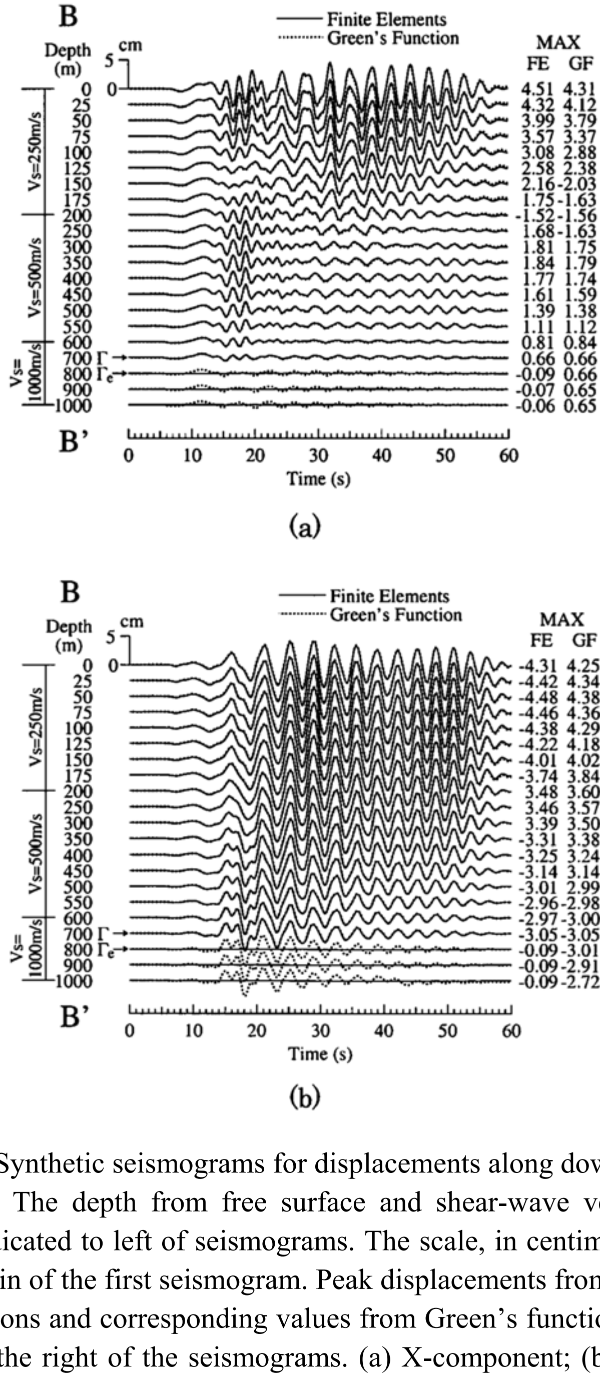

Figure 2.12 Synthetic seismograms for displacements along downhole line BB' (Figure 2.11). The depth from free surface and shear-wave velocity of each material is indicated to left of seismograms. The scale, in centimeters, is shown above the origin of the first seismogram. Peak displacements from finite-element DRM simulations and corresponding values from Green's functions calculations are shown to the right of the seismograms. (a) X-component; (b) Z-component (Yoshimura et al, 2003).

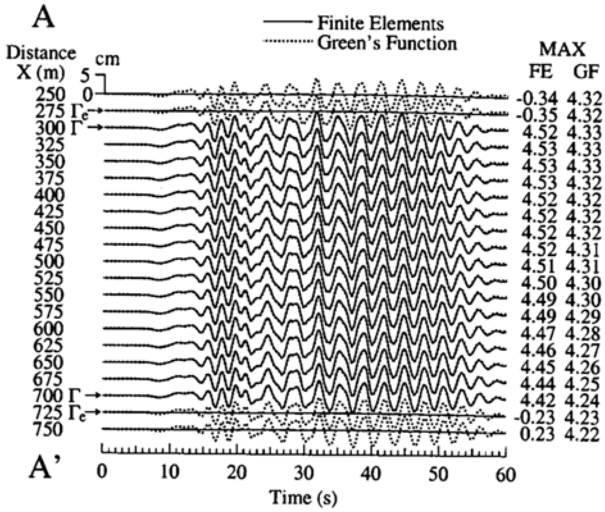

(a)

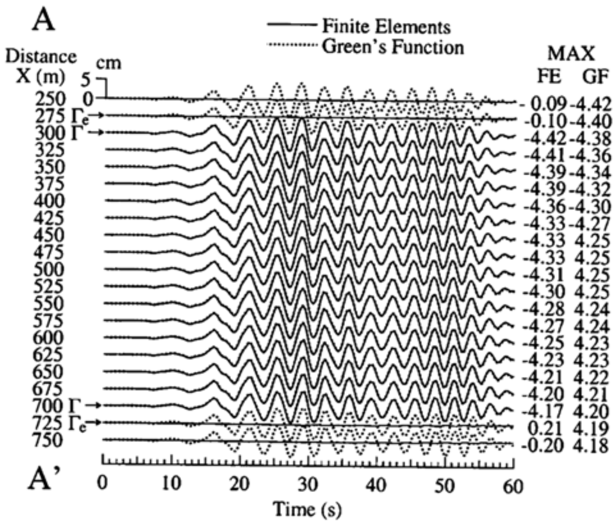

(b)

Figure 2.13 Synthetic seismograms for displacements along free-surface (horizontal) line AA' (Figure 2.11). The distance *x* is measured from the origin of the *x* axis of Figure 2.10 (Yoshimura et al, 2003).

2.4.2. Dynamic response of idealized basin and hill (Yoshimura et al., 2003)

To illustrate the applicability of the method, the authors has considered two examples of idealized cases: (i) stratigraphy variability in a basin and (ii) presence of topography, as hills.

In the first example is illustrated the applicability of DRM to more complex situations at the one that involves a local structure Ω with a sedimentary basin embedded into the same two-layer stratigraphic system considered in the previous section. The basin has the shape of a spherical cap and has a maximum depth of 100 m and a 150 m radius at its intersection with the free surface, as shown in Figure 2.14. It has a uniform shear-wave velocity of 125 m/s, P-wave velocity of 250 m/s, and density of 20 kN/m^3. The seismic source is identical to that for the unperturbed flat-layered system. The resulting displacement along the line BB' (Figure 2.14) are shown in Figure 2.15, together with the corresponding values for the background (flat-layered) structure.

As expected, the basin has the effect of magnifying the amplitude of the free-field ground motion.

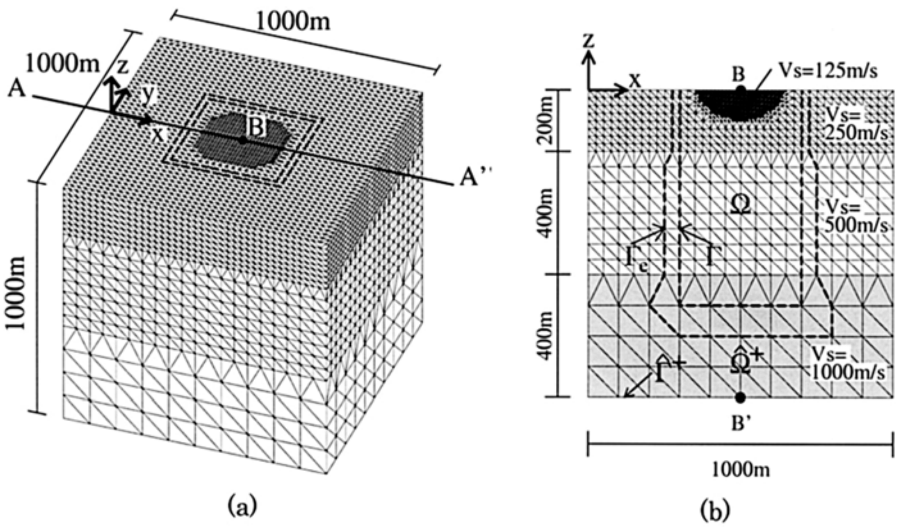

Figure 2.14 Homogeneous basin embedded in flat layered system. (a) Finite-element mesh; (b) cross section through AA' (Yoshimura et al, 2003).

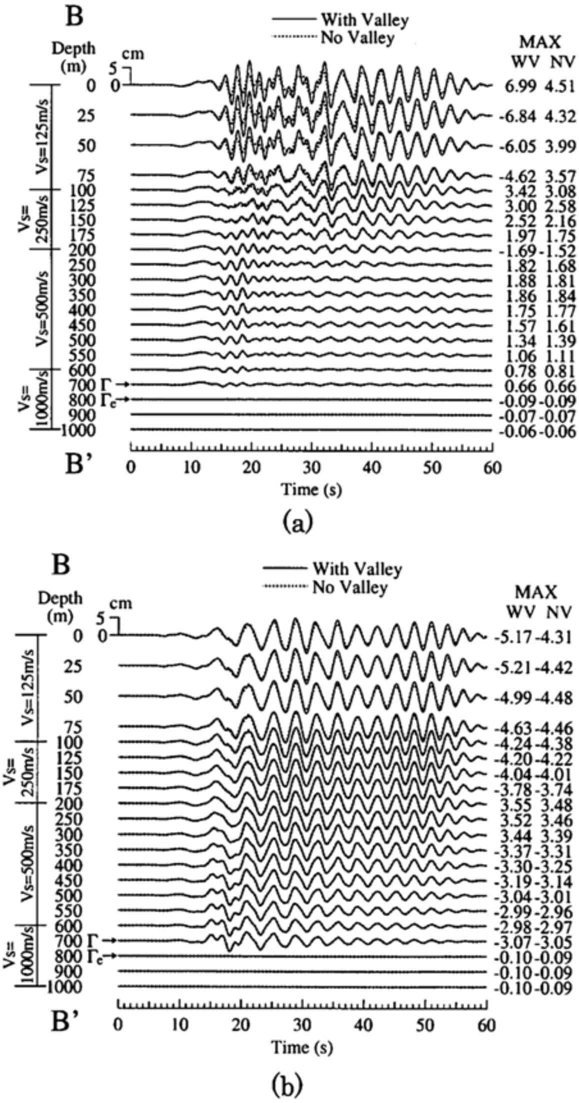

Figure 2.15 Synthetic seismograms for displacements along down hole line BB' (Figure 2.14b). The solid lines show the response with basin present. The dashed lines correspond to free-field motion (without the valley). The right-hand columns show peak values with and without basin. Traces for points within surface C represent total displacement; those for points outside this surface show residual displacements with respect to free-field surface motion of the corresponding points for the flat-layered system. (a) *X*-component; (b) *Z*-component (Yoshimura et al, 2003).

In the second example, the authors apply the DRM procedure to the analysis of topographic effects. They considered the case of a hill supported on the two-layered system, as shown in Figure 2.16. The ground motion for two variations of the hill problem has been used. In the first instance, the hill is assumed homogeneous with the same properties as the top layer of the background material; in the second, the hill has a weathered surface layer 25 m thick, with the same properties as those of the basin in the previous example. The hill has a square base 350 m x 350 m, it is 100 m high, and the lateral sides have a slope of 45°. The seismic excitation is the same as before. The hill's effect on the free-field ground motion is far from negligible. In Figure 2.17, it is seen that the prescribed seismic source excites primarily the fundamental mode of the hill. The peak amplitudes of the x and z (directions of slip motion at the source) components of displacement increase from the base to the top, and the maximum peak values occur on the eastward side of the crest for the x component of displacement and on the westward side and uphill plane for the vertical component.

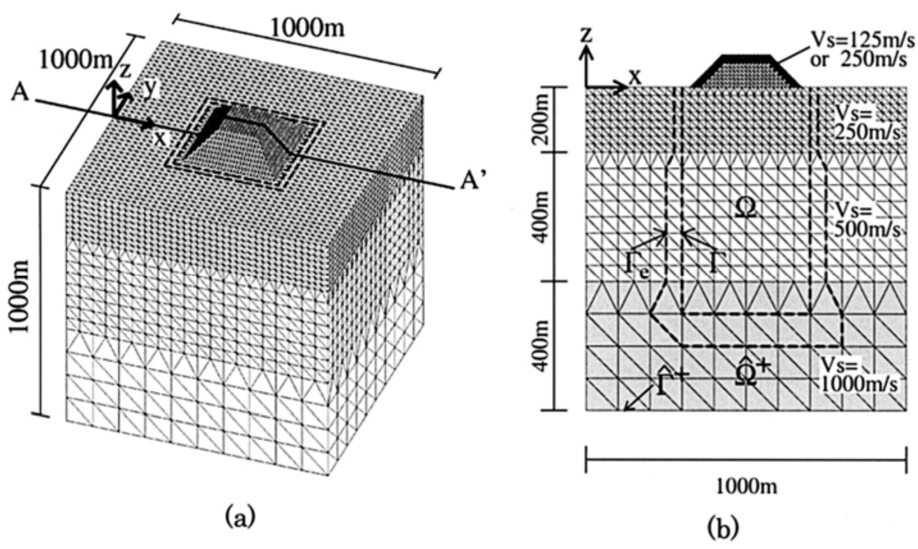

Figure 2.16 Hill on flat-layered system. (a) Finite element mesh; (b) cross section through line AA', which traverses the free surface of the flat-layered system and that of the hill. Two cases of hill are considered in the simulations: one for a homogeneous hill, in which its properties are the same as those of the top surficial layer, and the second in which the hill has a weathered layer with the same properties as those of the basin in Figure 2.14 (Yoshimura et al, 2003).

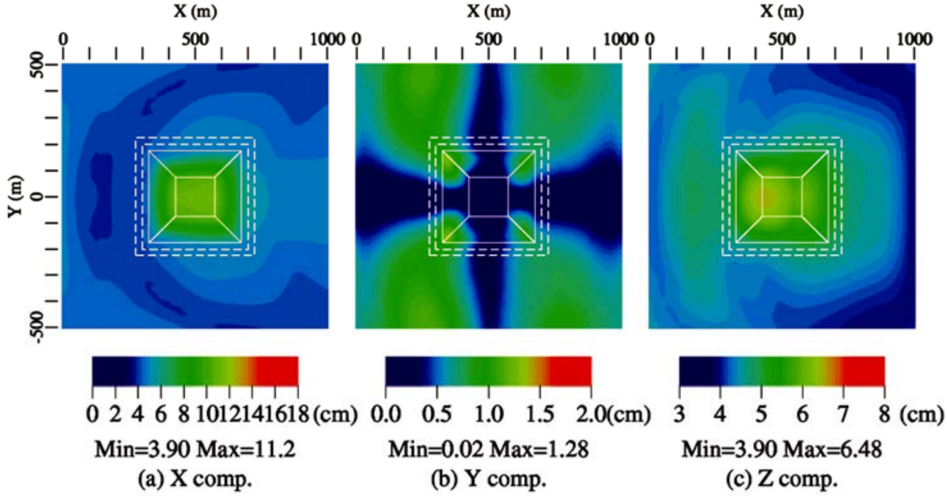

Figure 2.17 Spatial distribution of maximum value of displacement components of ground motion on free surface of uniform with V_s=125 m/s. (a) *X*-component; (b) *Y*-component; (c) *Z*-component (Yoshimura et al, 2003).

2.4.1. Underground structures vulnerability (Scandella, 2007)

A complete analysis of the seismic problem has been performed, which involves the simultaneous effects of the seismic source, the propagation path, the geological site conditions, and the soil-structure interaction. The auxiliary problem (Figure 2.18a) simulates the earthquake source and propagation path effects with a model that includes both the source and a background structure (external domain) from which the structure has been removed and replaced by the same material as the surrounding soil. The reduced problem (Figure 2.18b) models with high accuracy only the tunnel and a reduced portion of the surrounding soil (internal domain). Its input is a set of effective nodal forces evaluated on the basis of the ground displacement from the first step and applied in a strip of elements (dark boundary fill in Figure 2.18).

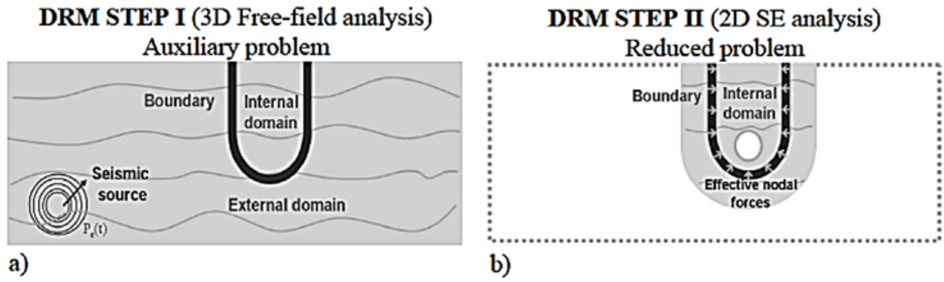

Figure 2.18 Scheme of the DRM procedure applied to the "Serro Montefalco" tunnel case: a) analysis of the source and the wave propagation in the half-space; b) wave propagation in the reduced domain including soil-structure interaction. The dark line denotes the effective boundary (Scandella, 2007).

The Ariano Irpino fault (ITGG092) has been selected as the scenario seismic source, because it is the closest one to the tunnel and it is characterized by an expected maximum magnitude Mw 6.9. It was the source of the December 5, 1456 earthquake, one of the most important natural events of the Italian seismic history, and it would represent a potential event with a minimum return period of 2000 years (DISS, 2006).

In agreement with Improta et al. (2004), the rock profile (figure 3.13) has been adopted as a generalized model for the Irpinia-Lucania Apennines.

The dynamic analysis has been performed considering a simplified circular tunnel characterized by an equivalent external radius of 5.85 m and a concrete lining thickness of 0.80 m. The mesh of the reduced problem, shown in Figure 2.19a, is characterized by the dynamic properties listed in in Figure 2.19b. A no slip condition at the interface between the soil and the lining has been considered.

Scadella (2007) performed also a simplified analysis of the transversal cross-section applying the closed form solution developed by Corigliano et al. (2006).

For the results, reference could be made to Scandella thesis (2007) available online.

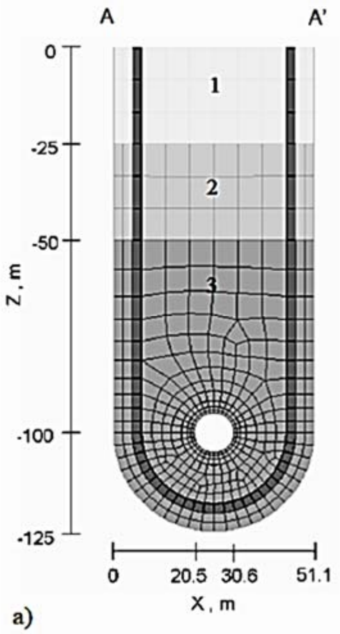

Layer	V_P (m/s)	V_S (m/s)	ρ (t/m^3)	Q_S
1	1039	600	1.80	30
2	1386	800	1.90	50
3	2252	1300	2.10	75
tunnel	3651	2236	2.50	80

b)

Figure 2.19 Step II of DRM: (a) model of the reduced problem including the transversal A-A' cross-section of the tunnel and (b) dynamic adopted properties (Scandella, 2007).

2.4.1. Christchurch city vulnerability (Guidotti, 2012)

To evaluate city vulnerability an estimation of the ground motion is required. If the site is in near source condition, we cannot ignore source effects (see chapter 1). The three-dimensional numerical simulation was realized, inclusive the following features: (i) kinematic description of the seismic source, (ii) horizontally layered deep geological model, (iii) a simplified but realistic description for the Cretaceous-Cenozoic alluvial Canterbury Plains, and (iv) a linear visco-elastic soil behaviour. Note that in these preliminary analyses the authors has considered a relatively rough model for the soil behaviour, by assuming a linear-visco elastic constitutive law, with a quality factor Q proportional to frequency (further details about the implementation of the viscoelastic soil behaviour can be found in Stupazzini et al., 2009).

Different three-dimensional numerical models were built for the Christchurch earthquake, in order to achieve the best fit with the ground motion observations, combining: (i) two different kinematic seismic fault solutions, based on recent seismic source inversion studies, and (ii) two simplified models for the shape of the interface between the alluvial soft soil sediments and the rigid volcanic materials (Figure 2.20 b and c).

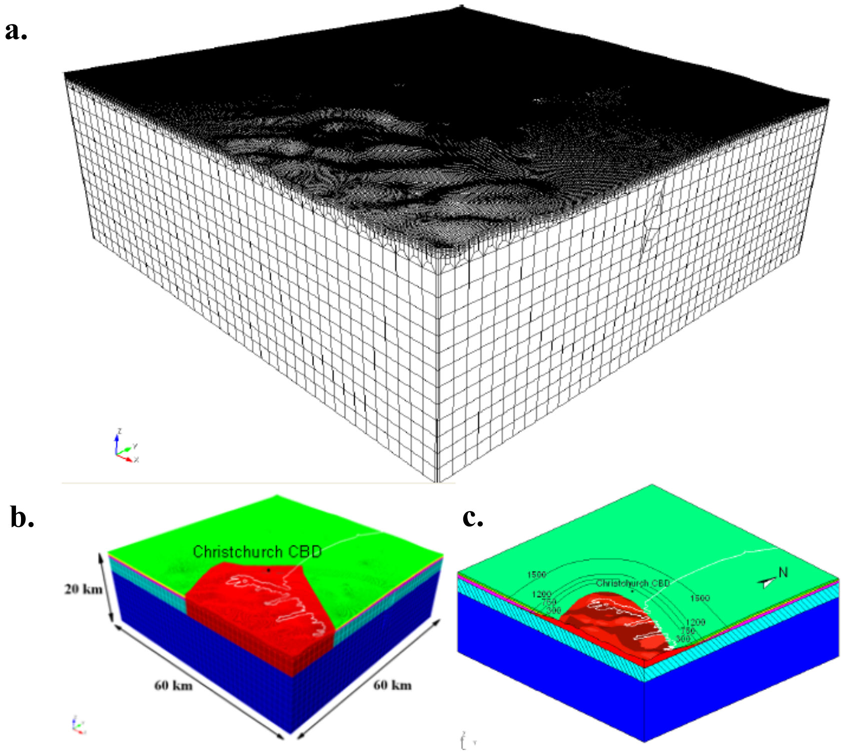

Figure 2.20 (a) 3D mesh of the Canterbury Plains relying on the kinematic seismic source inversion. (b) Corresponding "Step-like" model and (c) "Smooth" model, with depth contours of the contact between the alluvial soft sediments and the rigid volcanic materials (depth in meters). Position of the Canterbury Business District (CBD) is also shown (Guidotti, 2012).

The 3D model of the region of the South Island of New Zealand covers an area of approximately 60x60x20 km around the city of Christchurch, including the information available in the geological map Figure 2.20. The site is shown in Figure 2.21, where also the meshing process is illustrated.

As a starting point, the real configuration of the CBD has been considered, taking information on height and floor plan dimensions of the cluster of around 150 buildings, in an area having a dimension of about 1 km x 1 km.

For the results, reference could be made to Guidotti thesis (2007) available online.

a.

b.

c.

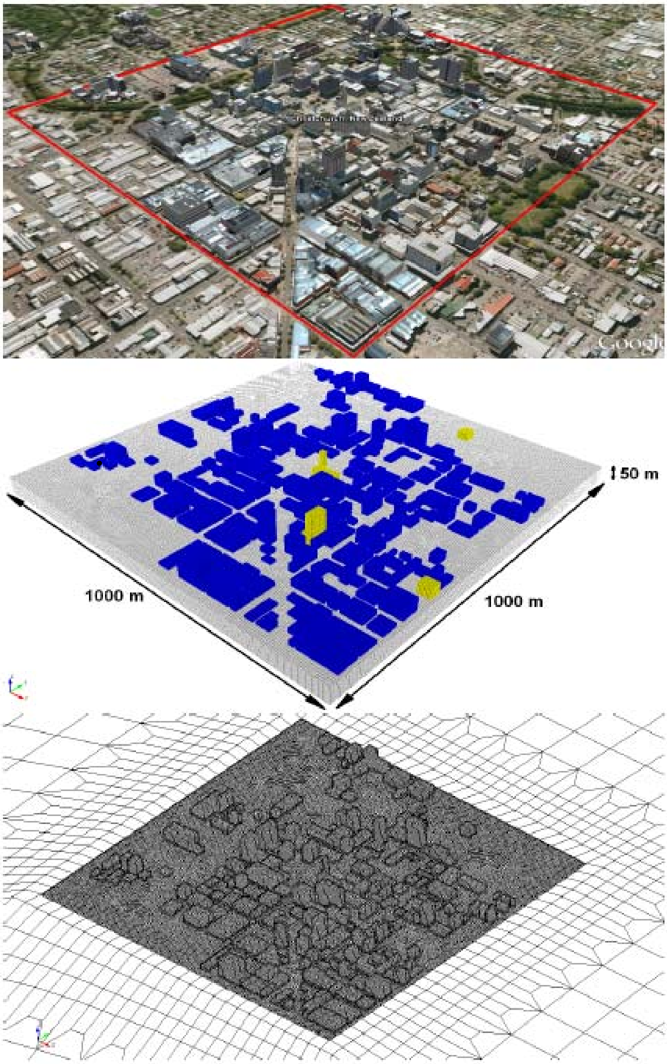

Figure 2.21 (a) Aerial view of the CBD area. The red contour defines the modelled area. (b) Corresponding three-dimensional model, independently meshed with element size around 5 m. Also foundations and soil around foundations are meshed. In yellow important buildings are highlighted. (c) Model of the CBD set into the model of the Canterbury Plains (Guidotti, 2012).

3. Model on a Regional Scale

3.1. Geological framework of Campano-Lucana platform

Since the selected case-history (Conza dam) belongs to the Campano-Lucana region, in this chapter details will be provided on the geological and seismological features of this region.

The Apennine mountain chain arose from the convergence between the African and Eurasian plates during the Cenozoic age. It belongs to the mountainous system of Africa that characterizes the Mediterranean area. The Apennine mountains are characterised by thrusts, verging towards the Adriatic foreland, which have involved crustal material.

In the Southern Apennines, from west to east the main paleogeographic zones are the Campano-Lucana platform, the Lagonegro-Molise basins (Ionian oceanic basin) and the Apulian platform (Figure 3.1). To the east of the Apulian platform another basin developed during the Mesozoic (e.g. the East Gargano basinal sediments), and this was coeval to the opening of the southern Adriatic basin. The forward propagation of thrusts piled up the paleogeographic domains, having in the hanging-wall of the thrusts units originally located westward relative to the footwall, e.g. the Liguride units thrusting the Tuscan nappe, which in tum was thrust onto the Cervarola unit, mainly composed of foredeep sediments, which has in the following footwall the Umbro-Marchigiano basin. To the south, the Campano-Lucana platform was thrust onto the Lagonegrese pelagic units, which in turn was thrust onto the Apulian platform. This occurred because thrust planes were running in some cases parallel to the pre-existing paleogeographic zones. Compressional tectonics began in the middle Cretaceous period, continuing to the Oligocene with continental collision. In the Tortonian age, the rift process started, which caused the opening of the Tyrrhenian Basin. The volcanic activity along the Tyrrhenian sea from Tuscany to Campania is linked to the extensional tectonics that stretched the lithosphere and thinned the crust.

The main process that determined the building of the accretionary wedge was the subduction of the Adriatic plate under the Apenninic chain. In the early phase, this subduction involved the oceanic lithosphere, and afterwards, the continental one. Casero et al. (1988) consider the remarkable Apennines uplift that happened during the Quaternary subduction of the lighter continental crust.

Between the late Tortonian and the lower-middle Pleistocene, the Tyrrhenian back-arc basin, the Apenninic chain and the foredeep migrated towards the East, following the hinge roll-back of the subducting Adriatic plate.

According to Patacca and Scandone (1989 and 2007), the southern Apennines are an Adriatic-verging fold and thrust belt, built on the SW border of the continental Apulian lithosphere, in subduction towards the SW, and they developed from the late Cretaceous until the Quaternary. The belt is associated with the Tyrrhenian back-arc basin to the West and with the Bradano foredeep to the East (Figure 3.1). The basin-thrust-belt-foredeep system migrated eastwards, overlying the Apulia Carbonate Platform (ACP) and progressively involved both the basin and carbonate platform paleogeografic domains. From West to East, the main paleogeografic domains that characterize the southern Apennines are the western carbonatic platform, the Lagonegro basin successions and the Apulia Basin.

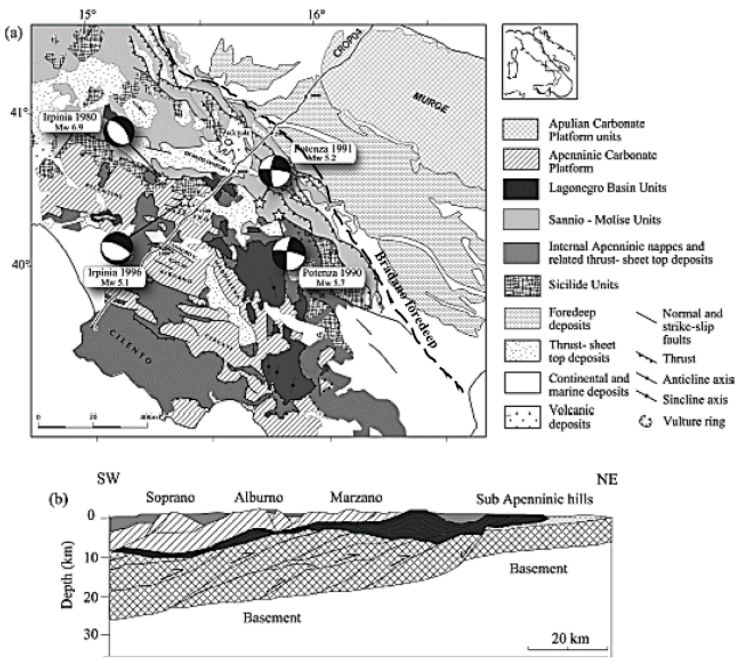

Figure 3.1 (a) Geological map of the Campania–Lucania region (proposed by Patacca & Scandone 2007) and focal mechanisms of main large recent earthquakes. (b) Schematic cross-section passing through the CROP04 seismic line (proposed by Scrocca et al. 2005). Figure from Matrullo et al. 2013.

During the Middle Pleistocene the Southern Apennine wedge was uplifted and involved by an extensional tectonic with a NE-SW direction responsible for the historical and present day seismic activity (Anderson and Jackson, 1987) and caused the extensive volcanism on the Tyrrhenian margin of the chain. The tectonic style of the chain is strongly variable because the carbonate platforms underwent brittle deformation, with the onset of higher magnitude. The basin terrains, instead, underwent a ductile deformation (Menardi and Rea, 2000).

The present structural complexity of the chain is due precisely to all these different palaeogeographic domains involved in the Southern Appenine thrust belt building (the carbonate platforms underwent brittle deformation whereas the basin domains underwent a ductile deformation) so as also to several deformational episodes that led to the formation of the chain. Since the lower-middle Pleistocene, the axial zone of the chain is in an extensional NE–SW regime. This regime is still active, as shown by the analysis of surface geological indicators, breakout and seismic data (Pantosti & Valensise, 1990; Frepoli & Amato, 2000; Montone et al., 2004; Pasquale et al., 2009; DISS Working Group, 2010; De Matteis et al., 2012), and it is responsible for the present seismicity in Southern Apennines.

3.2. Seismological framework of Campano-Lucana platform

The Campania-Lucania Region in the southern Apennines is one of the highest seismic hazard areas in Italy (Cinti et al., 2004). It has experienced numerous disastrous seismic events, among which there were those of 1694, 1851, 1857 and 1930. The most recent significant event (surface-wave magnitude of 6.9) was the complex normal-faulting 23 November 1980 Irpinia earthquake (Westaway and Jackson, 1984; Bernard and Zollo, 1989), which resulted in about 3,000 victims and huge damage to the historical and civil heritage. In this area the present-day seismicity is characterized by low-to-moderate magnitude events that are mainly concentrated along the seismogenic structures on which the 1980 Irpinia earthquake originated (Stabile et al., 2012).

The Figure 3.2 shows the available observations on the seismic history of Conza della Campania and the directions of the major seismic genetic faults identified based on earthquakes since the fifteenth century. The seismic activity more recently, according to studies performed by Ascone et al. (executed on earthquakes from 1981 to 2005 on the Southern Apennines), is mainly concentrated in three areas: (i) the area of the high Irpinia; (ii) Potentino area; (iii)

Castelluccio area at north of Pollino. A significant seismicity also is found in the 90s between San Giorgio La Molara, Benevento and Apice (Ascione et al., 2013).

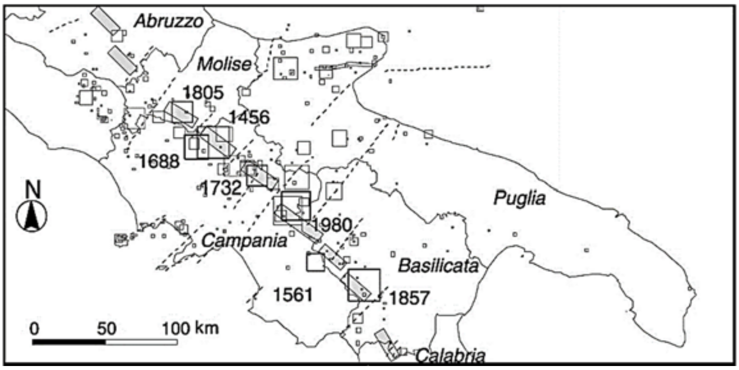

Figure 3.2 Seismotectonic scheme of the Southern Apennines. Squares are the historical earthquakes from CPTI 1999 catalog, thickest squares represent the larger earthquakes (M_{min} = 5.5). The gray rectangular boxes represent projections on the surface of the seismogenetic faults, dashed lines represent the transverse tectonic lineaments reported in the Database of Potential Source (Valensise and Pantosti, 2001). Figure from Vilardo et al., 2003.

The regional gravity and magnetic fields in Central and Southern ltaly were used to reconstruct the crustal structure and the top of the carbonatic sedimentary rocks (Corrado and Rapolla, 1981; Fedi and Rapolla, 1990). The only seismic data available in this area are some refraction and wide angle reflection profiles recorded in the 1970s (Italian Explosion Seismology Group, 1982). These data provide some indications about the depth of the Moho boundary in the transitional area between the Southern and Central Apennines but do not allow to define a detailed velocity model of the upper crust. Regional synthesis of the upper crustal structure of a large portion of Southern ltaly was realized by jointly interpreting geological studies and well and oil exploration seismic reflection data (Mostardini and Merlini, 1986; Casera et al., 1988; Roure et al., 1991). More detailed studies have been conducted in the studies carried out by Zollo et al. (2002) on active seismic tomography experiments in the Vesuvius area.

The analysis of regional seismicity to identify and geometrically characterize active fault structures and estimate the present tectonic regime requires an accurate determination of the spatial distribution of the earthquakes.

The knowledge of a realistic velocity structure is necessary to prevent artefacts in the location of hypocentres: inappropriate choice of the velocity model can lead to significant distortions and bias in the hypocentre positions.

In the thesis work, for the simulation of ground motion near the site of interest (Conza della Campania - AV), a summary of the most important geological and seismological studies has been performed referring to the main and most detailed publications available (Iannaccone et al., 1998; Improta et al., 2000; Improta et al., 2002; Improta et al., 2003; Corciulo et al., 2007; Convertito et al., 2009; Cantore et al., 2010; De Matteis et al., 2010; Amoruso et al., 2011; Amoroso et al., 2012; Matrullo et al., 2013).

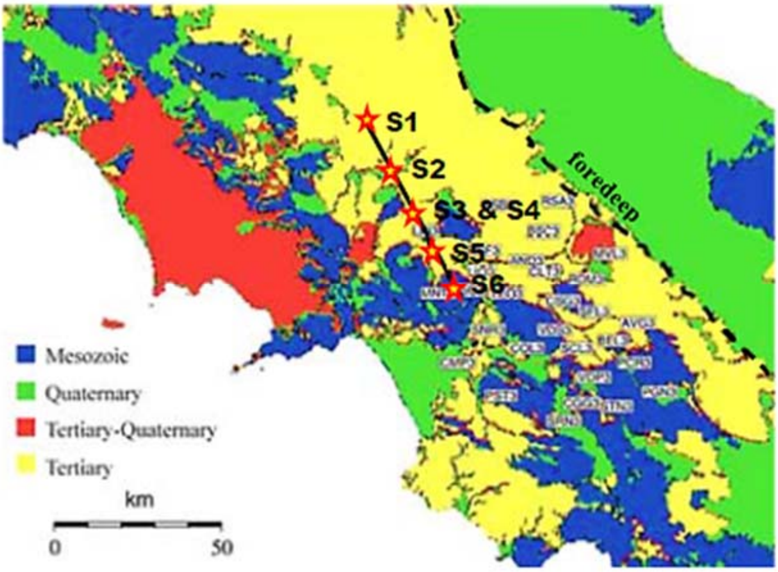

Figure 3.3 The Quaternary-Volcanic–Tertiary-Mesozoic (QVTM) site geological classification map. The labels indicate the locations of the ISNet seismic stations used for stratigraphic interpretation (from Convertito, 2009). The figure also shows the main seismic refraction profile and shot point, according to the experimental campaign carried out by Iannaccone et al. (1998).

3.3. Modelling: 3D approach

The structural setting of the Campania-Lucania region has been defined by several geological and geophysical studies, including: tomographic images (Amato & Selvaggi, 1993; Chiarabba & Amato, 1994; De Matteis et al., 2010), analysis and joint interpretation of gravity data, seismic reflection lines and subsurface information from many deep wells (Improta et al., 2003), seismic reflection analysis and investigations for hydrocarbon exploration (Mostardini & Merlini 1986; Patacca & Scandone 1989, 2001; Casero et al. 1991; Roure et al. 1991; Menardi&Rea 2000; Scrocca et al. 2005).

To define the 3-D model reference was made to the seismological models proposed by Iannaccone et al. (1998) and Improta et al. (2000, 2003).

3.3.1. Velocity structure

The modelling of seismic refraction data and the interpretation of the shallow crustal structure, up to a depth of 3÷4.5 km, derive from the study of stratigraphic, sonic velocity logs from oil exploration wells (Figure 3.4) and of three seismic profiles that cross the seismic refraction profile (Iannaccone et al., 1998; Improta et al., 2000). The seismic profile is 75 km long and oriented 150°N. Along this direction the geological structures are almost plane parallel allowing a more constrained interpretation of the seismic data. Six shots were fired (from S1 to S6 of Figure 3.3) at five sites with about 15 km spacing along the Line. Each shot consisted of 4-7 holes drilled to a maximum depth of 45 m and loaded with a explosive charges. A total of 81 portable seismic stations have been used. The seismic stations were deployed in a variable configuration according to the two objectives of the experiment.

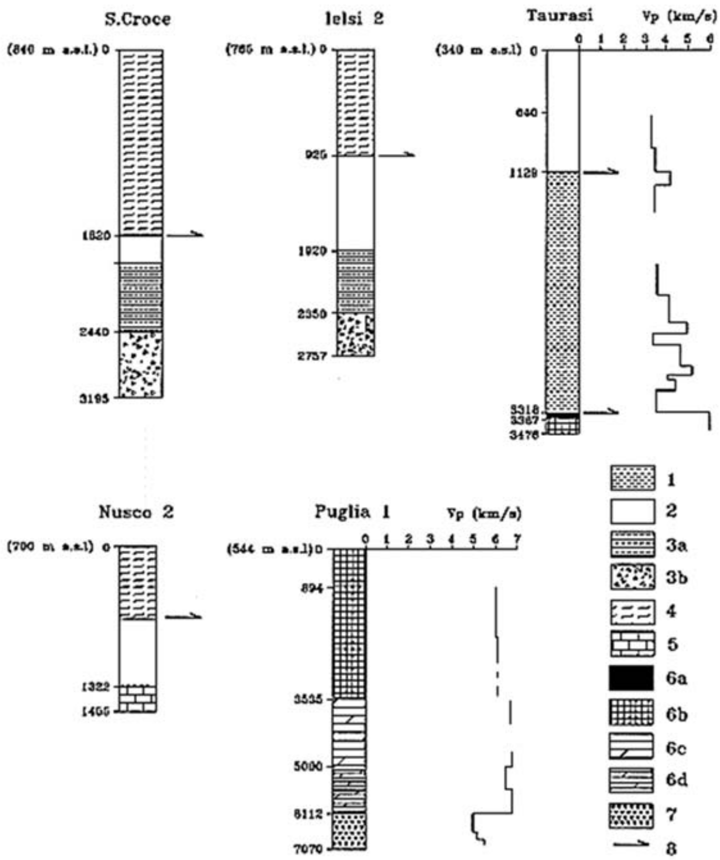

Figure 3.4 Stratigraphic and sonic velocity logs from wells located in the Sannio region and in the Apulia foreland. 1 — Late Tortonian–Upper Messinian thrust-sheets-top deposits; 2 — Upper Miocene siliciclastic flysch deposits of the Molise Basin (S. Croce and Ielsi 2 wells) or unconformably overlying the Western Carbonate Platform (Taurasi and Nusco 2 wells); 3 — Molise nappe: (a) clays, marls and marly limestones (Cenozoic upper sequence), (b) dolomitized breccias and calciturbidites (Mesozoic lower sequence); 4 —Paleogene-Lower Miocene varicoloured clays and basinal coarse-clastic lime resediments of the Sannio nappe; 5 — Mesozoic lime-stones of the Western Carbonate Platform; 6 — Apulia Carbonate Platform: (a) Messinian anhydrites, (b) Cretaceous-Lower Jurassic limestones and dolomit limestones, (c) dolomites of uncertain age, (d) Triassic dolomites and anhydrites of the Burano formation; 7 — Lower Triassic–Permian clastic deposits of the Verrucano formation; 8 — main thrust plane (Improta et al., 2000).

The main aspects of the velocity model proposed by Iannaccone et al. (1998) and Improta et al. (2000, 2003) are here summarized:

a) sedimentary rocks of basin and foredeep domains provide P-wave propagation velocities in the 3.0÷4.1 km/s range for the Tertiary deposits and 4.8 km/s for the Mesozoic successions;
b) in the North-Western segment (Benevento basin, shots S1 ÷ S5, Figure 3.5b-c-d) the surficial layer with a P-wave velocity of 3.3 km/s, corresponding to Tertiary portion of the Molise nappe, reaches its maximum thickness of about 2.5 km. Through 2-D simulation with elastic finite difference method (Graves,1996) it was deduced that within the first 5 km north of shot point S3, the presence of a thin shallow layer with a thickness of 0.35 km and a P-wave velocity of 2.0 km/s (first arrival time delays, Figure 3.5c) was detected. At depth of 1.5 km (gently deepens to 2.1 km of depth below shot S3) at the northern border a second layer has a velocity of 4.8 km/s;
c) in the South-Eastern segment (between shots S4 and S5, Figure 3.5c-d) the velocity from the value of 2.8 km/s, observed at the surface, increases with a gradient of 0.6 s-1, reaching a value of about 3.5 km/s at the bottom of the layer located at a depth of 0.8 km. South of shot S4, the velocity model is constrained by the seismic sonic log of the Taurasi 1 (Figure 3.4) well that provides a higher velocity of 3.3÷3.5 km/s at a depth of 0.3÷0.8 km, due to the propagation in the superficial sediments characterized by lower velocities;
d) according to Mostardini and Merlini (1986), a first seismic discontinuity with a velocity of 6.0 km/s observed at a depth ranging from 3.0 km to 4.8 km along the whole profile corresponds to the top of the Meso-Cenozoic limestones (Apulia Carbonate Platform), as inferred from well data;
e) higher velocities, up to 6.7 km/s, characterize the lower part of the Apulia Platform formed by Upper Triassic dolomites and evaporites of the Burano formation;
f) a deeper interface (6 to 8 km deep, Figure 3.5a) marked by a velocity of 6.7 km/s has been interpreted as a second-order discontinuity within the Apulia Carbonate Multilayer produced by a lithological transition between the Jurassic-Cretaceous carbonates and the Upper Triassic dolomites and evaporites of the Burano formation;
g) the deepest discontinuity, located at a depth of 9÷11 km, has been detected by intermediate-wide-angle reflected arrivals. Finite difference simulations, performed to model the observed amplitudes, suggest the existence of a strong velocity inversion at the reflecting boundary.

The latter hypothesis is mainly supported by:

(1) the sonic logs in Puglia area;

(2) the seismic reflection profiles for oil exploration recorded in the Apulia foreland and Bradano foredeep.

These considerations agree with the structural model of the Southern Apennines proposed by Mostardini and Merlini (1986), which is documented by 4 geological sections crossing the area of interest in NE-SW direction (from the Tyrrhenian to the Adriatic Sea, Figure 3.6).

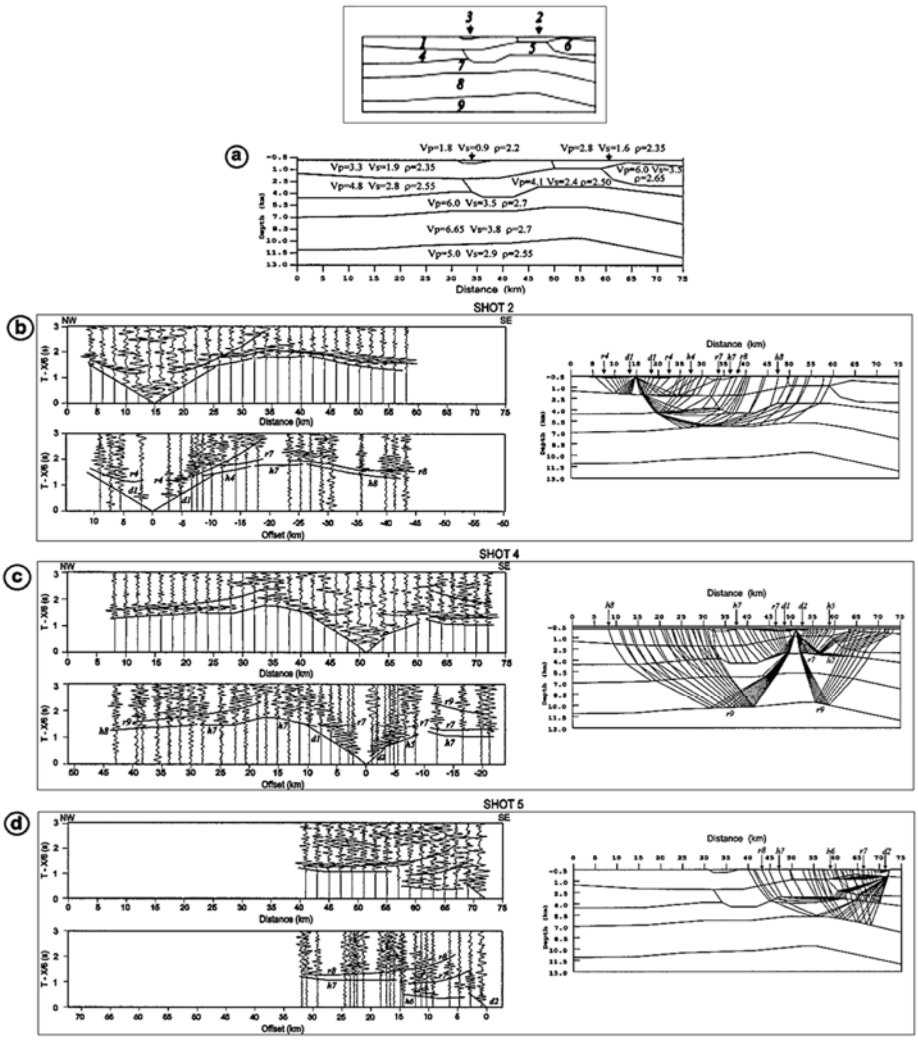

Figure 3.5 (a)-(d) Record section for shot point 2, 4 and 5. The data are plotted with normalized amplitude and reduced time scale, with a velocity reduction

of 6 km/s. The small letters and numbers represent, respectively, the type of analysed phase (d=direct, h=head waves, r=reflected) and the layer where the direct phase propagates or the refracted/reflected phase has been generated, see the numbered model in the upper figure (a). A seismic model, with the indication of ray path, for single shot point, are shown. Figure extract from Improta et al. (2000).

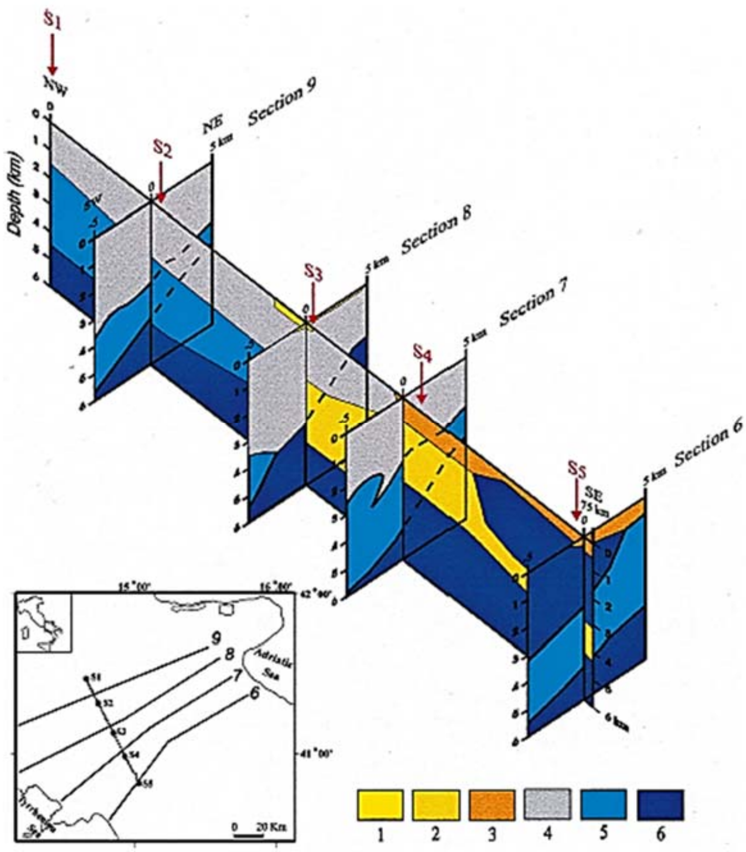

Figure 3.6 Comparison between the model carried out by seismic refraction data (Iannaccone et al., 1998 and subsequent) and the four geological sections proposed by Mostardini and Merlini (1986). The location of the four cross-sections is shown on the map at the bottom left. In figure, the colors indicate the classification of geological layers: 1 - Middle Pliocene deposits; 2 - Late Tortonian-Upper Messinian thrusts-sheets-top deposits; 3 - Upper Miocene flysch deposits unconformably overlying the Western Platform carbonates; 4 - Sannio and Molise nappes (Cenozoic upper sequence); 5 - Molise nappe (Mesozoic lower sequence); 6 -Western and Apulia Carbonate Platforms. Figure from Improta et al. (2000).

3.3.2. Final geological and geophysical consideration

As already known from long historical seismicity records elsewhere, long-lasting quiescence might alternate with clusters of closely spaced strong earthquakes. The long-term record confirms that long-lasting quiescence may punctuate fault activity, with major implications for seismic hazard assessment.

The combination of information on fault evidences at the surface and the hypocentre locations, estimated by using weak motion events, suggests that it is possible a decoupling between surface and deep fault zones and that outcropping fault planes cannot always be straightforwardly traced down to the hypocentral depths of weak motions.

3.3.3. 3D Model

Through the DRM approach (see chapter 2) the problem was solved into two successive steps: an external domain with regional extension containing the seismic source, and an internal detailed domain with a territorial spatial dimensions greatly reduced and containing the site of interest.

By implementing the main aspects of the velocity model developed by Iannaccone et al. (1998) and later by Improta et al (2000) and considering the four geological sections suggested by Mostardini & Merlini (1986), a 3D model of the Campania-Lucania region was developed (Figure 3.6) for the simulation of focal mechanism and propagation of elastic waves by the DRM. In the vertical direction the various lithotypes of the 3D model (Figure 3.7) was obtained by a suitable interpolation of stratigraphic information from the geological sections (see previous paragraph 3.1), on the surface the model has been connected with the simplified QVTM geological map of (Figure 3.3).

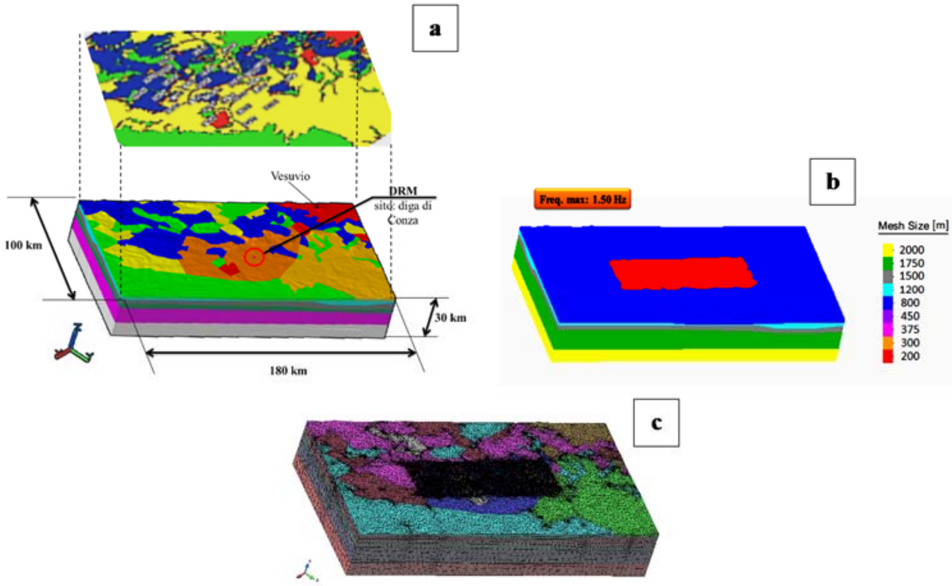

Figure 3.7 3D model of the external domain realized to study the input motion at the Conza site. (a) Comparison between QVTM map and the geological formations in the 3D model. (b) Contour of mesh size used in the mesh generation (maximum frequency around to 1.5 Hz). (c) Mesh of the model.

For the simulation of the focal mechanism, it was considered appropriate to refer to the fault system that generated the Irpinia 1980 earthquake. In particular, among several versions existing in literature, reference was made to that proposed by Westaway & Jackson, (1987) and Bernard & Zollo (1989).

Compared to a one-dimensional propagation medium, the main advantage of using a three-dimensional geometric model is the possibility of accounting for soil lateral stiffness variability, different arrival times of the various phases at different surface points.

The large distance between the various layer, although reproduce the arrival times and the maximum acceleration at various stations, do not allow to obtain a diffuse distribution of energy for the signals at the surface, but most of the energy is concentrated at the arrival of the various phases (Figure 3.8). Consequently, the signals at different observation points have a limited duration and an impulsive waveform at each arrival of any single phase. The model is not able to reproduce the superficial reverberations, due to local heterogeneity of a propagation medium, which, however, would lead to a reduction of the energy concentrated (pulse-like waveform), distributing such energy over time. Not even the introduction of material stiffness variation (around the average value) as a function of depth (to simulate a non-homogeneity inside the single layer) is sufficient to overcome the problem, because this variability is a continuous function in the spatial domain and then unable to generate new interfaces.

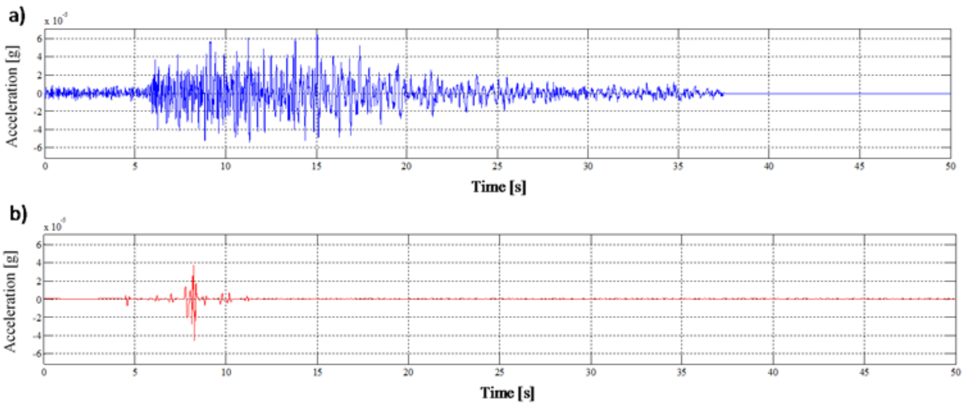

Figure 3.8 Comparison between the seismic motion (east-west component) recorded at the Avigliano station (a) for a weak-motion and the simulation (b) carried out with the stratigraphy proposed by Chiarabba et al., 2005 (see Figure 3.12).

For the superficial lithotypes a random stiffness variation in the simple elements of the mesh can be performed. As shown in Figure 3.9, there are no significant differences between the two signals obtained in the case of layers with constant or random varying stiffness. This is explained by the small size of the elements (10 times less than the smallest wavelength propagated). As a matter of fact, for the wave front the propagation medium is essentially homogeneous with stiffness close to the average value (Rotili, 2012; Chiaradonna et al., 2012; Landolfi, 2013; Sica et al., 2014). No further improvement can be obtained by inserting a horizontal layer with a random variability in stiffness, generating interfaces able to influence the propagation of the wave front (Figure 3.9).

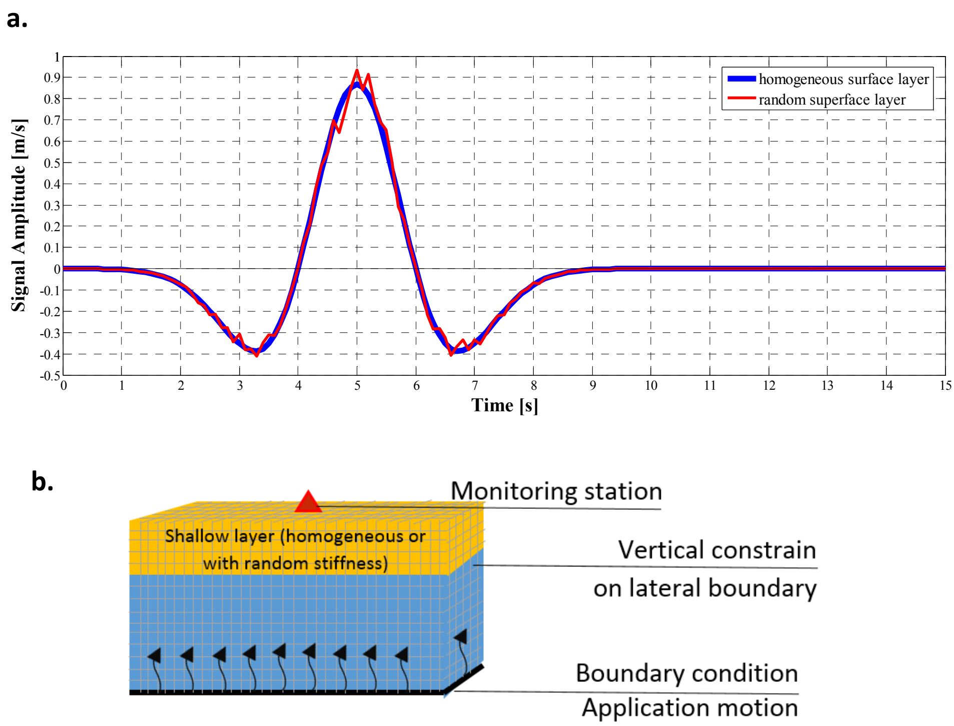

Figure 3.9 Comparison of the response on ground level of the 3D model (b) between a homogeneous surface layer and a spatial random varying stiffness in the same layer (a). The input is a wavelet with fundamental period of 4.5 s.

Accordingly, the 3-D modelling may be inappropriate for earthquake site response analyses, where other factors characterizing a signal are meaningful such as:

(i) duration;
(ii) waveforms;
(iii) frequency content (Fourier transform or elastic response spectrum);
(iv) synthetic parameters (i.e. PGA, PDV, PGD, period average and dominant period, Arias Intensity, Root Mean Square, etc.);
(v) number of cycles;
(vi) time distribution of the energy content (i.e. a spectrogram or more simply a cumulative-energy plot, etc.).

Duration, number of cycles, energy flux function and RMS of a signal are important in a problem of geotechnical engineering, because representative of signal energy distribution with the time. In fact, two signals with the same energy content, one of pulse-like type with a higher PGA value and one with higher number of cycles, have totally different effects in terms of plastic strain accumulation in soils. In particular, the pulse signal causes less deformation for the limited time-span in which such deformations are accumulated (Newmark 1965).

No less important is the frequency content of the signal, which regulates the dynamic response of the system. In particular, due to the amount of RAM and time computing required, it impossible to use a mesh able to propagate frequencies above 1.5 Hz. The mesh size is determined by considering the relation $k * V_S / f_{max}$, with k recommended less than 0.125. Such low frequencies are however not very significant in seismic response analysis, especially in near-source conditions where higher frequencies are significant in terms of energy content. These higher frequencies are essential for studying the asynchronism induced by a near-source seismic motion.

The above shortcomings make the 3D model unsuitable to solve the first stage (step 1) of the DRM (§2.2) for the scope in this research. Consequently, a 1-D (flat and parallel layers) stratigraphic model of the Irpinia-Lucania area was adopted.

3.4. Modelling: 1D approach

1-D velocity models are routinely adopted in seismological studies to estimate seismic source parameters as focal mechanisms and earthquake location.

3-D tomographic models are often obtained as perturbations of a 1-D reference model. The tomographic model are obtained by iterative methods and for this the results and the resolution estimates strongly depend on the choice of the initial model. 1-D layered velocity models are also required by several methods for the calculation of synthetic Green's function, such as the widely used discrete wavenumber approach (Bouchon, 2003). The 1-D approach has been used in the present work and for this reason more details will be provided.

In regions with strong lateral variations and irregular topographic surface, significant errors can be introduced by using simplified 1-D velocity models. In these cases, the complexity of geological structures can be represented only by 3-D velocity models. In other cases, however, one can partially account for velocity lateral variations by including station and/or source terms in the location procedure (Douglas, 1967; Pujol, 1988; Shearer, 1997) or path-dependent calibrations (Zhan et al., 2011). Geophysical and geological interpretations have shown (Cocco & Pacor, 1983; Westaway & Jackson, 1987; De Natale et al., 1987; Bernard & Zollo, 1989; Pantosti & Valensise, 1990; Pastosi et al. 1993; Iannaccone et al., 1998; Improta et al., 2000; Improta et al., 2002; Improta et al., 2003; Panza et al., 2003; Corciulo et al., 2007; Convertito et al., 2009; Lancieri & Zollo, 2009; Cantore et al., 2010; De Matteis et al., 2010; Amoruso et al., 2011; Amoroso et al., 2012; Matrullo et al., 2013) that there are important lateral variations of the properties of the medium mainly along the direction perpendicular to the Apenninic belt in the upper crust. This is consistent with the presence of a Platform domain in the SW direction and with the basin deposits in the NE direction. In addition, important lithological variations may be found along the chain, the most relevant being an abrupt deepening of the Apulian Carbonate Platform in the southeastern part of the investigated region (Improta et al., 2003).

At present the Irpinia area is characterized by several seismic swarms and low-magnitude background seismicity (M_L < 3.5) that delineates both NW–SE striking structures along the Apenninic chain (Irpinia fault system) and a nearby approximately E-W oriented transversely cutting the chain (De Matteis et al., 2012).

Many 1D velocity models have been developed for the Irpinia region at different spatial scales: for the analysis of the 1997–2002 Italian Seismic Catalogue (Chiarabba et al., 2005); for the study of the recent seismicity of the Lucania Apennines and Bradano foredeep (Maggi et al., 2009); for the characterization of the aftershocks of the 1980 Irpinia earthquake (Bernard & Zollo, 1989; Amato & Selvaggi, 1993; De Matteis et al., 2010). These velocity models have differences in *P*-wave velocity values and in number and depth of interfaces (Figure 3.12a and Figure 3.13). This is due to the different tools and data used by the authors in each study, as well as to the actual complexity of the propagation medium.

For the model at regional scale, several simulations were performed starting from the stratigraphic data available in literature (Figure 3.12). The calibration of the stratigraphy at regional scale was performed with reference to seismic events of low magnitude, to avoid that events of medium-high intensity (magnitude greater than 4) could affect the estimation of rock/soil stiffness. Conversely, medium-high seismic events may be adopted for identifying other parameters, such as magnitude and hypocentre of an earthquake.

Finally, the use of seismic events of greater intensity is to be avoided since if we consider recordings at short distances from the source it is no possible to model the fault as a point source.

We should considere an extended source and account for further uncertainties about: (i) fault geometry (strike & dip direction and their respective size);

(ii) distribution of the slip on the rupture surface; (iii) average direction of the slip; (iv) duration of the rise-time; (v) location hypocenter; (vi) distribution of isochrones on the fault surface.

Errors due to nonlinearity of soils and factors as source-site distance, source size and wavelengths, could be removed (Fraunhofer approximation) by using stations placed at greater distances from the source. This is straightforward if the rigid substrate is really flat with parallel layers (i.e. one-dimensional propagation in a medium with low lateral inhomogeneity). This condition is generally not realistic, especially in Central Southern Apennines (Figure 3.3). The use of distant stations would lead to wavefront paths and stratigraphy not consistent with those of the real propagation medium between the focal mechanisms of Irpinia 1980 event and the reference site (Conza).

Six earthquakes of magnitude between 1.5 and 2.5 with hypocenter within 5km from the event 1 (ID event 16076r of the 2013-08-16, time 03:56 UTC, M_L 2.6), were considered. The epicenters of these earthquakes are located in the Vietri Di Potenza municipality, distant no more than 20 km from the site considered.

The selected stations belong to the ISNet network (Copyright RISSC-Lab, Department of Physics of Federico II University and AMRA) and are distributed (average distance of less than 10 km) on the Campano-Lucano Apennine, in the south area of the first fault segment mobilized during the seismic event of 1980, more precisely between the towns of Lione and Sala Consilina. The epicentres are close to the geometric center of the ISNet monitoring zones (Figure 3.10).

As anticipated, the back-analysis was conducted with reference to the different stratigraphies, published in literature and reported in Figure 3.12a and Figure 3.13.

Figure 3.10 Location of the station of Irpinia Seismic Network (ISNet) and the epicenters of considered events.

3.4.1. Reference stratigraphy

A brief summary of the original model as proposed by Matrullo et al. (2013) will be reported.

The 1-D velocity model was obtained by calculating a *P*-wave 'Minimum 1-D model' (VELEST code, Kissling et al., 1995) through joint inversion of layered velocity models, station corrections and hypocentre locations, acting on a data set of over 1000 events occurred between 2005 and 2011, recorded at 42 seismic stations. Starting from the 1-D model (Figure 3.12a), a preliminary 3-D crustal velocity model was computed, to study the relation between station corrections and lateral velocity variations. Finally, refined 1-D station corrections are calculated by fixing the location of well-constrained events (Figure 3.12b). Moreover, by an evaluation of picking consistency on the arrival times by the "*modified Wadati diagram*" (Chatelain 1978), an average V_P/V_S ratio of 1.885 is estimated (Figure 3.11).

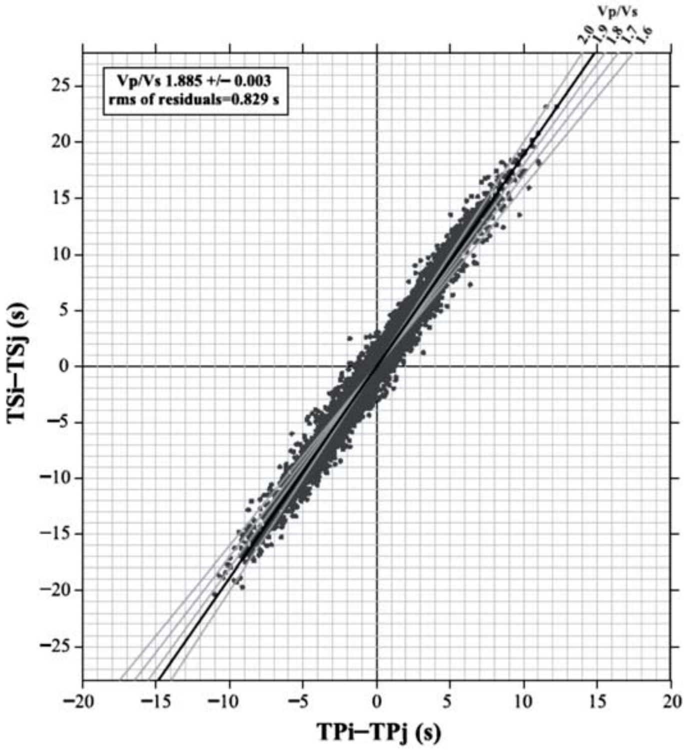

Figure 3.11 *Modified Wadati diagram* for each event and pair of station (i, j). On axis are reported the difference between P-phase ($T_{Pi} - T_{Pj}$) and S-phase ($T_{Si} - T_{Sj}$) arrival times. The black line provides the best-fitting of V_P/V_S ratio, while the grey lines show other theoretical ratios (from Matrullo et al. 2013).

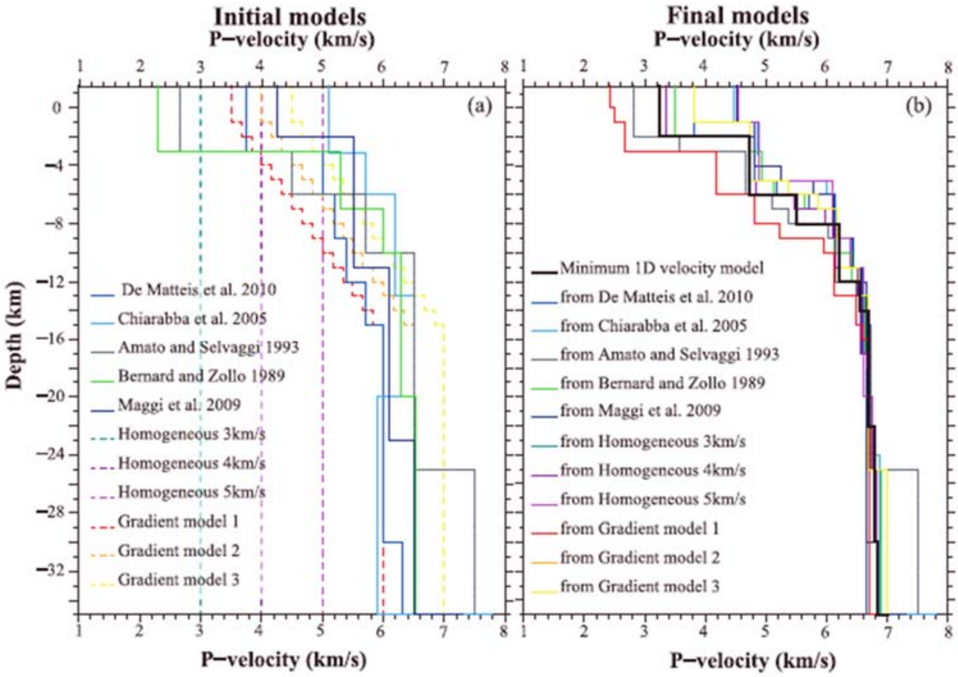

Figure 3.12 (a) 1D P-wave velocity structures used as initial models for the VELEST inversion procedure. (b) Final velocity models obtained from the VELEST inversion procedure starting from different initial models shown in (a). The ‘minimum’ 1D P-wave velocity model, obtained from an “average” of the 11 final models, is represented with a black thick line (from Matrullo et al. 2013).

Figures 3.14÷3.16 show comparisons between the recorded time-histories and those simulated for some stratigraphy models examined in Figures 3.12a and 3.13. The comparisons were made also in terms of Fourier spectra (figures 3.14c÷3.16c). The reproduced signals are extremely simple in terms of waveforms while the arrival times of the different wave fronts are well simulated.

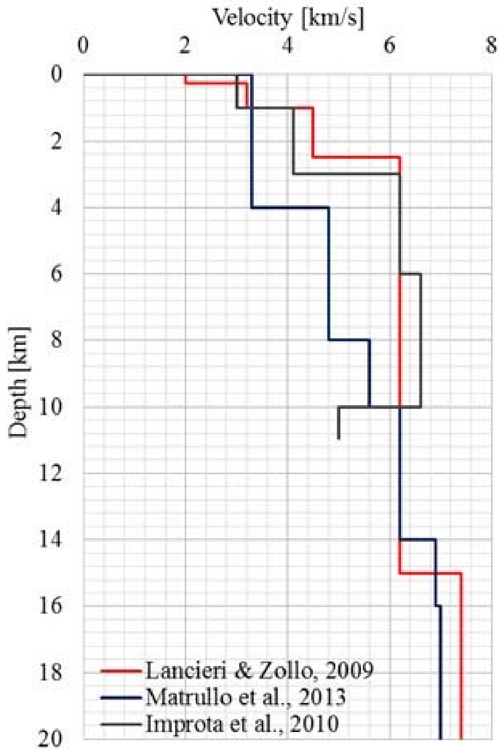

Figure 3.13 Comparison 1D stratigraphy between Matrullo et al. (2013), blue line, Lancieri and Zollo (2009), red line, and Improta et al. (2010), grey line.

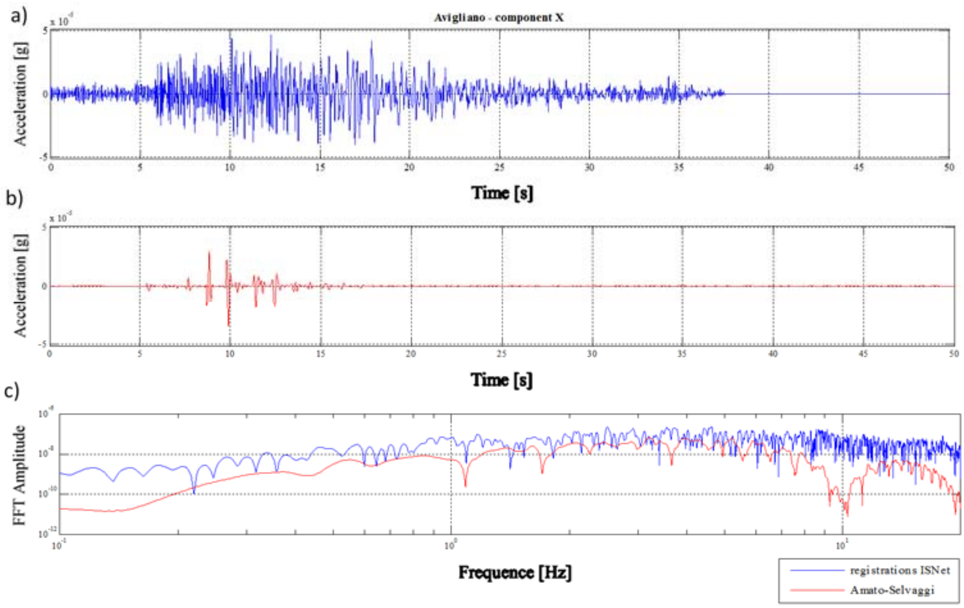

Figure 3.14 Comparison between the north-south time histories recorded at the Avigliano station (a) and the simulation (b) carry out with the stratigraphy proposed by Amato & Selvaggi (1993, Figure 3.12). (c) FFT comparison.

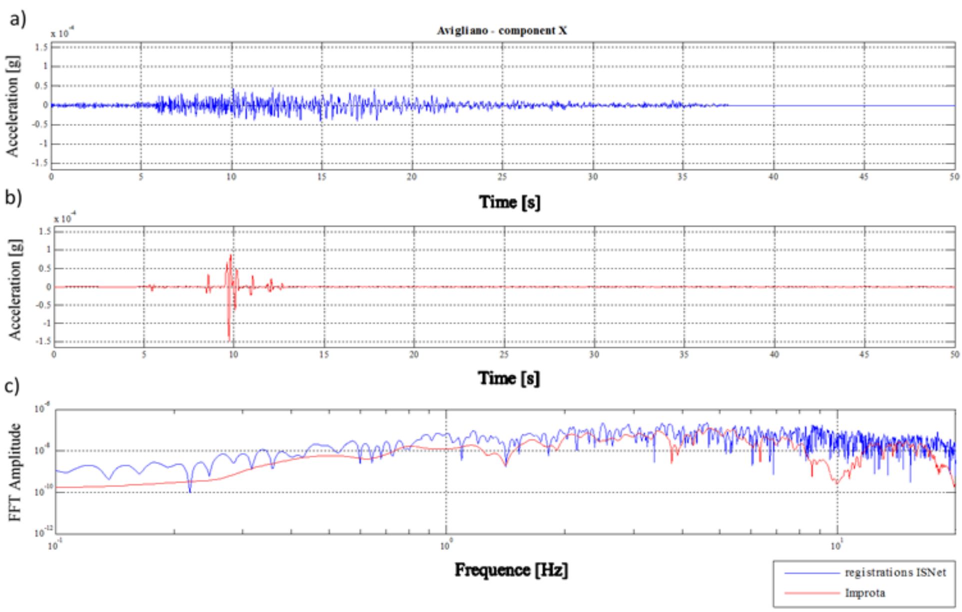

Figure 3.15 Comparison between the north-south time histories recorded at the Avigliano station (a) and the simulation (b) carry out with the stratigraphy proposed by Improta et al. (2000, Figure 3.13). (c) FFT comparison.

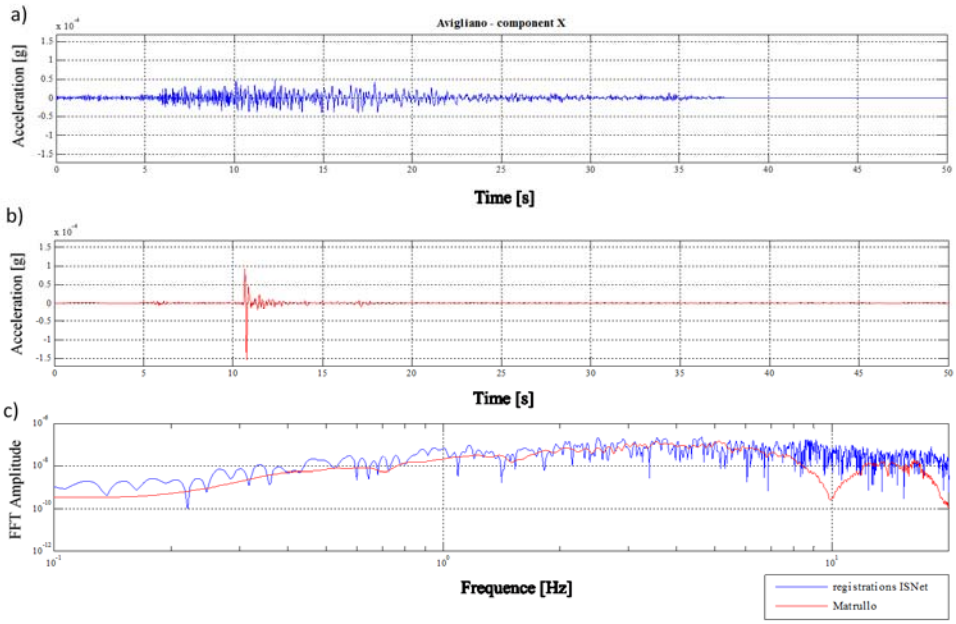

Figure 3.16 Comparison between the north-south time histories recorded at the Avigliano station (a) and the simulation (b) carry out with the stratigraphy proposed by Matrullo et al. (2013, Figure 3.12). (c) FFT comparison.

3.4.2. Calibration of velocity models by using empirical Green functions

The synthetic signals reproduced by the Matrullo stratigraphy, shown in Figure 3.12b have basically pulse-like waveforms in correspondence to the individual arrivals of the various phases (reflected, refracted and converted waves). However, the reverberations caused by the superficial layers in the upper part of the earth crust or local anomalies attributable to bi- and tri-dimensional effects are not taken into account in this model.

The duration and energy distribution (in time) of a signal is very important in the dynamic analysis of soil deposits and geotechnical structures, especially if we consider constitutive non-linear soil models. A pulse signal or a signal with multiple peaks in time, even if characterized by the same frequencies content, produce very different effects on soils and structures. This problem is crucial in the engineering field and should be overcome necessarily. Therefore, a random stratigraphic succession has been introduced in the upper layers, using a well-known approach in literature.

The simulations of synthetic signals at regional scale was carried out by implementing an algorithm based on empirical Green's functions (for the estimation of the propagation term) and a kinematic source model. The Green's functions are computed using the Discrete Wavenumber Method (DWM) introduced by Bouchon & Aki (1977). This method introduces a spatial periodicity of the sources to discretize the radiated wave field, and it is based on the Fourier transform in the complex frequency domain to calculate the Green's functions (see appendix A). Note the source and propagation terms, it is possible to determine the motion to the receiver by their convolution. This numerical formulation is implemented in the Axitra code by Coutant (1989). The code is widespread in the seismological field and numerous validations of the code have been performed (Bouchon, 2003; Amoruso et al., 2004).

Hisada (1994, 1995) described the critical cases for wavenumber integration codes: source and observer with the same depth, source close to the boundary between two layers and source on a boundary. These conditions should be avoid when the source position within the 1D velocity model is estabilished.

With reference to Q factor (defined as the reciprocal of damping ratio commonly adopted in geotechnical field), low values for shallow layers ($Q < 100$) and higher values for the deepest layers have been adopted, as suggested by Malagnini et al. in 2000 and Lancieri & Zollo in 2009.

Figures from 3.17 to 3.25 show comparisons in terms of acceleration time histories and elastic response spectra for the horizontal and vertical components at the stations of Caggiano, Marsico Nuovo and Satriano.

In all simulations, the source was assumed as a point (moment magnitude equal to 2) and the rise time was imposed equal to 0.075s. In addition, the adopted slip velocity function is triangular. Both on recorded signals and simulated ones a band-pass Butterworth filter (order 4) in the frequency range of 0.3 and 5 Hz was applied.

The Matrullo model shown in Figure 3.12b was enriched with a random variation of stiffness in the upper part of the model considering different thickness where the random variability was applied: 500m, 1000m and 1500m, the range of imposed variation corresponds to ±50% of the P-wave velocity that the original Matrullo model provides at the same depth.

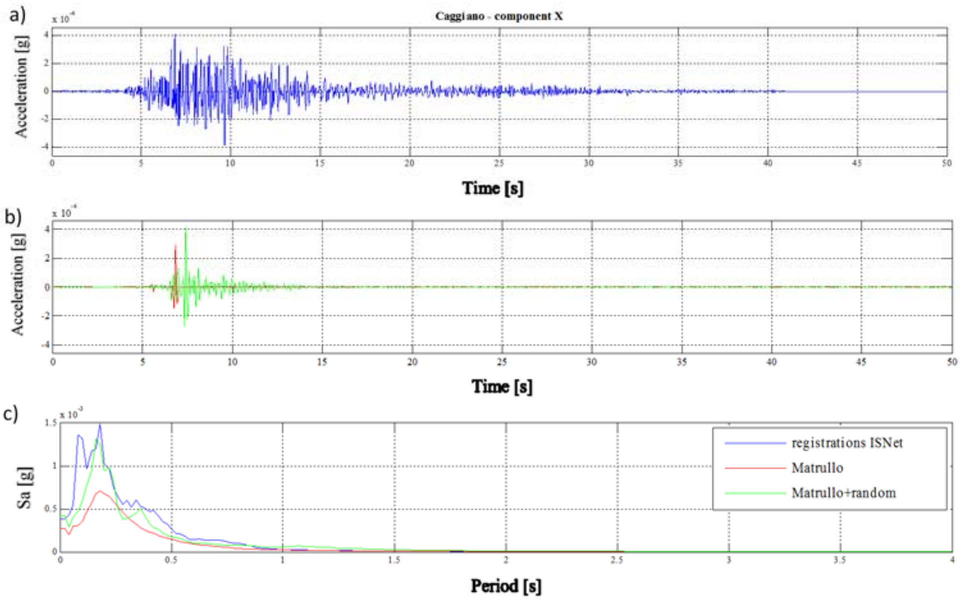

Figure 3.17 Comparison between the North-South acceleration time histories recorded (a) and simulated (b) at the Caggiano station and corresponding elastic spectra (c). Simulations were performed by implementing the original Matrullo et al. (2013) velocity model and the randomly modified (only in the upper part) version.

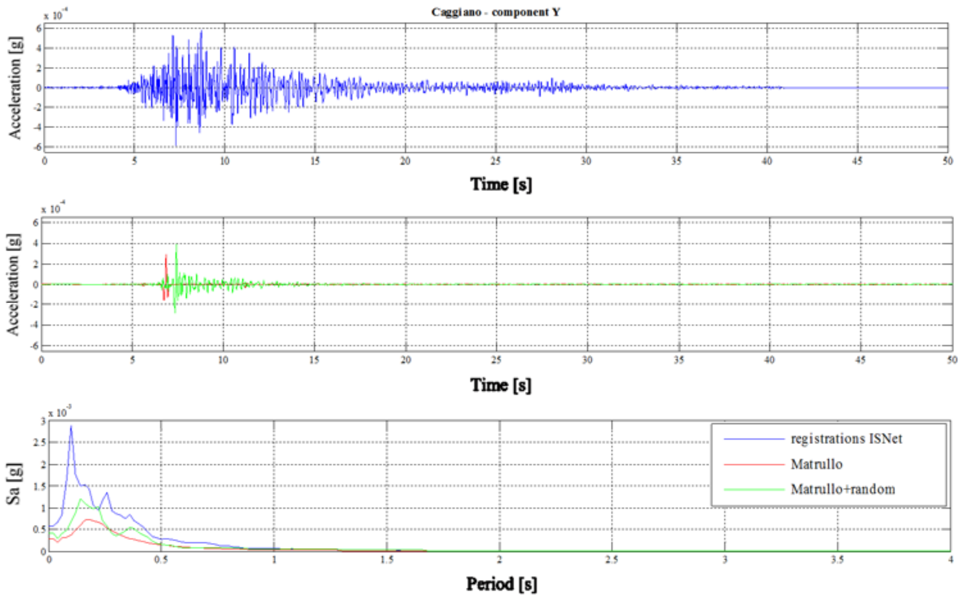

Figure 3.18 Comparison between the East-West acceleration time histories recorded (a) and simulated (b) at the Caggiano station and corresponding elastic spectra (c). Simulations were performed by implementing the original Matrullo et al. (2013) velocity model and the randomly modified (only in the upper part) version.

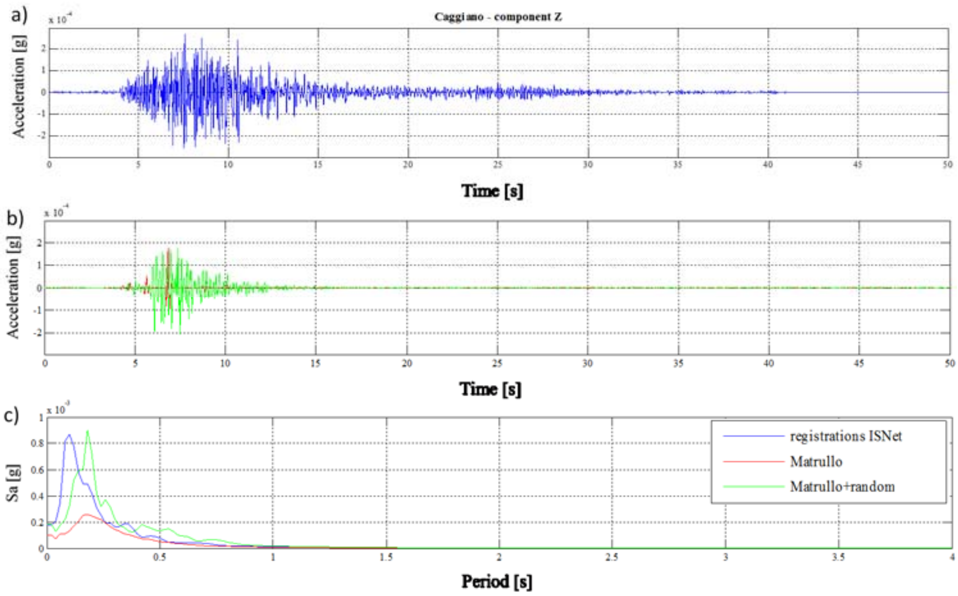

Figure 3.19 Comparison between the Up-Down acceleration time histories recorded (a) and simulated (b) at the Caggiano station and corresponding elastic spectra (c). Simulations were performed by implementing the original Matrullo et al. (2013) velocity model and the randomly modified (only in the upper part) version.

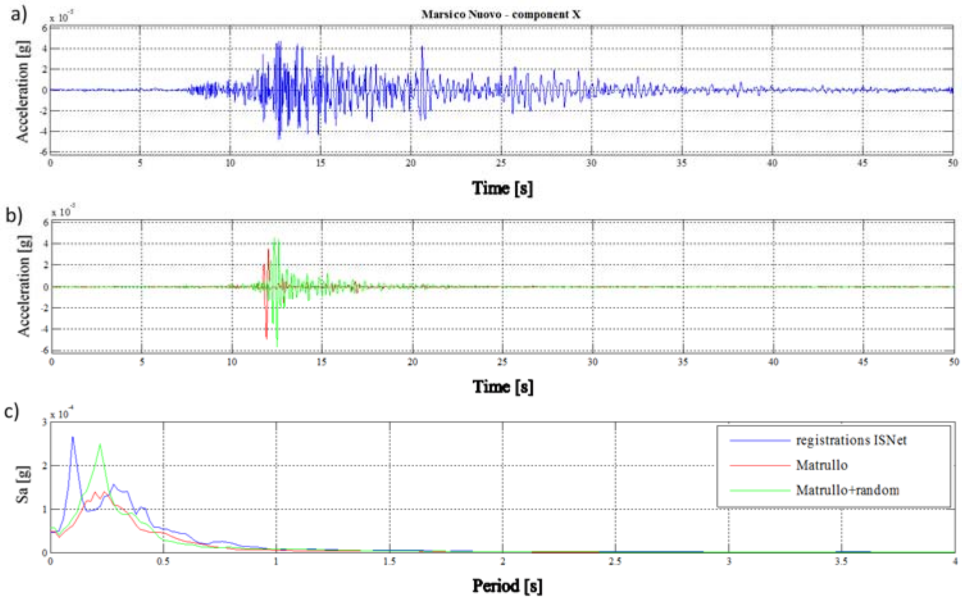

Figure 3.20 Comparison between the North-South acceleration time histories recorded (a) and simulated (b) at the Marsico Nuovo station and corresponding elastic spectra (c). Simulations were performed by implementing the original Matrullo et al. (2013) velocity model and the randomly modified (only in the upper part) version.

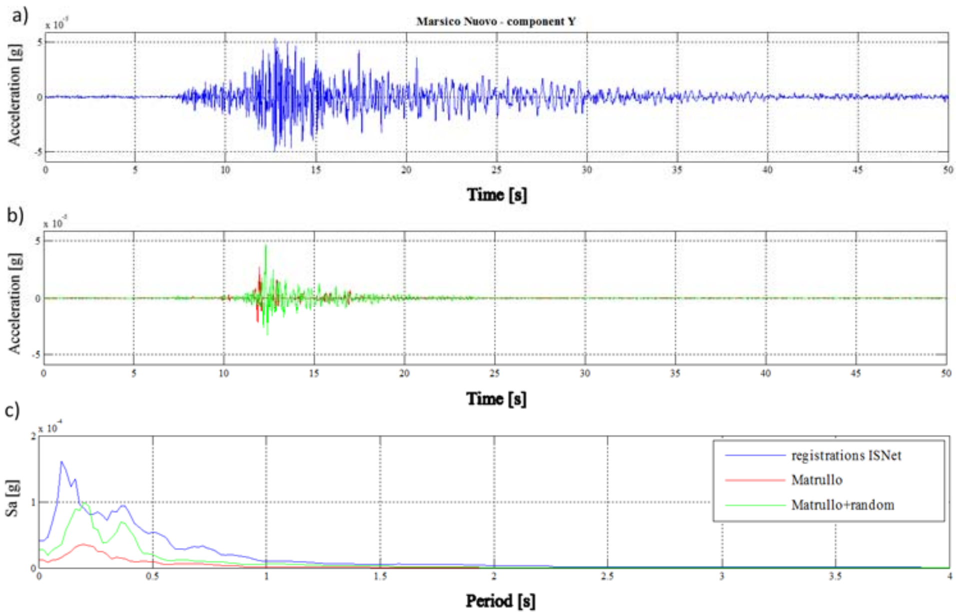

Figure 3.21 Comparison between the East-West acceleration time histories recorded (a) and simulated (b) at the Marsico Nuovo station and corresponding elastic spectra (c). Simulations were performed by implementing the original Matrullo et al. (2013) velocity model and the randomly modified (only in the upper part) version.

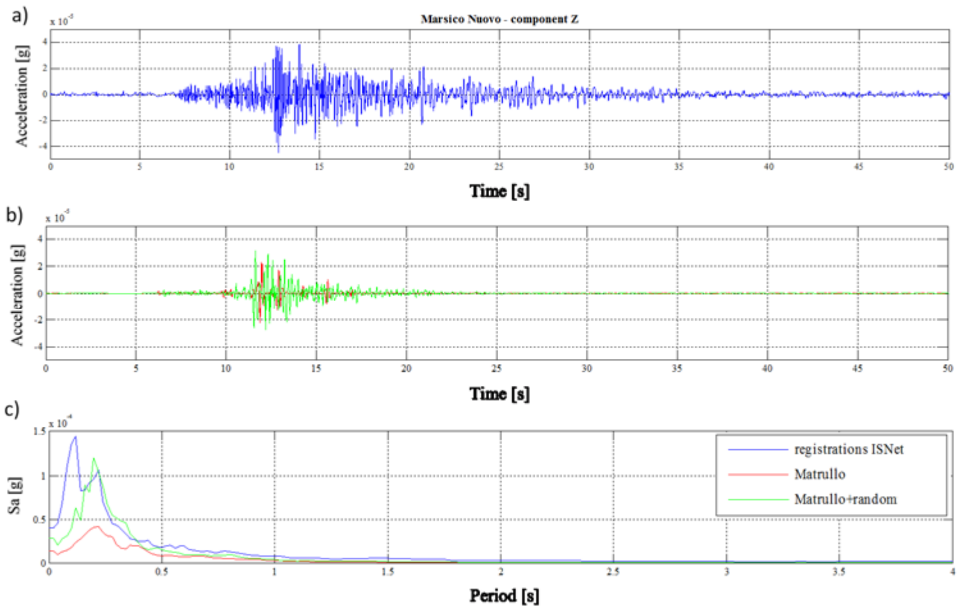

Figure 3.22 Comparison between the Up-Down acceleration time histories recorded (a) and simulated (b) at the Marsico Nuovo station and corresponding elastic spectra (c). Simulations were performed by implementing the original Matrullo et al. (2013) velocity model and the randomly modified (only in the upper part) version.

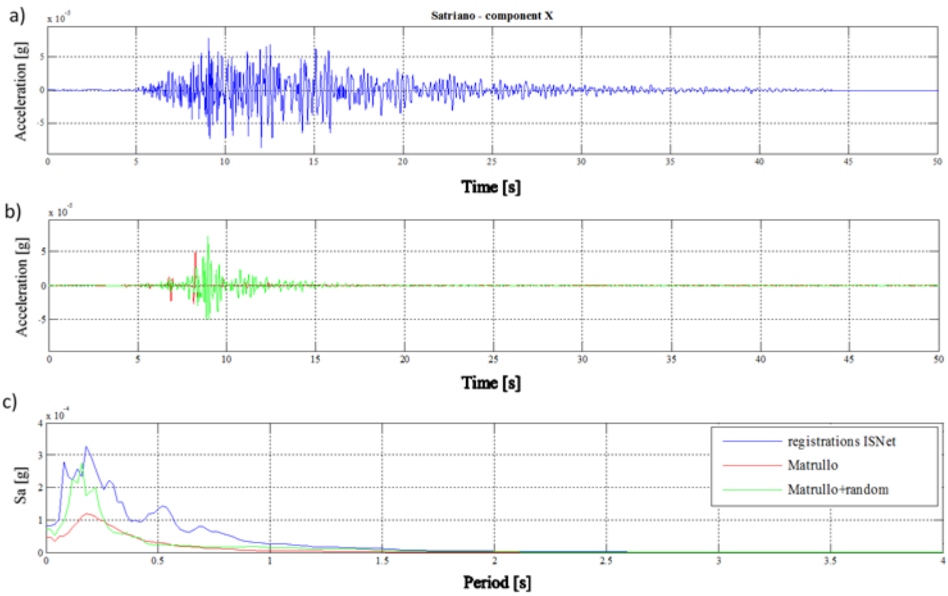

Figure 3.23 Comparison between the North-South acceleration time histories recorded (a) and simulated (b) at the Satriano station and corresponding elastic spectra (c). Simulations were performed by implementing the original Matrullo et al. (2013) velocity model and the randomly modified (only in the upper part) version.

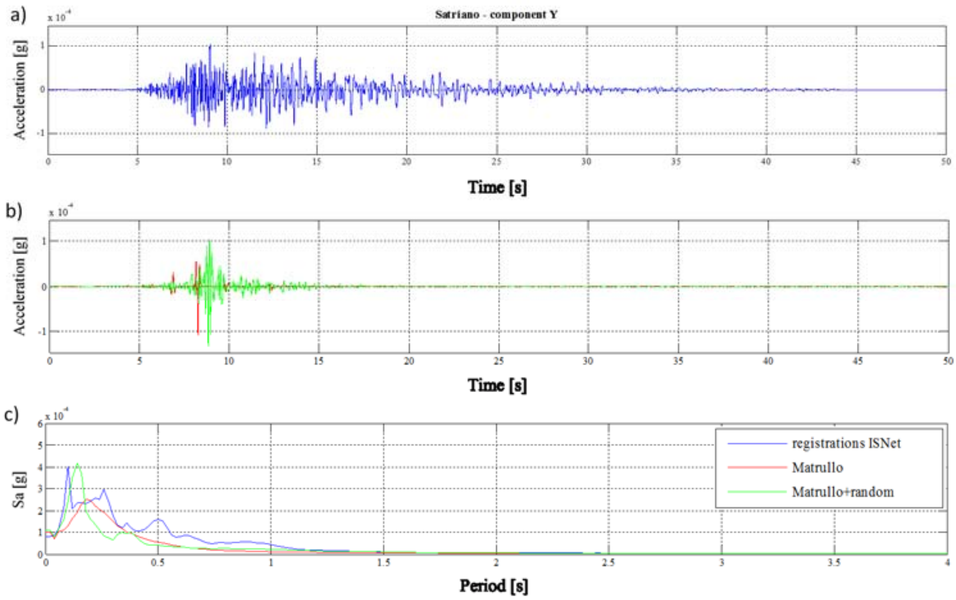

Figure 3.24 Comparison between the East-West acceleration time histories recorded (a) and simulated (b) at the Satriano station and corresponding elastic spectra (c). Simulations were performed by implementing the original Matrullo et al. (2013) velocity model and the randomly modified (only in the upper part) version.

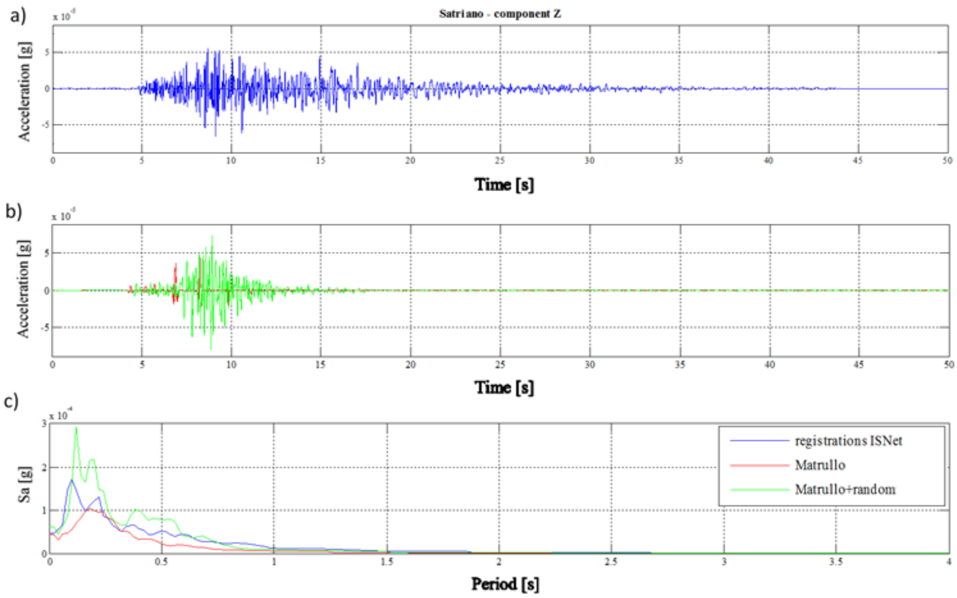

Figure 3.25 Comparison between the Up-Down acceleration time histories recorded (a) and simulated (b) at the Satriano station and corresponding elastic spectra (c). Simulations were performed by implementing the original Matrullo et al. (2013) velocity model and the randomly modified (only in the upper part) version.

In Figures 3.17÷3.25 is possible to observe a remarkable improvement of the fitting on spectral components, especially at high frequencies (low periods). The signal reproduced by considering only the original stratigraphy of Matrullo tends to strongly underestimate the spectral components with respect to the recorded signal. In particular, this happens for the North-South component of Caggiano and Satriano (respectively, Figure 3.17c and Figure 3.23c), as well as for East-West and Up-Down components of Marsico Nuovo (Figure 3.21c and Figure 3.22c). The fitting considerably improves when we consider the modified stratigraphy model (Matrullo + random).

In Figure 3.26 the comparison between predicted and measured signals is shown in terms of attenuation laws for PGV and PGA. The comparison is quite satisfactory. In particular, observing the data between 20 and 25 km or between 27 and 28.5 km, two higher values of PGA and PGV are observed. These peaks are well reproduced by the numerical simulations for all examined models. Since the same trend is obtained also using the original Matrullo model, this implies that there are two contributes due to reflections from deep interfaces, maybe related to the layers between depths of 4 and 10 km.

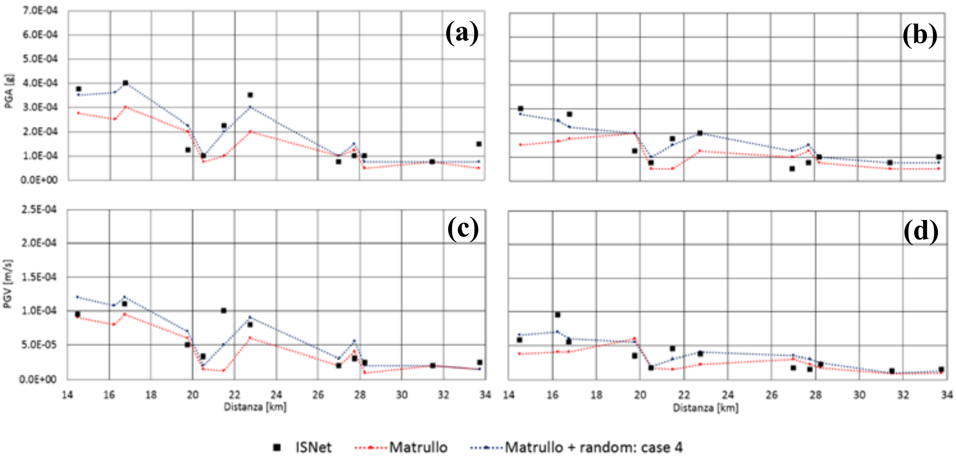

Figure 3.26 Comparison between observed and simulated attenuation law for PGA (a-b) and PGV (c-d). The horizontal PGA and PGV, obtained with vector composition of north-south and east-west components, are shown in figure (a) and (c). The vertical PGA and PGV are plotted in figure (b) and (d) respectively.

Among different random stratigraphies here considered, one defined as "Mastrullo + random: case 4" was selected because it minimizes the mean square error (cumulated on all stations and motion components) related to the spectral ordinates between periods 0.2-3s. Moreover, this model of velocity provides the highest values of the coherence function between the recorded and simulated signals (average value on the band of frequencies between 1 and 5 Hz, Figure 3.27). Finally, even the error function referred to FFT amplitudes (Hamming window of 100 and overlap of 50%) confirms that the selected model 4 provides the best-fitting to recorded data.

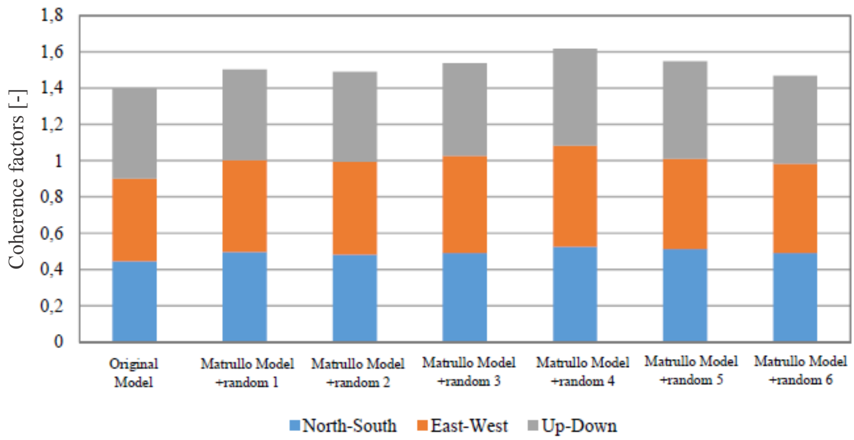

Figure 3.27 Mean value of coherence function (frequency band 1÷5 Hz) between the recorded and simulated signals.

3.4.3. Final considerations

The main limitations of a synthetic reproduction of an earthquake ground motion are essentially related to the proper simulation of high and low frequencies of the signal content.

At *long periods* (longer than about 1 second), strong ground motions are deterministic in the sense that seismological models are capable of matching not only the spectral amplitudes but also the waveforms of recorded long period ground motions, once the rupture model and the seismic velocity structure of the region surrounding the earthquake are known.

At *short periods* (shorter than about 1 second), strong ground motions become increasingly stochastic in nature. Seismological models are generally capable of matching the spectral amplitudes of ground motions to the shorter period, but are generally not capable of matching recorded waveforms.

3.5. Source model

The determination of the seismic source is on important aspect to determine the seismic hazard of a specific site. There are several approaches to face this issue and generally they may be distinguished in deterministic (DSHA) or probabilistic (PSHA) approach (Kramer, 1996). These approaches allow to determine the main parameters of a signal (PGA, PGV, PGD, Arias Intensity, duration, root mean square, the ordinates of the elastic and/or design response spectrum, etc.) and to perform scenario analysis using real or “artificial” accelerograms, Anyway, whatever the applied methodology, DSHA or PSHA, for the estimation of the seismic hazard (to be used for the seismic design and scenario analysis), it is possible to estimate only the synthetic parameters. No indication is instead provided on the expected waveforms at the site.

If same procedures are almost consolidated for far-fault zones (where a single set of three accelerograms is able to describe the ground motion), almost nothing has been done to estimate the seismic hazard at bedrock in near-fault conditions. Many studies over the past ten years (Sommerville, 2003; Iervolino & Cornell, 2008; etc.) have highlighted only some aspects concerning: (i) forward directivity occurrence; (ii) valuation of the pulse intensity; (iii) pulse period; (iv) shape of the elastic response spectrum and its variation in the proximity of the pulse period.

In general, seismic hazard (on bedrock level) is evaluated at territorial scale, i.e. with mesh sizes of the order of kilometers or tens of kilometers. In Italy, for example, such assessments are made on the basis of homogeneous seismogenic zones in regional or sub-regional areas and are not related to the individual faults. In near source conditions, as already discussed in chapter 1, it is appropriate to assess the effects of asynchronous motions. It is therefore important to evaluate the variations of the synthetic parameters based on a site-specific hazard analysis. For some structures, it is appropriate to have, also, the spatial variability is of ground motion (time-histories).

In this thesis, a determinist approach was then selected to reproduce the near-source ground motion with the above discussed simplifications on modelling both source and propagation media.

3.5.1. Source implementation

The source model is built by positioning a series of equally spaced, double couple point sources along the fault surface, each of them having the same strike, dip, rake and time history shape, but different intensity (moment), trigger time, rise time (thereby, also the maximum slip-velocity). The sum of point source seismic moments is set to be equal to the event seismic moment.

In order to set parameters for the finite source model we assume that the event magnitude (or seismic moment), location and focal mechanism are 'a priori' known from previous estimation carried out by Bernard & Zollo (1989).

A rough estimation of the fault length can be also derived from the event magnitude using the Wells and Coppersmith relationships:

$$RLD = 10^{\mathrm{a+b}*M_w} \tag{3.1}$$

$$RW = 10^{\mathrm{c+d}*M_w} \tag{3.2}$$

where RLD, RW and M_W are the subsurface rupture length, the downdip rupture width and the moment magnitude respectively, while a, b, c and d are regression coefficients.

The rupture velocity (V_R) is assumed constant and equal to the 80% of the shear waves velocity in the investigated area.

The elementary point source spacing and their rise-time are fixed on the basis of the maximum frequency chosen for the numerical accelerogram computation. The aliasing effect is avoided by positioning the elementary sources at a distance smaller than the minimum wavelength given by $\lambda = V_R/f_{ny}$, with f_{ny} is the selected Nyquist frequency.

It was decided to use at least 6 point sources for the minimum wavelength (Lancieri & Zollo, 2009), and consequently the source spacing is given by relation $\Delta s = \lambda/6$.

In addition, the signals emitted from each elementary source must overlap at the receiver, which means that it is necessary to verify (and correct if necessary) that the source duration (rise-time, r_t) of each point source has to be greater than the time needed by the rupture front to reach each single point source ($r_t \gg V_R/\Delta s$).

As stated above, low quality factor values (Q) were adopted for shallow layer, while higher Q factor values were used for the deepest layer (Lancieri & Zollo, 2009).

3.5.2. The 1980 Irpinia earthquake

The 1980 Irpinia earthquake is one of the most studied normal faulting event in the world. This earthquake (Ms = 6.9), occurred in the southern Apennines, is the largest earthquake in Europe in the past 50 years. A detailed discussion of the structural and tectonic setting of this area can be found in the works of Westaway and Jackson (1987) and Pantosti and Valensise (1990). Surface faulting was first reported by Westaway and Jackson (1984 and 1987) and later recognized over a broader area by Pantosti and Valensise (1990). Results from these studies allowed the identification of a fault scarp associated with the earthquake, which has a total length of 38 km. Several fault fragments were identified from an analysis of the surface rupture and each of these was associated to a different rupture episode of the Irpinia earthquake (Figure 3.28a), which has been detected by the analysis of both teleseismic and accelerometric data. The accelerograms recorded during this earthquake represent an important data set for investigating the source process in extensional regimes. Despite its complexity, detailed reconstructions of the faulting process have been made by various researchers. These investigations have been carried out successfully thanks to the complete geophysical data set, which includes seismometric data at teleseismic and local distances, strong motion data, surface faulting observations and elevation changes during the period of seismic activity (Westaway and Jackson, 1987; Bernard and Zollo, 1989; Pantosti and Valensise, 1990). A question which is remained unsolved was the dynamic behaviour of slip and the rupture development on the fault plane during the earthquake. The solution of this problem is complicated by the high number of source and medium parameters, as well as the results obtained by the analysis of geologic, geodetic and seismometric data, because they provide important physical constraints for the waveform modelling. The strong motion data contain important information on the details of the source mechanism: they can be used to provide an accurate picture of the space-time evolution of the rupture process. A multi-disciplinary approach allows the faulting process to be reconstructed, with emphasis being laid on the most distinctive features of the earthquake complexity. The source time function obtained at teleseismic distances (distances of over 2000 km) (Bezzeghoud, 1987; Giardini, 1992) revealed that the rupture was characterized at least by three different episodes occurring at 0 s, 20 s and 40 s. Westaway and Jackson (1987) proposed a source model based on forward modelling of teleseismic data that enhanced the presence of three main rupture episodes. The accelerograms recorded at several sites clearly show two distinct seismic events separated by a time lag of 40 s. The seismic radiation of the 20 s sub-event is not clearly visible on all the strong motion recordings because it is probably superimposed on the seismic radiation of the main rupture (most of the stations are located towards the northwest).

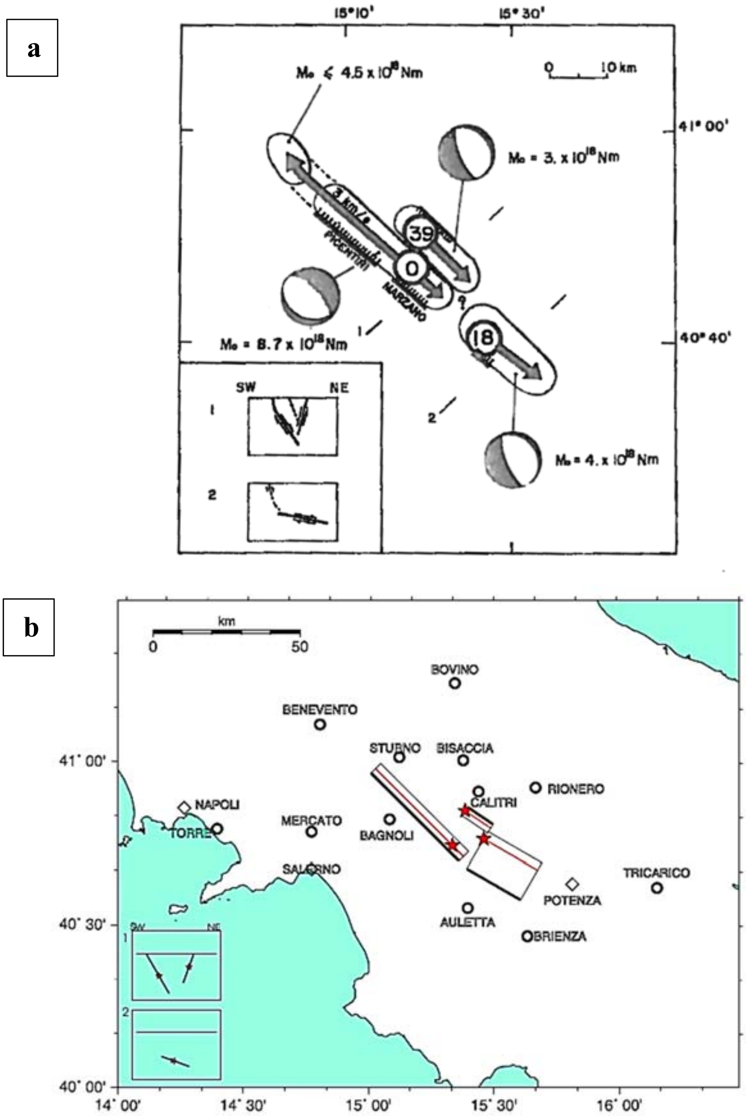

Figure 3.28 Irpinia 1980 earthquake fault model by Bernard & Zollo (1989). The event was characterized by three main rupture segments, nucleating at 0, 20 and 40 s. In figure (b) the red stars on grey left panels represent the nucleation points for three, while the bold black lines are the fault top (Lancieri & Zollo, 2009).

Westaway and Jackson (1987) and Bernard and Zollo (1989) also computed the fault plane solutions for the 20 s and 40 s sub-events (Figure 3.28b). All these solutions indicate that a complex system of normal faults was activated during the 1980 Irpinia sequence and that the amount of left-lateral strike-slip solution is negligible. Deschamps and King (1983) proposed a fault plane solution containing a significant left-lateral strike-slip component; this solution was later shown to rely on some ambiguous polarity readings (Westaway and Jackson, 1987). The location and the rupture mechanism of the 40 s fault fragment are mainly constrained by geodetic and strong motion data. No surface evidence of this sub-event was recognized. Various locations and geometries have been proposed for this fault fragment (Crosson et al., 1986; Westaway and Jackson, 1987; Bernard and Zollo, 1989; Siro and Chiaruttini, 1989; Pantosti and Valensise, 1990). Even if the geodetic data alone cannot resolve the exact position of this fault fragment, there is a diffuse agreement (Bernard and Zollo, 1989; Pantosti and Valensise, 1990) to locate the 40 s sub-event on a normal fault antithetic to the main fault and dipping 70°SW. The 20 s sub-event occurred along a further fault fragment located to the southeast of the main fault. Bernard and Zollo (1989) located this sub-event using the strong motion recordings. The principal controversy about this fault fragment concerns the dip angle. Based on surface breakage investigations Pantosti and Valensise (1990) proposed a dip angle of 70°, similar to that of the main event, while Bernard and Zollo (1989) proposed a dip angle of 20°. Clearly, only for the rupture geometry of the main rupture (0 s) is the agreement unanimous. A larger number of accelerograms are available for the main event than those available for the 40 s sub-event (only five accelerograms are available with a favourable signal-to-noise ratio) and for the 20 s sub-event (just three accelerograms have been associated with this sub-event). Cocco and Pacor in 1993 have studied the evolution of the rupture process along the main fault, believing that no more information on the source mechanism of the 20 s sub-event may be extracted from the strong motion data due to the poor source coverage. The uncertainties on fault geometry and the paucity of accelerograms complicate also the theoretical modelling of the 40 s rupture.

In order to study the distribution of the fault slip of the main event (0 s), Cocco & Pacor (1993) have preferred to constrain the fault geometry by using results from geological and geodetic investigations as well as data from aftershocks (Westaway and Jackson 1987, Bernard and Zollo, 1989; Pantosti and Valensise, 1990). The goal was to model the waveforms radiated by a purely normal fault, dipping 60° NE with a strike of 315°. The first two sub-events were separated by a strong barrier that impeded a continuous propagation of the rupture from the southern 0 s fault fragment to the 20 s one. The rupture arrest on this barrier and the following nucleation on the 20 s fault complicate any attempt to model the rupture propagation along the two fault fragments together as a single fault.

It is possible to conclude that the rupture history consists of a bilateral rupture propagation with a variable rupture velocity. It is evident that the second nucleation was located 18 km away from the hypocentre. This rupture behaviour allows reproduction of the observed waveforms, in particular those recorded at Sturno, Bagnoli Irpino and Calitri stations.

The slip velocity distribution consists of three main patches: the first one is located on the nucleation zone (120 cm/s) and extends to shallow depths.

With reference only to mainshock (0 s mechanism), Cocco & Pacor (1993) have showed that the region of highest slip velocity was close to the rupture nucleation. Moreover, two other regions of high slip velocity are localized at 15 km and 22 km away from the hypocentre, along the direction of strike. The rupture propagation towards the northwest was characterized by abrupt changes in rupture velocity. The behaviour of slip velocity along the fault is strictly related to the fault scarp height observed at the earth surface and seems to be controlled by the fault zone structure. The aftershocks are concentrated mostly close to the region of maximum co-seismic slip. This rupture model explains the dominant features of the rupture process on the assumed fault and the body-wave field radiated at frequencies ranging between 1 and 2 Hz.

Numerical simulation

For the scopes of this research work, reference was made for the first mechanism (0 s) to the inversion studies on the source by Cocco & Pacor (1993), whereas for the stratigraphy reference was made to the model of Bernard & Zollo (1989), widely accepted as the best characterization by the national and international scientific community.

The seismic moment resulting from the inversion proposed (Cocco & Pacor, 1993) is $1.9e^{19}$ N m, which is in close agreement with the value estimated by Bernard & Zollo (1989) for the main rupture and for the north-western extension ($1.3e^{19}$ N m). Cocco & Pacor (1993) have analyzed the strong motion accelerograms of the 1980 Irpinia earthquake in order to investigate the slip distribution and the rupture history during this event. The rupture model was studied first by means of a forward waveform modelling following a trial-and-error approach, and afterwards by applying a linearized inversion of ground motion waveforms. The forward waveform modelling and the spectral analysis of ground accelerations provided a reliable interpretation of the strong motion recordings, enhancing the most important features of the radiated wave field. Moreover, the rupture model resulting from the forward approach was used as starting model for the linearized inversion. A linearized tomographic inversion has been used with the aim to investigate slip velocity and rupture time distribution on an extended fault. Unlike other studies, the fault is not subdivided into sub-faults. Furthermore, the fault geometry is not part of the solution. To constrain the faulting mechanism, Cocco & Pacor (1993) have used the results obtained in other studies (Westaway and Jackson, 1987; Bernard and Zolo, 1989; Pantosti and Valensise, 1990; Amato and Selvaggi, 1921) mainly based on independent data (such as geodetic, geologic and local seismometric data).

The spatial distribution of the dip component of slip velocity shown in Figure 3.30 was obtained by the data inversion (Cocco & Pacor, 1993) imputed from a starting model (Figure 3.29a) with two patch having constant velocity slip, whose rupture time is shown in Figure 3.29b.

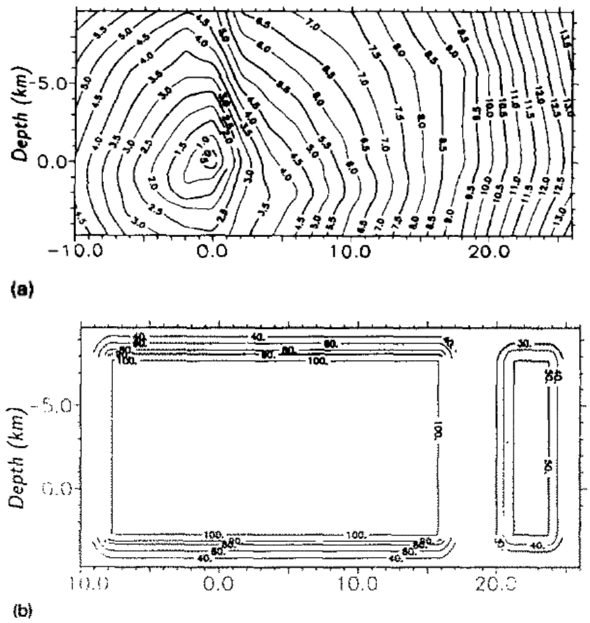

Figure 3.29 Starting model for data inversion. (a) Rupture time (s). The rupture velocity is constant (2.6 km/s). The Slip velocity (b) distribution (cm/s) consists of two patches: the first one homogeneously covers the portion of the fault plane modelled with the forward approach; the second patch is located on the northwestern extension of the earthquake rupture (Cocco & Pacor, 1993).

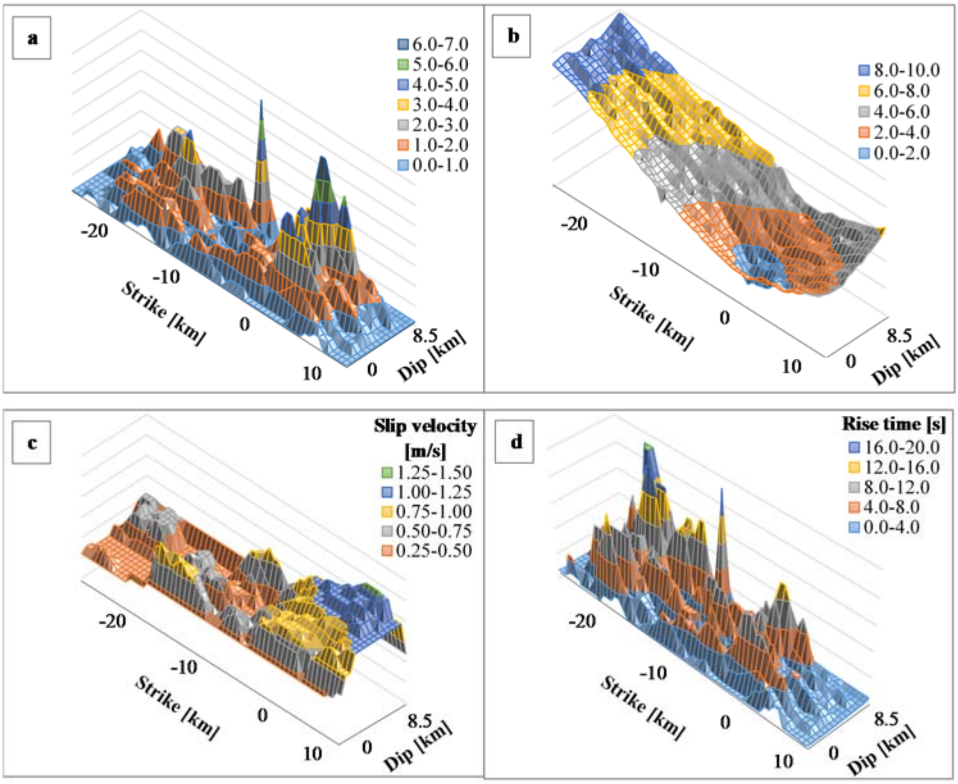

Figure 3.30 Source model of the first mechanism (Irpinia 1980 earthquake): (a) slip map; (b) rupture time distribution; (c) slip velocity and (d) rupture duration (modify from Cocco & Pacor, 1993).

Cocco & Pacor (1993) have shown that the results obtained from the waveform inversion indicate that the rupture was quite heterogeneous. Looking at the similarity of the solutions derived by the comparison of different inversion solutions obtained using different starting models in order to verify the effect of the initial conditions, the authors conclude that the results do not depend on the choice of the starting model.

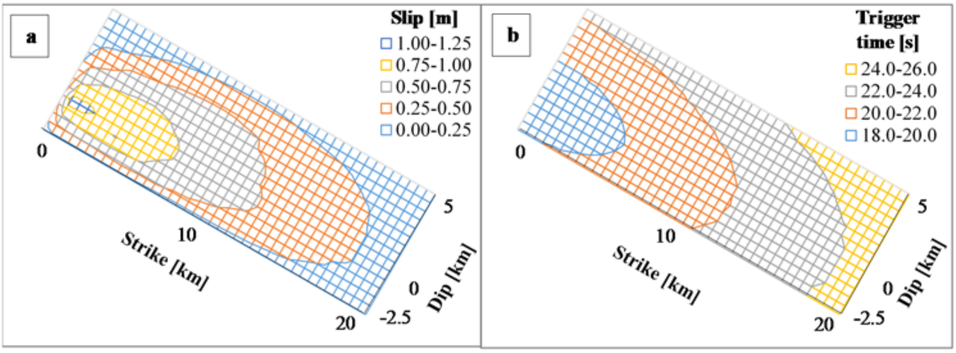

Figure 3.31 Source model of the second mechanism: slip map (a) and rupture time distribution (b).

For the second and the third sub-event of the 1980 earthquake no detailed information is available in literature. Simplifying assumptions were made accounting for the indications of Westaway & Jackson (1984, 1987) Bernard & Zollo (1987), Cocco & Pacor (1993), Lanceri & Zollo (2009) and Ameri et al. (2011).

In particular, on the basis of experimental observations, the second mechanism may be considered an extension of the first mechanism, although in delayed trigger. Many authors argue that the slip-map of the first mechanism consists of two different macro-patches and a bilateral rupture (Cocco & Pacor, 1993). The slip-map of the first mechanism may be assumed made of a single asperity of semi-circular shape with maximum intensity on the North side (i.e. at the hypocenter), in continuity with the rupture towards the South of the mechanism 1 (Figure 3.31).

For the third mechanism, consistently with what suggest by Lanceri & Zollo (2009) to define the shake-map of the earthquake of 1980, a map of slip (Figure 3.32) almost uniform has been considered, consisting of a roughness having size comparable to the characteristic length of the fault and maximum intensity at the hypocenter. The propagation of the rupture was assumed parallel to the strike as for the other two mechanisms and oriented according to Bernard & Zollo (1989).

For the second and third sub-events, the assumed distribution of slip consists of one asperity, with an average intensity consistent with the seismic moment proposed by Bernard and Zollo (1989) and regression studies by Wells & Coppersmith (1994). To the assumed slip-map at low frequencies, a random roughness having small asperities (high frequency slip-map, lower wavelengths excited) with k-square (Gallovič & Brokešová, 2007) or Gaussians (Del Gaudio, 2014) formulations or similar approaches was added.

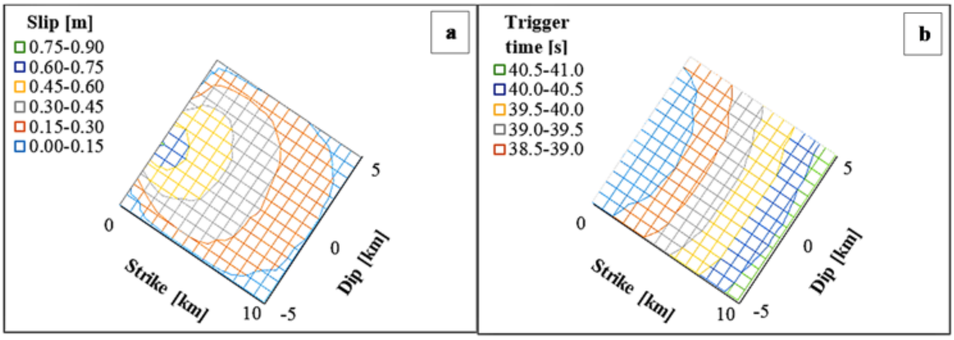

Figure 3.32 Source model of the third mechanism: slip map (a) and rupture time distribution (b).

3.5.3. Future seismic scenarios

For the site of Conza della Campania six different seismic scenarios were considered. For all scenarios, the stratification of the propagation medium unchanged is considered (paragraphs §3.4.1 and §3.4.2).

In constructing the future scenarios reference was made to the source mechanism activated during the 1980 Irpinia earthquake. In particular, the first and the third mechanism were considered. The second mechanism is quite far from the site and its contribute to the seismic motion is minor (Cocco & Pacor, 1993).

As shown in Figure 3.33, the assumed scenarios may be divided into two groups, each containing three events:

- 1a, 1b and 1c reproduce the first mechanism of the 1980 Irpinia earthquake;
- 3a, 3b and 3c reproduce the third mechanism of the 1980 Irpinia earthquake.

In the Figure 3.33 the numbers indicate the reference mechanism (1st and 3rd) and the letters indicate a different scenario in the adopted slip map.

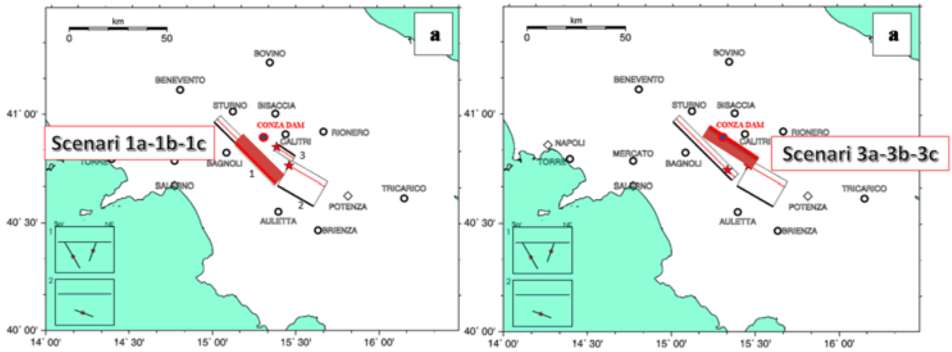

Figure 3.33 Future scenarios, simulated in this thesis work, for dynamic studies on Conza dam. In figure (a) are shown the scenarios based on first Irpinia 1980 mechanism, in figure (b) are reported the scenarios related the third event of Irpinia earthquake (modify by Lancieri & Zollo 2009).

Six different slip maps were used. To determine these maps, for each scenario were added two contributions (Del Gaudio, 2014): the first resulting by large asperities (low-frequencies slip map, LF); the second related to a stochastic distribution of 2D Gaussian functions (Figure 3.34) according to the formulation:

$$f(\vec{x}) = Ae^{-\frac{1}{\sigma^2}(\overrightarrow{x_0},\vec{x})^2} \qquad \textbf{(3.3)}$$

where $\overrightarrow{x_0}$ and $\vec{x}$ represent respectively the positions of the centre of the Gaussian and of a generic point on the fault surface; a indicates the amplitude of the slip, connected to the single Gaussian. It can be appropriately determined as a rate of the average value determined by the LF-slip map ($A_{(L)}=a \cdot slip_{mean} \cdot (l-l_{min})/(l_{max}-l_{min})$ with l, l_{min} and l_{max} the patch length, min and max dimension respectively and a is a weighting factor). Finally, the standard deviation, σ, is a function of the wavelength related to the characteristic size of the asperities:

$$\sigma = \frac{1}{2} \cdot max\{L; W\} \qquad \textbf{(3.4)}$$

where L and W are the strike and dip length, respectively.
By summing of several Gaussians, conveniently weighted on patch extension, the high-frequencies slip map (HF) is obtained.

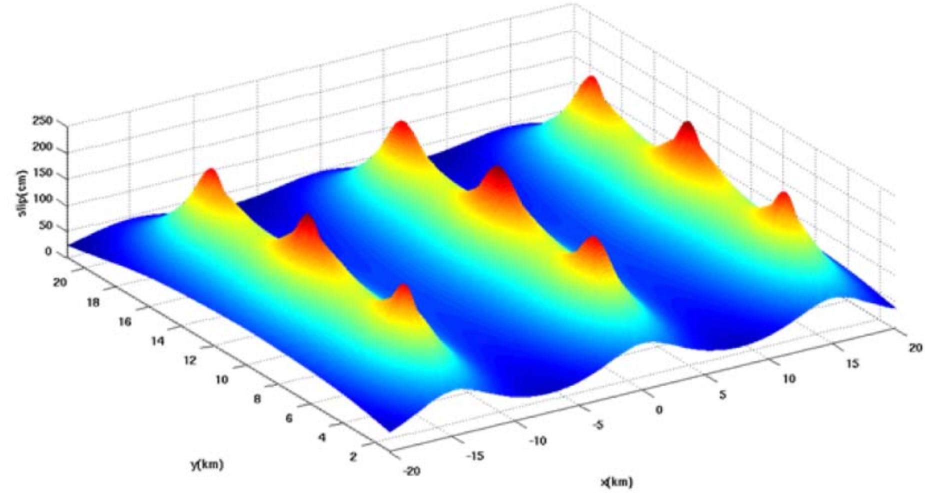

Figure 3.34 Overlap of nine, uniformly spaced, 2D Gaussian functions (Del Gaudio 2014).

As proposed by Del Gaudio (2014), the LF-slip map can be identified through inversion at low frequencies (f < 0.5 Hz) of the seismic source, while for higher frequencies random patches may be applied.

A slip broadband map (0 < f ≤ 7.5 Hz) is obtained by superimposing the LF and HF slip distribution. The seismic moment of broadband slip map is equal to the sum of the seismic moments of the LF and HF components. The expected seismic moment is obtained from the single LF slip map, while the high-frequency components may be small or large, because generated by the superposition of random distributions. Consequently, a redistribution of seismic moment (and of the displacements) should be later made.

For all scenarios the magnitude was set equal to 6.5, according to the historical seismicity in the Campano-Lucano Apennine.

As the position hypocenter regards, due to the stress drop caused by the 1980 Irpinia earthquake, the actual stress state acting on the three fault surface is now reduced and a stress migration (accumulation) moved along fault borders. It is therefore possible that a future triggering mechanism takes place on the outside of the pre-existing faults as already observed for San Andreas fault (Housner et al., 1990). For each of the two mechanisms at the base of the six design scenarios, the hypocenter was then placed at the edges of the fault segments activated during the 1980 Irpinia seismic sequence. An extension of the fault, outside the previously activated surfaces, was considered (Figure 3.33).

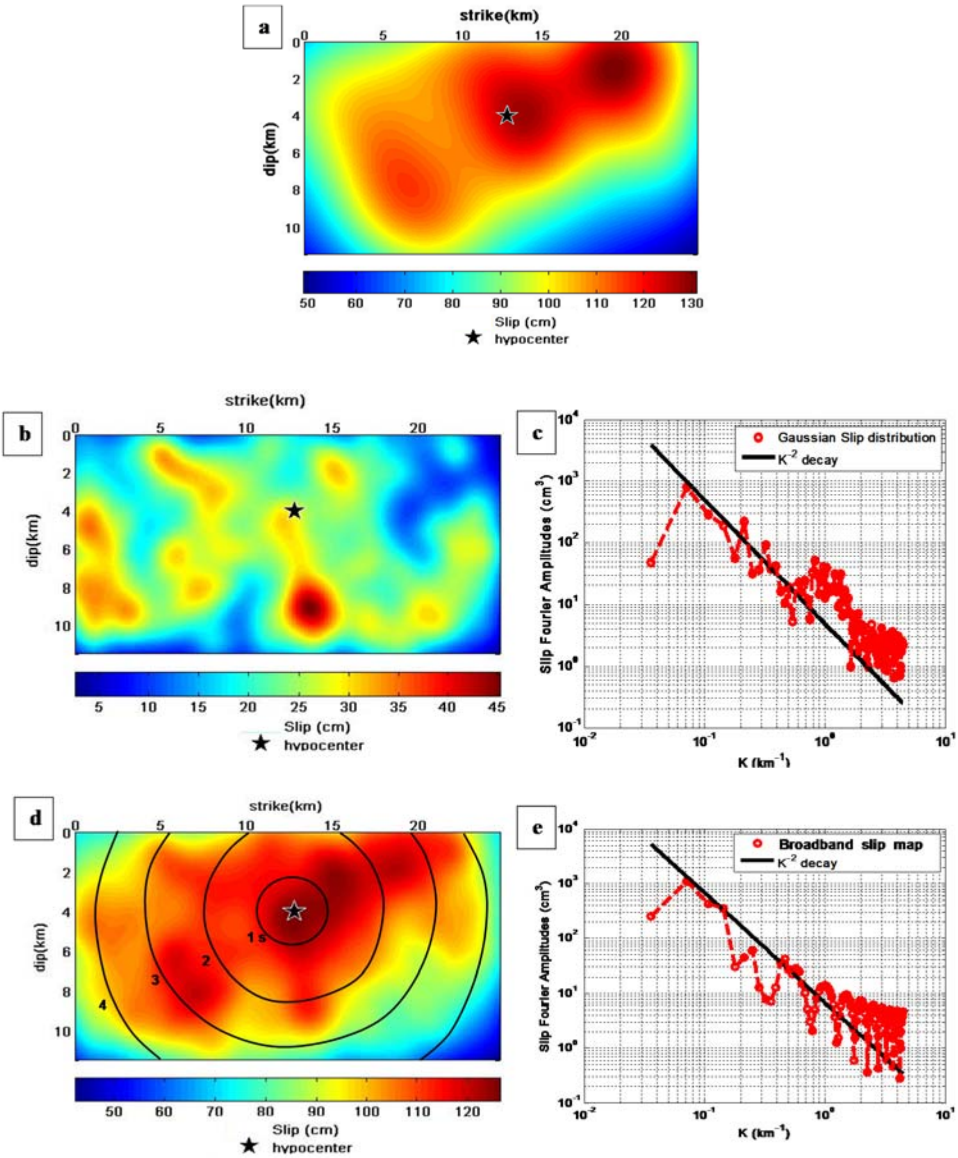

Figure 3.35 Scenario 3a. (a) LF-slip map containing three large asperities. (b) HF-slip map obtained by random application of 2D Gaussian functions of different sizes and positions. (c) Fourier amplitude of Gaussian slip distribution compared to an equivalent k^{-2} decay trend (black lines). (d) Broadband slip map (LF+HF) and the isochrones (black circumferences) relative to a 6.5 magnitude event. (e) Fourier amplitude of the final slip (figure d) compared to k^{-2} decay trend.

The planar extension was determined according to the relationships (3.1) and (3.2). A rupture propagation velocity of 0.8 V_S has been considered to define the isochrones.

For the seismic scenario 3a (Figure 3.33), in Figure 3.35 the LF and HF maps of slip are shown together with the isochrones and the final broadband. Finally, the Figure 3.36 shows the slip map of the other five scenarios simulated in this research work.

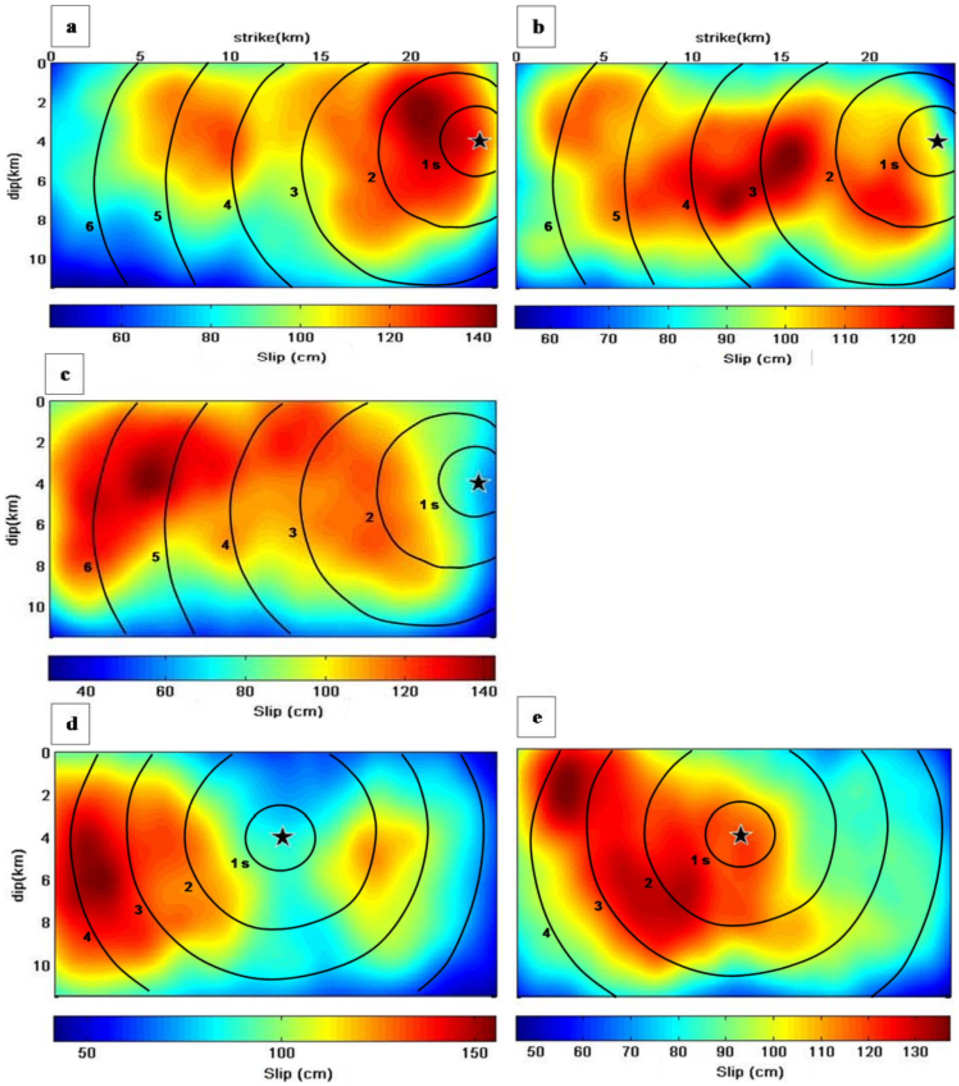

Figure 3.36 Slip map of the other five scenarios simulated. From figure (a) to (e), the scenarios 1a, 1b, 1c, 3a and 3c are shown. The corresponding isochrones are indicated with black lines.

4. Boundary Value Problem

4.1. Coupled formulation

Let the particles of the medium move with velocity $[v]$. In an infinitesimal time dt, the medium experiences an infinitesimal strain determined by the translations $v_i\, dt$ and the corresponding components of the strain-rate tensor, ξ, may be written as:

$$\xi_{ij} = \frac{1}{2}\left(v_{i,j} + v_{j,i}\right) \tag{4.1}$$

where partial derivatives are taken with respect to components of the current position vector $[x]$.

The equations of motion (4.7), together with the definitions (4.1) of the rates of strain, constitute nine equations in fifteen unknowns (6 + 6 components of the stress and strain rate tensors and 3 components of the velocity vector). Six additional relations are provided by the constitutive equations that define the behavior of the particular material at hand. Soil behavior is usually expressed in the form:

$$[\breve{\sigma}]_{ij} = H_{il}\left(\sigma_{ij}, \xi_{ij}, \kappa\right) \tag{4.2}$$

in which $\left[\breve{\sigma}_{ij}\right]$is the co-rotational stress-rate tensor, $[H]$ is a function of stress (σ_{ij}), strain-rate (ξ_{ij}) and history of loading (κ). The co-rotational stress rate $[\breve{\sigma}]$ is equal to the material derivative of the stress as it would appear to an observer attached to the material point and rotating with it at an angular velocity equal to the instantaneous angular velocity $[\omega]$ of the material. Its components are defined as:

$$[\breve{\sigma}]_{ij} = \frac{d\sigma_{ij}}{dt} - \omega_{ik}\sigma_{kj} + \sigma_{ik}\omega_{kj} \tag{4.3}$$

in which $d[\sigma\,]/dt$ is the material time derivative of $[\sigma\,]$, and $[\omega]$ is the rate of rotation tensor.

The differential equations describing the fluid-mechanical response of a porous multi-phase material are summarized below.

4.1.1. Darcy's Law

The fluid transport is described by Darcy's law and for a homogeneous, isotropic solid and constant fluid density, this law is given in the form:

$$q_i = -k_{il}\,\hat{k}_{(s)}\left[p - \rho_f\, x_j\, g_j\right]_l \tag{4.4}$$

where q_i is the specific flow vector, p is pore pressure, k is the tensor of absolute permeability of the medium, $\hat{k}_{(s)}$ is the relative permeability which is a function of fluid saturation s, ρ_f is the fluid density, g_i is i-th component of the gravity vector g. For saturated/unsaturated flow the air pressure is assumed to be constant and equal to zero.

4.1.2. Balance Laws

For small deformations, the fluid mass balance may be expressed as

$$-q_{i,i} + q_v = \frac{\partial \zeta}{\partial t} \tag{4.5}$$

where q_V is the volumetric fluid source in [1/sec], and ζ is the variation of fluid content or variation of fluid volume per unit volume of porous material due to diffusive fluid mass transport, as introduced by Biot (1956).

The balance of momentum has the form:

$$\sigma_{ij,i} + \rho g_i = \rho \frac{dv_i}{dt} \tag{4.6}$$

where $\rho = (1-n)\rho_S + n\, s\, \rho_W$ is the bulk density, and ρ_S and ρ_W are the densities of the solid and fluid phase, respectively. Note that $(1-n)\rho_S$ corresponds to the dry density of the matrix, ρ_d (i.e., $\rho = \rho_d + n\, s\, \rho_w$).

If the acceleration dv/dt is zero the equation (4.6) provides static equilibrium of the medium, and so it reduces to:

$$\sigma_{ij,j} + \rho g i = 0 \tag{4.7}$$

4.1.3. Equilibrium equation of the liquid phase

The variables that govern the fluid diffusion in a porous medium are the pore pressure, p, saturation, s, and mechanical volumetric strains, ϵ. In particular, the response equation for the pore fluid constitutive equation is formulated as:

$$\frac{1}{M}\frac{\partial p}{\partial t}+\frac{n}{s}\frac{\partial s}{\partial t}=\frac{1}{s}(q_v-q_{i,i})-\alpha\frac{\partial \epsilon}{\partial t} \tag{4.8}$$

where n is the porosity, M is the Biot modulus [N/m^2] and α is the Biot coefficient (Appendix C).

The coupled deformation-diffusion process is formulated within the framework of the quasi-static Biot theory. Various types of fluids, including gas and water, can also be represented.

4.1.4. Range of applicability of the different coupled formulations

Zienkiewicz et al. (1980), starting from the generalized Biot theory, derived two simplified formulations applicable only if the actions induced by the external loads are such that the inertial terms are, all or in part, negligible:

- *u-p formulation*, in which the inertial terms of the fluid displacement relative to soil are neglected;
- *quasi-static or consolidation formulation*, in which all inertial terms are absent.

In relations (4.9), (4.10) and (4.11) display the equilibrium equations of the fluid phase, respectively, for the complete, reduced and quasi-static formulation:

<u>*complete*</u>

$$-p_{,i}+\rho_f g_i=k_{ij}^{-1}\dot{w}_i+\rho_f\ddot{u}_i+\rho_f\frac{\ddot{w}_i}{n} \tag{4.9}$$

<u>*u-p*</u>

$$(k_{ij}p_{,j})_{,i}-\dot{\varepsilon}_{ii}-(k_{ij}\rho_f g_j)_{,i}=-(k_{ij}\rho_f\ddot{u}_j)_{,i}+n\frac{\dot{p}}{K_f} \tag{4.10}$$

<u>*quasi-static*</u>

$$(k_{ij}p_{,j})_{,i}-\dot{\varepsilon}_{ii}-(k_{ij}\rho_f g_j)_{,i}=n\frac{\dot{p}}{K_f} \tag{4.11}$$

where k is the mean permeability, K_f the water bulk modulus, u the soil displacement and w the relative soil-water displacement.

With reference to the one-dimensional problem shown in Figure 4.1, in which is represented a periodic force $q = \bar{q}e^{i\omega t}$ on the surface of a homogeneous elastic medium on impermeable layer, Zienkiewicz et al. (1980) established the limits of the use of various treatises (Figure 4.2). In particular, they are referred to the dimensionless values: Π_1 function essentially of the permeability (*k*) of the porous medium; Π_2 function of the ratio between the speed of load application (pulsation ω) and the dominant frequency of the system ($1/\hat{T}$). Always in Figure 4.2 have been identified three areas of applicability of the various formulations of the theory of Biot:

- Zone I: slow phenomena, where we can also apply the *quasi-static* formulation (in addition to the other two);

- Zone II: phenomena of average speed, in which we can apply the *reduced u-p* formulation (in addition to complete formulation);

- Zone III: fast phenomena, in which only the complete Biot formulation can be applied.

We can also see that for $\Pi_1 \leq 10^{-2}$ the soil behaviour can be considered completely drained, while the case of behaviour completely undrained we have for $\Pi_1 \geq 10^{-2}$.

The above concepts have been particularized for the application problem of this research, and it has been found that at least a *u-p* formulation must be used. The latter differs from equation (4.11) only for the term $-(k_{ij}\rho_f\ddot{u}_j)_{,i}$.

A simple algorithm that added up step by step on the pore pressure of the single node the $-(k_{ij}\rho_f\ddot{u}_j)_{,i}$ value, calculated with reference to the values of the previous step, was developed to switch the *u-p* formulation, starting from the quasi-static case (4.11).

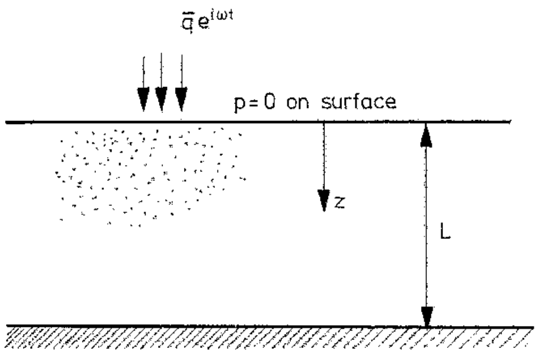

$$p = 0 \qquad z = 0$$

$$\begin{matrix} u = 0 \\ \mathrm{d}p/\mathrm{d}z = 0 \end{matrix} \quad \text{or} \quad \left.\begin{matrix} u = 0 \\ w = 0 \end{matrix}\right\} \quad z = L$$

$\beta = \dfrac{\rho_f}{\rho}$	ratio between fluid density (ρ_f) and bulk density of bi-phase medium (ρ)
$\omega = \dfrac{2\pi}{T}$	angular frequency;
T	period of pulsation;
$\hat{T} = \dfrac{2L}{V_c}$	natural period of the system;
L	characteristic length of the system;
$V_c = \sqrt{\dfrac{E_{oed} + M}{\rho}}$	compression wave velocity in saturated porous medium;
E_{oed}	oedometric stiffness;
M	Biot modulus;
$\Pi_1 = \dfrac{kV_c^2}{g\beta\omega L^2} = \dfrac{2}{\beta\pi}\dfrac{k}{g}\dfrac{T}{\hat{T}^2}$;	
$\Pi_2 = \pi^2\left(\dfrac{T}{\hat{T}}\right)^2$.	

Figure 4.1 Scheme of the model analyzed by Zienkiewicz et al. (1980). Homogeneous layer subject at a periodic force on the surface.

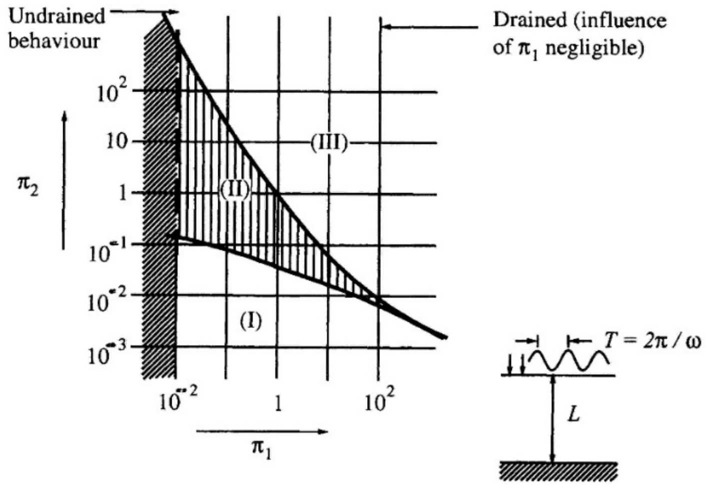

Figure 4.2 Areas of validity for different formulations of the Biot theory. (Zienkiewicz et al, 1980).

4.2. Soil constitutive law

Soils can rarely be described as ideally elastic or perfectly plastic, but simple elastic and plastic models form yet the basis for the most traditional geotechnical engineering calculations. With the advent of cheap powerful computers the possibility of performing analyses based on more realistic models has become widely available. One of the aims of this paragraph is to describe the basic ingredients of a soil model and to demonstrate pro and cons of different type of soil models in numerical analyses. Such analyses are often regarded as mysterious black boxes but a proper appreciation of their worth requires an understanding of the features of the constitutive models on which they are based.

4.2.1. Simplified models

4.2.1.1. Hysteretic model

The equivalent-linear method has been in use for many years to calculate wave propagation (time histories and response spectra) in soil and rock under seismic excitation. The method does not *directly* capture any nonlinear effects because it assumes linearity during the solution process; strain-dependent modulus and damping functions are only roughly taken into account considering an equivalent deformation for the entire signal (as in Shake, QUAD4, etc.), in order to approximate some *effects* of nonlinearity (damping and material softening). Although fully nonlinear codes (e.g. Abaqus, Diana, GeoMadrid for FEM code, and Flac for DEM) are capable - in principle - of modeling the correct physics, they are difficult to be applied in routine computations. One reason is that the available constitutive models are too complicated and, then, there is the need for a long calibration process to define all parameters.

A further motivation to use a hysteretic damping model is to overcame the need for additional damping to avoid numerical spurious oscillation.

Formulation

Nonlinear stress/strain response implies stiffness modulus degradation. If we consider an ideal soil, in which the stress depends only on strain (not on the number of cycles or time), we can derive an incremental constitutive relation from the degradation curve, described by $\frac{\bar{\tau}}{\gamma} = M_s$, where $\bar{\tau}$ is the normalized (on G_0) shear stress, γ is the shear strain and M_S is the normalized secant modulus.

$$\bar{\tau} = M_s\gamma \tag{4.12}$$

Once defined the normalized secant modulus, the normalized tangent modulus may be written as:

$$M_t = \frac{d\bar{\tau}}{d\gamma} = M_s + \gamma\frac{dM_s}{d\gamma} \tag{4.13}$$

The incremental shear modulus in a nonlinear simulation is then given by $G_0 * M_t$, where G_0 is the small-strain shear modulus of the material.

Note that the Masing rule is used when applying the formulation presented in (4.13). For the first loading cycle, both stress and strain axes are scaled by one-half compared to those for subsequent cycles.

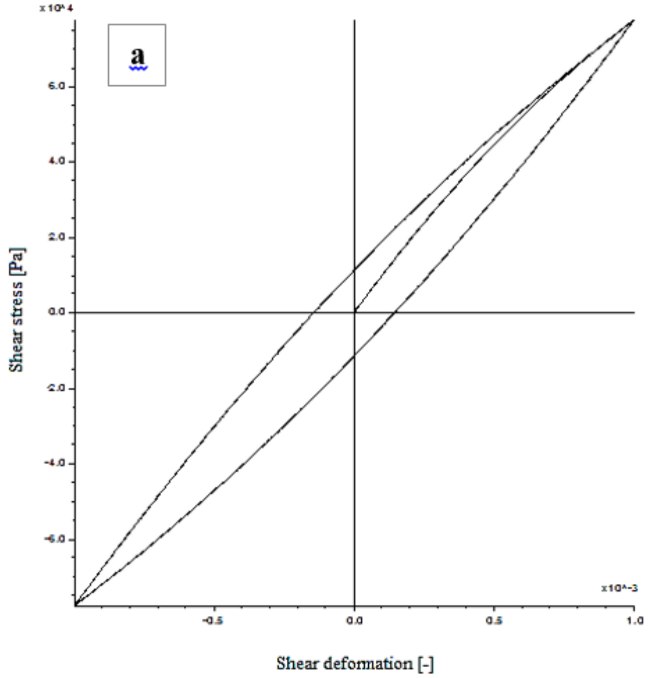
a
x10^4
6.0
4.0
2.0
0.0
-2.0
-4.0
-6.0
Shear stress [Pa]
x10^-3
-0.5
0.0
0.5
1.0
Shear deformation [-]

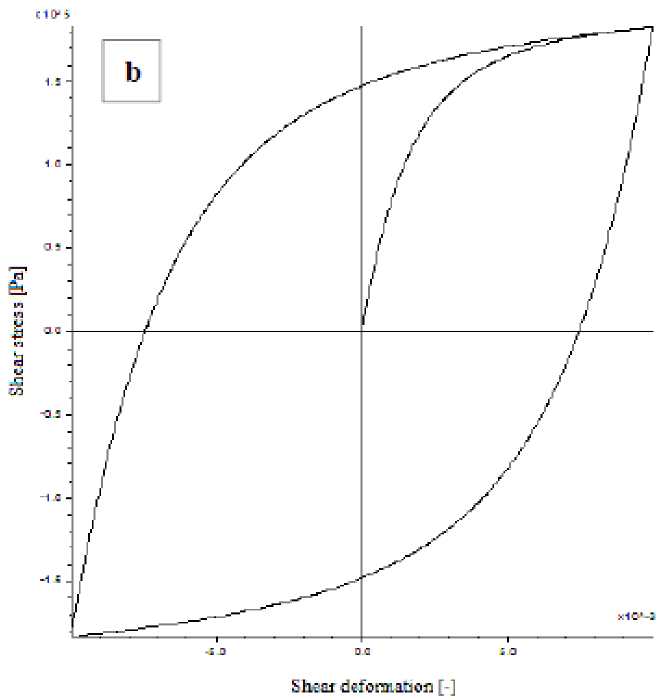
b
1.5
1.0
0.5
0.0
-0.5
-1.0
-1.5
Shear stress [Pa]
-5.0
0.0
5.0
Shear deformation [-]

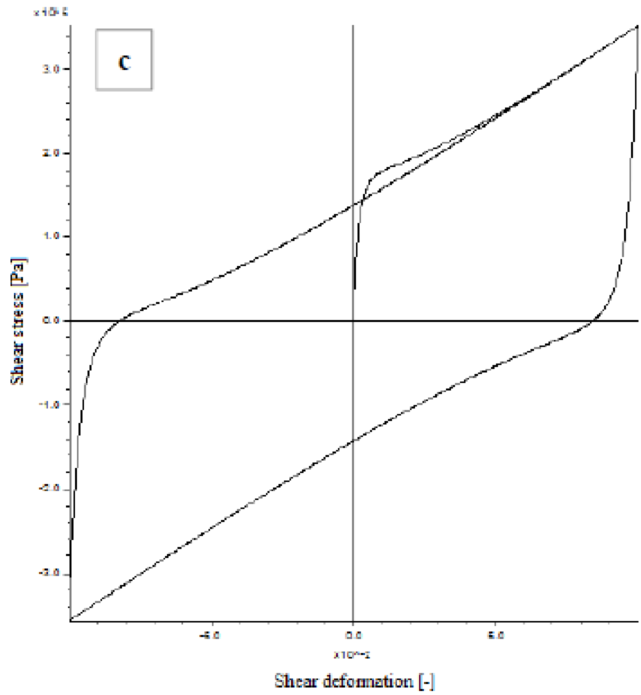

Figure 4.3 Shear stress vs shear strain predicted by mens the hysteretic model for three different imposed shear strains: (a) 0.1%, (b) 1% and (c) 10%.

Many hysteresis models are developed by noting that the S-shaped curve of modulus versus logarithm of cyclic strain can be represented by sigmoidal curves.

The sigmoidal curves are monotonic within the defined range of strains and have the appropriate asymptotic behavior, this makes the functions well-suited for the purpose of representing modulus degradation curves. In this model formulation, the secant modulus, M_S, can be expressed as:

$$M_s = y_o + \frac{a}{1 + exp(-(L - x_o)/b)} \tag{4.14}$$

where a, b, x_O and y_O are parameters regulating the curvature and position of the $G/G_0 - \gamma$ curve, to calibrate on experimental data. In equation (4.14), the strain variable is hidden in L which is logarithmic strain with base 10.

4.2.1.2. Damage Model

Under seismic loads, irreversible volumetric strains of the soil skeleton may occur due to grain rearrangement. If the voids are filled with fluid, then the pressure of the fluid increases, and the effective stress acting in the soil decreases.

This mechanism has been modelling by Finn (1975), and later noted by Byrne (1991) who provided a simplified version of the Finn empirical equation, that relates the increment of volume decrease, $\Delta\epsilon_{vd}$, to the cyclic shear-strain amplitude, γ:

$$\frac{\Delta\epsilon_{vd}}{\gamma} = C_1 exp\left(-C_2\left(\frac{\Delta\epsilon}{\gamma}\right)\right) \tag{4.15}$$

where C_1 and C_2 are model parameters. The author suggests to express C_2 as function of C_1, according to $C_2 = \frac{0.4}{C_1}$, so (4.15) that only one parameter is required. Byrne (1991) has noted that, C_1, can be derived from relative densities, D_r, as follows.

$$C_1 = 7600(D_r)^{-2.5} \tag{4.16}$$

Further, using an empirical relation between D_r and the normalized standard penetration test values, $(N_1)_{60}$:

$$D_r = 15(N_1)^{1/2}{}_{60} \tag{4.17}$$

then,

$$\mathrm{C_1} = 8.7(\mathrm{N_1})^{-1.25}{}_{60} \tag{4.18}$$

In the three-dimensional case (4.15) should be expressed in tensorial notation. The six strain components are as follows:

$$\epsilon_1 = \epsilon_1 + \Delta \mathrm{e}_{12} \tag{4.19}$$

$$\epsilon_2 = \epsilon_2 + \Delta \mathrm{e}_{23} \tag{4.20}$$

$$\epsilon_3 = \epsilon_3 + \Delta \mathrm{e}_{31} \tag{4.21}$$

$$\epsilon_4 = \epsilon_4 + \frac{(\Delta \mathrm{e}_{11} - \Delta \mathrm{e}_{22})}{\sqrt{6}} \tag{4.22}$$

$$\epsilon_5 = \epsilon_5 + \frac{(\Delta e_{22} - \Delta e_{33})}{\sqrt{6}} \tag{4.23}$$

$$\epsilon_6 = \epsilon_6 + \frac{(\Delta e_{33} - \Delta e_{11})}{\sqrt{6}} \tag{4.24}$$

Denoting the previous point by superscript ($^{\circ}$), and the one before that with ($^{\circ\circ}$), the previous unit vector, n_i^o , in strain space is computed:

$$v_i = \epsilon_i^o - \epsilon_i^{oo} \tag{4.25}$$

$$z = \sqrt{v_i v_i} \tag{4.26}$$

$$n_i^o = \frac{v_i}{z} \tag{4.27}$$

where subscript *i* takes the values 1 to 6, and repeated indices imply summation.

The projection *d* of the new vector, $\epsilon_1 - \epsilon_i^o$, from the old point to the new point is given by the dot product of the new vector with the previous unit vector:

$$d = (\epsilon_1 - \epsilon_i^o) n_i^o \tag{4.28}$$

Using the rule that *d* must be negative, the new strain segment corresponds to a reversal compared to the previous segment. It is important to monitor the absolute value of *d* and do the following calculation when it passes through a maximum, d_{max}, provided that a minimum number of timesteps has elapsed (to prevent the reversal logic being triggered again on transients that immediately follow a reversal). This threshold number of timesteps is controlled by the latency, which is set to 50.0 in the runs.

$$\gamma = d_{max} \tag{4.29}$$

$$\epsilon_i^{oo} = \epsilon_i^o \tag{4.30}$$

$$\epsilon_i^o = \epsilon_i \tag{4.31}$$

Having obtained the engineering shear strain, we insert it into (4.15) and obtain $\Delta\epsilon_{vd}$. It is then possible to update ϵ_{vd}, as follows, and save it for use in (4.15).

$$\epsilon_{vd} = \epsilon_{vd} + \Delta\epsilon_{vd} \tag{4.32}$$

We also save one-third of $\Delta\epsilon_{vd}$ and revise the direct strain increments input to the model at the next cycle:

$$\Delta\epsilon_{11} = \Delta\epsilon_{11} + \frac{\Delta\epsilon_{vd}}{3} \tag{4.33}$$

$$\Delta\epsilon_{22} = \Delta\epsilon_{22} + \frac{\Delta\epsilon_{vd}}{3} \tag{4.34}$$

$$\Delta\epsilon_{33} = \Delta\epsilon_{33} + \frac{\Delta\epsilon_{vd}}{3} \tag{4.35}$$

One effect that has been shown to be very important is the effect of rotation of principal axes: volume compaction may occur even though the magnitude of deviatoric strain (or stress) is kept constant. Such rotations of axes occur frequently in earthquake situations.

4.2.2. Advanced soil constitutive models: overview

A constitutive model is a mathematical description of the stress–strain relationship for a given material. Conventional plasticity models require the definition of: (i) the yield surface, (ii) the flow rule or plastic potential and (iii) the hardening rule including strain hardening and yield surface translation rules. The complexity of a constitutive model depends on the type of material to be simulated. However, unlike structural materials (e.g., concrete, steel), soil behaviour is governed by the presence of water in addition to solid (soil particles). The complex nature of clays cannot be simulated satisfactory by simple models (e.g., von Mises, Mohr-Coulomb), as their behavior is known to be dependent on confining pressure and over-consolidation ratio (OCR), and they exhibit a significant degree of anisotropy in the in-situ state. The dependence on confining pressure and to some extent on OCR can be simulated by the Modified Cam-Clay model (MCC) (Roscoe and Burland, 1966), which is based on Critical State Soil Mechanics (CSSM) theory developed at Cambridge University (Roscoe and Poorooshasb, 1963; Roscoe et al., 1963, 1958).

Over the years, a number of constitutive models have been developed to simulate the cyclic loading of cohesive and non-cohesive soils (with emphasis, for these last, on cyclic mobility and/or flow liquefaction), which may be divided into several categories depending on their fundamental characteristics, such as multi-surface models (e.g. Iwan, 1967; Mròz, 1967 and 1969; Prevost, 1978; Cubrinovski & Ishihara, 1998; Yang et al., 2003; Yang & Elgamal, 2008), two-surface models (e.g. Poorooshasb & Pietruszczak, 1986; Manzari & Dafalias, 1997; Gajo & Wood, 1999; Papadimitriou et al., 2001; Papadimitriou & Bouckovalas, 2002; Loukidis & Salgado, 2009), bounding surface models (e.g. Hachiguchi & Ueno, 1977; Wang et al., 1990; Li et al., 1999, Li, 2002) and generalized plasticity models (e.g. Pastor et al., 1990; Iai et al., 1992; Ling & Liu, 2003; Ling & Yang, 2006). Furthermore, there are models that are built on classical elastoplasticity by complementing it with key constitutive concepts, like the multi-laminate concept (e.g. Park & Byrne, 2004), an endochronic densification law (e.g. Lopez-Querol & Blazquez, 2006), the middle surface concept (e.g. Yang et al., 2006), the disturbed state concept (e.g. Park & Desai, 2000) and the multiple-mechanism concept (e.g. Aubry et al., 1982; Hujeux, 1985; Aubry et al., 1990). In addition to the above, there are models that go beyond elastoplasticity, like the hypoplastic ones (e.g. Bauer & Wu, 1993). These models postulate that the stress-strain rate relationship depends not only on the current stress state but also on the stress rate itself. In accordance with this concept, the dependence of the plastic strain rate direction on the stress rate direction has been introduced. Hypoplastic constitutive models have been developed since 1980's and now they have established a solid base for an alternative description of soil behaviour, without an explicit definition of yield and potential surfaces (Pastor et al., 1990). Recent hypoplastic models (Iai et al., 1992; Yang et al., 2003) include the concept of critical states and have been successfully adopted for solving different boundary value problems within coarse-grained soils. The progress of hypoplastic models for fine-grained soils has been delayed. Rate-dependent (Li et al. 1999; Yang & Elgamal, 2008) and rate-independent (Manzari & Dafalias, 1997; Papadimitriou et al., 2001) hypoplastic models for clays may be very promising.

One of the main aspects of soil behaviour, incorporated in many elasto-plastic constitutive models, is the presence of a surface in the stress-porosity space which bounds all possible stress states (state boundary surface). Hypolastic models do not incorporate the state boundary surface explicitly in the mathematical formulation. However, as demonstrated by Hashiguchi & Ueno (1977) for a particular hypoplastic model developed for clay, state boundary surface is implicitly predicted by the constitutive equation.

Iwan (1967) and Mròz (1967, 1969) independently, have been the first to introduce models with several surfaces, enclosing each other, of progressively larger size. As the stress point reaches a larger surface, the stiffness reduces, resulting in increased hysteretic work. A bounding surface framework, presented for metals by Dafalias and Popov (1975) and then incorporated for soils by Dafalias (1986b), Dafalias and Herrmann (1986), and Anandarajah and Dafalias (1986), is another approach to simulate plastic deformations within the yield surface. Unlike in the models by Iwan and Mròz, stiffness change within the yield surface is continuous in the bounding surface formulation. In addition, the formulation does not require storing in memory a finite number of surfaces for better simulation of stiffness reduction for the stress states inside the yield surface.

The bounding surface framework is popular due to its simplicity and has been incorporated into different models to simulate soil response. In the bounding surface formulation, the yield surface is replaced by a bounding surface, which accounts for loading history. The bounding surface allows development of plastic deformation for the stress states inside it. A Simple ANIsotropic CLAY plasticity (SANICLAY) model developed by Dafalias (1986a), Dafalias et al. (2006) allows simulations of induced anisotropy by incorporation of rotational and distortional hardening in a so-called yield surface, which encloses the very small elastic domain.

Although these models present the foregoing differences in their fundamental characteristics, the most recent ones usually share constitutive ingredients that have offered improved simulations. Specifically, since the mechanical response of sand is characterized by infinite normal consolidation lines (NCL) depending on the initial conditions of void ratio and confining pressure, the critical state constitutive models that retained the unique NCL idealization from clay response had difficulties in producing quantitatively accurate simulations for all initial conditions. Hence, the introduction of the state parameter ψ of Been & Jefferies (1985) in constitutive equations, either implicitly (by Jefferies, 1993, for monotonic loading) or explicitly (by Manzari & Dafalias, 1997, for both monotonic and cyclic response), allowed the use of a single set of model constants for successful simulations for any initial void ratio or confining pressure. Thereafter, this concept has been implemented in many constitutive models regardless of their fundamental characteristics (e.g. the bounding surface model of Li et al. (1999), the two-surface model of Papadimitriou & Bouckovalas (2002), Dafalias & Manzari (2004) and the generalized plasticity model of Ling & Yang (2006)).

In addition, various functions of integrals of strain histories during the shearing phase have appeared in the literature as scalar multipliers of the plastic modulus (e.g. in the generalized plasticity model of Pastor et al., 1990). Such a plastic modulus multiplier was first explicitly related to evolving sand fabric by Papadimitriou (1999) and Papadimitriou et al. (1999) in their integrated approach to account, not only for the densifying effect related to contractive phases of shearing, but also for the opposite effects related to dilation. In parallel, focusing merely on sand fabric evolution due the dilation, Dafalias & Manzari (1999) proposed a scalar multiplier of the dilatancy aiming primarily on accurately simulating the cyclic mobility phase of shearing. This constitutive concept related to evolving sand fabric has continued to appear in the literature, in different forms of scalar multipliers of either the plastic modulus (e.g. in generalized plasticity models by Ling & Liu, 2003; Ling & Yang, 2006; in two-surface models

Papadimitriou et al., 2001; Papadimitriou & Bouckovalas, 2002), or of the dilatancy (e.g. in multi-surface models Yang et al., 2003; Yang & Elgamal, 2008; in two-surface models Dafalias & Manzari, 2004), or as an endochronic densification law (Lopez-Querol & Blazquez, 2006).

Given the foregoing recent advances, many constitutive models are now able to simulate the hysteretic response of sands for small to medium shear strains (Vucetic, 1994) and to reproduce the excess pore pressure build-up in undrained loading under large cyclic shear strains, as well as the well-known ‘‘butterfly’’ shaped loops in the effective stress path that are related to cyclic mobility. Nevertheles, quantitative accuracy of the response for all cyclic strain levels with the same set of model constants has been demonstrated by Papadimitriou et al. (2001) and Papadimitriou & Bouckovalas (2002), who adopted the constitutive two-surface model of Manzari & Dafalias (1997), and introduced two key constitutive elements: (a) a Ramberg-Osgood type non-linear hysteretic formulation of the “elastic” moduli, that governs shear modulus degradation and hysteretic damping increase for small to medium cyclic shear strains, and (b) a scalar multiplier of the plastic modulus, as defined in Papadimitriou et al. (1999) and Dafalias & Manzari (2009), which governs soil response from medium to large cyclic shear strains.

Although many plasticity based models have been proposed for soils, alternative approaches, same in contrast with the plasticity theories were developed such as these based on thermodynamic frameworks (Coleman and Gurtin, 1967 and Lubliner, 1972).

Ziegler (1983) introduced the concept that a constitutive model of a deformable solid may be completely defined by the use of two potential functions: energy and dissipation. These two functions allow the constitutive low to be written in a compact and consistent framework for the computation of the stress-strain response. Collins and Houlsby (1997) developed an approach called “hyperplasticity” theory which adopts Ziegler’s concept. These hyperplastic models have been developed only in the late 90s and even now encounter many difficulties to replace more established theories, such as the Generalized and Bounding Surface Plasticity models.

A summary of the main aspect of the Generalized and Bounding Surface Plasticity will be reported, following the work of Zienkiewicz et al. (1999) and Papadimitriou et al. (2001), respectively.

4.2.2.1. Generalized plasticity

In the following, boldface characters will be used for tensors, uppercase (such as D) denoting fourth-order tensors D_{ijkl} and lower case (such as a) for second-order tensors σ_{ij}.

It is convenient to use a vector matrix representation of tensorial magnitudes in numerical computations; fourth-order tensors corresponding to matrices and second order tensors to vectors.

The convention for products and its matrix equivalence is:

$$A{:}B \equiv A_{ijkl}B_{ijkl} \quad \text{vs} \quad AB \equiv A_{ij}B_{ij} \tag{4.36}$$

Double dot denotes contracted product in last two indexes.

The response of the material does not depend on the velocity, whereby the stress varies the relationship between the increments of stress and strain can be written as:

$$d\epsilon = \Phi(d\sigma) \tag{4.37}$$

Where Φ is a function of the increment of the stress tensor $d\sigma$ and variables describing the "state" (or history) of the material. This is a general relation embracing most nonlinear, rate-independent constitutive laws.

An inverse form is:

$$\mathrm{d}\sigma = \Psi(\mathrm{d}\epsilon) \tag{4.38}$$

As the material response does not depend on time,

$$\lambda d\epsilon = \Phi(\lambda d\sigma)$$

where $\lambda \in \Re_+$ is a positive scalar (Darve 1990).

Consequently, Φ is a homogeneous function of degree 1, which can be written as:

$$\Phi = \frac{\partial \Phi}{\partial (d\sigma)}{:}\, d\sigma \tag{4.39}$$

from which the increments of stress and strain are related by:

$$\begin{aligned} d\epsilon &= C{:}\, d\sigma \\ d\sigma &= D{:}\, d\epsilon \end{aligned} \tag{4.40}$$

where:

$$C = \frac{\partial \Phi}{\partial (d\sigma)} \tag{4.41}$$

is a fourth-order tensor, homogeneous, of degree zero in $d\sigma$. Before continuing, some basic properties of *C* will be described.

We will consider a uniaxial loading-unloading-reloading test schematized in Figure 4.4 where the Constitutive tensor *C* is a scalar, the inverse of the slope at the point C.

As can be seen, the slope depends on the stress level, being smaller at higher stresses. However, if we compare the slopes at points A_1, A_2 and A_3, they are not the same, and *C* depends on past history (stresses, strains, modification of material microstructure, etc.)

Taking a closer look at point C, it can be seen that, for a given point, different slopes are obtained in "loading" and "unloading", which implies a dependence on the direction of stress increment.

This dependence is only on the direction, as *C* is a homogeneous function of degree zero on $d\sigma$.

Therefore, in this simple one-dimensional case, it is possible to write for loading:

$$d\epsilon_L = C_L : d\sigma \tag{4.42}$$

and for unloading:

$$d\epsilon_U = C_U : d\sigma$$

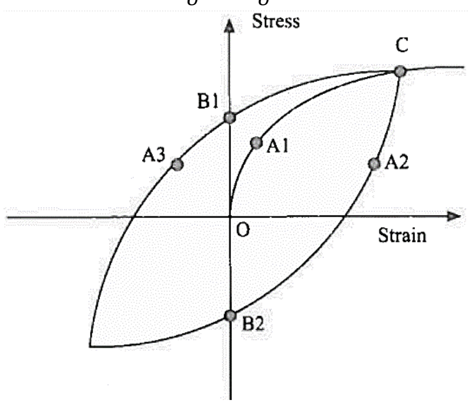

Figure 4.4 General stress-strain behaviour (Zienkiewicz et al, 1999).

If we consider an infinitesimal cycle followed by $d\sigma$, the total change of strain is not zero. This kind of constitutive law, (4.43), has been defined by Darve (1990) as incrementally non-linear.

$$d\epsilon \quad = d\epsilon_L + d\epsilon_U = (C_L - C_U) : d\sigma \neq 0 \tag{4.43}$$

There are several alternatives to introduce the dependence on the direction of the stress increment, among which it is worth mentioning the multilinear laws proposed by Darve and co-workers in Grenoble (Darve and Labanieh, 1982), or the hypoplastic laws of Dafalias (1986) or Kolymbas (1991). However, the simplest consists of defining in the stress space a normalized direction n for any given state of stress, such that all possible increments of stress are separated into two classes, loading and unloading:

$$\begin{aligned} d\epsilon_L &= C_L : d\sigma \quad \text{for} \quad n : d\sigma > 0 \qquad \text{(loading)} \\ d\epsilon_U &= C_U : d\sigma \quad \text{for} \quad n : d\sigma < 0 \qquad \text{(unloading)} \end{aligned} \tag{4.44}$$

Neutral loading corresponds to the limit case for which:

$$\boldsymbol{n} : \boldsymbol{d\sigma} = \boldsymbol{0} \tag{4.45}$$

This is the starting point of the Generalized Theory of Plasticity, introduced by Zienkiewicz and Mroz (Mroz & Zienkiewicz, 1985) and later extended by Pastor and Zienkiewicz (Zienkiewicz, Leung & Pastor, 1985; Pastor et al., 1985, Pastor; Zienkiewicz & Chan 1990).

Introduction of this direction discriminating between loading and unloading defines a set of surfaces which is equivalent to those used in Classical Plasticity as will be shown later, but these surfaces need never be explicitly define.

Continuity between loading and unloading states requires that constitutive tensors for loading and unloading are of the form:

$$C_L = C^e + \frac{1}{H_L} n_{gL} \cdot n \tag{4.46}$$

and

$$C_U = C^e + \frac{1}{H_U} n_{gU} \cdot n \tag{4.47}$$

where n_{gL} and n_{gU} are tensors of unit norm, different for each model because regulate the behavior of them, and $H_{L/U}$ two scalar functions defined as loading and unloading plastic moduli.

The strain increment can be decomposed into two parts:

$$d\epsilon = d\epsilon^e + d\epsilon^p \tag{4.48}$$

If C^e is elastic tensor, one obtained:

$$d\epsilon^e = C^e + d\sigma \tag{4.49}$$

and

$$d\epsilon^p = \frac{1}{H_{L/U}}\left(n_{gL/U} \cdot n\right): d\sigma \tag{4.50}$$

We note that irreversible plastic deformations have been introduced without the need for specifying any yield or plastic potential surfaces, nor hardening rules. All that is necessary to specify are two scalar functions $H_{L/U}$ and three directions, $n_{gL/V}$ and n.

To account for softening behaviour of the material, i.e., when H_L is negative, definitions of loading and unloading have to be modified as follows:

$$\begin{aligned} d\epsilon_L &= C_L: d\sigma \quad \text{for} \quad n: d\sigma^e > 0 \; (loading) \\ d\epsilon_U &= C_U: d\sigma \quad \text{for} \quad n: d\sigma^e < 0 \; (loading) \end{aligned} \tag{4.51}$$

where $d\sigma^e$ is given by:

$$d\sigma^e = (C^e)^{-1}: d\epsilon \tag{4.52}$$

In the case of cyclic loading, to obtain the values of H_L, n and n_g, suitable interpolation rules are used. In particular, n is interpolated from $-n$ to n using a linear law. The direction of plastic flow is obtain again by defining a suitable dilatancy at C, d_{Cg} which is interpolated from an initial value d_{g0} to:

$$d_{gD} = (1+\alpha)\left(M_g - \eta_D\right) \tag{4.53}$$

The initial value of the dilatancy at the reversal point d_{g0} is given by:

$$d_{g0} = (1+\alpha)\left(M_g - C_g\eta_B\right) \tag{4.54}$$

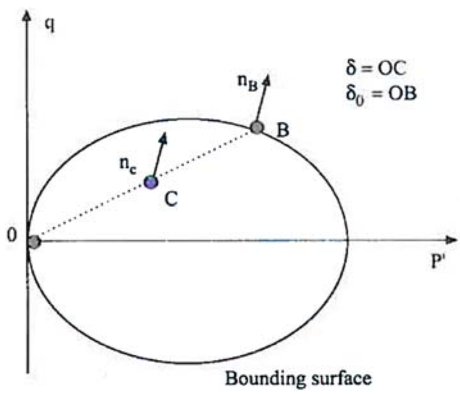

Figure 4.5 Interpolation rule with reference at plastic surface. Zienkiewicz et al, 1999).

Where the constant C_g ($0 < C_g < 1$) varies with the density, being dose to zero for medium-loose sands.

The plastic modulus is interpolated between an initial value H_{u0} and its final value at the image point on the mobilized stress surface H_D.

The initial value can be assumed to be infinite to decrease a possible accumulation of plastic strain under very low amplitude cycles.

$$H = H_{U0} + f(H_D - H_{U0}) \tag{4.55}$$

where f is an interpolation function depending on the relative position of the points B, C and D and which is 1 when C and D coincide. Concerning the rule to obtain the image stress point D, there are several alternative possibilities. For instance, it can be obtained as the intersection of the straight line joining the reversal and the stress point with the mobilized stress surface, as depicted in Figure 4.6.

This interpolation law provides a smooth transition between unloading to reloading. In fact, unloading may be considered as a new loading process. It is important to remark that direction of plastic flow and unit vector n will not be functions of the stress state only, but of the past history as well.

4.2.2.2. Bounding surface: theory and model

If the number of surfaces is reduced to two, i.e., the outer or consolidation and the inner or yield, a field of hardening moduli can still be described by prescribing the variation between both surfaces. This model was independently proposed by Krieg (1975) and Dafalias and Popov (1975), and evolved to what is known today as "Bounding Surface Theory" (Dafalias and Herrmann, 1982; Dafalias, 1986; Wang Dafalias and Sben 1990; Kaliakin and Dafalias 1989 and Bardet, 1989).

A similar approach, the "sub-loading surface model" was proposed by Hashiguchi and Ueno (1977) and Hashiguchi, Imamura and Ueno (1989).

On the bounding surface, plastic strain develops according to classical plasticity theory, with directions n and n_g given by the normals to the bounding and plastic potential surfaces, and the plastic modulus obtained through application of the consistency condition describing material hardening or softening properties. In the case of loading processes beginning at the bounding surface, the results coincide with those of classical plasticity. However, for loading processes inside it, such as many occur in cyclic loading, the difference is that bounding surface models are able to introduce plastic deformations by using some interpolation rules relating the stress point C (Figure 4.6) to an image P_{BS} of it on the BS (Figure 4.6). Simple interpolation rules were proposed by Dafalias and Herrmann (1982), and by Zienkiewicz, Leung and Pastor (1985).

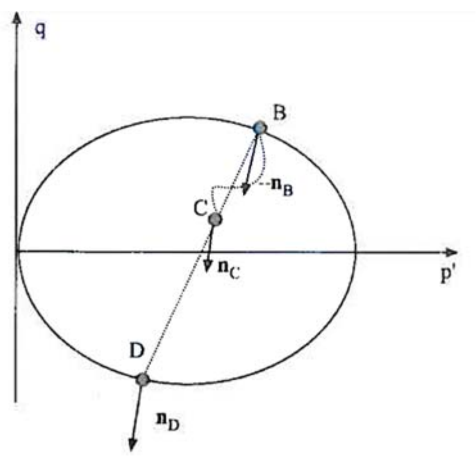

Figure 4.6 Bounding surface interpolation rule. (Zienkiewicz et al, 1999).

Then, to obtain the image point P_{BS}, a line was drawn passing through the origin and point P, its intersection with the bounding surface being taken as the image point. Directions n and n_g in P were assumed to be those at P and the plastic modulus was interpolated according to a simple law:

$$H_L = H_L^{BS} \left(\frac{\delta_0}{\delta}\right)^{\gamma} \tag{4.56}$$

where $\boldsymbol{\delta}$ is the distance from the origin to the stress point P, and $\boldsymbol{\delta_0}$ the distance between the origin and the image point P_{BS}, being a parameter of the model (Figure 4.6).

The main shortcoming of early BS models was their inability to reproduce plastic deformations which develop when unloading, and it was overcome within the more general framework of generalized plasticity (Pastor, Zienkiewicz and Leung, 1985). Hence, the model was of bounding surface type for loading, but plastic deformations during unloading were introduced within the more general framework of generalized plasticity. A further step was given by Pastor, Zienkiewicz and Chan, introducing a full generalized plasticity model in Pastor and Zienkiewicz (1986) and Pastor, Zienkiewicz and Chan (1990), which was applied by the authors to reproduce the behaviour of both cohesive and frictional soils under monotonic and cyclic loading.

Model outline

As shown in Figure 4.7, the yield surface has the form of an open wedge with the apex at the origin of axes, and its yield function is given by (Manzari and Dafalias 1997) where $\boldsymbol{\eta} = \frac{\boldsymbol{q}}{\boldsymbol{p}} = p$ = deviatoric stress ratio; and scalars m and $\boldsymbol{\alpha}$= tangents of angles related to the opening and the location of the bisector of the yield surface, respectively. While m remains constant throughout shearing, the value of $\boldsymbol{\alpha}$ changes for shear paths that cause plastic strains. In other words, isotropic hardening is neglected, while kinematic hardening is incorporated via the evolution of $\boldsymbol{\alpha}$. Scalar s is an auxiliary parameter taking the value of s = +1 when $(\boldsymbol{\eta} - \boldsymbol{\alpha}) \geq \boldsymbol{0}$, and s = -1 in the opposite case. Hence, its use in (4.57) replaces the cumbersome $\pm$ sign, a useful analytical tool for subsequent equations as well.

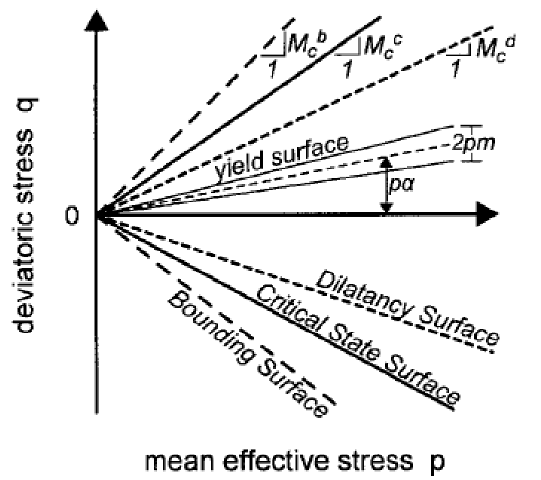

Figure 4.7 Model Surfaces in p-q Space.

$$f = \frac{q}{p} - \alpha \mp \eta - \alpha - sm = 0 \tag{4.57}$$

Besides the yield surface, the model incorporates the use of three more surfaces: the critical state, bounding and dilatancy surfaces. As shown in Figure 4.7, all three surfaces have the form of open wedges with the apex at the origin of the p-q axes. In Figure 4.8, a viewing of the projection on □-plane of the model surfaces is shown.

Their shape for triaxial compression is fully defined by slopes Mc, Mb, and Md (collectively $\boldsymbol{M_c^{c,d,b}}$). Similarly, their shape for triaxial extension is fully defined by slopes $\boldsymbol{M_e^{c,d,b}}$. Following Manzari and Dafalias (1997), slopes $\boldsymbol{M_{c,e}^{c}}$ are constant model parameters. On the contrary, $\boldsymbol{M_{c,e}^{b}}$ and $\boldsymbol{M_{c,e}^{d}}$are continuous functions of $\boldsymbol{M_{c,e}^{c}}$ and the ever-changing value of the state parameter $\boldsymbol{\psi}$ as:

$$M_{c,e}^{b} = M_{c,e}^{c} + k_{c,e}^{b}\langle -\psi \rangle \tag{4.58}$$

$$M_{c,e}^{d} = M_{c,e}^{c} + k_{c,e}^{d}\psi \tag{4.59}$$

where $\boldsymbol{k_{c,e}^{b}}$ and $\boldsymbol{k_{c,e}^{d}}$= model parameters and $\langle \quad \rangle$ are the Macauley brackets yielding: $\langle \boldsymbol{A} \rangle = \boldsymbol{A}$ if $A > 0$ and $\langle \boldsymbol{A} \rangle = \boldsymbol{0}$ if $\boldsymbol{A} \leq \boldsymbol{0}$. It is noted that (4.58) without the Macauley brackets was first proposed by Wood et al. (1994). Although $\boldsymbol{M_{c,e}^{b,d}}$dependence on $\boldsymbol{\psi}$ could be more complicated for greater accuracy [e.g., Li et al. (1999) and Li and Dafalias (2000)], the linear form of (4.58) and (4.59) is considered adequate for the present needs.

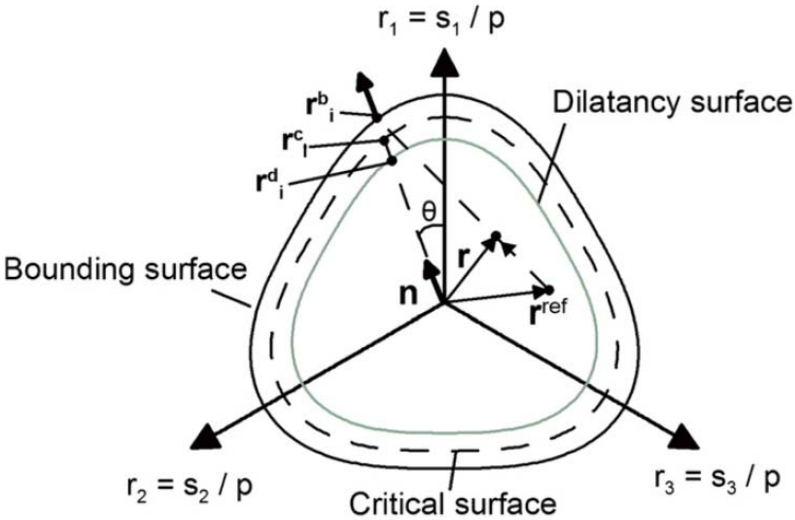

Figure 4.8 Model surfaces and mapping rule in the $\boldsymbol{\pi}$-plane of the deviatoric stress ratio space.

The strain increment $\boldsymbol{d\varepsilon_{p,q}}$ is deconvoluted into $\boldsymbol{d\varepsilon^{e}_{p,q}}$ and $\boldsymbol{d\varepsilon^{p}_{p,q}}$, the elastic and the plastic components. *Alternative* subscripts *p* and *q* denote the volumetric and deviatoric parts of each strain component. For any effective stress increment (*dp*, *dq*), the elastic strains are given by

$$d\varepsilon_q^e = \frac{dq}{3G_t} \tag{4.60}$$

$$d\varepsilon_p^e = \frac{dp}{K_t} \tag{4.61}$$

where K_t and G_t = tangential bulk and shear moduli, respectively.

The plastic strain components are given by

$$d\varepsilon_q^p = s\sqrt{\frac{2}{3}}\langle L\rangle \tag{4.62}$$

$$d\varepsilon_p^p = D\left|d\varepsilon_q^p\right| \tag{4.63}$$

where the scalar D = dilatancy coefficient used to define the flow rule of the formulation, and the scalar L = loading index, given by

$$\boldsymbol{L = s\frac{p}{k_p}d\eta} \tag{4.64}$$

In (4.64), $d\eta$ is the incremental change of the deviatoric stress ratio $\eta = q/p$, and K_p is the plastic modulus. Note that the Macauley brackets in (6) ensure that nonpositive values of L lead to $d\varepsilon_{p,q}^p = 0$. Practically, the sign of L determines the loading conditions: $L > 0$ for loading, $L < 0$ for unloading, and $L = 0$ for neutral loading.

Non-linear hysteretic "elastic" moduli

Departing from Manzari and Dafalias (1997), the tangential elastic moduli K_t and G_t are interrelated via a constant elastic Poisson's ratio $\boldsymbol{\nu}$. Furthermore, G_t decreases smoothly during shearing similarly to the widely used nonlinear hysteretic stress-strain relation of Ramberg and Osgood (1943). In particular, the tangent shear modulus is expressed as

$$G_t = \frac{G_{max}}{T} \tag{4.65}$$

The maximum value of shear modulus G_{max} is given by a generalization of the well-established formula of Hardin (1978) as

$$G_{max} = \frac{Bp_a}{0{,}3 + 0{,}7e^2}\left(\frac{p}{p_a}\right)^{0,5} \tag{4.66}$$

where B = model parameter.

The value of scalar T is given by

$$T = \begin{Bmatrix} \mathbf{1+2\left(\frac{1}{a_1}-1\right)\left(\frac{|\eta-\eta_0|}{\eta_1}\right)}, \textit{first loading} \\ \mathbf{1+2\left(\frac{1}{a_1}-1\right)\left(\frac{|\eta-\eta_{SR}|}{2\eta_1}\right)}, \textit{unload and reload} \end{Bmatrix} \leq \mathbf{1+2\left(\frac{1}{a_1}-1\right)} \quad (4.67)$$

where η_{SR} and η_0= deviatoric stress-ratios at the last shear reversal (SR) and at consolidation, respectively. Scalars a_1 and $\eta_1$are parameters whose physical meaning will be described below. SR for the elastic strain formulation is defined at a point where the deviatoric strain increment $d\varepsilon_q$ changes sign (i.e., when $\left[d\varepsilon_q^{(i)}\ d\varepsilon_q^{(i-1)}\right]$, where (*i-1*) and (*i*) denote successive steps in the forward integration scheme).

For the shear loop of Figure 4.9, which is characterized by a deviatoric stress ratio amplitude $\eta_c \leq \eta$, analytical integration leads to the following expression for the secant shear modulus ratio:

$$\frac{G_s}{G^0_{max}} = \frac{1}{1+\left(\frac{1}{a_1}-1\right)\left(\frac{\eta_c}{\eta_1}\right)} \quad (4.68)$$

Since $\eta_C = (G_S/G^0_{max})(G^0_{max}/p_0)\gamma_c$ and $\eta_1 = 2a_1(G^0_{max}/p_0)\gamma_1$.

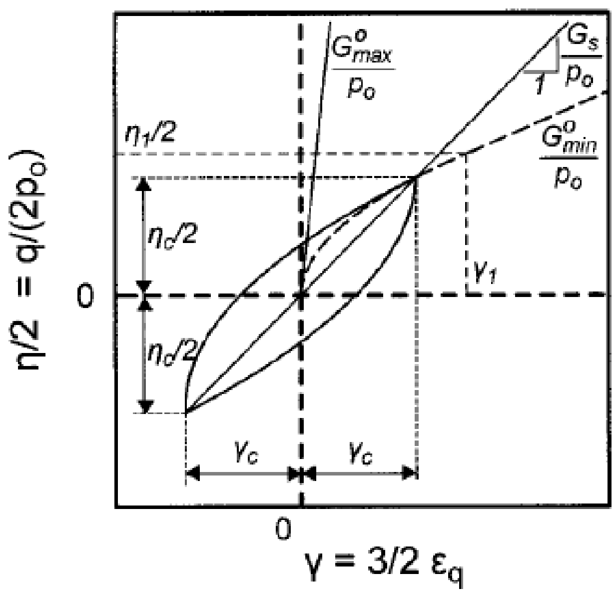

Figure 4.9 Analytical Estimation of Elastic Deviatoric Stress-Strain Relation (*G*max = Const).

Plastic modulus

The plastic modulus K_p in (4.64 is related to the distance from the bounding surface d^d as

$$K_p = p h_b h_f d^b \tag{4.69}$$

The scalar parameters p, h_b, and h_f are nonnegative, so that the sign of K_p is governed by the sign of d^b.

4.3. Dynamic numerical formulation

Numerical distortion of the propagating wave can occur in a dynamic analysis as a function of the modelling conditions. Both the frequency content of the input wave and the wave-speed characteristics of the system will affect the numerical accuracy of wave transmission. Kuhlemeyer and Lysmer (1973) show that, for accurate representation of wave transmission through a model, the spatial element size, Δl, must be smaller than approximately one-tenth to one-eighth of the wavelength associated with the highest frequency component of the input wave:

$$\Delta l \leq \left(\frac{1}{10} \div \frac{1}{8}\right) \lambda_{min} \tag{4.70}$$

where λ_{min} is the wavelength associated with the highest frequency component of the input motion and stiffness property of soil media ($\lambda_{min} = V_S / f_{max}$).

For dynamic input with a high peak velocity and short rise-time, the Kuhlemeyer and Lysmer requirement may necessitate a very fine spatial mesh and a corresponding small timestep. The consequence is that reasonable analyses may be prohibitively time- and memory-consuming. In such cases, it may be possible to adjust the input by recognizing that most of the power for the input history is contained in lower-frequency components. By filtering the history and removing high frequency components, a coarser mesh may be used without significantly affecting the results.

The aspect relative to the timestep determination is faced in detail in the appendix with references to the dynamic soil-fluid coupled formulation (§C.2).

4.3.1. Dynamic loading and boundary conditions

When the ground is modeled with a discrete model using the technique of finite element or finite difference techniques there is the problem to represent an infinite domain with a model of finite size.

Compared to the real domain, the discretized model is delimited by fictitious borders which in the mathematical model should reproduce the same actions coming from the indefinite excluded domain. The problem becomes particularly difficult when dynamic problems should be analyzed, as the boundaries of the model must also ensure the correct transmission of energy outside the discretized domain (radiative condition).

In seismic problems borders must not alter the input signal which generally is applied in the nodes of the lower boundary of the model.

In modeling dynamic problems, the borders may be classified in absorbent or non-absorbent: the former reproduce the radiative condition, the latter not.

Non-absorbent, or elementary bordes, are fixed if they impose a condition of zero displacement (Dirichlet condition) along the border nodes or free if they impose a condition of zero force (Neumann condition).

In the first case, the reflected wave has the same amplitude but opposite phase with respect to the incident wave.

In the second case the reflected wave has the same amplitude and phase of the incident wave.

Viscous frontiers, proposed by Lysmer & Kuhlemeyer (1969), are local borders that absorb only the volume waves (P and S) with plane wave front acting normally to the border. They provide an exact solution for the one-dimensional (vertical) propagation of volume waves in a linear elastic medium.

Viscous boundaries

If a subsoil with horizontal stratification is hit by a plane wave front which propagates in the vertical direction, the problem geometry can be considered one-dimensional.

Assume, also, that the medium is linearly elastic, with a single-phase and neglect volume forces.

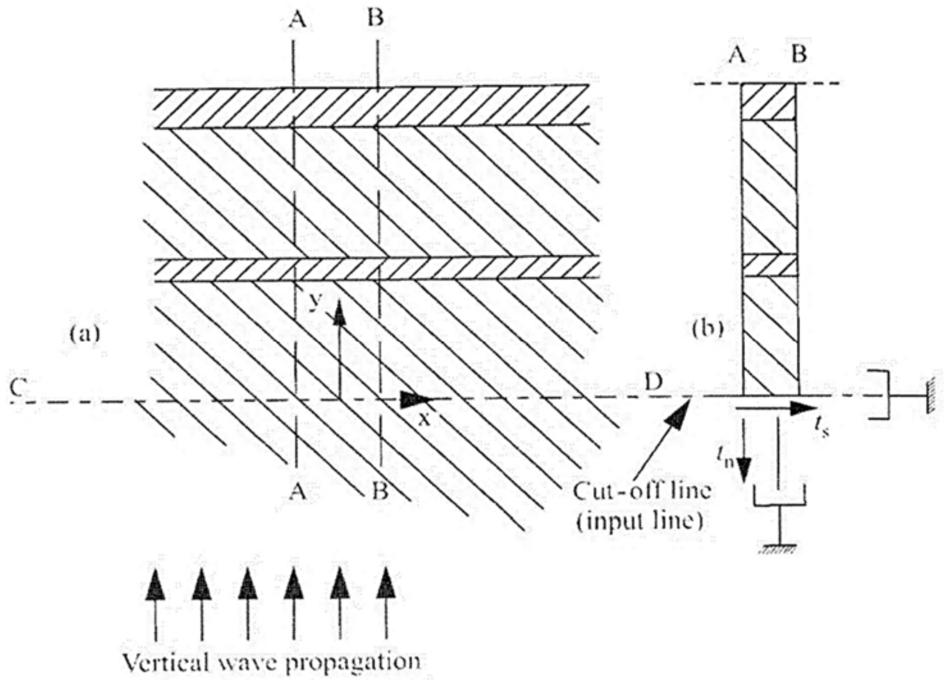

Figure 4.10 One-dimensional propagation of bulk waves. (Zienkiewicz et al., 1980)

In these hypotheses, the equilibrium equation (4.6) reduces to the following expression:

$$\sigma_{ij,i} - \rho \frac{dv_i}{dt} = 0 \tag{4.71}$$

that in the reference system (x, y) of Figure 4.10a, may be expressed in the two equations:

$$\frac{\partial \sigma_{xy}}{\partial y} - \rho \ddot{u}_x = 0 \tag{4.72}$$

$$\frac{\partial \sigma_{yy}}{\partial y} - \rho \ddot{u}_y = 0 \tag{4.73}$$

The stress, σ_{xy} and σ_{yy}, may be expressed through the elastic relationships:

$$\sigma_{xy} = G\frac{\partial u_x}{\partial y} \tag{4.74}$$

$$\sigma_{yy} = \overline{K}\frac{\partial u_y}{\partial y} \tag{4.75}$$

where G and $\overline{K}$ indicate respectively the shear stiffness and the oedometric modulus of soil.

The equations (4.72) and (4.73) then become:

$$\frac{\partial^2 u_x}{\partial y^2} - \frac{\rho}{G}\ddot{u}_x = 0 \tag{4.76}$$

$$\frac{\partial^2 u_y}{\partial y^2} - \frac{\rho}{\overline{K}}\ddot{u}_y = 0 \tag{4.77}$$

Equation (4.76) represents a shear wave that propagates with velocity $V_s = \sqrt{\frac{G}{\rho}}$.

It is the sum of an in-going shear wave, which travel in the positive direction along y (u_{xI}), and out-going shear wave, which travel in the negative direction (u_{xO}):

$$u_x = u_{xI}(y - V_S t) + u_{xO}(y + V_S t) \tag{4.78}$$

Similarly, equation (4.77) provides a P-wave which travels with velocity $V_p = \sqrt{\frac{\overline{K}}{\rho}}$.

It is the combination of an incident wave u_{yI} and an out-going wave u_{yO} for which we have:

$$u_y = u_{yI}(y - V_P t) + u_{yO}(y + V_P t) \tag{4.79}$$

To the border *CD* the waves that propagate into the interior of the model must be canceled while outgoing waves u_{xO} and u_{yO} should remain unchanged (radiative condition).

This condition can be reproduced by imposing that along the border *CD* tangential stress t_x and a normal stress t_y act according to the following relationships:

$$t_x = \sigma_{xy} = \frac{G}{V_S}\frac{\partial u_x}{\partial t} \tag{4.80}$$

$$t_y = \sigma_{yy} = \frac{\overline{K}}{V_P}\frac{\partial u_y}{\partial t} \tag{4.81}$$

Conditions (4.80) and (4.81) correspond to position two viscous dampers in the tangential and normal direction to the border (Figure 4.10b).

The expressed radiative condition can also be applied to bi or tri-dimensional geometries placing the viscous dampers in each node of the border but, differently from the one-dimensional case, the radiative condition is not exact since it does not simulate the correct transmission of waves impinging obliquely at the border.

4.3.2. Dinamic Damping

When performing dynamic analyses, it is preferable to add a damping term $F_i^{D\,<l>}$ in the equation of motion (B.31 in the appendix) to mitigate spurious oscillations produced by the numerical algorithm. The relation (B.31), therefore, becomes:

$$F_i^{<l>} + F_i^{D\,<l>} = M^{<l>}\left(\frac{dv_i}{dt}\right)^{<l>} \qquad l = 1, n_n \tag{4.82}$$

Considering $F_i^{<l>}$ as the sum of surface forces T_i, volume B_i and actions P_i, equation (4.82) may be written as:

$$\left[\left[\frac{T_i}{3}+\frac{\rho b_i V}{4}\right]\right]^{<l>}+P_i^{<l>}+F_i^{D\,<l>}=M^{<l>}\left(\frac{dv_i}{dt}\right)^{<l>} \qquad l=1,n_n \tag{4.83}$$

with $F_i^{D\,<l>}$ opposite sign of $F_i^{<l>}$.

It is possible to define this term as a function of nodal velocity in the following way:

$$F_i^{D\,<l>}=C^{<l>}v_i{}^{<l>} \qquad l=1,n_n \tag{4.84}$$

The damping matrix $C^{<l>}$ can be defined as a linear combination of the mass matrix and damping, according to the classical formulation of Rayleigh:

$$\mathrm{C}=\alpha\,\mathrm{M}+\beta\,\mathrm{K} \tag{4.85}$$

where α and β are numerical coefficients chosen to minimize the high frequency oscillations induced numerically by the numerical algorithm.

The adoption of the damping matrix $\mathbf{C}$ can be useful when the level of induced deformation is very low and the hysteretic damping of the soil and viscous effects of the fluid cannot eliminate the spurious oscillations of the system, with abnormal generation of a significant energy content at higher frequencies. Such high frequencies can be controlled by adding a damping term which is function of the velocity vector, the intensity of which is strongly influenced by the presence of high frequencies. However, if the constitutive model contains an adequate representation of material hysteresis that occurs in a real material, no additional damping would be necessary. The Raylingh damping formulation is unpopular with code users because it often involves a drastic reduction in time step and a consequent increase in solution time.

Hysteretic damping may be used also conjunction with other damping schemes (as Rayleigh damping).

In the thesis a hysteretic damping formulation defined hysteretic damping was adopted. It is respectful of the Masing criteria (1926) and associated to reproduce soil modulus degradation with increasing the strain level (§4.2.2).

5. Model at the Site Scale

5.1. Introduction

In this chapter, the analysis performed in the second step of the DRM procedure (Chapter 2) will be described, namely those related to the detailed model at the site scale. The case-history of the Conza dam has been selected because it is located very close to the fault system of the 1980 Irpinia earthquake and as a result suffered huge damage.

The topic of the present work is to clarify whether the observed damage on the Conza dam could have been amplified by possible effects of the near-source propagation the dam experienced.

As highlighted in §1.3.2 with reference to simple embankments, higher shear strains and a strong asynchronism of the seismic motion at the base are expected compared to what could occur to an embankment located in far-fault conditions. With the proposed innovative approach, the seismic motion at the base of the detailed model is derived from simulating the seismogenic fault acting in the area (step I of DRM) and then from transmission of the actions to each node of the boundary of the small model (step II of DRM).

During the PhD research activity a unified approach was developed and validated, in which the seismic motion is not obtained from the “outside” by selecting natural accelerograms (spectrum-compatible) from a general database where different source mechanisms are included, but obtained directly from the model.

In the field of earth dams the use of advanced models presupposes the reliability of the analysis, i.e., the ability to reproduce the observed behavior of the dam in the most salient aspects.

In particular, it is important to mention:

- The possibility to model the different phases of the dam life with continuity, introducing the seismic event in the normal exercise of the dam (Sica, 2001);
- The possibility to reliably interpret the temporal and spatial evolution of the quantities measured on the dam body and derive from them, variables not measured or unmeasurable, which are equally important for assessing dam safety.

Rigorous analysis in effective stresses allows to highlight the real behavior of the dam body and of the foundation against expected seismic scenarios and to highlight the real resources or deficiencies of the structure, taking into account a number of factors that simplified analysis neglect.

Due to the importance of earth dams the mathematical and numerical procedures that should be selected to analyze their seismic response must be consistent with the analysis objectives. In the case of earth dams the analyses should be primarily aimed to verify safety against the watertightness risk. Earthquakes can induce negligible effects or decrease dam watertightness. The severity of the seismic-induced effects mainly depends on the characteristics of the earthquake and vulnerability of the structure.

The phenomena of global instability, embankment compaction, break of the watertightness element, liquefaction or localized erosion, are dangerous effects that an earthquake could cause to earth dams. The above seismic damages, should be verified individually through different simplified procedures or at once through advanced modelling.

The pseudo-static (Terzaghi, 1950; Ambraseys, 1960; Seed and Martin, 1966) and the pseudo-dynamic approach (Newmark, 1965; Makdisi and Seed, 1978) have been adopted in the past to check the phenomena of global instability and seismic performance of earth dams, respectively. In addition, empirical correlations have been used to verify liquefaction occurrence (Seed and Idriss 1971; Iwasaki et al., 1982; and Boulounger & Idriss, 2004).

The recent developments of refined constitutive models that account for important features observed at the soil volume scale (non-linearity, non reversibility, dependence on loading history, hysteresis, effect of number cyclic loading) and the implementation of coupled dynamic formulations (Chapter 4) in robust numerical algorithms and computer codes, provide more refined tools to simultaneously analyze the various aspects related to the seismic response of earth dams. These approaches are suitable to describe the overall response of dams since they provide predictions in terms of stress, pore pressures and strains.

It is important to enhance that the static and dynamic response of an earth dam are jointly connected since soil behavior strongly depends on the history of previous loading.

The application of an advanced modelling in general has the following well-known drawbacks:

- the need to define several parameters of the soil constitutive laws. Often field and laboratory tests that are available are of the traditional type and inadequate for the purpose;
- the difficulty in convergence of the numerical algorithm that implements high degree of "non-linearity", the latter included not only in the soil constitutive law but also in the adopted field equations;
- the variability of the spatial domain during the simulation of the construction phases;
- the variability of the static and hydraulic boundary conditions during the simulation of the construction and operational phases;
- the introduction of different seismic accelerations in any point of the boundary of the small DRM domain during the simulation of the seismic stage.

All this could generate long calculation time even with high performant computers that are available nowadays. Moreover the need of back-analysing the observed response of the dam to quantitatively define the soil parameters required, to bypass the lack of a proper geotechnical characterization, could make a very onerous overall computation.

At the end of this chapter, after having modelled the selected case history to reproduce its static and seismic response to the 1980 Irpinia earthquake accounting for the source simulation described in Chapter 3, the prediction of the dam response to future seismic scenarios will be provided (§5.5.2.2). These scenarios have been (§3.5.3) modelled with the same procedure adopted for the 1980 Irpinia earthquake. The important aspect to stress is that these further predictions of dam response accounts for the memory of the 1980 event.

5.2. "Conza della Campania" dam

The Conza dam has been deeply investigated by Brigante (2010) who interpreted the monitoring data of the static and seismic response of the structure from construction to 2002. Reference is made to this previous work to derive the required information necessary for the scope of the present research.

The Conza dam is a zoned earth dam located in the Irpinia region in the core of the Southern Apennines (Italy) around 20 km north of the third mechanism of the 1980 Irpinia earthquake.

It is characterized by a maximum height equal to 46 m. The maximum water storage of the reservoir is of about 77 million m^3, for a plan dimension of 5x3 km.

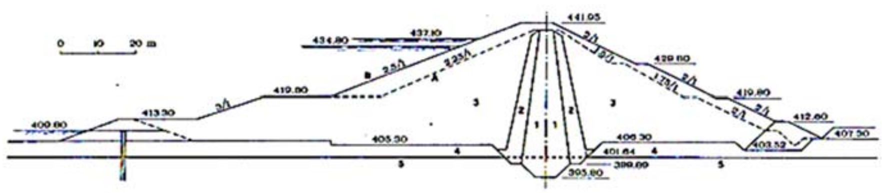

Figure 5.1 Cross Section of the Conza dam: A) original section, B) final section. Different zones: 1) core, 2) filters, 3) shell, 4) alluvial material, 5) foundation clay (Brigante, 2010).

The construction work began in May 1979 and were soon suspended after the 1980 earthquake.

The Conza Dam is an interesting case (and not rare for the Central Southern Apennines) of a dam subjected to a seismic event of high intensity with the epicenter located close to the site. (Figure 5.2).

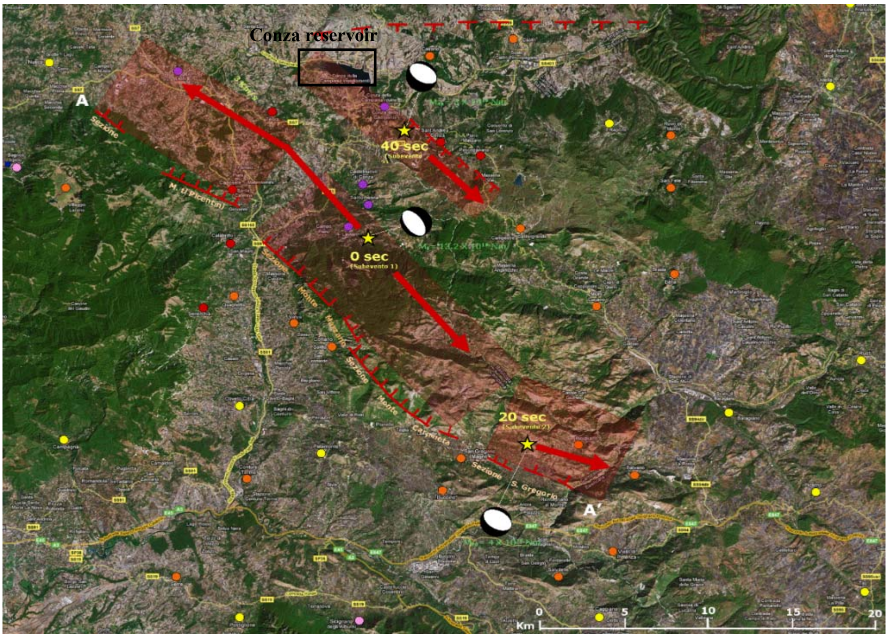

Figure 5.2 Location of Conza Dam and faults activated during the 1980 Irpinia event (INGV).

At the time of the 1980 seismic event, the embankment was partly achieved: the shell reached about 420m a.s.l. and the core about 415 m a.s.l.. Therefore, in correspondence with the main section, the total height was approximately 18 m. However, in correspondence to the center of the longitudinal axis and for a length of approximately 120m (section 4), the dam height resulted 5 meters lower (Figure 5.4).

The damage caused by the Irpinia earthquake was very evident: settlements and cracks suffered by the dam body. The interpretation of measurements, carried out by Brigante (2010), highlights that the 1980 earthquake caused significant permanent settlements: at the foundation level of the order of 40 cm and about 60 cm at the top of the dam.

Lower settlements were measured along the section 4 which, as stated above, is in correspondence with the dam portion of lower height at the time of the 1980 earthquake (Figure 5.3).

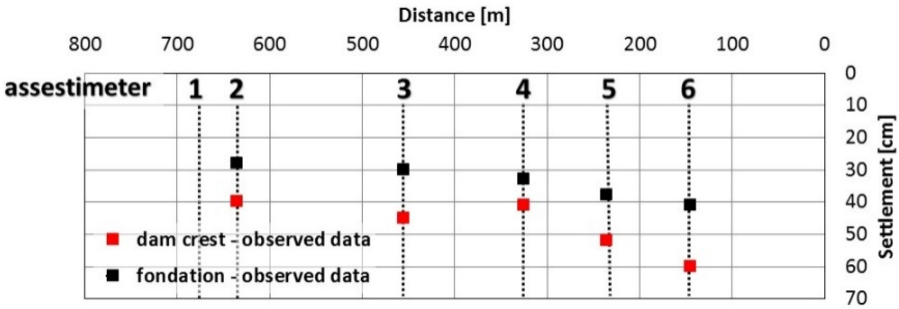

Figure 5.3 Embankment and foundation settlements in correspondence to the instrumented sections of the Conza Dam (Brigante, 2010).

The construction work started again in June 1985 until1992. The impounding stage started in 1993.

The original design did not contemplate seismic actions since the site was not considered prone to high seismic hazards before 1980.

Therefore, after the 1980 earthquake, the design was reconsidered and dam geometry suitably changed to account for seismic actions (Figure 5.4).

A new experimental campaign on dam soils was performed (7 dilatometric verticals in the core, 6 cross-hole tests and geophysical investigations with the seismic refraction method made in the shells and foundation).

The new design was done in respect of the regulations in force at the time (Ministerial Order dated 24/03/1982).

The position of the core resulted no more centered with respect to the vertical axis of symmetry of the cross-section.

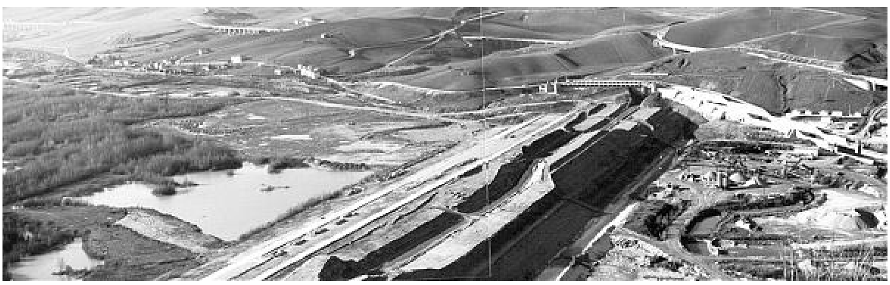

Figure 5.4 Conza della Campania dam during the construction of the embankment (www.prolococompsa.it and wikimapia.org). A lower height of the embankment is observed in the middle (section 4 of Figure 5.5).

During the first and second construction stage, the Conza dam was equipped with: (i) USBR cross-arms inside the core to measure settlements along 6 verticals (see Figure 5.5); (ii) piezometric cells for measurement of pore pressures and tension cells placed at the vertical 2, 4 and 6.

USBR cross-arms and open standpipe piezometers were also installed in the downstream shell of the embankment.

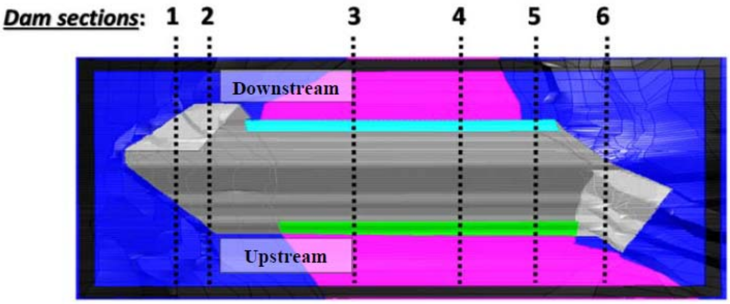

Figure 5.5 Plan view of the Conza Dam with indication of the instrumented sections.

5.3. Soil materials of the earth dam

Core

The material is "silt-clay" with medium-high plasticity ($I_p \approx 20\%$).

The core was created with layers of height at 0.5 m.

The dry unit weight $\gamma_{S,opt}$ and the water content w_{opt} at the optimum of the Proctor are respectively around 17 kN/m and 22%.

The permeability was estimated of the order of 10^{-10} m/s.

For the core, in addition to traditional geotechnical characterization from tests conducted during the construction work, 7 dilatometric tests were carried out after the seismic event of 1980. Also, an oedometric test on a sample retrieved at a depth of 1.7 m was carried out.

The angle of friction has been derived (see Brigante, 2010) from empirical correlations with the plasticity index (Jamiolkowski et al. 1979) and a value of 25° was cautiously adopted.

For the remaining parameters, the literature values were firstly adopted and then changed by a back-analysis of the observed dam response during construction and seismic-stages, as suggested in previous interpretations of other case-histories (Sica, 2001; Sica et al. 2008; Sica & Pagano, 2009).

For the core and cofferdam, the non-linear variation of the initial stiffness with the main effective stress *p'* is expressed by the following relation:

$$G_0 = G_1 \cdot \left(\frac{p'}{p_r} \right)^{\alpha} \tag{5.1}$$

where p_r is a reference pressure (1 MPa), G_1 is the initial stiffness at the reference confining pressure p_r and α regulates the variation of G_0 with p' (or depth). G_1 and α should be calibrated with experimental results and they were assumed equal to 554 MPa and 0.3 respectively. As deduced from the experimental law obtained on Camastra dam (Pagano et al., 2008). This dam has the same typology of Conza with almost the same features of core soils and construction techniques. To determine E_0 the elastic relation $E_0 = 2(1+\upsilon')G_0$ has been used, with a value of the Poisson coefficient ν' of 0.3.

Regarding the $G/G_0 - \gamma$ curves of the cofferdam and core, reference was made to resonant column (RC) tests performed on the soil of the Marana Capicciotti dam (Cascone & Rampello, 2003; Rampello et al., 2009), having a grain size and plasticity index similar to the materials of the Conza core.

Shell

The shells may be classified as "sandy gravel".

The material has been placed by layers of 0.8m in height.

The dry unit weight and the water content at the optimum of Proctor standard are 23 kN/m and 3% respectively.

The permeability is of the order of 10^{-5} m/s.

For the estimation of the mechanical properties at low strain the cross-hole tests carried out after the Irpinia 1980 earthquake were considered.

No further experimental tests exist and literature values were adopted for all the other geotechnical properties. These values have changed during the back analysis of the observed response to calibrate soil stiffness at larger strains.

For the shells and the toe drain, the elastic stiffness at small strain is expressed by the following relations:

$$G_0 = G_1 \cdot f_{(e)} \cdot \frac{(p')^{\alpha}}{(p_r)^{\alpha-1}} \tag{5.2}$$

where p' represents the mean effective stress, p_r is a reference pressure (1 MPa), $f_{(e)}$ is the void index function proposed by Hardin & Richart (1963), G_1 and α are parameters to be calibrated with experimental results ($G_1 \approx 8$ MPa and $\alpha = 0.75$). To determine E_0 a value of the Poisson coefficient of 0.2 has been assumed.

Filters

The material adopted for the filters comes from alluvium used for the construction of the shell after appropriate sieving (d_{max} = 10mm).

The mean value of permeability was equal to about 5×10^{-5} m/s, which is of the same order as the material used for the shells.

Foundation

The foundation soils of the embankment are the so-called "blue-gray clay" formation, typical of the Ofanto river valley. This formation is inorganic clay of medium high plasticity with w_L between 45% and 75% and I_p between 25% and 50%.

The physical properties of the foundation soils of the Conza dam are as follows:

- natural unit weight (γ_{nat}) of 23 kN/m^3;
- natural water content (w_{nat}) 15%;
- porosity 25%;
- degree of saturation between 97% and 99%.

Above the gray-blue clay there is an alluvial layer with a thickness of about 5 m, characterized by the soils of the shells.

Undrained triaxial tests (UU) on samples retrived at a depth of 0.8 m provides c_u around 1000 kPa.

The friction angle φ' has been assumed equal to 20°, as indicated in the original design of the dam. The effective cohesion (150 kPa) was desumed from triaxial tests in neighboring sites.

After the earthquake of 1980 cross hole tests and one oedometric test (on a sample taken at a depth of one meter) were conducted on the foundation soils.

The V_S values estimated by cross-hole test vary from 800 m/s to 1000 m/s.

In the numerical analysis, a linear variation of V_S with depth was assumed.

The parameters of stiffness at large strain levels were obtained during the back-analysis on the construction phase.

5.4. Numerical modeling

5.4.1. Geometry

The Conza dam has been analyzed by a three-dimensional model. For the case at hand, the use of a 3D model is not justified by the complexity of the geometry (as the case of Camastra or Menta dam), or by the variability of the foundation level along the longitudinal axis, or by the narrow shape of the valley (see El Infiernillo dam).

For the Conza dam, for instance, the foundation level at the base of the embankment is horizontal and the considerable extension in plan (about 850m) makes the stiffening effects exerted by the abutments negligible, as highlighted by Gazetas (1987) by comparing the results of 2D vs 3D dynamic analyses of dams in narrow canyon valleys.

The choice of a three-dimensional model fulfils the objectives of the present research, that is, to investigate the dynamic response of the dam under a near source propagation by differentiating the input motion in all nodes of the dam basement.

As enhanced in the previous chapters, asynchronous motions may reduce the inertial stresses (Bilotta et al., 2010) but may increase the spatial variability of strains and consequently of settlements in the dam body. Differential settlements due to asynchronous motions at the dam base (higher than those evaluable by traditional approaches) increase the risk of crack formation. Cracks may be dangerous as regards both shell stability and watertightness of those dam elements assuring it (core in zoned dams, upstream mat in CFR dams, etc.). For dams, even the operation limit state should be verified to assure the functionality of the dam. In this case small differential settlements can limit the use of pipelines, tunnels of inspection, other hydraulic organs or, moreover, promote piping inside small cracks.

To highlight the importance of accounting for variability of the motion at the dam base, it is worth noting that greater the extension in plan of the structure, the expected variability of the seismic motion at the base is greater. The occurrence of asynchronous motion, indeed, is related to the wavelength associated to the earthquake and propagation media. In near-source conditions high frequencies prevail, which induce shorter wavelengths comparable (or minor) to the characteristic dimensions of the dam. Indeed, in the case of large dams both longitudinal and cross-sections may be affected by the sway motion due to short wavelengths.

The 3D geometry of the site model and its discretization (II step of the DRM) are shown in Figure 5.6.

Figure 5.7 shows the interface surfaces between the external and internal domain with the effective forces $\boldsymbol{P}^{eff}$ computed according to Bielak et al. (2003) formulation.

The discretization of the domain ensures that there are at least 8÷10 elements for wavelength, with higher values in correspondence of the dam body, according to the equation (4.70).

Since the extended external model of the DRM (step 1) does not allow ground notion to generate with frequencies higher than 5÷7 Hz, the discretization of the internal domain was regulated on f_{max} = 7.5 Hz, consistently with the outer domain.

a

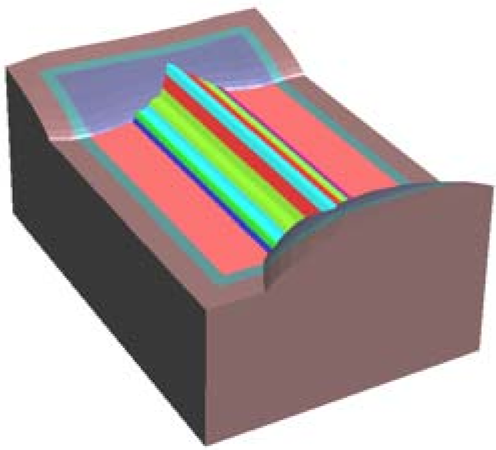

b

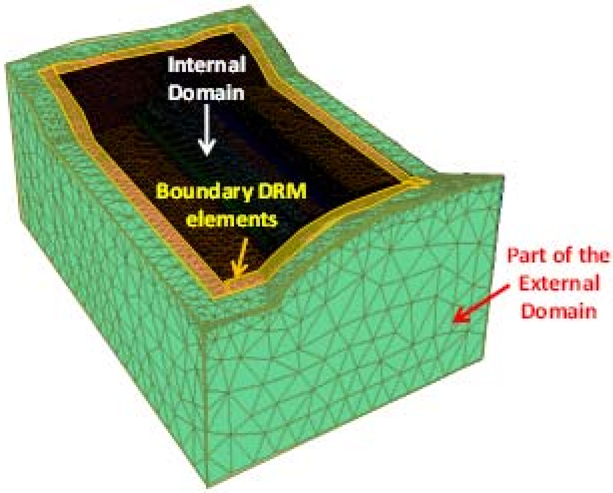

Figure 5.6 (a) Details of the site model including the Conza dam. (b) Discretized model with indication of the external and internal domain together with the interface zone between them.

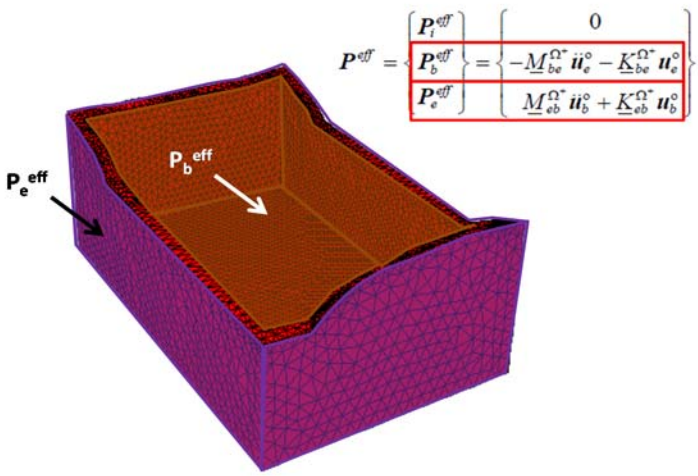

Figure 5.7 Interface zone with analytical formulation of the effective forces according to Bielak et al. (2003).

5.4.2. Interaction between the phases

As the interaction between the soil phases in the various zones of the dam regards, the fine-grained materials (core and filters) were modelled by a two-phase coupled formulation (§4.1), while the coarser materials of the shells were treated by a decoupled approach assuming a completely drained behaviour (no phase interaction).
The drawback of a two-phase formulation is the inability to account for those peculiar phenomena of partially saturated soils such as:

- undrained compressibility;
- collapse due to saturation of the shells during the first filling of the dam.

In the case-history of Conza, the hypothesis of complete saturation, however, is very plausible since the initial degree of saturation is higher than 90% on average.

5.4.3. Constitutive models

Recalling the two steps of the DRM approach, in the following paragraph details will be provided on the constitutive law adopted for each zone of the reduced model, which at the site scale includes the Conza dam.

For elements belonging to the interface zone between the internal and external domain, a linear visco-elastic law acquired. For all other materials present in the model an elastic plastic behaviour was assigned.

Both for fine-grained and coarse-grained materials of the dam, the initial shear stiffness (G_0), was related to the confining pressure (p'). At the start of each analysis stage $G_0(p')$ was updated.

For the coarse-grained materials of the shells a traditional Mohr-Coulomb model was adopted.

For the fine-grained materials of the core, two different models have been considered: one for the static and another for the dynamic analysis.
Under static or quasi-static loading conditions a modified version of the Mohr-Coulomb elasto-plastic model was adopted. This version has a cap which defines the elastic region on the hydrostatic axis in stress space. In addition to the parameters of the Mohr-Coulomb model (angle of friction, cohesion, traction cut-off and dilatancy), the cap version has an additional

parameter which is analogous to the parameter p_{c0} of the Cam-clay model. It was evaluated through the available oedometric test, by computing the OCR in the core material. The Mohr-Coulomb with cap allows for better simulation of the construction stage of the dam but it is not suitable for dynamic analyses. For this reason, the Finn model was added, for core material, to the Mohr-Coulomb elasto-plastic law. In particular, for the estimation of residual volumetric strain the relation proposed by Byrne (1991) was used (§4.2.1.2).

The use of two different models for the core is possible because an identical formulation of yielding and resistance criterion is adopted.

Finally, the behaviour of the material from small to medium strains is controlled by a hysteretic model as function of the shear strain induced each instant by the earthquake. shows the comparison between the reference experimental data (Cascone & Rampello, 2003) and those obtained using the hysteretic model (§4.2.1.1). Table 5.1 provides the values adopted to fit the experimental data.

In Table 5.2 the values obtained fitting the $G/G_0 - \gamma$ curve, for coarse-grained materials proposed by Costanzo et al. (2011) on experimental data of Melito dam (Lirer, 2008), has been reported. Figure 5.9 shows the curve related to the parameters of Table 5.2.

For the filters, the shear modulus reduction curves have been referred to the data in the literature (Seed et al., 1986).

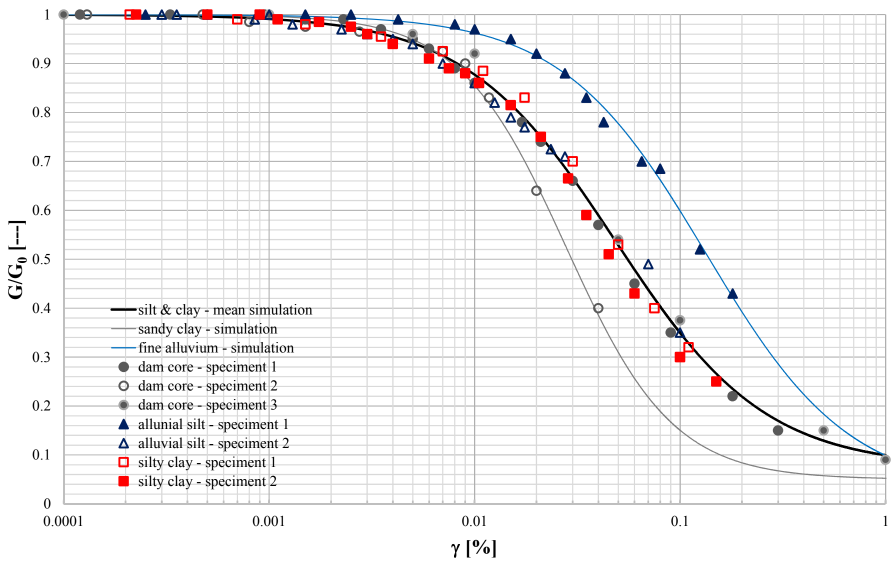

Figure 5.8 $G/G_0 - \gamma$ curves for fine grained materials: experimental data (scattered indicators) on Marana Capacciotti dam (Cascone & Rampello, 2003) and simulation with the hysteretic damping model (continuous curves).

Parameter	***a***	***b***	***x₀***	***y₀***
Silt & clay - mean	*0.925*	*-0.365*	*-1.315*	*0.075*
Sandy clay	*0.95*	*-0.26*	*-1.555*	*0.05*
Fine alluvium	*0.975*	*-0.35*	*-0.875*	*0.025*

Table 5.1 Parameters adopted for the hysteretic model of the core.

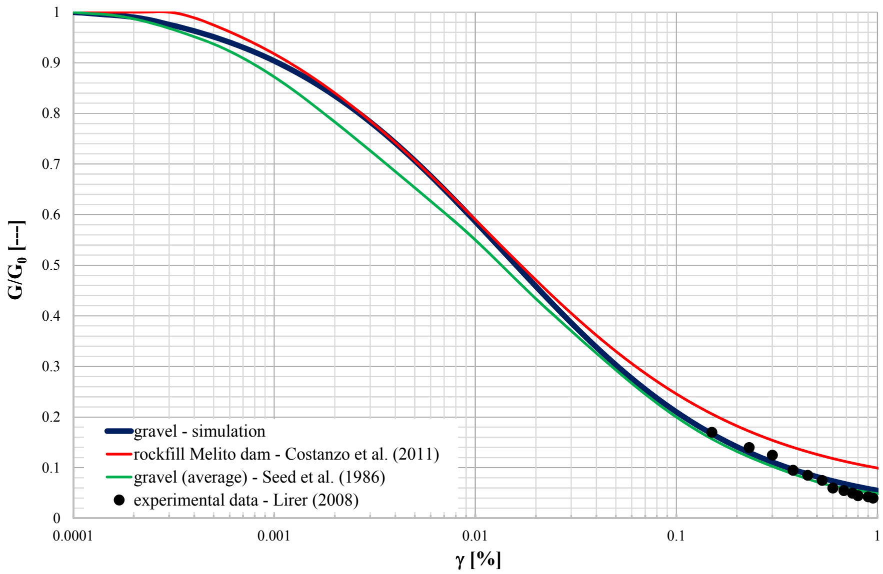

Figure 5.9 $G/G_0 - \gamma$ curves for the shells: experimental data (large-strain, p'=400 kPa) Melito dam (points), simulation with the hysteretic damping model (blue line) and literature functions (red and green lines).

Parameter	***a***	***b***	***x_0***	***y_0***
rockfill	*1.025*	*-0.600*	*-1.850*	*0.01*

Table 5.2 Parameters adopted for the hysteretic model of the shells.

5.4.4. Static stages before the 1980 seismic event

Construction of the Conza dam embankment has been simulated in accordance with the real loading history desumed from work reports.

Before starting the construction phase of the dam embankment, a geostatic stresses field was generated in the foundation with a gravity load procedure.

The dam construction consists of the activation of one row of elements for each step of construction for a total number of 6 horizontal layers with thickness from 5 to 7 meters.

Any layer activation was realized by the following steps:

- application of the well-known procedure called "dense liquid method" for which the behaviour of the material is assimilated to that of a liquid having its own weight but no stiffness. This latter is later restored at the activation of the following soil layer. In this way, the analysis reproduces the stress and strain induced in the dam by the real loading history distribution (Mattar and Naylor, 1988).

At this stage average value of the soil stiffness for each layer are adopted by "gravity loading procedure";

- introduction of material stiffness dependency on the mean effective stress p'. Such phase has been coded in different subroutines written by the built-in programming language of the adopted analysis code;
- Regeneration of the stresses acting on the embankment and foundation, according to the new stiffness and strength distribution;
- Modification with the previously defined subroutines of strength and stiffness distribution according to the new distribution of stresses;

The weight of the layer had been applied in a very short period of time (vertical portion of the step function).

Before moving to the next construction step, a phase of consolidation (horizontal portion the step function) has been applied, which corresponds to the actual placement of the layer.

The impounding stage started in September 1992, almost 11 years after the 1980 earthquake and 4 years after the end of the II construction stage.

The simulation of the reservoir impounding has been done by:

- applying water pressure on the upstream side of the dam assuming a hydrostatic distribution regulated by to the current level of the reservoir;
- initialization of the pore pressure (hydrostatic pressure) in the nodes of the wet boundary;
- applying the stress ($\sigma_n = \gamma_w h$) along the upstream side of the shell to have (together with the hydraulic condition) zero effective stresses on the wet boundary of the dam.

5.4.5. Dynamic stage

The dynamic analysis has been made by means the same mathematical and numerical modelling used for the simulation of the static phases.

The initial state of the dynamic analysis in terms of stresses, pore pressures and soil model internal variables comes from the static analysis. In such a context, dynamic analyses have continuity with the static analysis, thanks to a unified approach where time is a variable of the problem such as it occurs in reality.

The input motion for the dynamic analysis has been derived from the application of DRM (step I) and thus a diversified motion was applied to each node of the interface zone between the external and internal domain (Figure 5.6).

All along the boundary of the reduced model the effective forces, determined by step I of DRM, have been applied. These are able to reproduce the effect induced by the seismic source (present only in the outer model) on each node of the interface zone.

The external part of these interface elements has already considered an absorbent boundary. In fact, if the domain part present uses one level of higher damping, fixed or free borders can be used in place of the absorbing boundary conditions (ABCs) without committing significant errors (Bielak et al., 2003; Scandarella, 2007; Smerzini, 2010). Besides, in the thesis to reduce the effect of reflections at the boundaries (other the ABCs), a double value of damping in the external domain has been preferred to include.

At the bottom and lateral boundary of the reduced model, absorbing elements, coherently to Lysmer & Kuhlemeyer (1969) formulation, were placed to reproduce the radiative condition (§4.3.1). To enable the latter, during the simulation of the earthquake, all degrees of freedom of the boundary nodes had been released, being blocked during the previous static phase.

The analyses were performed using an explicit integration method, in which the time step is calculated as the minimum time employed by the wavefront to traverse the elements of the mesh (i.e. the ratio between the minimum size and the V_S). For example, the analysis of a seismic event with a total duration of 80 seconds requires the execution of about 800’000 time steps (Δt approximately equal to 10^{-4}s), equivalent to more than 24 hours of processing with the available calculation tools.

To characterize the free oscillations of the dam, the dynamic analysis has extended beyond the actual duration of the seismic solicitation, for an interval of time approximately equal to the 1/3 of the actual duration of the earthquake. This time had considered sufficient to reach a stationary conditions so that no further accumulating plastic strains and excess pore pressures in the dam core occur.

In the analysis, a modest viscous damping is also used of the Rayleigh type, to improve the numerical stability of the analysis. This contribution is defined by a minimum damping ratio $\xi_{\min}$, that for this type of problems is taken typically close to unity, and the frequency associated with it, which is assumed equal to the fundamental frequency of the deposit, determined by a preliminary linear analysis (natural period around 0.6s).

Difference between the proposed approach and the traditional one

To evaluate the effect of the near-source propagation on the seismic response of the selected dam, a traditional approach has also been applied in order to compare predictions obtained from both solutions.

The seismic input motion (in the x, y and z) was applied only at the lower border of the detailed model, thus simulating a sub-vertical propagation (Figure 5.10).

The external domain (step I DRM) provided the input motions at all nodes of the interface zone and for the traditional approach just one time-history was selected: in correspondence of the reduced model base (point 6 of Figure 5.18).

Having to compare the two approaches in the same conditions and geometrical discretization (so that the diversity of the results can not be attributed to the geometry or size of the mesh used) the use of a common model was mandatory.

In the traditional approach, beyond the application of the dashpots, along the lateral boundary of the model, the free-field motion has been imposed (Itasca, 2005).

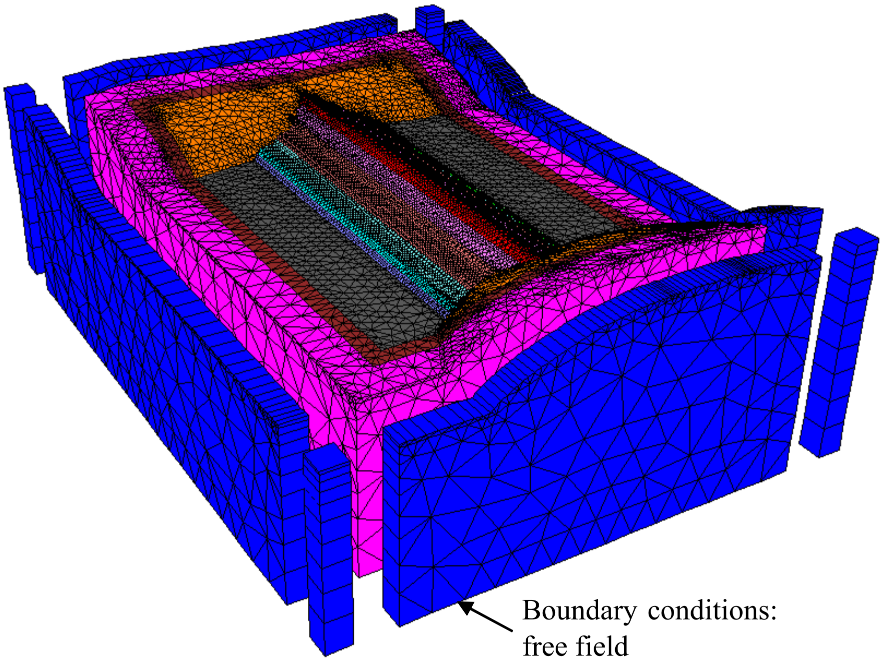

Figure 5.10 Model used for traditional analysis. The free field boundary conditions used solely in this approach are reported in blue.

5.5. Results of the performed simulation

5.5.1. Static analysis

Due to the lack of a suitable experimental characterization on Conza Dam soils, typical of most case-histories of dams built in the last century, a back-analysis has been made by updating soil stiffness (at medium-large strain level), trying to fit the settlements measured during the first (before the 1980 Irpinia earthquake) and the second (after the 1980 earth) construction stage.

Figures 5.11 to 5.16 show some results of the simulation of the static stage in terms of vertical displacements (Figures 5.11-5.12), of pore pressures (Figures 5.13 to 5.15) and vertical stress states (Figure 5.16).

In Figure 5.12, the high settlement values in the middle of the dam include also the 1980 seismic-induced settlement.

In Figure 5.17 the shear stiffness contour in function of the stress state in three different conditions is shown: final of first and second construction and of maximum reservoir.

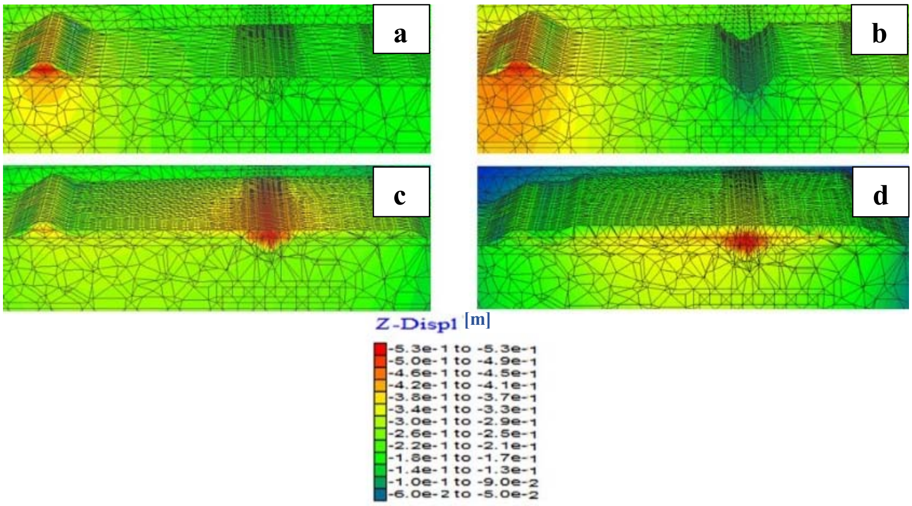

Figure 5.11 Contour of vertical displacements relative to the first construction phase: (a) cofferdam realization; (b) excavation of the foundation plane; (c) and (d) construction layer by layer of core, filters and shells.

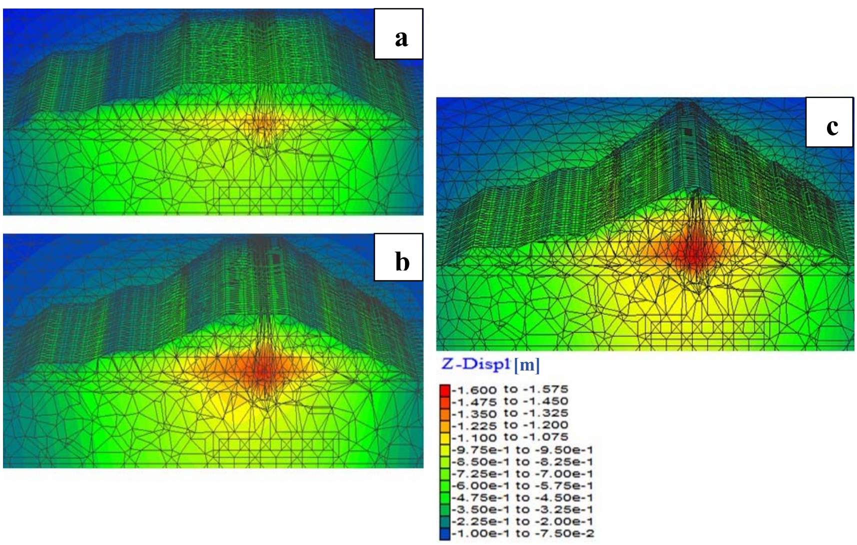

Figure 5.12 Contour of vertical displacements relative to the second construction phase: (a) and (b) different analysis steps; (c) final construction**.**

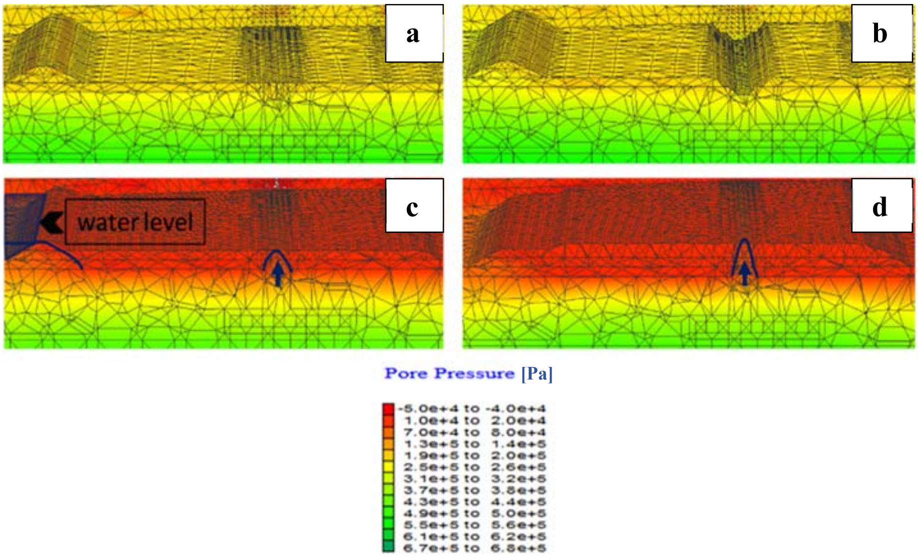

Figure 5.13 Contour of pore-pressure relative to the first construction phase: (a) Cofferdam realization; (b) excavation of the foundation plane; (c) and (d) different construction steps of core, filters and shells.

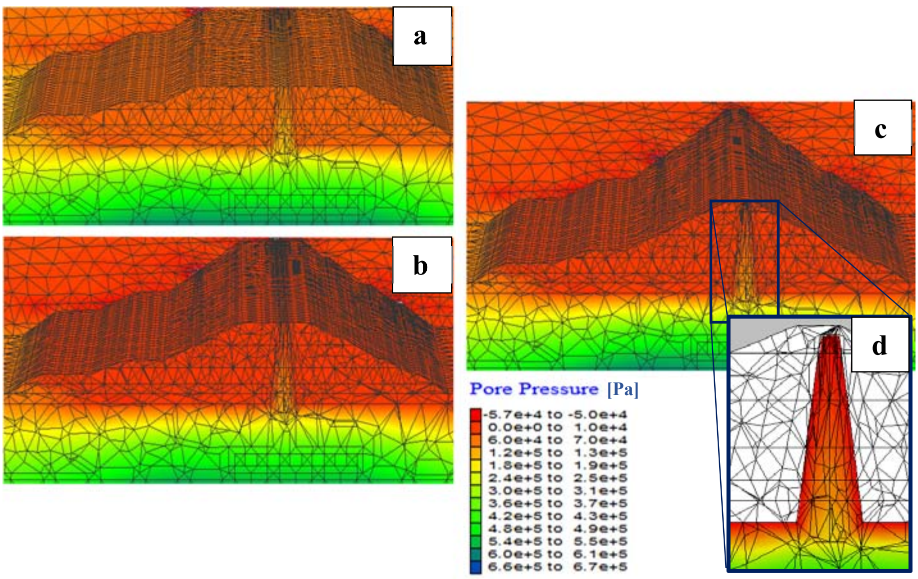

Figure 5.14 Contour of pore-pressure relative to the second construction phase: (a) and (b) different construction steps; (c) final step of construction; (d) zoom, for final step, relatively to the core.

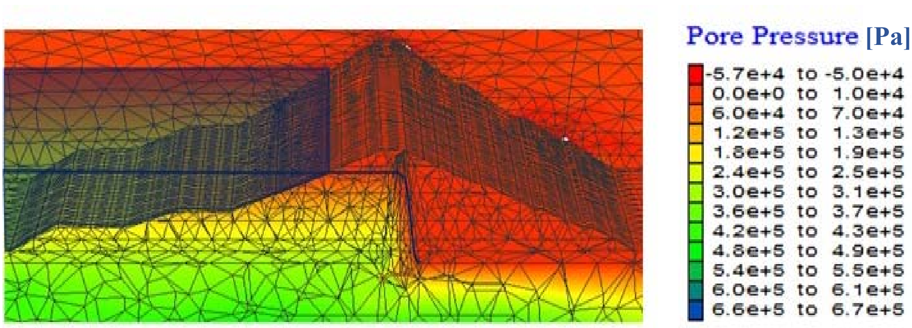

Figure 5.15 Pore-pressure at the end of the reservoir filling.

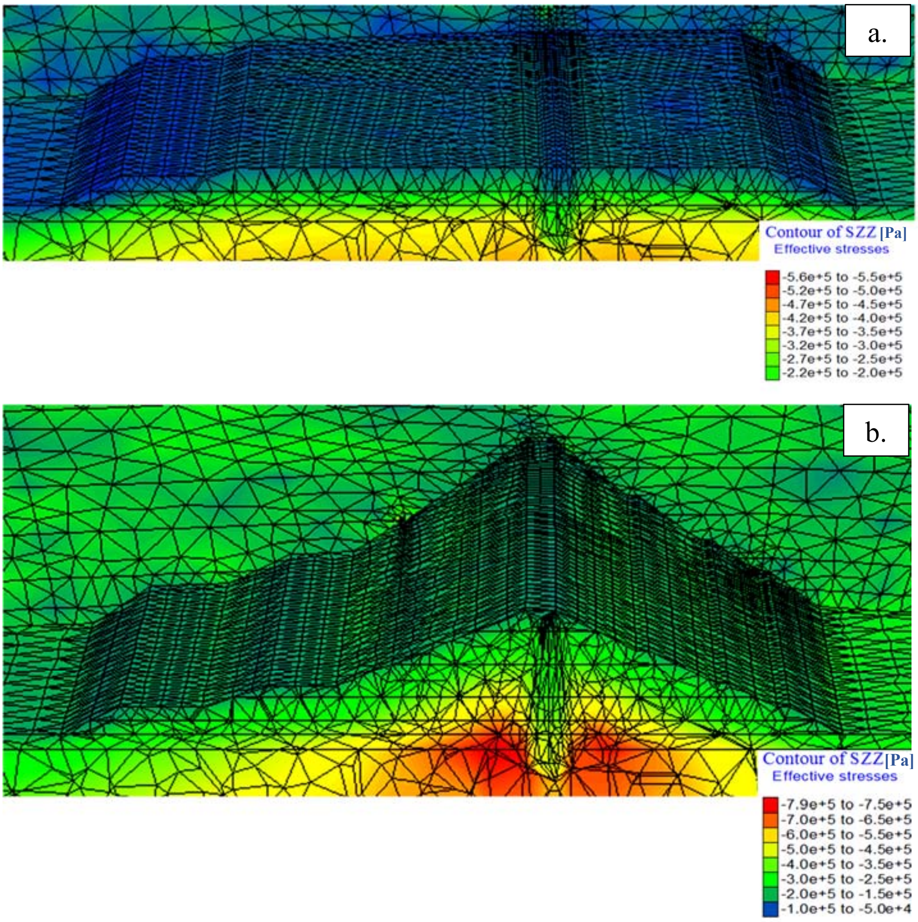

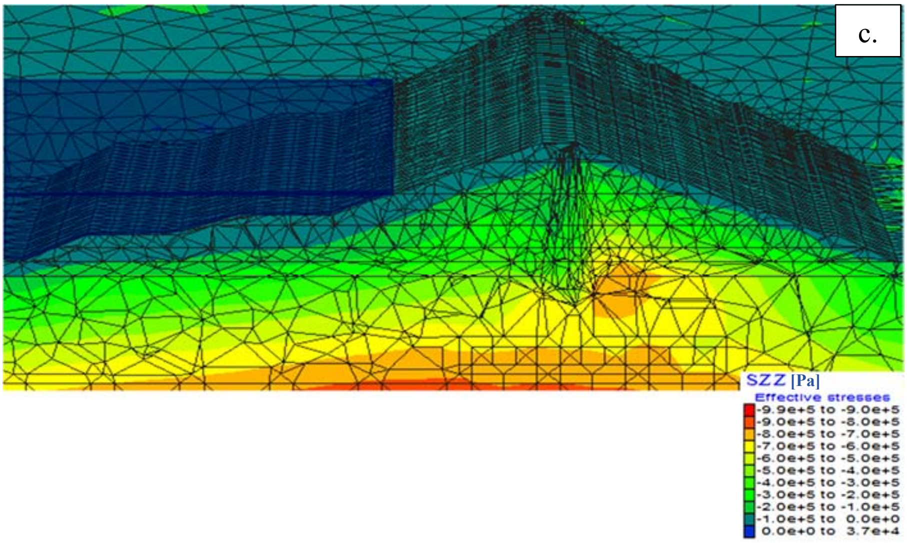

Figure 5.16 Vertical effective stress: (a) step before the Irpinia earthquake; (b) final step of construction; (c) end of reservoir filling.

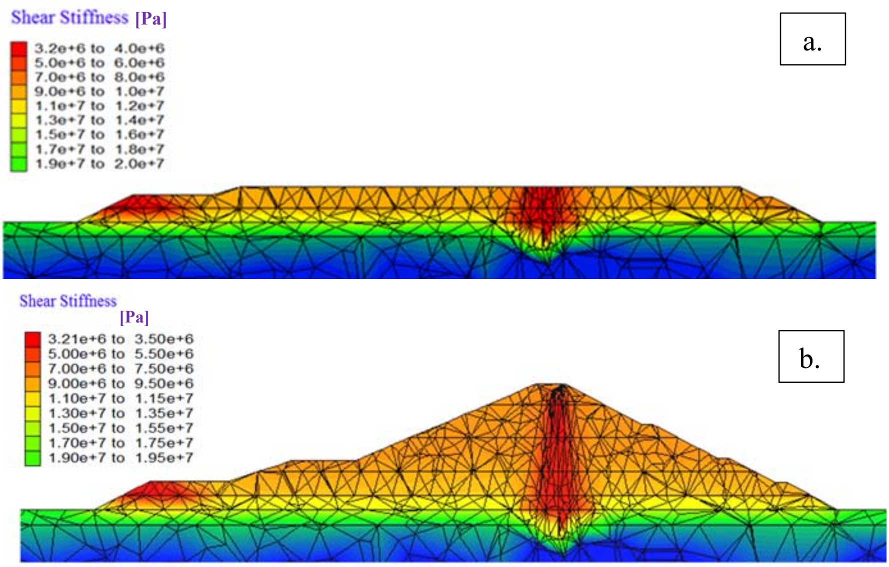

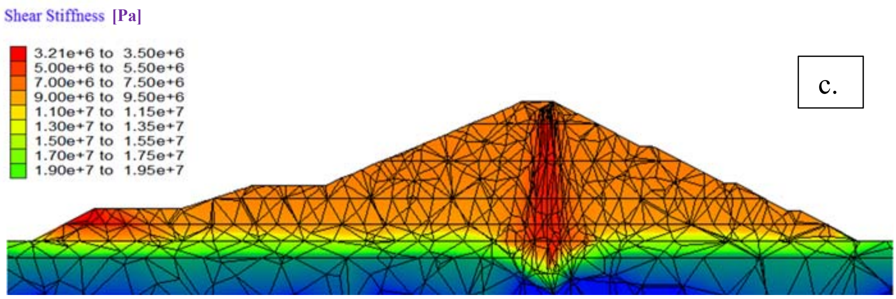

Figure 5.17 Shear stiffness: (a) before the Irpinia earthquake; (b) end of construction; (c) maximum water level.

5.5.2. Dynamic analysis

The results of the dynamic analysis refer to the simulation of the 1980 Irpinia earthquake and of future seismic scenarios.

For the sake of clarity, the points shown in Figure 5.18 will be adopted to discuss the variability of the input motion at the roof of the bedrock in reduced model of DRM.

In Figure 5.19 acceleration time histories in x-direction relative to the six nodes reported in Figure 5.18 are shown. A strong variability in ground motion can be observed.

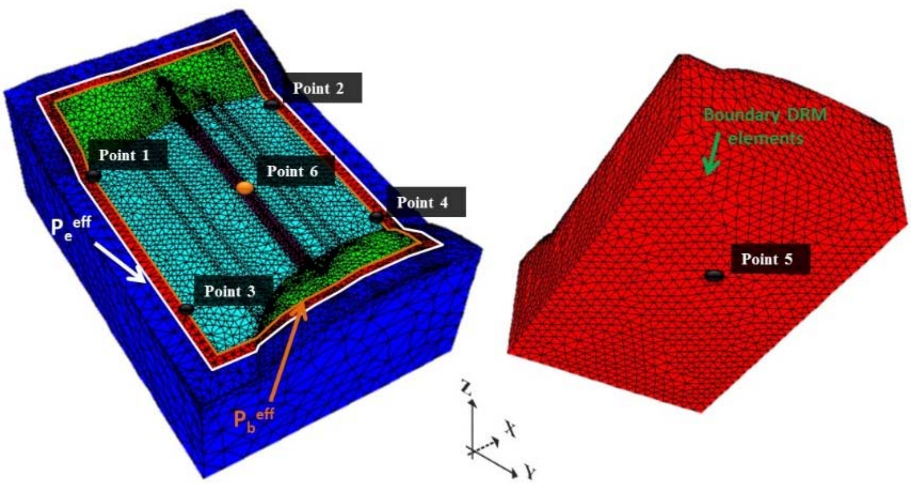

Figure 5.18 Reference points: points from 1 to 4 belong to the DRM interface on the outcropping bedrock; point 6 is placed on the foundation level in

correspondence of the central section of the dam; point 5 is placed at the bottom of the DRM interface below point 6.

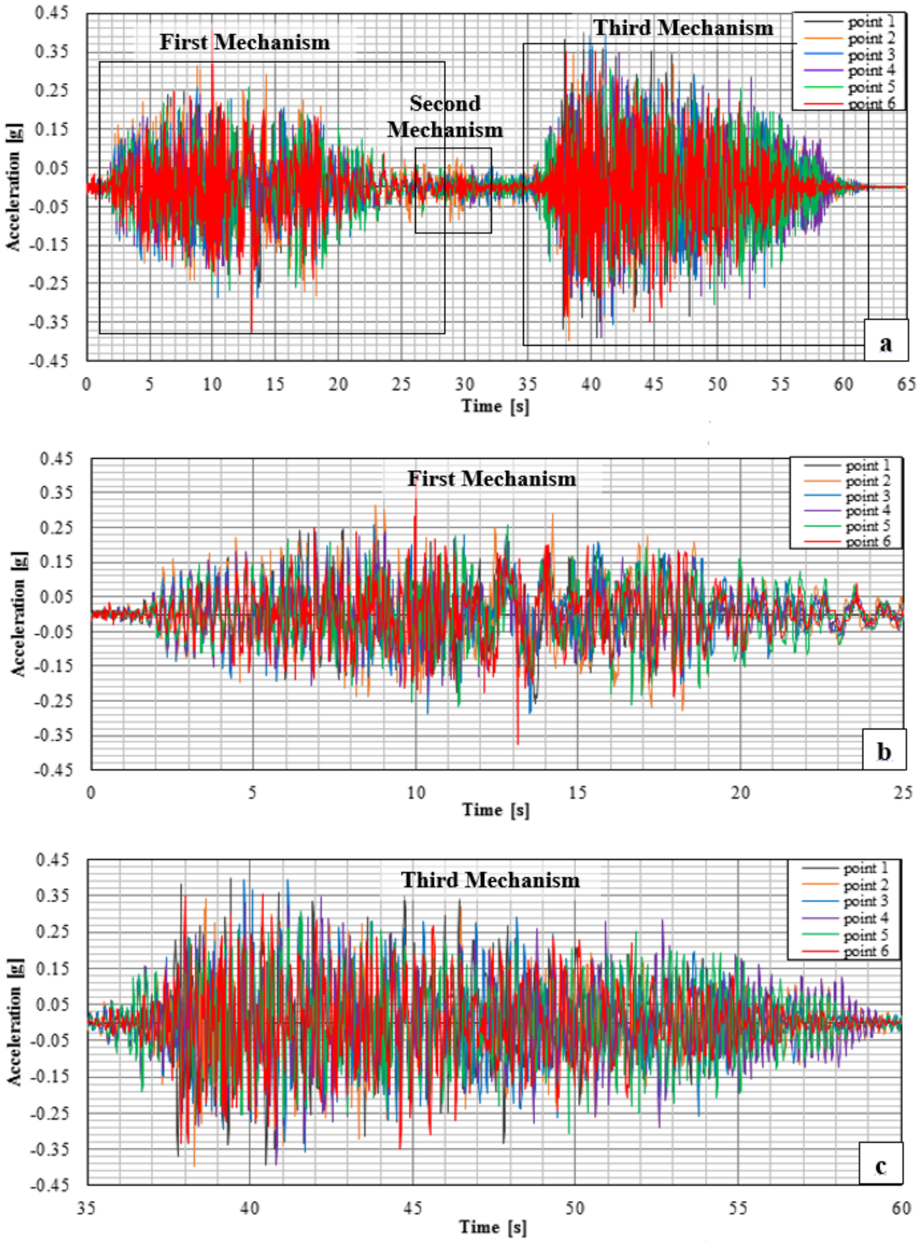

Figure 5.19 Acceleration time-histories in x direction for the selected monitoring points. a) total time history; b) window on the first mechanism and c) on the third mechanism.

It is worth noting that all time histories are characterized by a higher PGA during the third mechanism of the 1980 Irpinia earthquake. This is apparently unexpected considering the higher magnitude of the first mechanism. This behavior could be justified invoking the shorter distance between the dam and the source of the third mechanism (Chapter 3). If reference is made, for example, to the time history of point 6, a similar response is also detectable on the recording available at Calitri station during the 1980 Irpinia earthquake, being also Calitri as Conza, closer to the third mechanism of the 1980 source.

The registrations of Calitri (Figure 5.20) present lower amplitude in comparison to simulations obtained in Conza since a greater distance between the source and former site exists.

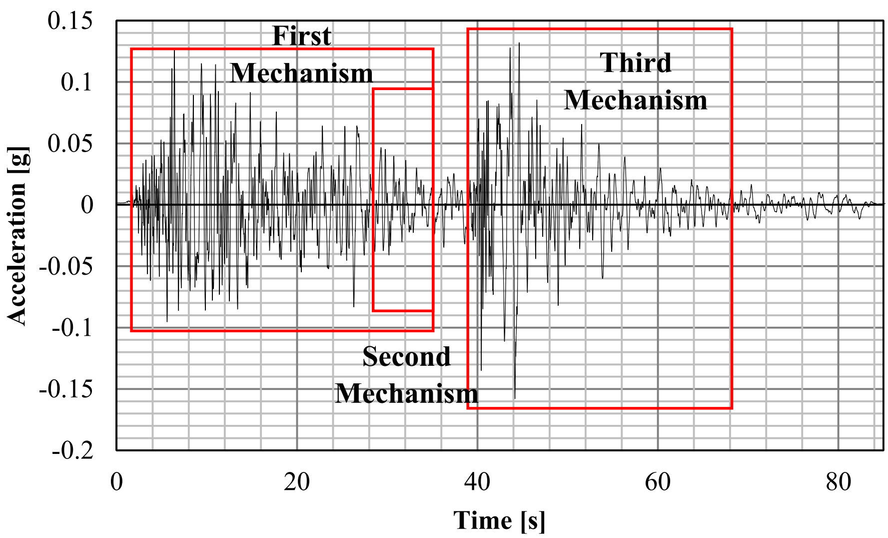

Figure 5.20 Acceleration time history recorded at Calitri during the 1980 Irpinia earthquake, projected along the x direction of the DRM model.

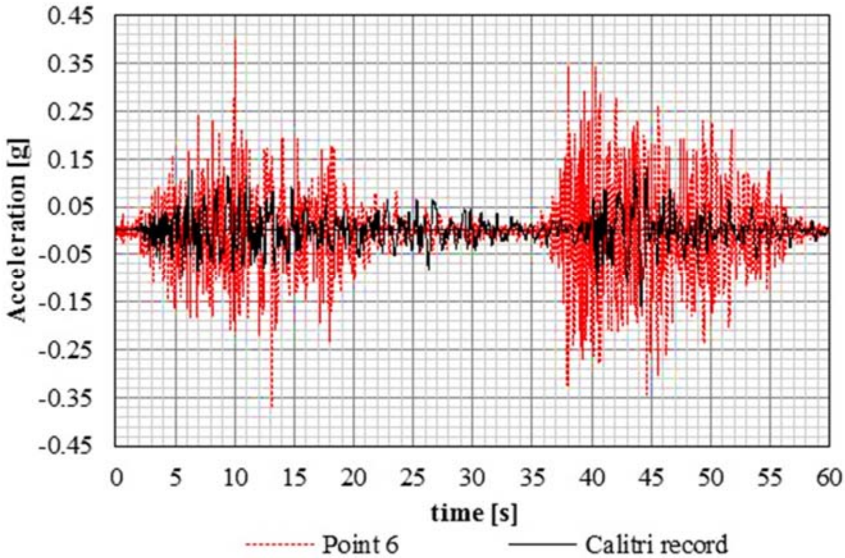

Figure 5.21 Comparison between the acceleration time history (along x direction) for point 6 of the DRM model and Calitri registration of Irpinia earthquake.

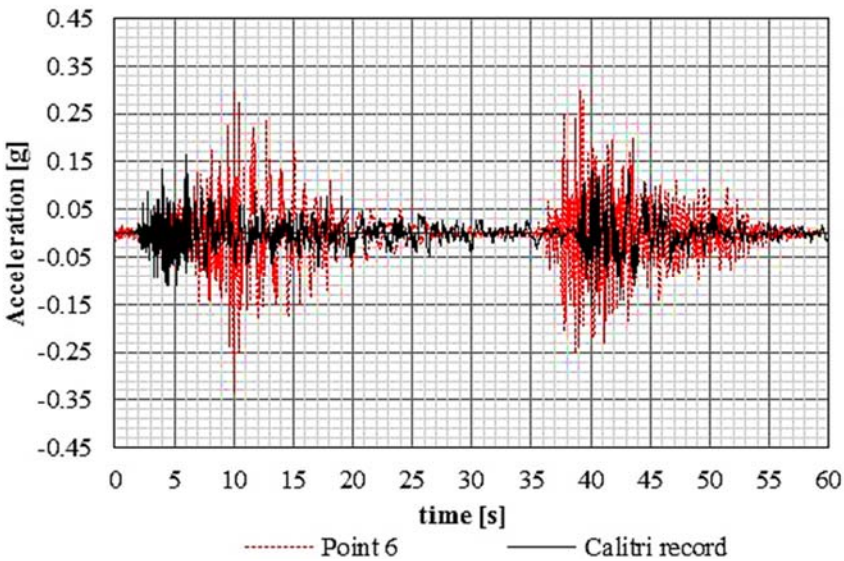

Figure 5.22 Comparison between the acceleration time history (Up-Down component) for point 6 of the DRM model and Calitri registration of Irpinia earthquake.

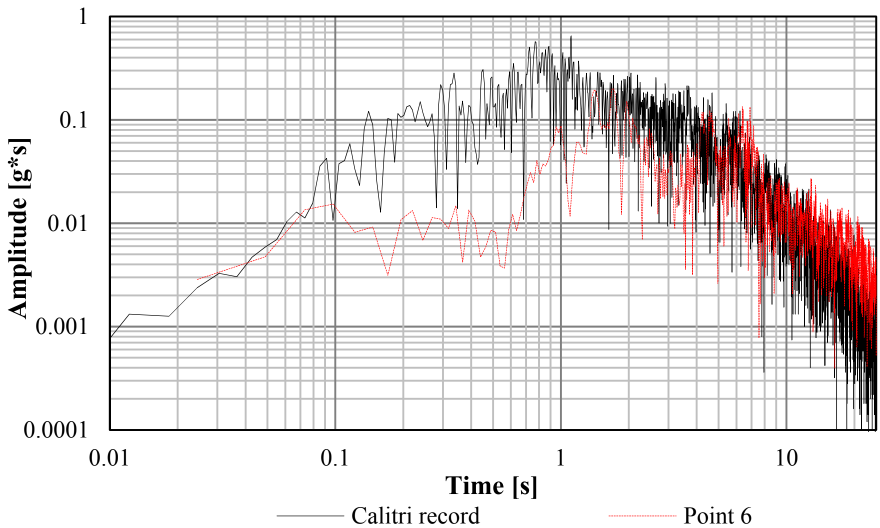

Figure 5.23 Comparison between the Fourier spectra of the signal (x component) recorded at Calitri in 1980 (black line) and simulated by DRM (point 6).

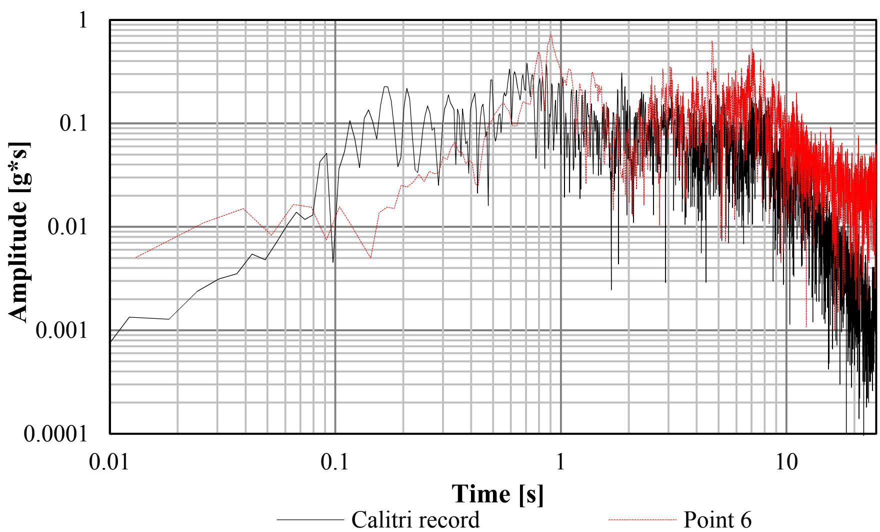

Figure 5.24 Comparison between the Fourier spectra of the signal (Up-Down) recorded at Calitri in 1980 (black line) and simulated by DRM (point 6).

The same consideration made for x components of the motion may be observed for the other two components (y and z).

In particular, the Up-Down components (Figure 5.22), simulated (point 6) and recorded (Calitri), are comparable to the horizontal ones as expected in near-fault conditions (Figure 5.21).

In Figure 5.23 and 5.24 the Fourier spectra of the accelerograms, related to Figure 5.21 and 5.22 respectively, are shown and a good agreement of spectral shape are highlighted.

This assures the proper simulation of the source mechanism by DRM approach.

5.5.2.1. *Effects of the 1980 Irpinia earthquake on the dam embankment*

In Figure 5.25 the vertical displacements after the simulation of the Irpinia earthquake are shown. In the figure higher settlements can be observed in correspondence of the connection between the dam and the western abutment. Settlements between 70 and 80 cm (red shade) were computed.

Conversely slightly lower vertical displacements are found on the eastern abutment. From the global view of the seismic-induced displacements with the DRM approach, it emerges that the western part of the dam body together with the abutment suffers a huge subsidence phenomenon, more pronounced than for the eastern part. These displacements are co-seismic, further deformations in the dam body and foundation are expected during the post-seismic consolidation due to dissipation of excess pore water pressures.

From Figures 5.25 and 5.26 it is possible to observe a portion of the central part of the dam (section 4) that is lower height, since it was not yet built at the time of the 1980 Irpinia earthquake.

Figure 5.26 shows the vertical displacement computed according to the traditional approach, by adopting a unique input motion at base of the dam, or better at the roof of the bedrock (motion of point 6 in Figure 5.18).

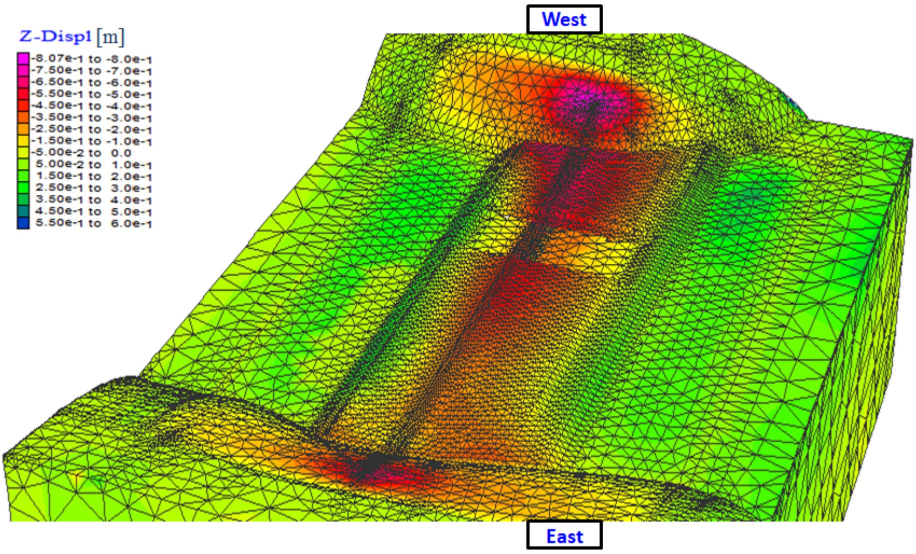

Figure 5.25 Computed vertical displacements due to the Irpinia earthquake by the DRM proposed approach.

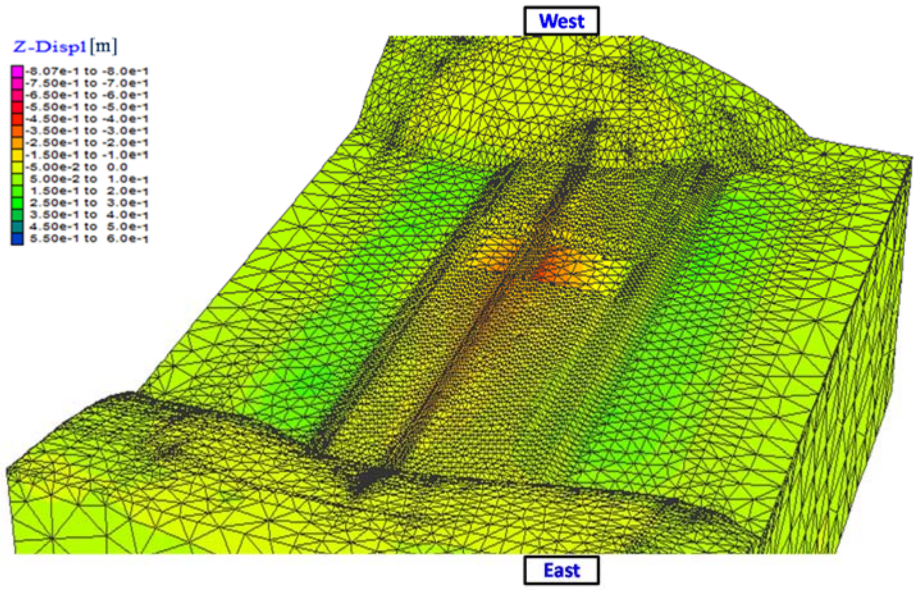

Figure 5.26 Computed vertical displacements due to the Irpinia earthquake by the traditional approach.

The comparison between Figures 5.25 and 5.26 highlights important differences between the two approaches. In particular, the DRM approach provides:

- comparable vertical displacements of the dam body, for intensity and trend, with the experimental measures;
- settlements growing in west direction;
- maximum seismic-induced displacement in correspondence to section 6 of the embankment;
- settlements of the foundation level about 20 cm lower than settlements in crest.

Instead, the traditional approach provides:

- reduced values of the vertical displacements of the dam body (maximum value about 40 cm);
- settlements growing in the middle of the embankment;
- maximum displacement in correspondence to section 4;
- settlements of the foundation level of about 20 cm;
- about zero settlements in section 1 and 6.

In Figure 5.25, the maximum settlement corresponds, unexpectedly, to the lower part of the dam body in 1980 (section 4). This unexpected response predicted only by the DRM approach may be justified by comparing the results of computed settlements with those measured at the time of 1980 earthquake and interpreted by Brigante (2010).

From Figure 5.27 a good agreement between settlements measured in correspondence to the foundation and crest of the embankment with settlements predicted by the proposed DRM approach can be observed.

The trend of computed settlements along the longitudinal axis of the dam reproduces the observed values in all monitored sections fairly well (higher values towards section 6, that is, the western abutment).

Conversely, in the case of the traditional approach (Figure 5.28) the computed settlements do not fit the measured trend. The maximum settlements in the foundation and at the embankment crest are about 50% lower than the measured ones.

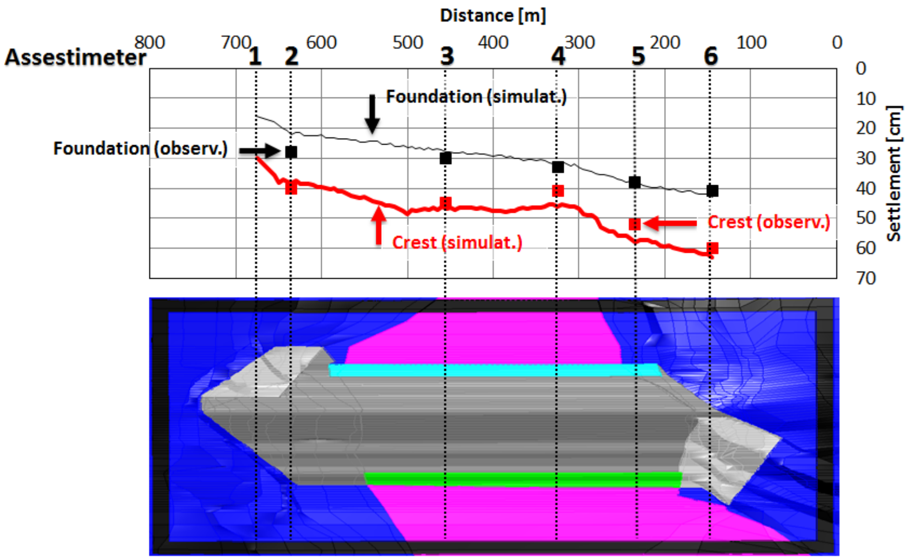

Figure 5.27 Comparison between numerical solution (proposed approach) and experimental data. The red line represents the simulated crest settlements in the longitudinal section, while the thin black line represents the foundation settlements. Red and black points represent the crest and foundation observation, respectively.

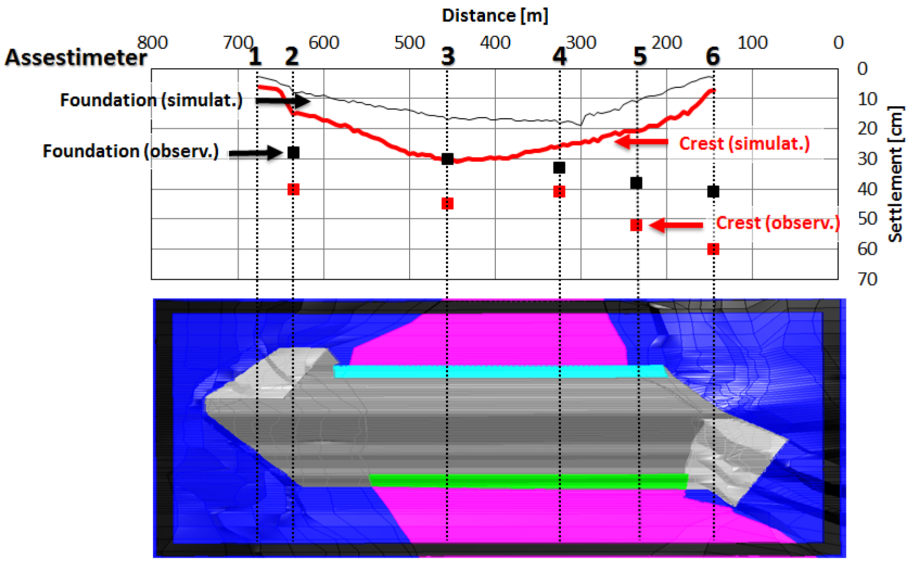

Figure 5.28 Comparison between numerical solution (traditional approach) and experimental data. The red line represents the simulated crest settlements in longitudinal section, while the thin black line represents the foundation settlements. Red and black points represent the crest and foundation observation, respectively.

It is important to emphasize that both the DRM and traditional analyses have been carried out adopting the same geometry, mesh and constitutive laws of materials. Accordingly the variation of the results is all attributable to the seismic input, which in the DRM approach is diversified for each node of the interface elements (Figure 5.7) between the external and internal domains.

Figures 5.29 and 5.30 show the time histories of vertical displacements for six points along the longitudinal axis (points from A to F) and 3 points on the cross-section N°4 (points G, C and H) for the DRM and traditional approach, respectively.

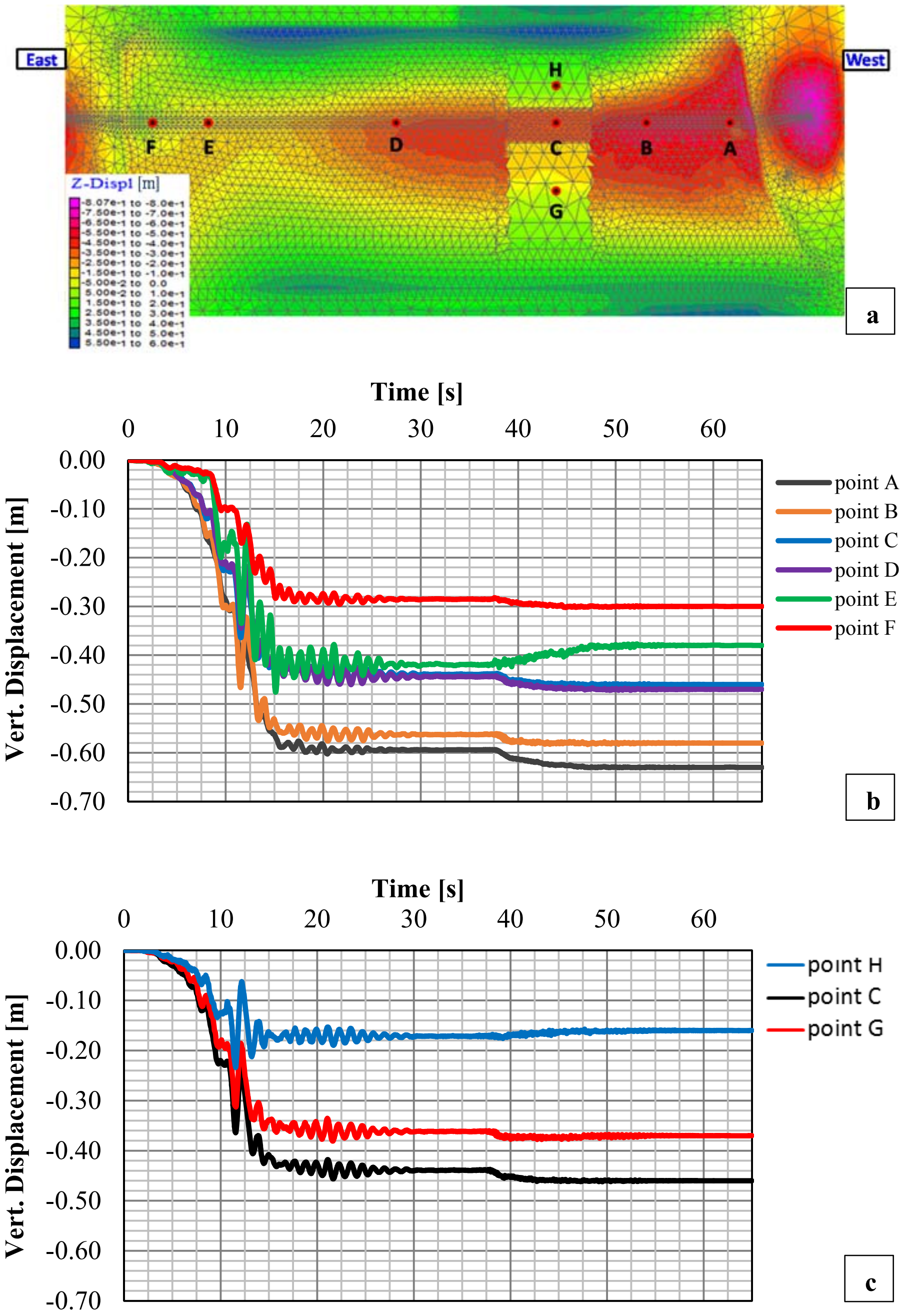

Figure 5.29 Time-history of vertical displacements computed for some points along the boundary of the dam in the DRM approach. (a) Point location, (b) results along the longitudinal section and (c) in the cross-section 4 (H-C-G).

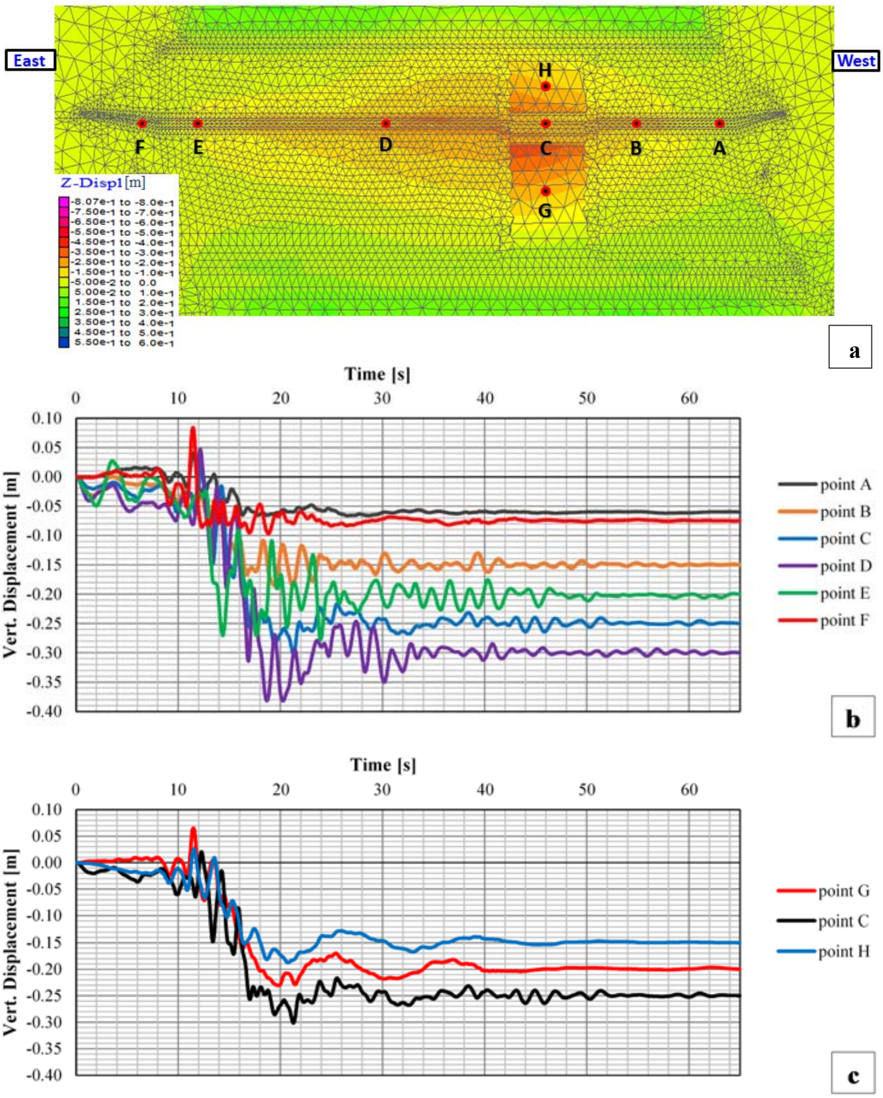

Figure 5.30 Time-history of vertical displacements computed for some points along the boundary of the dam in the traditional approach. (a) Point location, (b) results along the longitudinal section and (c) in the cross-section 4 (H-C-G).

In both approaches, however, is the first mechanism of the 1980 event to induce the higher permanent deformation while no further contribution is given by the third mechanism whose seismic intensity at the site is even higher than that of the first mechanism (Figures 5.19 and 5.20). This aspect acts as a kind of "memory" effect that soil exhibits. Further accumulation of plastic strains occurs only if stress states much higher than those experienced by the dam during the first mechanism of the 1980 event will be induced.

Figure 5.31 accounts for PGA amplification (in respect to dam foundation) of the x-component of acceleration, in correspondence to the six monitored cross-sections of the dam. Higher amplification is found at the cross sections n. 3 of the dam where PGAs of 0.55g are computed with the DRM approach. The dashed line in Figure 5.31 highlights the variability of the input motion at the base of the dam, variability that, as stated up to now, only the DRM approach may account for.

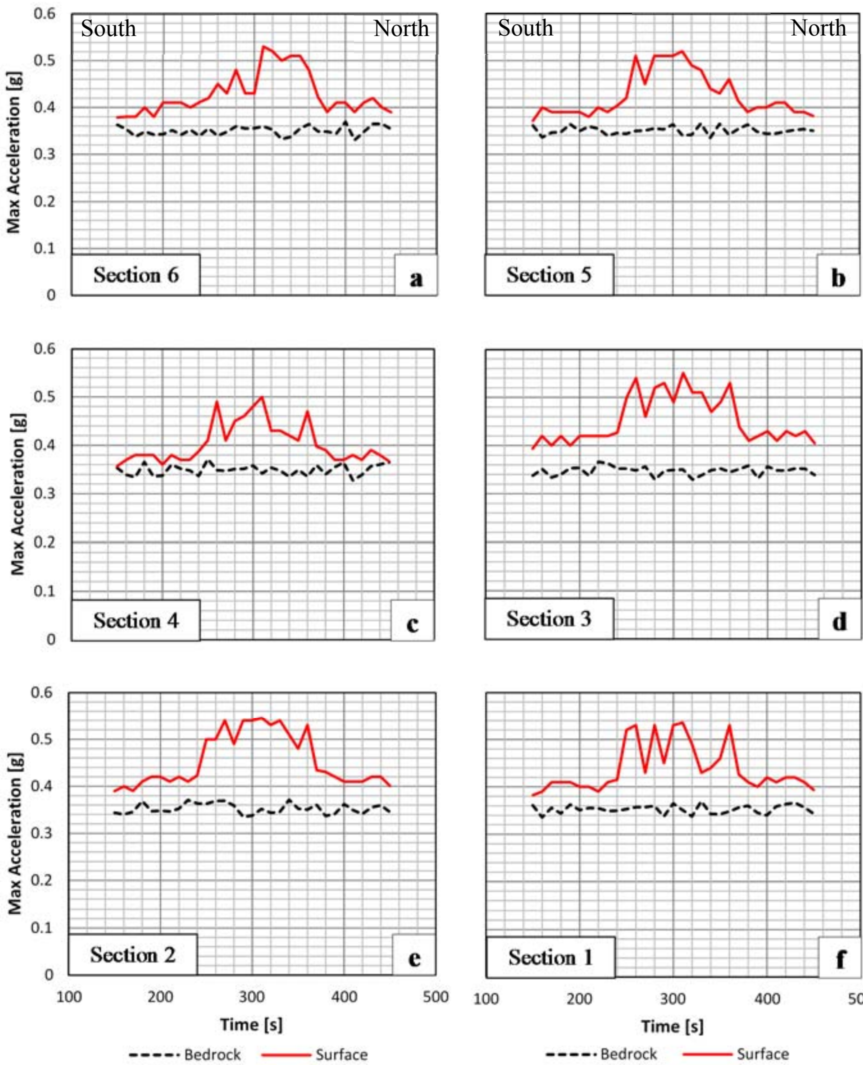

Figure 5.31 Peak ground acceleration along the dam boundary (red line) and foundation (black dashed line) in correspondence to the six monitored cross-sections.

During the 1980 Irpinia earthquake, permanent settlements of the dam body and of the valley were measured. No information is available on the seismic-induced pore water pressures in the dam core (the dam was not yet impounded at that time). Predictions carried out by the DRM approach combined to the Finn-Byrne constitutive model of the core soils (§ 4.2.1.2) provides excess pore water pressures (Figure 5.32) of 230 kPa and 160 kPa at the core base (point A) and middle height (point B) respectively.

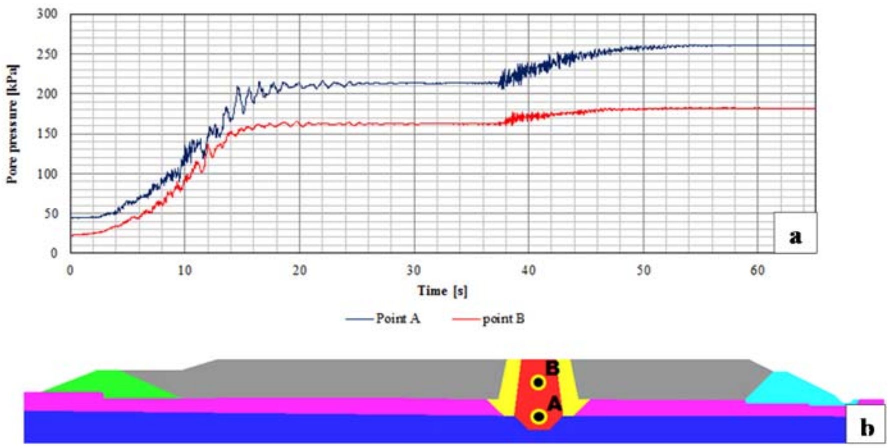

Figure 5.32 Pore-pressure history for two nodes in the core during the Irpinia earthquake simulation.

Once again as observed for settlements, it is possible to see a rapid accumulation of pore pressures during the first mechanism of the 1980 Irpinia earthquake and a lower contribute of the third mechanism. These predictions should be corroborated in the future by suitable laboratory investigation on core soils to calibrate the amount of excess pore water pressures on the number of cycles.

5.5.2.2. *Future seismic scenarios*

As anticipated in Chapter 3, scenario analyses were carried out to evaluate dam response in its actual configuration (maximum dam height and reservoir level). In particular, six seismic scenarios are considered: (i) three slip-maps for the first mechanism of the Irpinia earthquake (scenarios 1a, 1b and 1c); (ii) three slip-maps for the third mechanism (scenarios 3a, 3b and 3c).

Figures 5.33 and 5.34 show time histories and Fourier spectra of the accelerograms (x-direction) for point 6 (Figure 5.18) of section 3. It is worth noting that any other point could have been selected but the choice of point 6 was motivated by the fact that its motion was adopted as reference one in performing the dynamic analysis of the dam by means of the traditional approach.

From Figures 5.33 and 5.34 it emerges that the two seismic mechanism (1 and 3) at the foundation of the dam provides almost the same PGA (0.35÷0.38g) but duration of the strong motion stage and Fourier spectra (Figure 5.34) may be different with the obvious consequences on seismic-induced deformation in the embankment and abutments.

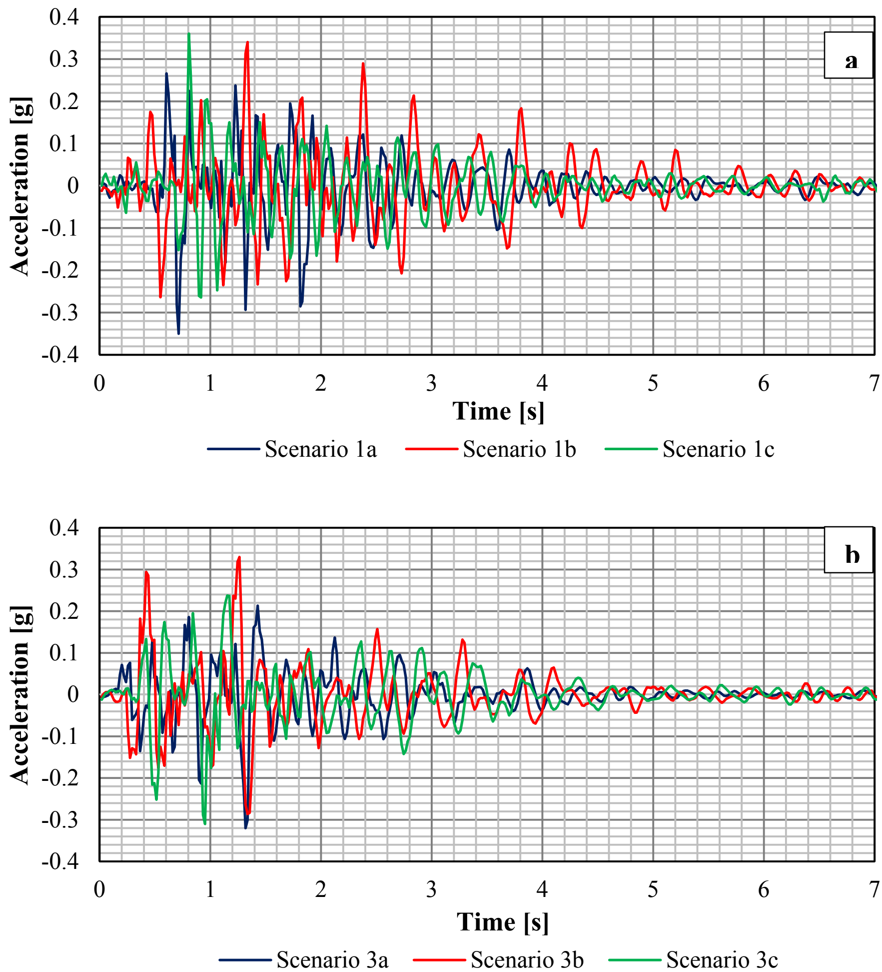

Figure 5.33 Time histories of x-acceleration at point 6 for mechanism 1 (a) and mechanism 3 (b).

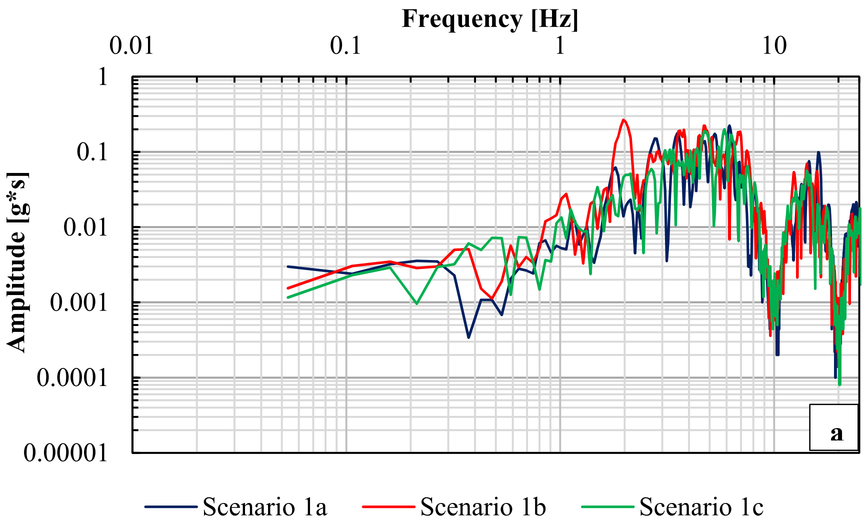

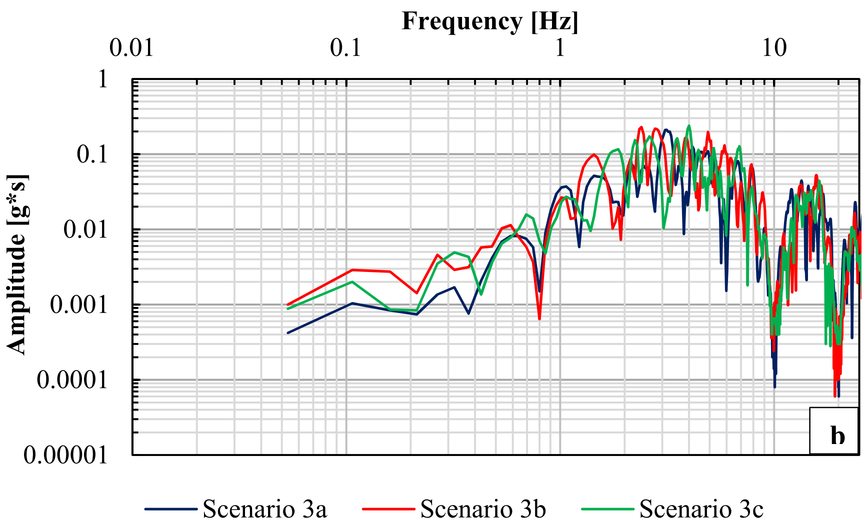

Figure 5.34 Fourier spectra of x-acceleration at point 6 for mechanism 1 (a) and mechanism 3 (b).

With reference to section 3 of the dam, Figure 5.35 plots the peak accelerations at the base and along the dam boundary. A PGA amplification of about 1.5 is found again, as computed for the 1980 event (but with a lower height of the embankment). This response may be justified considering that in Figure 5.35 the amplification factor is primarily affected by topography effects of the dam (H=50m) while in 1980 amplification of the signal (Figure 5.31) may be primarily due to the low stiffness of the embankment layers (G_0 *(p')*).

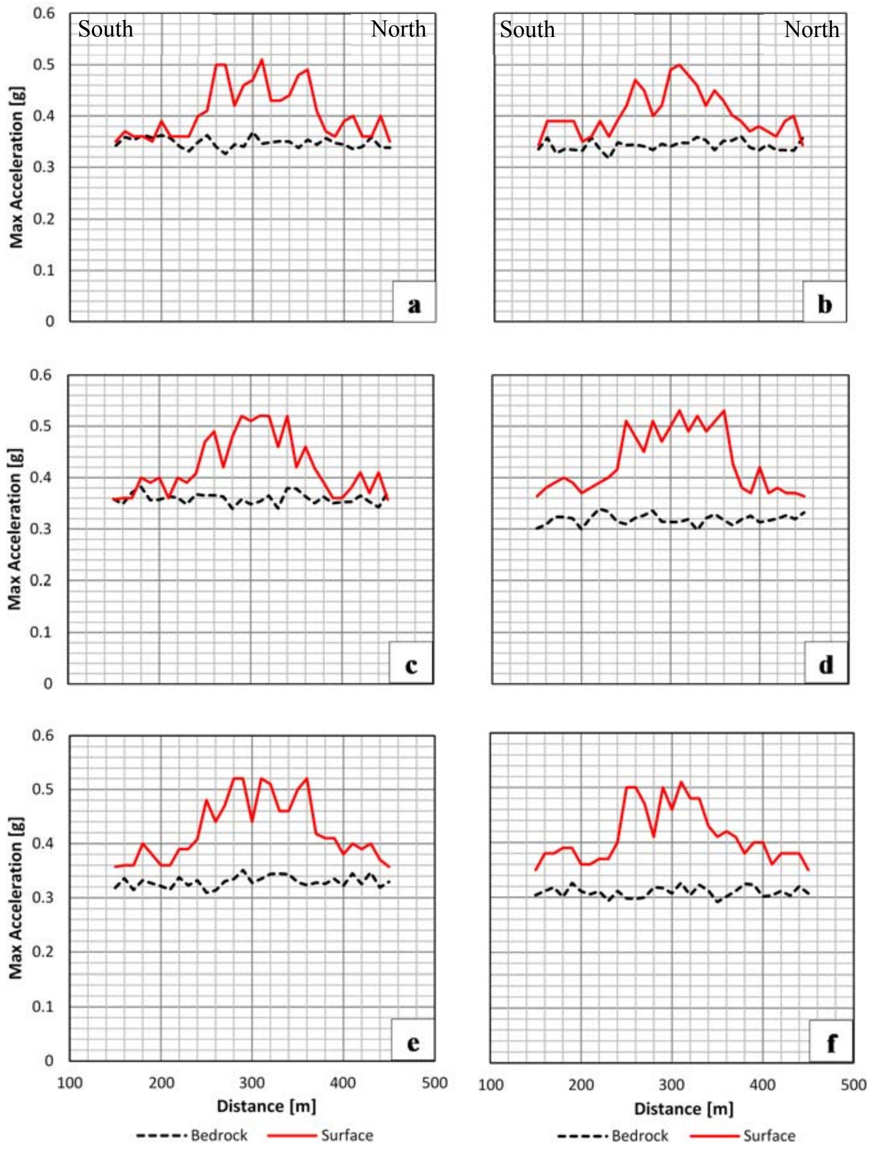

Figure 5.35 Peak acceleration (x-direction) at the base (dashed line) and along the dam boundary (red line) of cross-section 3 and for the 6 simulated seismic scenarios.

In Figure 5.36, the contours of the vertical displacements of the dam for the six scenarios considered are provided. The maximum settlement does not exceed 10 cm which is much lower than the value estimated and observed during the 1980 earthquake with a minor height of the dam embankment. This response may be justified by several factors:

(i) modified geometry of the dam after the 1980 event designed to account for seismic actions;
(ii) hardening of soils which “remember” the shaking of the 1980 earthquake. Further analyses were carried out in time sequence with the real events (1980 earthquake, construction, impounding, consolidation).

In dependence of the seismic scenarios, different settlement contours are plotted (Figure 5.36) and it is not straightforward to establish the most critical scenario for the dam body. However, a trend may be envisaged. Higher settlements are computed in the west side when mechanism 1 triggers. Conversely, mechanism 3 is more dangerous for the eastern part. In addition, for a fixed source mechanism, a different slip-map can affect the system response. For example, the slip-maps with the maximum value of slip concentrated at higher depth, due to the different radiative path, tend to generate subsidence mainly in the middle of the embankment (see scenarios 1c and 3b).

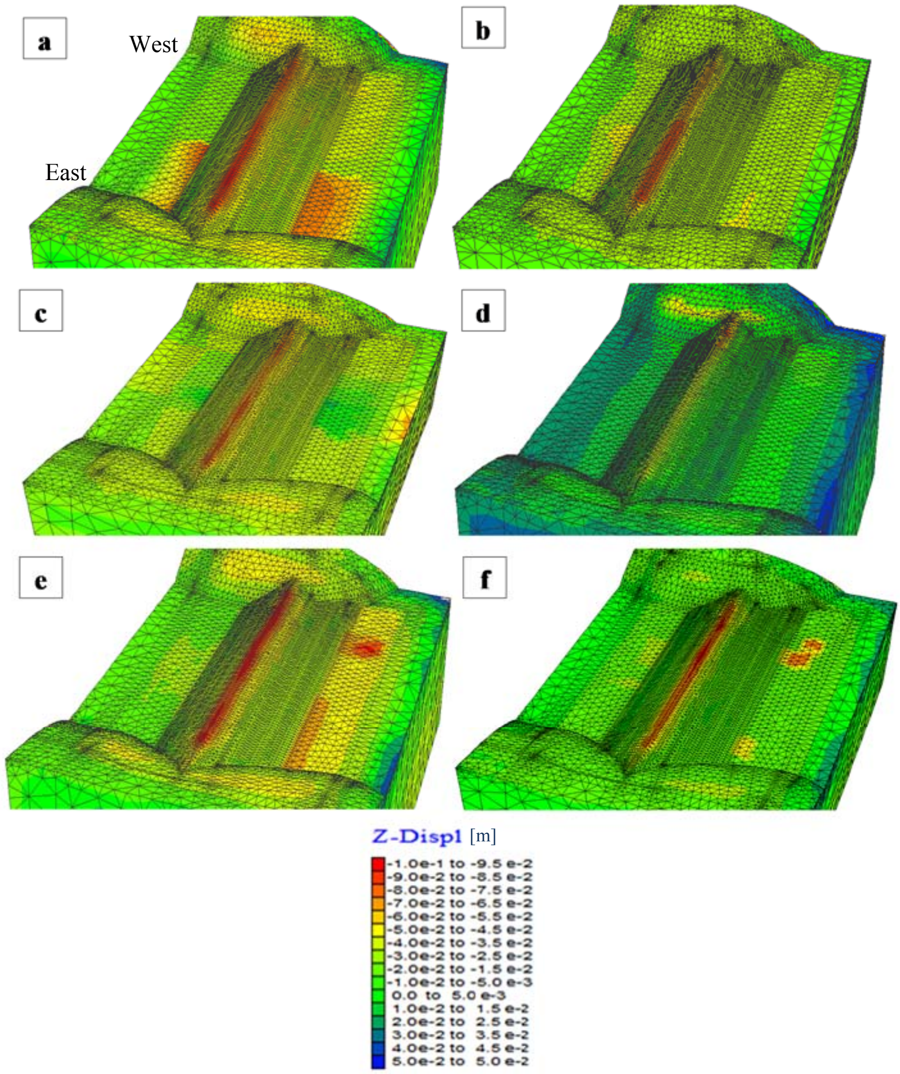

Figure 5.36 Vertical displacements computed in the dam by the DRM approach with the six simulated seismic scenarios.

In Figure 5.37, the same scenarios were reproduced with the traditional approach. In this case, no significant difference is found between the various scenarios. Maximum settlements are around 2-3 cm generally in correspondence of the central part of the dam.

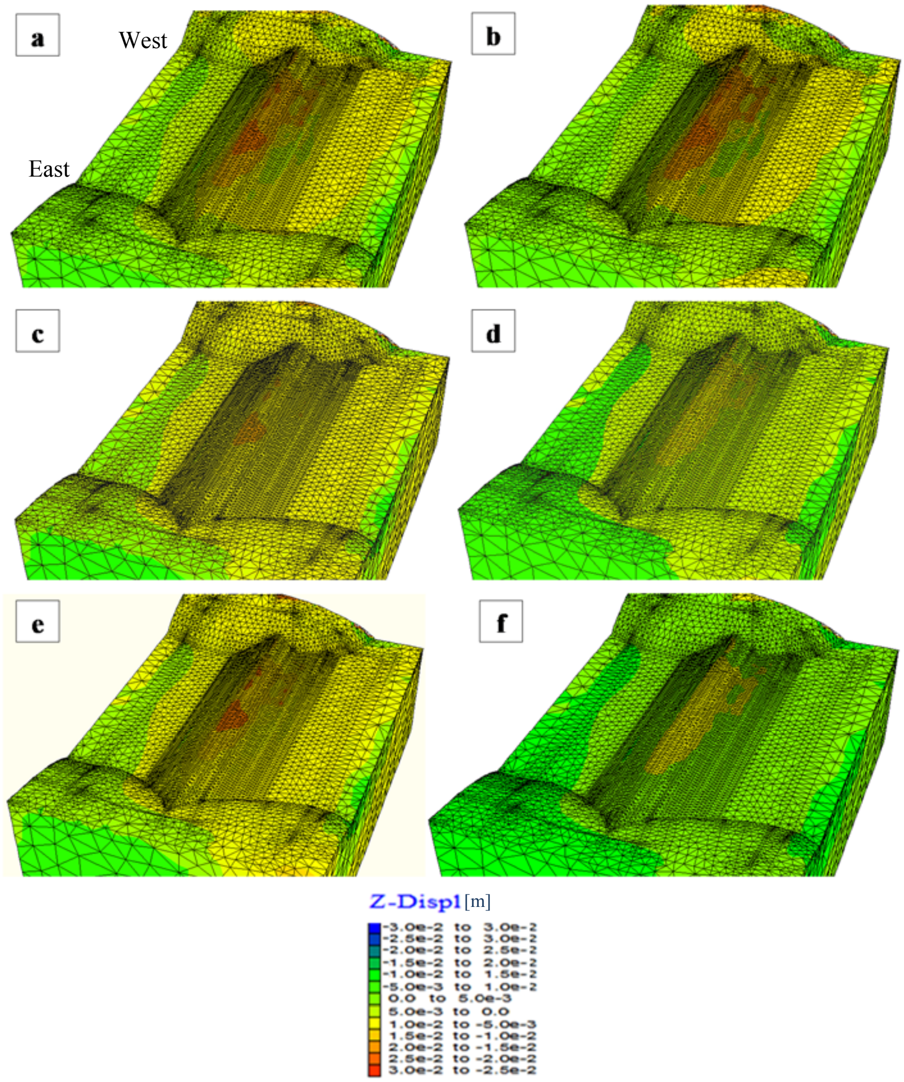

Figure 5.37 Vertical displacements computed in the dam by the traditional approach with the six simulated seismic scenarios.

To assure the reliability of the predicted dam response to the simulated seismic scenarios, the estimated settlements of the Conza dam in its actual configuration were compared to the experimental data collected by Swaisgood (2003) on a worldwide dam database. It is worth noting that most dams considered by Swaisgood (2003) in its database experienced near-source seismic propagation. For earthquakes with high magnitudes (M=5.8÷8.3) most dams are placed within 20 km from the seismic source.

The settlement predictions obtained for Conza dam with the DRM approach (variability of the input motion) is consistent with the observed response for an earthquake magnitude of 6.5 (1980 first mechanism). The traditional approach provides dam permanent settlements much lower than those associated with the magnitude of simulated earthquake (Figure 5.38).

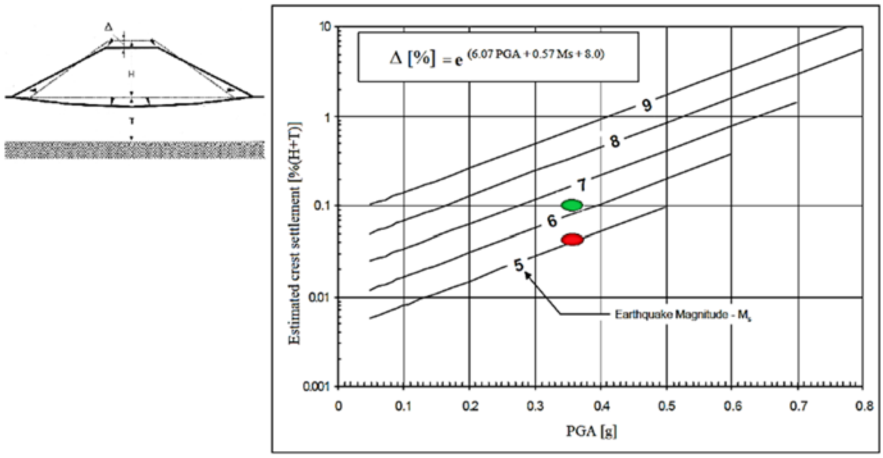

Figure 5.38 Chart for estimating crest settlement (modification from Swaisgood, 2003). In green the range of the results carried out by the DRM approach is reported. In red the prediction range related to the traditional approach is showed.

Final remarks

Accelerometric and velocimetric recordings acquired in different sites located at a short distance from seismic sources, during several earthquakes worldwide, have shown the variability of seismic motion characteristics in near-source conditions. In particular, in the vicinity of the seismic source the presence of a bimodal spectral shape on at least one of the components of motion was observed (Somerville 2005). A significant energy content at high frequencies is observed, due to minor dissipation occurred during the short wave path form the seismic source and the site. The spectral peak at low frequencies, however, is probably caused by the presence of an impulsive component induced by the phenomenon of “forward directivity” (Somerville 2005). Other typical characteristics of the near-source motion are: the presence of residual displacements at the ground level, or evidence of the fault on the surface ("fling-step"); high PGA, PGV and PGD values compared to those recorded far from the source (far-field conditions) for earthquakes with the same magnitude; the presence of a not-negligible vertical motion, with reference to the horizontal components; the almost simultaneous arrival of S and P waves due to the short source-site distance; further P and S waves contribute to both horizontal and vertical motions because the wave fronts approach the surface with an inclination which can be very different from the sub-vertical (as it happens for sites far from the focal mechanism). Finally, the frequency content of the signal depends on the focal mechanism, i.e. geometry and direction of fracture propagation, slip map and source-site relative position.

In geotechnical earthquake engineering, it is particularly important to characterize both the frequency content of the seismic signal and its asynchronism at the bedrock. In this context, the seismic response of structures characterised by predominant longitudinal development (such as dams, road embankments, tunnels, bridges, pipelines) can be significantly influenced by kinematic and dynamic effects due to the near-source wave propagation. The asynchronism of the seismic motion at the base of an earth embankment, for example, may induce unsafe stress states.

As already pointed out by Corigliano et al. (2011), the earthquake response analysis in near-source conditions can not be separated from the simulation of the source mechanism and of the propagation process, since the variation of seismic motion along the boundary of the analysis domain is closely related to: (i) the geometry of the source (extension in plan and corners of the strike and dip); (ii) the direction and value of the sliding average; (iii) the position and number of asperities on the fault surface; (iv) the mean rise-time; (v) the site-source distance; (vi) the propagation medium (number of layers and the mechanical properties of each layer); (vi) to the extension of the study area. All these aspects were considered to reconstruct the seismic motion in each node at the border of the interest domain. This seismic motion will naturally be different from that that occurred in 1980 but equivalent from the engineering point of view. For this aim, a calibration of the 1D velocity model of the propagation medium, between the site and the source, has been realized, through the use of empirical Green functions. When the boundary value problem also contains the source mechanism over the structure of interest, the calculation times are notoriously long, because the size of the mesh elements is regulated by the maximum frequency of the signal that wants to propagate in the domain in exam. Furthermore, the need to simulate the presence of the interstitial fluid and the inelastic behavior of the soil, also through constitutive models which are not overly complex, makes the numerical simulation more expensive. To address this problem, in the context of the research project the approach called Domain Reduction Method (DRM), proposed by Bielak et al. in 2003, is defined. With this procedure it is possible to decouple the study of the dynamic response of the structure from the problem of the generation of the seismic motion at bedrock level. The first (model 1), containing the source and a simplified stratification (one-dimensional) of the subsoil; the second (model 2), detailed, containing the real topography of the site, as well as the structure object of study (earth dam).

In the thesis the mathematical-numerical modeling of a representative case study has been addressed. The choice is on the Conza della Campania dam, as it is positioned in a very short distance from the first and third fault segment of the 1980 Irpinia earthquake. This latter has hit the dam when was still in the construction phase (height of the embankment less than half of the maximum of the project), causing total settlements in axis to the core around 70 cm, of which about 50% is attributable to the settlements of the foundation plan. In fact, looking at the monitoring data interpreted by Brigante (2010), it is possible to see that the settlements induced by the earthquake along the longitudinal axis of the dam are not constant, but they grow in a west direction, that is moving to the right shoulder. There are not conditions to justify the variation of the profile of the deformation measured along the longitudinal axis of the dam (no significant variations of the foundation level and stratigraphy). Therefore, the possibility of a non-uniform seismic motion at the site (for reduced distance from the Irpinia earthquake fault system) has been investigated. For this aim, the dynamic response of the dam with a three-dimensional model, contemplating the effects of asynchronous motion to the base of the dam, was simulated. To verify the effects of seismic motion diversification at the base of large embankments located near the source, it is possible to compare the estimates of the seismic response of a dam through the innovative approach developed with the traditional methodology, valid in far-fault conditions. This latter assumes the use of a single set of 3 accelerograms (one for each component of motion) to be inserted at the lower border of the model.

A comparison between the monitoring data of the effects induced by the 1980 earthquake and the numerical predictions obtained, shows that the integrated model is able to reproduce, much more realistically, the response that the Conza dam expressed following the Irpinia earthquake, with settlements of a higher magnitude in the vicinity of the west abutment to the centreline. The results of the analysis show that, at equal mechanical properties of materials, the diversification of the seismic input at the base of the dam may have caused an increment of seismic-induced deformation, and a non-uniform distribution along the longitudinal development of the dam body, an effect that is reflected in the experimental data.

Future earthquake scenarios, with the same magnitude of the 1980 earthquake, induced low permanent displacements in the dam body. The justification is related to the important “memory” effect the 1980 earthquake preserved in the soil.

Comparing innovative and traditional approaches, an increase of settlement (up to three times) is observable in the use of the DRM approach. It is important to underline that the traditional approach does not provide comparable values (underestimating the damage) with the relationships between maximum settlement, magnitude and PGA proposed by Swaisgood (2003) on a database of monitored dams.

As further improvements of the performed study, an extended source model is required by setting up a 3D refined scheme of Campano-Lucano Apennine, enough realistic at high frequencies.

For the model at the site scale, the analyzes were carried out by assigning to the materials of the reference dam a constitutive model able to simulate only some salient aspects of the response of soils under cyclic and dynamic loading. A further advancement of scientific research in this field could be the use of advanced constitutive models, which can better simulate the nonlinear response of the soil from small to large strain levels (Bounding Surface Plasticity).

A. APPENDIX.
Discrete Wavenumber Method formulation (Bouchon, 2003)

A.1. Introduction

The evaluation of Green's functions for elastic media is an important topic in several fields such as seismology or acoustics. Since the pioneering work of Lamb (1904), many approaches have been proposed to evaluate the response of elastic solids to excitation due to transient point sources. The methods proposed for the calculation of the Green's functions are, however, often very complex and, in many cases, only provide approximate solutions. The discrete wavenumber method, introduced by Bouchon and Aki (1977), provides a way to accurately calculate the complete Green's functions for many problems.

The principle of the method may be traced back to Rayleigh (1896, 1907), who demonstrated that waves reflected by a sinusoidally corrugated surface propagate only at discrete angles that he referred to as the orders of the spectrum.

The existence of discrete orders in the horizontal wavenumber spectrum is an immediate consequence of the periodicity of the reflecting surface. Aki and Larner, (1970), extended Rayleigh's approach to study the scattering of plane waves in the vicinity of a periodic irregular surface with the use of complex frequency. In the same way, the discrete wavenumber (DWN) method introduces a spatial periodicity of sources to discretize the radiated wave field, and relies on the Fourier transform in the complex frequency domain to calculate the Green's functions.

A.2. Principle of the Method

We shall begin with a short consideration of the 2-D case, as the principle of the method is easier to describe in this case. The steady-state radiation from a line source in an infinite homogeneous medium can be represented as a cylindrical wave or, equivalently, as a continuous superposition of homogeneous and inhomogeneous plane waves. Therefore, denoting by *x* and *z* the horizontal and vertical axes in the plane normal to the line source, any variable such as displacement or stress can be written in the form

$$F(x,z;\omega) = e^{i\omega t}\int_{-\infty}^{\infty} f(k,z)e^{-ikx}\,dk \tag{A.1}$$

where x is the frequency and k is the horizontal wavenumber. Equation (A.1) still holds for an extended two-dimensional source located in a medium which is homogeneous in any horizontal plane.

When the medium is finite or vertically heterogeneous, the integral kernel has poles and singularities, and the integration over the horizontal wavenumber becomes mathematically and numerically complicated. One simple way to overcome these difficulties is to replace the single-source problem, whose solution is expressed by (A.1), by a multiple-source problem where sources are periodically distributed along the x axis.

Then, equation (A.1) is replaced by:

$$G(x,z;\omega) = \int_{-\infty}^{\infty} f(k,z)\,e^{-ikx}\sum_{m=-\infty}^{\infty} e^{ikmL}\,dk \tag{A.2}$$

where L is the periodicity source interval and the e^{ixt} term accounts for time dependence.

Equation (A.2) reduces to:

$$\mathrm{G(x,z;\omega)} = \frac{2\pi}{\mathrm{L}}\sum_{\mathrm{n}=-\infty}^{\infty} \mathrm{f(k_n,z)\,e^{-ik_nx}} \tag{A.3}$$

with $k_n = \frac{2\pi}{L}n$, which in turn, if the series converges, can be approximated by the finite sum equation

$$G(x,z;\omega) = \frac{2\pi}{L}\sum_{n=-N}^{N} f(k_n,z)\,e^{-ik_nx} \tag{A.4}$$

In moving from equation ((A.1) to equation (A.4), we have greatly reduced the calculation. In so doing, however, we have changed the problem from one of a single source, to one involving an infinite number of periodic sources, as illustrated in Figure A.1. The DWN method calculates equation (A.4), that is $G(x, z; \omega)$, instead of evaluating equation (A.1).

The second stage of the method is to retrieve the single-source solution from the multiple-source problem that we have solved in the frequency domain. This would be straightforward if we could calculate the continuous Fourier transform of G, as we could then isolate the single source solution in the time domain, provided that we have chosen an appropriate value for L.

In practice, however, we can only calculate G for a certain number of frequencies and use the discrete Fourier transform to obtain the time domain solution. Thus, on one hand we deal with a signal which has an infinite time response (because of the infinite set of sources), while on the other hand, we use the discrete Fourier transform, which yields a signal of finite duration $T = 2\pi/\Delta\omega$, where $\Delta\omega$ is the angular frequency sampling used in calculating G. This can indeed be accomplished by performing the Fourier transform in the complex frequency domain:

$$g(x, z; t) = \int_{-\infty+I\omega_I}^{\infty+i\omega_I} G(x, z; \omega) e^{i\omega t}\, d\omega \tag{A.5}$$

where ω_I denotes the constant imaginary part of the frequency and is chosen such that:

$$e^{\omega_I T} \ll 1 \tag{A.6}$$

This last equation ensures the attenuation, over the time window T, of the previously infinite time response solution. Thus, provided that we have chosen L large enough so that no disturbance arrives at the receiver (x, z) from the next closest source in the time window of interest T, the time-domain single-source solution $f(x, z;\ t)$ is obtained from the frequency-domain multiple-source calculation $G(x, z;\ \omega)$ by:

$$f(x, z; t) = e^{-\omega_I t} \int_{-\infty}^{\infty} G(x, z; \omega) e^{i\omega_R t} d\omega_R \tag{A.7}$$

where the integral is computed by using the FFT.

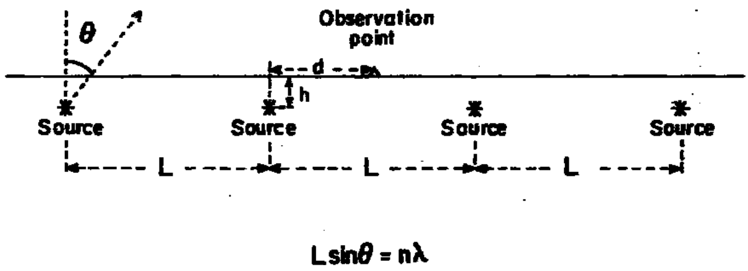

Figure A.1 Physical interpretation of the DWN method. The single source is replaced by an infinite array of sources distributed horizontally at equal interval L. For a given radiation wavelength k, corresponding to a specific frequency of excitation, the elastic energy is radiated in discrete directions h only (Bouchon, 2003).

Equation (A.6) shows that ω_I is only a function of the length of the time window T considered. The results should not be sensitive to the particular value of ω_I chosen, as long as it provides enough attenuation for the disturbances which arrive after the time window of interest T to be negligible. Values in the range:

$$\omega_I = \left[-\frac{\pi}{T}, -\frac{2\pi}{T}\right] \tag{A.8}$$

are recommended for most applications.

It is worth noting here that disturbances which arrive in the time range $[T, 2T]$ will be attenuated by $e^{\omega_I T}$, while disturbances in the time range $[2T, 3T]$ will be attenuated by $e^{2\omega_I T}$, and so on. The choice of ω_I may also be justified by the fact that the frequency spectrum $G(\omega)$ is not discrete, as would be the case with real frequencies, but is continuous with a bandwidth proportional to ω_I (Larner, 1970). Choosing values in the range of relation (A.8) implies that the bandwidth of the spectral lines is of the order of the frequency interval. Thus, the calculated signals may also be considered as resulting from a nearly continuous sampling of the frequency domain. Figure A.2, we present a comparison of the numerical results obtained through these equations with an analytical solution. The case considered involves an explosive line source in a half-space, as it is one of the rare cases where an analytical solution exists (Garvin, 1956). The comparison shows the high accuracy of the DWN method.

A.3. Discretization in Various Coordinate Systems

The simplest type of elastic source in three-dimensions is an isotropic point source. The wave field radiated by such a source can be conveniently represented by the displacement potential, which, for a steady-state excitation, is given by:

$$\phi(R;\omega) = \frac{-V_s(\omega)}{4\pi R} e^{i\omega(t-R/\alpha)} \tag{A.9}$$

where V_s is the volume change at the source and a denotes the compressional wave velocity.
In the shallow earth, where boundaries are nearly horizontal and where the medium properties change primarily with depth, using this spherical wave representation would be cumbersome, so we must express the wave field in more appropriate coordinate systems.

One possibility is to use a Cartesian system with the *z* axis running vertically. In such a system, the wave field is expressed as a double integral over the two components of the horizontal wavenumber, *kx* and *ky*, through the Weyl integral (Lamb, 1904; Aki and Richards, 1980):

$$\phi(x,y,z;\omega) =$$
$$= \frac{iV_s(\omega)}{8\pi^2} \int_{-\infty}^{\infty} \int_{-\infty}^{\infty} \frac{1}{\nu} e^{-i\nu|z|} e^{-ik_x x} e^{-ik_y y} dk_x dk_y \tag{A.10}$$

with

$$\nu = \sqrt{\frac{\omega^2}{\alpha^2} - k_x^2 - k_y^2} \qquad Im(\nu) < 0$$

where the origin of the coordinate system is taken at the source, and the $e^{i\omega t}$ dependence is understood.

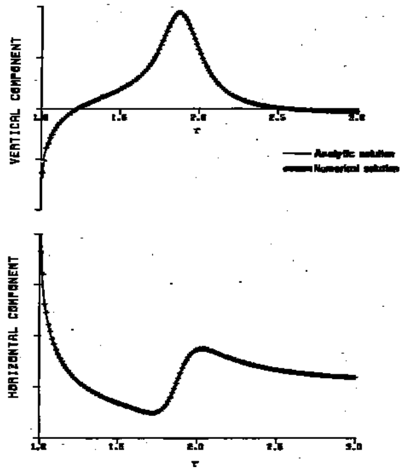

Figure A.2 Comparison between numerical and analytical solutions for the surface displacement due to a buried explosive line source with step-function time dependence. Computations are made for a Poisson ratio of 0.25 and a ratio of distance R to source depth equal to 10. $\tau = t\alpha = R$, where t is time and α is the compressional wave velocity. The analytical displacements are infinite at the time of P -wave arrival ($\tau = 1$). (Bouchon, 2003).

The generalization of the previous results from 2-D to 3-D is straightforward and leads to the following expressions (Bouchon, 1979):

$$\phi(x, y, z; \omega) = \frac{iV_s(\omega)}{2L_xL_y} \sum_{n_x=-N_x}^{N_x} \sum_{n_y=-N_y}^{N_y} \frac{1}{\nu} e^{-i\nu|z|} e^{-ik_{nx}x} e^{-ik_{ny}y} \qquad \text{(A.11)}$$

with

$$k_{nx} = \frac{2\pi}{L_x} n_x, k_{ny} = \frac{2\pi}{L_y} n_y,$$

for which the corresponding multiple-source problem is a periodic array of sources distributed at equal intervals *Lx* in the *x* direction, and *Ly* in the *y* direction. In many wave propagation problems, the elastic wave field may also be conveniently expressed in a cylindrical coordinate system with *z* as the vertical axis.

The wave field is then represented as an integral over the horizontal wavenumber through the Sommerfeld integral:

$$\phi(r,z;\omega) = \frac{iV_s(\omega)}{2L_xL_y}\int_0^{\infty}\frac{k}{\nu}J_0(kr)e^{-i\nu|z|}dk \tag{A.12}$$

with $\nu = \sqrt{\frac{\omega^2}{\alpha^2} - k^2}$, $Im(\nu) < 0$ and where J0 denotes the zeroth order Bessel function.

The discretization of this equation can also be achieved by replacing the single source by a periodic arrangement of sources which, in this case, consists of the original point source plus an infinite array of circular sources centered around the point source and distributed at equal radial interval L (Bouchon, 1981). This physical arrangement leads to:

$$\phi(r,z;\omega) = \frac{iV_s(\omega)}{2}\sum_{n=0}^{N}\frac{k_n}{\nu_0}J_0(k_nr)e^{-i\nu_n|z|}dk \tag{A.13}$$

with $k_n = \frac{2\pi}{L}n$.

The comparison between the two geometric source arrangements resulting in discretizations (A.11) and (A.13) is shown in Figure A.3

Once the source radiation has been decomposed, through equations (A.4), (A.11), or (A.13), into a superposition of waves propagating with discrete wavenumbers, the effect of plane boundaries and flat layers is taken into account by using, for each horizontal wavenumber component, the corresponding plane-wave reflection and transmission coefficients at the medium surface and interfaces, and summing up all the wavenumber contributions. This is best done by calculating, for each wavenumber involved in the source radiation, the corresponding reflectivity and transmissivity matrices of the layered medium (Kennett, 1974; Kennett and Kerry, 1979; Muller, 1985). The truncation of the wavenumber series is easily determined for each frequency by a simple convergence criterion which compares the new wavenumber contribution to the current sum of the series, and stops the calculation when the new contribution becomes negligible.

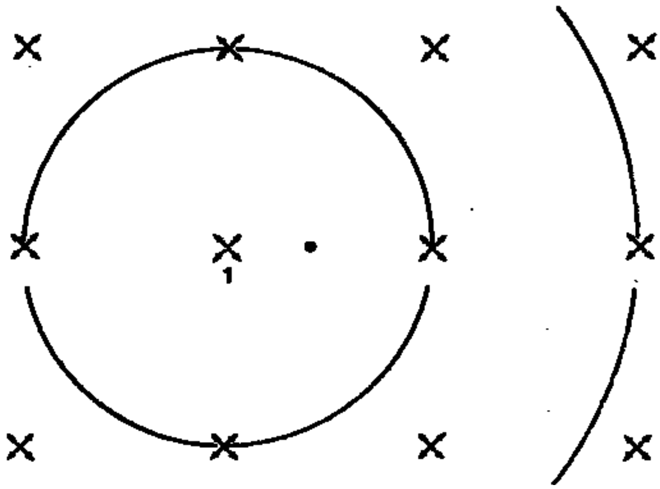

Figure A.3 Geometries of source-receiver configurations leading to the discretization: a circular source array for the k discretization scheme and a rectangular network for the (kx , ky) discretization method. Source 1 is the original single-source problem. The black dot shows the receiver location (Bouchon, 2003).

The accuracy of the two discretization schemes (A.11) and (A.13) can be measured by comparing synthetic seismograms obtained using these equations, as the two schemes are independent.

This is done in Figure A.4, where the similitude of the results demonstrates the accuracy of the DWN method. In most applications, the k discretization scheme will be preferred over the kx, ky scheme because it involves only one summation and the resulting calculation is faster. One such application is displayed in Figure A.5.

For other types of problems, other schemes of discretization may be devised. For instance, in the case of a source in a borehole, common in exploration geophysics, it is convenient to use, for equation (A.9), the expression:

$$\phi(r,z;\omega) = \frac{-V_s(\omega)}{4\pi^2}\int_{-\infty}^{\infty} K_0(\nu r)e^{-ikz}dk \tag{A.14}$$

with $\nu = \sqrt{\frac{\omega^2}{\alpha^2} - k^2}$, $Im(\nu) < 0$, where *(r, z)* are cylindrical coordinates centered at the source and z runs along the borehole axis, k is now the vertical wavenumber (in the case of a vertical borehole), and where K_0 denotes the zeroth-order modified Bessel function of the second kind.

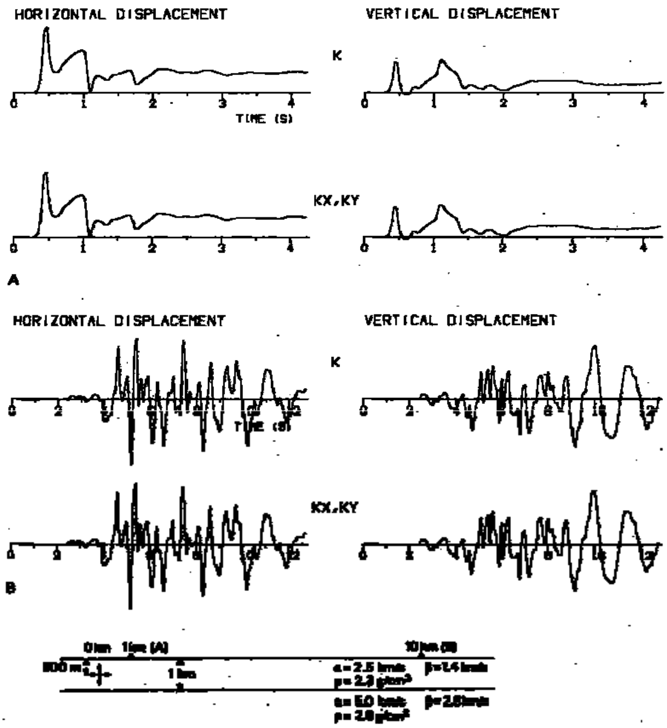

Figure A.4 Comparison of surface displacements obtained using the k and (*kx*, *ky*) discretization schemes for an explosion in a layer over a half-space model. The source-time function is $\frac{1}{2}[1 + tan\,h(t/t_0)]$ with $t_0 = 0.1\ s$. First motions are up and away from the source (Bouchon, 2003).

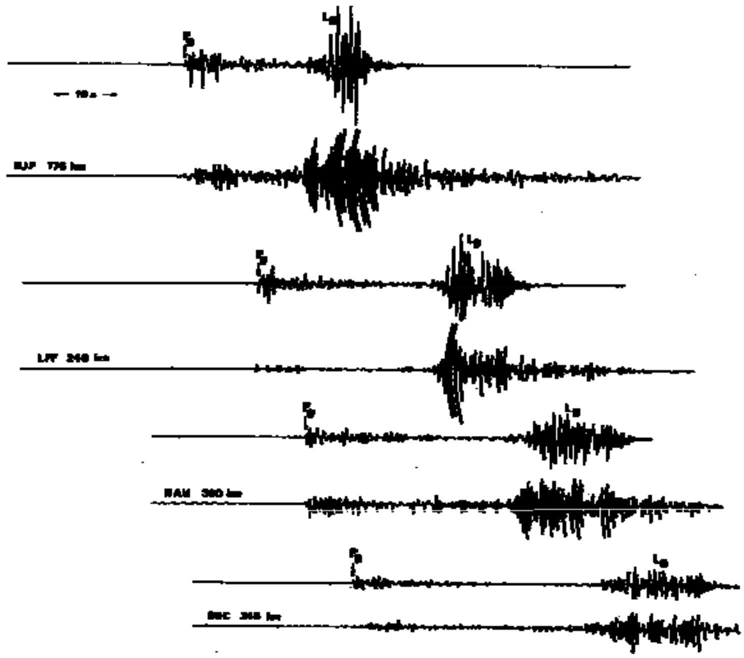

Figure A.5 Comparison of the vertical short-period seismograms synthesized (upper trace) and observed (lower trace) at four stations for a small earthquake in central France. The epicentral distance of each station is indicated. The propagation model used in the calculation consists of four crustal layers overlaying a mantle half-space. The source is a double-couple point with the mechanism of the earthquake and located at a depth of 10 km. The slip time dependence is a ramp function with a rise time of 0.2 s (Bouchon, 1982a).

The discretization of this expression, which was introduced by Cheng and Toksöz (1981), yields:

$$\phi(r,z;\omega) = \frac{-V_s(\omega)}{2\pi L} \sum_{n=-N}^{N} K_0(\nu_n r) e^{-ik_n z} \tag{A.15}$$

and corresponds to a periodic arrangement of point sources distributed at interval L along the z axis.

Expression (A.15) is convenient to use in a borehole environment because, in this form, cylindrical boundaries of the borehole, tubing, mud casing, and/or borehole tool can be taken into account through propagator matrices or reflectivity/transmissivity matrices similar to the ones in flat layer media. An example of such a calculation is displayed in Figure A.6.

A.4. Case of a Generalized and Extended Source

We now consider the case where the point source is a force with Cartesian components *Fx*, *Fy*, *Fz*. We express its radiation in a discretized form similar to (A.13). We assume again that the cylindrical coordinate system is centered at the source and that the *z* axis is vertical. We have for the compressional and rotational potentials:

$$\phi(r,\theta,z;\omega) =$$
$$= \frac{1}{2L\rho\omega^2}\left[sgn(z)F_z\sum_{n=0}^{N}k_nJ_0(k_nr)e^{-i\nu_n|z|}\right.$$
$$-i\big(F_x\cos\theta +$$
$$\left.+F_y\sin\theta\big)\sum_{n=0}^{N}\frac{k_n^2}{\nu_n}J_1(k_nr)e^{-i\nu_n|z|}\right]$$

$$\psi(r,\theta,z;\omega) =$$
$$= \frac{1}{2L\rho\omega^2}\left[iF_z\sum_{n=0}^{N}\frac{k_n}{\gamma_n}J_0(k_nr)e^{-i\gamma_n|z|}\right. \qquad \text{(A.16)}$$
$$+sgn(z)\big(F_x\cos\theta$$
$$\left.+F_y\sin\theta\big)\sum_{n=0}^{N}J_1(k_nr)e^{-i\gamma_n|z|}\right]$$

$$\chi(r,\theta,z;\omega) =$$
$$= i\,\frac{F_y\cos\theta + F_x\sin\theta}{2L\rho\beta^2}\sum_{n=0}^{N}J_1(k_nr)e^{-i\gamma_n|z|}$$

with $\gamma_n = \sqrt{\frac{\omega^2}{\beta^2} - k_n^2},\ Im(\gamma_n) < 0$ and $sgn(z) = 1\, for\ z > 0, sgn(z) = -1\, for\ z < 0$ where ρ is the density, β the shear-wave velocity, and J_1 is the Bessel function of the first order.

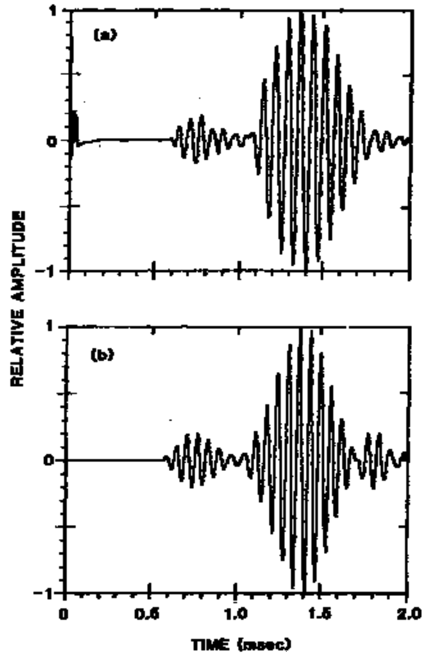

Figure A.6 A comparison between (a) actual and (b) synthetic full waveform acoustic log microseismograms in a limestone formation. The source is a pressure point located in a fluid-filled cylindrical borehole. Parameters used are $\alpha = 5{,}95\ km/s,\ \beta = 3{,}05\frac{km}{s}, \rho = 2{,}3$ for the geological formation, and $\alpha = 1{,}83\ km/s,\ \rho = 1.2$ for the fluid. The borehole radius is 6.7 cm. The synthetic microseismogram is calculated by discretizing the source radiation in the vertical wavenumber domain (Cheng et al., 1982).

Any type of elastic source can be represented by a combination of point forces. In particular, a generalized point source is commonly represented in seismology by its moment tensor m_{ij} where m_{xx}, m_{yy}, and m_{zz} represent three force dipoles oriented along the Cartesian axes, while $m_{xy} = m_{yx}$, $m_{xz} = m_{zx}$, and $m_{yz} = m_{zy}$ are double couples with force oriented along the first axis index and arm along the second axis index. Expressions for the radiation from an arbitrary moment tensor source can then be obtained by linear operations on equations (A.16).

Of particular interest is the radiation from a double-couple source, as such a body source is equivalent to a point of shear dislocation. Denoting by (s_x, s_y, s_z) the components of the unit vector in the slip direction and by (n_x, n_y, n_z) those of the normal to the fault, the corresponding moment tensor components are:

$$m_{ij} = -\mu slip(\omega)\Delta S(s_i n_j + s_j n_i) \quad \text{(A.17)}$$

where μ is the rigidity and ΔS is the elementary fault surface on which slip occurs.

The simplest way to calculate the elastic radiation from an extended source is usually to represent the source by a superposition of elementary point sources.

Although analytical expressions of the radiation can sometimes be derived in the frequency-wavenumber domain for particular cases, the point-source superposition is generally more versatile. In the case of an earthquake, for instance, the fault can be discretized into a two-dimensional array of double-couple points distributed on the fault plane at a spacing smaller than the shortest wavelength considered in the problem. Each point radiates with a phase delay $e^{-i\omega t_r}$, where t_r denotes the time for rupture to propagate from the hypocenter to the particular fault location. Slip amplitude and duration may vary at each point. The summation of all the elementary contributions is done in the frequency-wavenumber domain, and does not affect the calculation of the reflection/transmission and reflectivity/transmissivity matrices. One important aspect of the DWN method is that the method calculates the complete elastic wave field, including both static and dynamic contributions (see §1.2).

B. APPENDIX.
Numerical DEM formulation (Itasca, 2012)

B.1. Introduction

The analyses in this thesis were carried out at the University of Sannio with FLAC3D(*) code (Itasca, 2012).

In the performed analyses, the considered boundary value problem has been solved by implementing the following ingredients: a finite difference technique combined to a discrete model approach and to a dynamic solution.

- *Finite-difference technique*: first-order space and time derivatives of a variable are approximated by finite differences, assuming linear variations of the variable over finite space and time intervals, respectively.

- *Discrete-model approach*: the continuous medium is replaced by a discrete equivalent system, in which all forces involved (inertial, body and surface forces, internal source, etc.) are concentrated at the nodes of a 3D mesh representing the analysis domain. For the purpose of defining velocity variations on given space intervals, the medium is discretized into constant strain-rate elements of tetrahedral shape (Figure B.1) whose vertices are the nodes of the 3D mesh.

- *Dynamic-solution*: the inertial terms in the equations of motion are used as numerical means to reach the equilibrium state of the system under consideration. The equations of motion for a continuum are transformed into discrete forms of Newton's law at the nodes. The resulting system of ordinary differential equations is then solved numerically using an explicit finite difference approach in time domain.

(*) Prof. F. Guadagno and Dr. P. Ravellino are gratefully acknowledged for coordinating the purchase of the Flac 3D license under the auspicious of the GEMME Project.

B.2. Finite Difference Approximation to Space Derivatives

The finite difference formulation components of the strain-rate tensor for the tetrahedron are derived below as a preliminary step to derive the nodal formulation of the equations of motion. The tetrahedron nodes are identified by number from 1 to 4 and, by convention, face *n* is opposite to node *n* (Figure B.1).

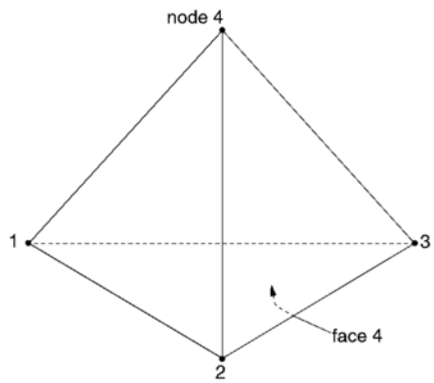

Figure B.1 Tetrahedron.

By application of the Gauss divergence theorem to the tetrahedron, we can write:

$$\int_V v_{i,j} dV = \int_S v_i n_j ds \tag{B.1}$$

where the integrals are taken over the volume and the surface of the tetrahedron, respectively, and $[n]$ is the exterior unit vector normal to the surface.

For a constant strain-rate tetrahedron, the velocity field is linear, and $[n]$ is constant over the surface of each face. Hence, after integration, (B.1) yields:

$$V v_{i,j} = \sum_{f01}^{4} \bar{v}_i^{(f)} n_j^{(f)} S^{(f)} \tag{B.2}$$

where the superscript (*f*) relates to the value of the associated variable on face f, and $\bar{v}_i$ is the average value of velocity component i.

For a linear velocity variation, we have:

$$\bar{v}_i^{(f)} = \frac{1}{3} \sum_{l=1, l\neq f}^{4} v_i^l \tag{B.3}$$

where the superscript (f) relates to the value at node l.

Substitution of (B.3) in (B.2) yields, reorganizing terms by node contribution:

$$V v_{i,j} = \frac{1}{3} \sum_{l=1}^{4} v_1^l \sum_{f=1, f\neq l}^{4} n_j^{(f)} S^{(f)} \tag{B.4}$$

If we replace v_i by 1 in (B.1) we obtain, by application of the divergence theorem:

$$\sum_{f=1}^{4} n_j^{(f)} S^{(f)} = 0 \tag{B.5}$$

Using this last relation, and dividing (B.4) by V, we get:

$$v_{i,j} = -\frac{1}{3V} \sum_{l=1}^{4} v_i^l n_j^{(l)} S^{(l)} \tag{B.6}$$

and the components of the strain-rate tensor may be expressed as:

$$\xi_{i,j} = -\frac{1}{6V} \sum_{l=1}^{4} \left(v_i^l n_j^{(l)} + v_j^l n_i^{(l)} \right) S^{(l)} \tag{B.7}$$

B.3. Nodal Formulation of the Equations of Motion

The nodal formulation of the equations of motion will be derived below by application of the theorem of virtual work. Approximations on the form of the nodal inertial terms will be made by using those terms as means to reach the solution corresponding to the equilibrium equations (4.2).

Fixing time, t, we consider an equivalent static problem governed at any instant in time by the equilibrium equations:

$$\sigma ij,j + \rho Bi = 0 \tag{B.8}$$

with body forces defined as (see (4.1)):

$$B_i = \rho\left(b_i - \frac{dv_i}{dt}\right) \tag{B.9}$$

In the framework of the finite difference approximation adopted here, the medium is represented by a continuous assembly of constant-strain tetrahedral subjected to body forces $[B]$. The nodal forces $[f]^n$, with n = (1,4), acting on a single tetrahedron in "static" equilibrium with the tetrahedron stresses and equivalent body forces, are derived by application of the theorem of virtual work. After application of a virtual nodal velocity $\delta[v]^n$ (it will generate a linear velocity field $\delta[v]$ and a constant strain-rate $\delta[\xi\ ]$ inside the tetrahedron), we equate the external rate of work done by the nodal forces $[f]^n$ and body forces $[B]$ with the internal work rate done by the stresses σij under that velocity.

Whereas the superscript refers to the nodal value of a variable and considering Einstein summation convention on indices i and j, the external work rate may be expressed as:

$$E = \sum_{n=1}^{4} \delta v_i^n f_i^n + \int_V \delta v_i B_i \, dV \tag{B.10}$$

while the internal work rate is given by:

$$I = \int_V \delta\xi_{ij}\sigma_{ij} dV \tag{B.11}$$

Using (B.7), we can write, for a constant strain-rate tetrahedron:

$$I = -\frac{1}{6}\sum_{l=1}^{4}\left(\delta v_i^l \sigma_{ij} n_j^{(l)} + \delta v_j^l \sigma_{ij} n_i^{(l)}\right) S^{(l)} \tag{B.12}$$

The stress tensor is symmetric, and defining a vector T^l with components:

$$T_i^l = \sigma_{ij} n_j^{(l)} S^{(l)} \tag{B.13}$$

we obtain:

$$I = -\frac{1}{3}\sum_{l=1}^{4} \delta v_i^l \, T_i^l \tag{B.14}$$

After substitution of (B.9) in (B.10), the external work rate may be expressed as follows:

$$E = \sum_{n=1}^{4} \delta v_i^n f_i^n + E^b + E^I \tag{B.15}$$

where E^b and E^I are the external work-rate contributions of the body forces ρb_i and inertial forces, respectively. For a constant-body force ρb_i inside the tetrahedron, we can write:

$$E^b = \rho b_i \int_V \delta v_i \, dV \tag{B.16}$$

while E^I may be expressed as:

$$E^I = -\int_V \rho \delta v_i \frac{dv_i}{dt} dV \tag{B.17}$$

According to the finite difference approximation done earlier, the velocity field varies linearly inside the tetrahedron. To describe it, we adopt a local system of reference axes x_1', x_2', x_3', with origin at the tetrahedron centroid, and write:

$$\delta v_i = \sum_{n=1}^{4} \delta v_i^n \, N^n \tag{B.18}$$

where N^n (with n = 1,4) are linear functions of the form:

$$N^n = c_0^n + c_1^n x_1' + c_2^n x_2' + c_3^n x_3' \tag{B.19}$$

and $c_0^n, c_1^n, c_2^n, c_3^n$ (with n = 1,4) are constants determined by solving the systems of equations:

$$N^n\left(x_1'^j, x_2'^j, x_3'^j\right) = \delta_{nj} \tag{B.20}$$

where δ_{nj} is the Kronecker delta. By definition of the centroid, all integrals of the form: $\int_V x_j' \, dV$ vanish, and substitution of (B.18) for δv_i in (B.15) yields, using (B.19):

$$E^b = \rho b_i \sum_{n=1}^{4} \delta v_i^n c_0^n V \tag{B.21}$$

Using Cramer's rule to solve (B.20) for c_0^n,we obtain, taking advantage of the properties of the centroid:

$$c_0^n = \frac{1}{4} \tag{B.22}$$

From (B.21) and ((B.22), we may write:

$$E^b = \sum_{n=1}^{4} \delta\, v_i^n \frac{\rho b_i V}{4} \tag{B.23}$$

Also, substitution of (B.18) for δv_i in (B.17) gives:

$$E^I = -\sum_{n=1}^{4} \delta\, v_i^n \int_V \rho N^n \frac{dv_i}{dt} dV \tag{B.24}$$

Finally, with expressions (B.23) for E^b and (B.24) for E^I , (B.15) becomes:

$$E = \sum_{n=1}^{4} \delta\, v_i^n \left[f_i^n + \frac{\rho b_i V}{4} - \int_V \rho N^n \frac{dv_i}{dt} dV \right] \tag{B.25}$$

For static equilibrium of the tetrahedron in the framework of the equivalent problem, the internal work rate (see ((B.14)) equals the external work rate expressed by (B.25) for *any* virtual velocity. Hence, we must have, rearranging terms:

$$-f_i^n = \frac{T_i^n}{3} + \frac{\rho b_i V}{4} - \int_V \rho N^n \frac{dv_i}{dt} dV \tag{B.26}$$

For small spatial variations of the acceleration field around an average value inside the tetrahedron, the last term in (B.26) may be expressed as follows:

$$\int_V \rho N^n \frac{dv_i}{dt} dV = \left(\frac{dv_i}{dt}\right)^n \int_V \rho N^n \, dV \tag{B.27}$$

For constant values of ρ inside the tetrahedron, and using the properties of the centroid mentioned above (see (B.19)) and (B.22), we may write:

$$\int_V \rho N^n \frac{dv_i}{dt} dV = \frac{\rho V}{4} \left(\frac{dv_i}{dt}\right)^n \tag{B.28}$$

In the context of this analysis, the mass $\frac{\rho V}{4}$ involved in the above inertial term is replaced by a fictitious nodal mass m^n, whose value will be determined below in order to ensure numerical stability of the system on its route to equilibrium. Accordingly, (B.28) becomes:

$$\int_V \rho N^n \frac{dv_i}{dt} dV = m^n \left(\frac{dv_i}{dt}\right)^n \tag{B.29}$$

and (B.26) may be written as:

$$-f_i^n = \frac{T_i^n}{3} + \frac{\rho b_i V}{4} - m^n \left(\frac{dv_i}{dt}\right)^n \tag{B.30}$$

The equilibrium conditions for the equivalent system may now be established by requiring that, at each node, the sum of the statically equivalent forces, $-[f]$, of all contributing tetrahedra and nodal contributions $[P]$ of applied loads and concentrated forces be zero. To express those conditions, we adopt a notation where a variable with superscript $<l>$ refers to the value of the variable at a node with label l in the global node numbering. The symbol $[[.]]^{<l>}$ is used to represent the sum of the contributions at global node l of all tetrahedra meeting at that node. With those conventions, we may write the following expressions of Newton's law at the nodes:

$$F_i^{<l>} = M^{<l>} \left(\frac{dv_i}{dt}\right)^{<l>} \qquad l = 1, n_n \tag{B.31}$$

where n_n is the total number of nodes involved in the medium representation, the nodal mass $M^{<l>}$ is defined as:

$$M^{<l>} = \left[[m]\right]^{<l>} \tag{B.32}$$

and the *out-of-balance force* $[F]^{<l>}$ is given by:

$$F_i^{<l>} = \left[\left[\frac{T_i}{3} + \frac{\rho b_i V}{4}\right]\right]^{<l>} + P_i^{<l>} \tag{B.33}$$

This force is equal to zero when the medium has reached equilibrium.

B.4. Explicit Finite Difference Approximation to Time Derivatives

Taking into consideration the constitutive equations, chapter 4 (equation 4.2), and the relation (B.7) between deformation rate and nodal velocities, (B.31) may be expressed formally as a system of ordinary differential equations of the form:

$$\frac{dv_i{}^{<l>}}{dt} = \frac{1}{M^{<l>}} F_i^{<l>} * \\ * \left(t, \left\{v_i^{<1>}, v_i^{<2>}, v_i^{<3>}, \dots, v_i^{<p>}\right\}^{<l>}, \kappa\right) \; L = 1, n_n \tag{B.34}$$

where the notation $\{\}^{<l>}$ refers to the subset of nodal velocity values involved in the calculation at global node l (see (B.31)). In FLAC3D, this system is solved numerically using an explicit finite difference formulation in time. In this approach, the velocity of a material node is assumed to vary linearly over a time interval Δt, and the derivative on the left-hand side of (B.34) is evaluated using central finite differences, whereby velocities are stored for times that are displaced by half timesteps with respect to displacements and forces. Nodal velocities are computed using the recurrence relation:

$$v_i{}^{<l>}\left(t + \frac{\Delta t}{2}\right) = v_i{}^{<l>}\left(t - \frac{\Delta t}{2}\right) + \frac{\Delta t}{M^{<l>}} F_i{}^{<l>} * \\ * \left(t, \left\{v_i^{<1>}, v_i^{<2>}, v_i^{<3>}, \dots, v_i^{<p>}\right\}^{<l>}, \kappa\right) \tag{B.35}$$

In turn, the node location is similarly updated using the central finite difference approximation,

$$x_i^{<l>}(t + \Delta t) = x_i^{<l>}(t) + \Delta t v_i^{<l>}\left(t + \frac{\Delta t}{2}\right) \tag{B.36}$$

It can be shown that first-order error terms vanish when the finite difference scheme embodied in (B.35) and (B.36) is used (i.e., the scheme is second-order accurate).

Nodal displacements are calculated in the code from the relation:

$$u_i^{<l>}(t + \Delta t) = u_i^{<l>}(t) + \Delta t u_i^{<l>}\left(t + \frac{\Delta t}{2}\right) \tag{B.37}$$

with $u^{<l>}(0) = 0$.

C. APPENDIX.
Numerical Time-Step estimation

C.1. Uncoupled and Coupled Formulation

When planning a simulation involves coupled flow, the time scale associated with the processes should be estimated. Knowledge of the problem time scales help in the assessment of maximum grid dimension, minimum element size and timestep. In addition, if the time scales of the different processes are very different, it may be possible to analyze the problem using a simplified (uncoupled) approach.

Time scales may be estimated using the definitions of characteristic time given below.

<u>Characteristic time of the mechanical process</u>

$$t_c^m = \sqrt{\frac{\rho}{K_u + 4/3G}} L_c \tag{C.1}$$

where K_U is the undrained bulk modulus, G is the shear modulus, ρ is the mass density, and L_C is the length characterizing the coupled flow (characteristic length).

<u>Characteristic time of the diffusion process</u>

$$t_c^f = \frac{L_c^2}{c} \tag{C.2}$$

where L_C is the characteristic length (L_c= *volume of flow domain/area of flow domain*), and c is the diffusivity defined as mobility coefficient k divided by storativity S:

$$c = \frac{k}{S} \tag{C.3}$$

For a coupled, saturated, deformation-diffusion analysis, S is the elastic storage and c is the true diffusivity or generalized *coefficient of consolidation* defined as:

$$c = \frac{k}{\frac{1}{M} + \frac{\alpha^2}{K + 4G/3}} \tag{C.4}$$

Where M is the Biot modulus, α is Biot coefficient ($M = K_f/n$ with $\alpha = 1$ for incompressible grains), K is the drained bulk modulus.

There are some properties worth noting on the above definitions.

1. In an explicit integration scheme, timestep corresponds to the shortest time needed for the perturbation to propagate from one gridpoint to the next. The magnitude of the timestep can be estimated using the smallest element size for L_C in equation (C.2). It is important to note that the explicit fluid flow timestep is calculated basing on *fluid diffusivity*, even in a coupled simulation. The timestep magnitude may be thus estimated from the formula by substitution in (C.2), and using the smallest zone size L_Z for L_C - i.e.:

$$\Delta t = min\left(\frac{L_z^2}{kM}\right) \tag{C.5}$$

2. In a coupled flow problem, the true diffusivity is controlled by the stiffness ratio R_k (i.e., the stiffness of the fluid versus the stiffness of the matrix):

$$R_k = \frac{\alpha^2 M}{K + 4/3G} \tag{C.6}$$

With this definition for R_k, (C.4) may be expressed in the following two forms:

$$c = kM\frac{1}{1 + R_k} \tag{C.7}$$

$$c = \frac{k}{\alpha^2}\left(K + \frac{4}{3}G\right)\frac{1}{1 + \frac{1}{R_k}} \tag{C.8}$$

If R_k is small (compared to 1), (C.7) shows that the standard explicit timestep (see (C.5)) can be considered as representative of the system diffusivity.

If R_k is large (i.e., M is large compared to $(K + 4G/3)/\alpha^2$ $(or\ K_f >> (K + 4G/3)n)$), the explicit timestep will be very small and the diffusivity problem will be controlled by the matrix (see (C.5) and (C.8)). The value for

M (or K_f) can be reduced in order to increase the timestep and reach faster steady-state computationally. (C.8) indicates that if M (or K_f) is reduced such that R_k = 20, then the diffusivity should be within 5% of the diffusivity for infinite M (or K_f). Whereby the time scale is respected with the same accurateness.

If the matrix is very stiff (or the fluid highly compressible) and R_k is very small (<< 1), the diffusion equation for the pore pressure can be uncoupled, since the diffusivity is controlled by the fluid (Detournay and Cheng, 1993). The modeling technique will depend on the driving mechanism (fluid or mechanical perturbation):

1. In mechanically driven simulations, the pore pressure may be assumed to remain constant. In an elastic simulation, the solid behaves as if there is no fluid; in a plastic analysis, the presence of the pore pressure may affect failure. This modeling approach is adopted in slope stability analyses.

2. In pore-pressure driven elastic simulations, volumetric strains will not significantly affect the pore-pressure field, and the flow calculation can be performed independently. The fluid modulus (M or K_f) must be set to zero during mechanical cycling, to prevent additional generation of pore pressure.

If the matrix is very soft (or the fluid incompressible) and R_k is very large (>> 1), then the system is coupled, with a diffusivity governed by the matrix. The modeling approach will also depend on the driving mechanism.

In mechanically driven simulations, calculations can be time-consuming. It may be possible to reduce the value for M (or K_f), such that R_k = 20, without significantly affecting the response.

In most practical cases of pore-pressure driven systems, experience shows that the coupling between pore pressure and mechanical fields is weak. If the medium is elastic, the numerical simulation can be performed with the flow calculation in flow-only mode and then in mechanical-only mode (with fluid modulus set to zero) to bring the model to equilibrium.

Finally, it is important to note that, in order to preserve the true diffusivity (and hence the characteristic time scale) of the system, the fluid modulus M (or K_f) must be adjusted to the value

$$M^a = \frac{1}{\frac{1}{M} + \frac{\alpha^2}{K + \frac{4}{3}G}} \tag{C.9}$$

or

$$K_f^a = \frac{n}{\frac{n}{K_f} + \frac{1}{K + 4G/3}} \tag{C.10}$$

during the flow calculation (see (C.4)), and to zero during the mechanical calculation to prevent further adjustments by volumetric strains (Berchenko 1998). Note that, in any case, Kf should not be made higher than the physical value of the fluid (2×10^9 Pa for water).

C.2. Dynamic Formulation

The finite-difference formulation is identical to that described in Chapter 4, except that "real" masses are used at gridpoints rather than the fictitious masses used for optimum convergence in the static solution scheme. Each tetrahedral sub-zone contributes one - quarter of its mass (computed from zone density and area) to each of the four associated gridpoints. In finite-element terminology this is equivalent to use a diagonal mass matrix.

The calculation of critical timestep is:

$$\Delta t_{crit} = min\left\{\frac{V}{C_p A^f}\right\} \tag{C.11}$$

where Cp is the p-wave speed, V is the tetrahedral sub-zone volume, and A^f_{max} is the maximum face area associated with the tetrahedral sub-zone. The min{} function is taken over all elements. A safety factor of 0.5 is used, because (C.11) is only an estimate of the critical timestep. Hence, the timestep used for dynamic analyses, Δt_d, when no stiffness-proportional damping is used, is:

$$\Delta t_d = \Delta t_{crit}/2 \tag{C.12}$$

If stiffness-proportional damping is used, the timestep must be reduced, for stability. Belytschko (1983) provides a formula for critical timestep, Δt_β, that includes the effect of stiffness-proportional damping:

$$\Delta t_\beta = \left\{\frac{2}{\omega_{max}}\right\}\left(\sqrt{1+\lambda^2}-\lambda\right) \tag{C.13}$$

where ω_{max} is the highest eigenfrequency of the system, and λ is the fraction of critical damping at this frequency. Both ω_{max} and λ are function of an eigenvalue solution, but can be estimated through:

$$\omega_{max} = \frac{2}{\Delta t_d} \tag{C.14}$$

$$\lambda = \frac{0.4\beta}{\Delta t_d} \tag{C.15}$$

Given:

$$\beta = \xi_{min}/\omega_{min} \tag{C.16}$$

where $\xi_{min}$and $\omega_{min}$are the damping fraction and the angular frequency specified for Rayleigh damping. The resulting value of Δt_β is used as the dynamic timestep if stiffness-proportional damping is in operation.

C.3. Dynamic Multi-stepping (Itasca, 2012)

The maximum stable timestep for dynamic analysis is determined by the largest material stiffness and smallest zone in the model (see (C.11)). Often, the stiffness and zone size can vary widely in a model (e.g., in the case of a finely discretized stiff structure located on a soft soil). A few zones will then determine the critical timestep for a dynamic analysis even though the major portion of the model can be run at a significantly larger timestep.

A procedure known as *dynamic multi-stepping* is available in some FEM and DEM codes with explicit formulation of time-integration, to reduce the computation time required for a dynamic calculation. In this procedure, zones and gridpoints in a model are ordered into classes of similar maximum timesteps. Each class is then run at its timestep and information is transferred between zones at the appropriate time.

Dynamic multi-stepping uses a local timestep for each individual gridpoint and zone. At the start of an analysis, the grid is scanned and the local stable timestep for each gridpoint, Δt_{gp} , is determined and stored. The value of Δt_{gp} depends on size, stiffness and mass of the neighboring sub-zones (as shown in (C.11)), attached structural elements and interfaces. The global timestep, Δt_G, is determined as the minimum of all Δt_{gp}, as in the standard formulation.

Integer multipliers, M_{gp} , to the global timestep are then determined for each gridpoint according to the algorithm illustrated by the flow chart in Figure C.1. This algorithm ensures that multipliers are powers of 2. In the current implementation, M_{gp} is set to 1 for nodes that are assigned a null material model, connected to structural elements, attached to other gridpoints, or part of a quiet boundary. All zones are then scanned, and an integer multiplier, M_Z, is calculated for each zone as the minimum of the multipliers for the four surrounding gridpoints.

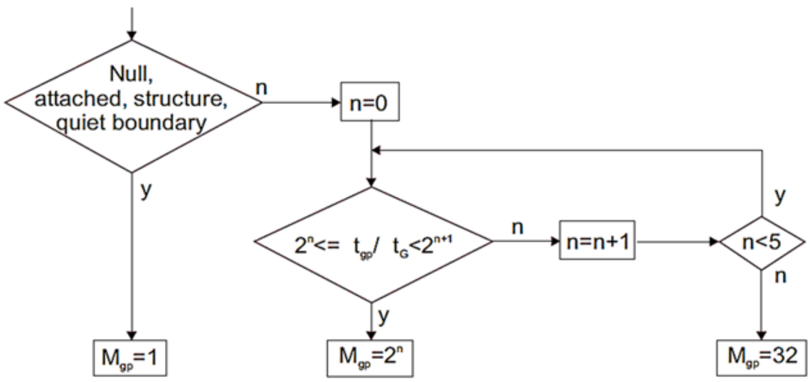

Figure C.1 Flow chart for determination of gridpoint multiplier, M_{gp}.

Calculations for a zone (i.e., derivation of new stresses from surrounding gridpoint velocities; accumulation of gridpoint forces from stress components) are only performed every M_Z timesteps. In all expressions involving a timestep, the global timestep is replaced by $\Delta t_G M_z$.

Calculations for a gridpoint (i.e., derivation of new velocities and displacements from gridpoint force sums) are only performed every M_{gp} timesteps; otherwise, the force sums are reset to zero, which is normally done after every motion calculation. In all expressions involving a timestep, the global timestep is replaced by $\Delta t_G M_{gp}$.

The effect of the prescriptions described above is to skip calculation of selected gridpoints and zones, thereby speeding up the overall calculation. The use of gridpoint and zone multipliers (M_{gp} and M_Z, respectively) ensures the following characteristics:

1. The force sum at each gridpoint is composed of component forces from each connected zone at the same point in time. The simultaneous nature of the component forces is guaranteed by the fact that multipliers are powers of two. Arbitrary integral multipliers would not have this characteristic.
2. Velocities seen by a zone (at the four surrounding gridpoints) are not updated between zone updates. This is guaranteed by the fact that the zone multiplier is the minimum of the surrounding gridpoint multipliers. Since stress increments are derived from strain and displacement increments, the displacement contribution of a gridpoint is felt by a zone at each update, even though the gridpoint is updated less frequently than the zone. In short, the total displacement increment of the gridpoint is divided into M_{gp} / M_Z equal parts.

This scheme is accurate for dynamic simulations that represent waves with frequencies well below the natural frequencies of individual elements, condition guaranteed by the relation between wavelength and critical timestep.

References

Aagaard B. T., Graves R. W., Rodgers A., Brocher T. M., Simpson R. W., Dreger D., Petersson N. A., Larsen S. C., Ma S., and Jachens R. C., 2010. *Ground-motion modeling of Hayward fault scenario earthquakes, part II: Simulation of long-period and broadband ground motions*. Bull. Seismol. Soc. Am., Vol. 100, no. 6, pp. 2945-2977

Aagaard B. T., J. F. Hall, and T. Heaton, 2001. *Characterization of near-source ground motions with earthquake simulations*. Earthquake Spectra; 17, 07. 07

Aagaard B. T., T. M. Brocher, D. Dolenc, D. Dreger, R. W. Graves, S. Harmsen, S. Hartzell, S. Larsen, K. McCandless, S. Nilsson, N. A. Petersson, A. Rodgers, B. Sjögreen, and M. L. Zoback, 2008. *Ground-motion modeling of the 1906 San Francisco earthquake, Part II: Ground-motion estimates for the 1906 earthquake and scenario events.* Bull. Seismol. Soc. Am. 98, 1012-1046.

Abe K., 1981. *Magnitudès of large shallow earthquakes from 1904-1980.* Phys. Earth Planet. Interiors 27, 72-92

Abe K., and S. Noguchi, 1983a. *Detennination of magnitude for large shallow earthquakes 1898-1917.* Phys. Earth Planet. Interiors 32, 45-59

Abe K., and S. Noguchi, 1983b. *Revision of magnitudes of large shallow earthquakes, 1897-1912.* Phys. Earth Planet. Interiors 33, 1-11

Abouseeda H. and Dakoulas P., 1998. *Non-linear dynamic earth dam-foundation interaction using a BE-FE method.* Earthquake Eng Struct Dyn; 27:917-36

Abrahamson N. A., 2000. *Effects of rupture directivity on probabilistic seismic hazard analysis*. In Sixth International Conf. Seismic Zonation, Oakland, California. Earthquake Engineering Research Inst

Abrahamson N. A. and R. R. Youngs, 1992. *A stable algorithm for regression analyses using the random effects model.* Bull. Seismol. Soc. Am. 82, 505-510

Abrahamson N. A. and Shedlock, K., 1997. *Overview, Seis. Res*. Letters 68, 9-23

Abrahamson N., 2001. *Incorporating effects of near fault tectonic deformation into design ground motions*. A presentation sponsored by EERI Visiting Professional Program, hosted by the University at Buffalo, October 26, 2001 http://mceer.buffalo.edu/outreach/pr/abrahamson.asp)

Abrahamson N.A. and K Shedlock, 1997. *Overview of ground motion attenuation relations.* Seismological Research Letters, 68: 9-23

Abrahamson N.A. and P.G. Somerville, 1996. *Effects of the hanging wall and footwall on ground motions recorded during the Northridge Earthquake.* Bull. Seism. Soc. Am., 86, S93- S99

Abrahamson N.A. and R.R. Youngs, 1992. *A stable algorithm for regression analyses using the random effects model.* Bull. Seism. Soc. Am., 82, 505-510

Abrahamson N.A. and W.J. Silva, 1997. *Empirical response spectral attenuation relations for shallow crustal earthquakes*. Seismological Research Letters, 68: 94-127

Abrahamson N.A., 2000. *Effects of rupture directivity on probabilistic seismic hazard analysis.* Proceedings of the 6th International Conference on Seismic Zonation, Palm Springs, Earthquake Engineering Research Institute

Abrahamson N.A. and Silva W.J., 1997. *Empirical response spectral attenuation relations for shallow crustal earthquakes*. Seismol Res Lett; 68(1):94-127

Abrahamson N.A. and Youngs R.R., 1992. *A stable algorithm for regression analyses using the random effects model.* Bull Seismol Soc Am; 82(1):505-10

Acharya H. K., 1979. *Regional variations in the rupture-length empirical Relationships among Magnitude, Rupture Length, Rupture Width, Rupture Area, and Surface Displacement magnitude relationships and their dynamical significance.* Bull. Seism. Soc. Am. 69, 2063-2084

Achilleas G. Papadimitriou, George D. Bouckovalas, Konstantinos I. Andrianopoulos, 2013. *Methodology forestimating seismic coefficient for performance-based design of earth dams and tallem bankments.* Soil Dynamics and Earthquake Engineering 56 57-73.

Adachi T. and Oka F., 1982. *Constitutive equations for normally consolidated clay based on elasto-viscoplasticity.* Soils and Foundations; 22(4), 57-70

Agip, 1982. *Aeromagnetic Survey of Italy*. A Few Interpretative Results. Agip Internal Report

Agresti A., 2002. *Categorical Data Analysis.* Wiley, New York, 710 pp

Akai K., Ohnishi Y., Murakami T. and Horita M., 1979. *Coupled stress flow analysis in saturated/unsaturated medium by finite element method.* Proc. Third Int. Conf. Num. Meth. Geomech. 1: 241-249, Aachen

Akaike H., 1974. *A new look at the statistical model identification*. IEEE Trans Autom. Control, 6, 716-723

Aki K. and P.G. Richards, 1980. *Quantitative Seismology: Theory and Methods*. W.H. Freeman and CoVols 1 and 2. 932 pp, San Francisco.

Aki K., 1967. *Scaling law of seismic spectrum.* J. Geophys. Res. 72, 1217-1231

Aki K., 1979. *Characterisation of barriers of an earthquake fault.* J. Geophfla. Ru., 84 (Bll), 618G-6147

Aki K., 1984. *Asperitiea, barrier, characteristic earthquakea and strong motion prediction.* J. Gcophp. Res., 89 (B7) ,6867-6872

Akinci A., L. Malagnini, and F. Sabetta, 2010. *Characteristics of the strong ground motions from the 6 April 2009 L'Aquila earthquake, Italy.* Soil Dyn. Earthquake Eng. 30, 320-335

Akkar S. and J. J. Bommer, 2010. *Empirical equations for the prediction of PGA, PGV and spectral accelerations in Europe, the Mediterranean region, and the Middle East.* Seismol. Res. Lett. 81, 195-206

Akkar S. and Bommer J.J., 2006. *Influence of long-period filter cut-off on elastic spectral displacements.* Earthquake Engineering and Structural Dynamics; 35(9):1145-1165.Copyright q 2010 John Wiley and Sons, Ltd. Earthquake Engng Struct. Dyn. 2010; 39:1039-1062 doi: 10.1002/eqe

Akkar S. and Bommer J.J., 2007. *Empirical prediction equations for peak ground velocity derived from strongmotion records from Europe and the Middle East.* Bull Seismol Soc Am 97:511-530. doi: 10.1785/0120060141

Akkar S., U. Yazgan, and P. Gulkan, 2005. *Drift estimates in frame buildings subjected to near-fault ground motions*. J. Struct. Eng. 131, no. 7, 1014-1024

Alavi B. and H. Krawinkler, 2000. *Design considerations for near-fault ground motions.* Proceedings of the U.S. - Japan Workshop on the Effects of Near-Fault Earthquake Shaking, San Francisco, March 20-21

Alavi B. and H. Krawinkler, 2001. *Effects of near-fault ground motions on frame structures*. Technical Report Blume Center Report 138, Stanford, California

Alavi B. and Krawinkler H., 2000. *Consideration of near-fault ground motion effects in seismic design*. Proceedings 12th World Conference on Earthquake Engineering, New Zealand

Albano M., 2013. *Numerical modeling of the seismic performance of bituminous faced rockfill dams.* PhD Thesis, Università degli studi di Cassino e del Lazio Meridionale

Albee A. L. and J. L. Smith, 1966. *Earthquake characteristics and fault activity in southern California.* In Engineering Geology in Southern California , R. Lung and D. W. Proctor (Editors), Association of Engineering Geologists, Los Angeles Section, 9- 34

Alessandrini B., Rove and A. Cocco M. and Mazza S., 1990. *Computation of ground displacement from strong-motion accelerograms using the exact deconvolution technique*. Bull. Seismol. Sot. Am., SO: 1753-1761

Alexander D. E., 1981. *Preliminary assessment of landslides resulting from the earthquake of 23rd November 1980 in Southern Italy, Disasters S ,* 376-383

Alexander D. E., 1982. *The earthquake of 23rd November 1980 in Campania and Basilicata, Southem Italy.* International Disaster lnstitute, London

Allen R., 2007. *The ElarmS earthquake early warning methodology and application across California*. In: Gasparini P (ed) Earthquake early warning systems. Springer, Berlin, pp 133-152

Alonso E. E., Gens A. and Josa A. 1990. *A constitutive model for partially saturated soil*. Géotechnique 40 No. 3, 405-430

Alonso E.E. and Romero E., 2003. *Collapse behaviour of sand*. Proceedings of the 2nd Asian Conference on Unsaturated Soils. Osaka. 325-334

Alonso E. and Pinyol N., 2009. *Slope stability under rapid drawdown conditions*. Universitat Politècnica de Catalunya, Barcelona

Al-Tabbaa A. and Wood, D.M., 1989. *An experimentally based 'bubble' model for clay*. Proc. of NUMOG3, 91-99

Al-Tabbaa A., 1987. *Permeability and Stress-Strain Response of Speswhite Kaolin*. PhD Thesis, Cambridge University

Alterman Z., and F. C. Karal, Jr., 1968. *Propagation of elastic waves in layered media by finite difference methods.* Bull. Seism. Soc. Am; 58, 367-398

Amaike F., 1987. *Seismic explorations of the buried fault associated with the 1948 Fukui earthquake.* J. Phys. Earth 35, 285-308

Amand P. and Virieux J., 1995. *Non linear inversion of synthetic seismic reflection data by simulated annealing, 65th Ann*. Internat. Mtg: Soc. Expl. Geophy. Expanded Abstracts, 612-615

Amato A. and Selvaggi, G., 1993. *Aftershock location and P-wave velocity structure in the epicentral region of the 1980 Irpinia earthquake.* Ann. Geofis., 36(1), 3-15

Amato A. and Selvaggi G., 1992. *Aftershock relocation and crustal structure in the epicentral region.* In: E. Boschi (Editor), Proc. Workshop Irpinia 10 anni dopo (Napoli, Italy, Nov. 19901, Editrice Compositori, Bologna (in press)

Amato A. and Montone P., 1997. *Present day stress field and active tectonics in southern peninsular Italy*. Geophys. J. Int., 130, 519-534.

Amato A., Chiarabba C., Malagnini L. and Selvaggi G., 1992. *Three-dimensional P-velocity structure in the region of the MS=6.9 Irpinia, Italy, normal faulting earthquake*. Phys. Earth Planet. Inter., 75, 111-119

Amato A., Cocco M., Pantosti D. and Valensise G., 1989. *Investigating a complex earthquake with a multidisciplinary approach: the 1980, Irpinia, normal faulting event (M, 6.9)*. EOS Trans. Am. Geophys. Union, 70: 1226

Ambraseys N., Smit P., Douglas J., Margaris B., Sigbjörnsson R., Ólafsson S., Suhadolc P. and Costa G., 2004. *Internet site for European strong-motion data.* Bollettino di Geofisica Teorica ed Applicata, 45, 3, pp. 113-129

Ambraseys N., 1975. *Studies in historical seismicity and tectonics.* In Geodynamics Today, The Royal Society, London, 7- 16

Ambraseys N., 1988. *Engineering seismology.* Earthquake Eng. Struct. Dyn. 17, 1-105

Ambraseys N., J. Douglas, S. K. Sarma, and P. M. Smit, 2005. *Equations for the estimation of strong ground motions from shallow crustal earthquakes using data from Europe and Middle East: Horizontal peak ground acceleration and spectral acceleration*. Bull. Earthquake Eng. 3, 1-53

Ambraseys N., 1960. *The seismic stability of earth dams*. In: Proceedings of the second world conference on earthquake engineering, vol. 2, Tokyo, Japan; p. 1345-63

Ambraseys N., Smit P., Berardi R., Rinaldis D., Cotton F. and Berge C., 2000. *Dissemination of European Strong- motion Data (Cd-Rom Collection)*. European Commission, Dgxii, Science, Research and Development, Bruxelles

Ambraseys N.A. and Menu J.M., 1988. *Earthquake-induced ground displacements*. Earthquake Eng Struct Dyn;16:985-1006

Ambraseys N., 1960. *The seismic stability of earth dams.* In: Proceedings, Second World Conference on Earthquake Engineering, Tokyo, Japan; 2: p. 1345-63

Ambraseys N. and Menu J.M., 1988. *Earthquake-induced ground displacements*. Earthquake Eng Struct Dyn; 16:985-1006

Ambraseys N. and Sarma S.K., 1967. *The response of earth dams to strong earthquakes*. Geotechnique; 17(3):181-213

Ameri G., F. Gallovič F. Pacor and A. Emolo, 2009. *Uncertainties in strong ground-motion prediction with finite-fault synthetic seismo- grams: An application to the 1984 M 5.7 Gubbio, central Italy, earthquake.* Bull. Seismol. Soc. Am. 99, 647-663

Ameri G., Massa M., Bindi D., D'Alema E., Gorini A., Luzi L., Marzorati S., Pacor F., Paolucci R., Puglia R. and Smerzini C., 2009. *The 6 April 2009 Mw 6.3 L'Aquila (Central Italy) Earthquake: Strong-motion Observations*. Seismological Research Letters, 80, 6, pp. 951-966.

Ameri G., F. Pacor, G. Cultrera and G. Franceschina, 2008. *Deterministic ground-motion scenarios for engineering applications: The case of Thessaloniki, Greece.* Bull. Seismol. Soc. Am. 98, 1289-1303

Ameri G., Massa M., Bindi D., D'Alema E., Gorini A., Luzi L., Marzorati S., Pacor F., Paolucci R., Puglia R. and Smerzini C. 2009b. *The 6 April 2009 MW 6.3L'Aquila (Central Italy) earthquake: Strong-motion observations.* Seismol. Res. Lett.,Vol. 80, No. 6, pp. 951-966

Ameri G., Emolo A., Pacor F. and Gallovič F., 2011. *Ground-Motion Simulations for the 1980 M 6.9 Irpinia Earthquake (Southern Italy) and Scenario Events*. Bulletin of the Seismological Society of America, Vol. 101, No. 3, pp. 1136-1151, doi: 10.1785/0120100231

Ammon C., Velasco, A. and Lay T., 1993. *Rapid estimation of rupture directivity: application to the 1992 Landers (Ms = 7.4) and Cape Mendocino (Ms = 7.2) California earthquakes. Geophys. Res. Lett.,* 20, 97-100

Amorosi A. and Kavvadas M., 1999. *A plasticity-based constitutive model for natural soils: a hierarchical approach*. In D. Kolymbas (Ed.), Proc. III Euroconference on Constitutive Modelling of Granular Materials, Horton, Greece, pp. 413-438

Amoruso A., Crescentini, L. and Scarpa, R., 2002. *Source parameters of the 1908 Messina Straits, Italy, earthquake from geodetic and seismic data.* J. geophys. Res., 107, doi: 10.1029/2001JB000434

Amoruso A., Crescentini L. and Fidani C., 2004. *Effects of crustal layering on source parameter inversion from coseismic geodetic data*. Geophys. J. Int.159, 353-364 doi: 10.1111/j.1365-246X.2004.02389.x

Anderson D. G. and Richart F.E., 1976. *Effect of straining on shear modulus of clays.* Journal of the Geotechnical Engineering Division (ASCE). Voi. 102, No.GT9, pp. 975-987

Anderson H. J. and Jackson J. A., 1987. *Active tectonics of the Adriatic region*. Geophys. J. R. astr. Soc., in press

Anderson H. J., 1985. *Seismotectonics of the western Mediterranean.* PhD thesis, University of Cambridge

Anderson J. C. and V. Bertero, 1987. *Uncertainties in establishing design earthquakes.* J. Struct. Eng. 113, no. 8, 1709-1724

Anderson J.G. and Hough S.E., 1984. *A model for the shape of the Fourier amplitude spectrum of acceleration at high frequencies*. Bull. Seismol. Sot. Am., 74: 1969-1993

Andrea Bizzarri and Harsha S. Bhat, 2012. *The Mechanics of Faulting: From Laboratory to Real Earthquakes*

Andrianopoulos K.I., Papadimitriou A.G. and Bouckovalas G.D., 2005. *Bounding surface models of sands: pitfalls of mapping rules for cyclic loading*. In: Proceedings of the 11th international conference of IACMAG, Torino, June 19-24, Vol. 1, p. 241-248

Andrianopoulos K.I., 2006. *Numerical modeling of static and dynamic behavior of elastoplastic soils.* Doctorate Thesis; Department of Geotechnical Engineering, School of Civil Engineering, National Technical University of Athens (in Greek)

Andrianopoulos K.I., Papadimitriou A.G. and Bouckovalas G.D., 2007. *Use of a new bounding surface model for the analysis of earthquake-induced liquefaction phenomena*. In: Proceedings of the Fourth International Conference on Earthquake Geotechnical Engineering; paper No. 1443

Andrianopoulos K.I., Papadimitriou A.G. and Bouckovalas G.D., 2009. *Bounding surface plasticity model for the seismic liquefaction analysis of geostructures*. Soil Dynamics and Earthquake Engineering; under review

Andrianopoulos K.I., Papadimitriou A.G. and Bouckovalas G.D., 2009. *Explicit integration of bounding surface model for analysis of earthquake soil liquefaction*. International Journal for Numerical and Analytical Methods in Geomechanics; doi:10.1002/nag.875

Andrianopoulos K.I., Papadimitriou A.G. and Bouckovalas G.D., 2010. *Bounding surface plasticity model for the seismic liquefaction analysis of geostructures*. Soil Dynam Earthq Eng; 30(10):895-911

Andrianopoulos K.I., Papadimitriou A.G., Bouckovalas G.D. and Karamitros D.K., 2014. *Insight into the seismic response of earthdams with an emphasis on seismic coefficient estimation*. Comput Geotech; 55(1):195-210

Amorosi A. and Elia G, 2008. *Analisi dinamica accoppiata della diga Marana Capacciotti.* Rivista Italiana di geotecnica 4

Ansal A., A. Akinci, G. Cultrera, M. Erdik, V. Pessina, G. Tonuk and G. Ameri, 2008. *Loss estimation in Istanbul based on deterministic earthquake scenarios of the Marmara Sea region (Turkey).* Soil Dyn. Earth. Eng. 29, 699-709

Anzidei M., Baldi P., Casula G., Galvani A., Mantovani E., Pesci A., Riguzzi F. and Serpelloni E., 2001. *Insights into present-day crustal motion in the central Mediterranean area from GPS surveys.* Geophys. J. Int., 146, 98-110

Anzidei M., Boschi E., Cannelli V., Devoti R., Esposito A., Galvani A., Melini D., Pietrantonio G., Riguzzi F., Sepe V. and Serpelloni E., 2009. *Coseismic deformation of the destructive April 6, 2009 L'Aquila earthquake (Central Italy) from GPS data*. Geophys. Res. Lett., Vol. 36, No. 17, L17307

Aoi S. and H. Fujiwara, 1999. *3-D finite difference method using discontinuous grids.* Bull. Seism. Soc. Am.; 89, 918-930

Arca S., Bonasia V., Gaulon R., Pingue, F., Ruegg, J. C. and Scarpa R., 1983. *Ground movements and faulting mechanism associated to the November 23, 1980 Southern ltaly earthquake.* Boll. geod. sciaffini, XLII, 137-147

Archilleas G. Papadimitriou, George D. Bouckovalas, Yannis F. Dafalias, Members and ASCE, 2001. *Plasticity model for sand under small and large cyclic strains*. Journal of geotechnical and geoenvironmental. Engineering / November

Archuleta R.J., 1984. *A faulting model for the 1979 Imperial Valley Earthquake*. J. Geophys. Res., 89: 4559-4585

Archuleta R.J. and Hartzell S.H., 1981. *Effects of fault finiteness on near-source ground motion*. Bull. Seism. Soc. Am.; 71: 939-957

Arthur J. R. F., Bekenstein S., Germaine J. T. and Ladd C. C., 1981. *Stress path tests with controlled rotation of principal stress directions*. Laboratory shear strength of soil, ASTM STP 740, ASTM,West Conshohocken, Pa

Arulanandan K. and Scott R.F. (Eds.), 1993. *Proceedings of VELACS symposium*. A.A. Balkema, Rotterdam
Arulanandan K. and Sybico J., 1992. *Post liquefaction settlement of sands, Proceedings, Wroth Memorial Symposium*. England: Oxford University
Arulmoli K., Muraleetharan K. K., Hossain M. M., and Fruth L. S., 1992. *VELACS: Verification of liquefaction analyses by centrifuge studies; laboratory testing program-Soil data report*. Res. Rep., The Earth Technology Corp
Arulmoli K., Muraleetharan K.K., Hossain M.M. and Fruth L.S., 1992. *VELACS verification of liquefaction analyses by centrifuge studies.* Laboratory Testing Program, Soil Data Report, Research Report, The Earth Technology Corporation
athje E.M. and Bray J.D., 2000. *Nonlinear coupled seismic sliding analysis of earth structures*. J Geotech Geoenviron Eng ASCE;126(11):1002-14
Ascione A., Mazzoli S, Petrosino P. and Valente E., 2013. *A decoupled kinematic model for active normai faults: Insights from the 1980, Ms = 6.9 Irpinia earthquake, soutbem Italy*. Geological Society of America Bulletin, 125, no. 7-8;1239-1259
Atik L. A., N. Abrahamson, J. J. Bommer, F. Scherbaum, F. Cotton and N. Kuehn, 2010. *The variability of ground-motion prediction models and its components.* Seismol. Res. Lett. 81, no. 5, 794-801
Atkinson G. M., and D. M. Boore, 2006. *Earthquake ground-motion prediction equations for eastern North America.* Bull. Seismol. Soc. Am. 96, 2181-2205
Atkinson G.M. and Sonley E., 2000. *Empirical relationships between modified Mercalli intensity and response spectra*. Bull Seism Soc Am; 90(2):537-44
Atkinson J. H., Richardson D. and Stallebrass S. E., 1990. *Effect of recent stress history on the stiflhess of overconsolidated soil.* Géotechnique. Vol. 40, No.4, pp. 531-540
Atzori S., Hunstad I., Chini M., Salvi S., Tolomei C., Bignami C., Stramondo S., Trasatti E., Antonioli A. and Boschi E., 2009. *Finite fault inversion of DInSAR coseismic displacement of the 2009 L'Aquila earthquake (Central Italy)*. Geophys. Res. Lett., Vol. 36, No. 15, L15305
Aubry D., Chouvet D., Modaressi H. and Modaressi A., 1985. *GEFDYN 5: Logiciel d'analyse du comportement statique et dynamique des so1s par éléments finis avec prise en compte du couplage sol-eau-air.* Rapport scientifique, Ecole Centrale Paris
Aubry D., Benzenati I. and Modaressi A., 1991. *A coupled statie/dynamic strain and pore pressure analysis for em.bankm.ent dams*. Dam. En.g 1991;11(1):53-94
Aubry D., Benzenati I. and Modaressi A., 1993. *Numerical predictions for Model n. 1, 2, and 7.* In: Arulanandan, Scott, editors. Verification of numerical procedures for the analysis of soil liquefaction problems. Rotterdam: Balkema; 1993. p. 45-66. p. 315-22 and p. 817-22
Aubry D., Hujeux J.C., Lassoudiere F. and Meimon Y., 1982. *A double memory model with multiple m.echanism. for cyclic soil behaviour*. In: International Symposium on Numerical Models in Geomechanics, Zurigh. p. 13
Ausilio E., Costanzo A., Tropeano G. and Silvestri F., 2009. *Evaluation of seismic displacements of a natural slope by simplified methods and dynamic analyses*. In: Kokusho A, Tsukamoto A, Yoshimine A, editors. Performanc based design in earthquake geotechnical engineering. London: Taylor and Francis Group; p. 955-62
Ausilio E., Silvestri F., Troncone A. and Tropeano G., 2007. *Seismic displacement analysis of homogeneous slopes: a review of existing simplified methods with reference to Italian seismicity*. In: Earth geotechnical engineering, Fourth ICEGE, Thessaloniki, Greece; 1614 p
Aydingun O. and Adalier K., 2003. *Numerical analysis of seismically induced liquefaction in earth embankment foundations*. Part I. Benchmark model. Can. Geotech. J., 40, 4, pp. 753-765
Aydinoğlu M. N., 1980. *Unified formulations for soil-structure interaction, in Proc*. 7th World Conf. Earthquake Engineering, Istanbul, Turkey, 8-13 September 1980, Vol. 7, 121-128
Aydinoğlu M. N., 1993. *Consistent formulation of direct and substructure methods in nonlinear soil-structure interaction.* Soil Dyn. Earthquake Eng. 12, 403-410
B. Bemstein 1965., *Hypoelasticity and elasticity. Arch. Rational Mech. Anal. 6 (1960) 89-104. Reprinted in: C.Truesdell (ed.), Continuum Mechanicsm.* The International Science Review Series. Gordon and Breach, New York.CrossRef
B. Bemstein and J.L. Ericksen, 1958. *Work functions inhypoelasticity*. Arch. Rational Mech. Anal. 1 396-409
B.Bernstein, 1960. *Relation between hypoelasticity and elasticity*. Trans. Soc. Rheol. 4 23-28. CrossRef
Baker J.W., 2007. *Quantitative classification of near-fault ground motions using wavelet analysis*. Bulletin of the Seismological Society of America; 97(5):1486-1501
Baker J.W., 2009. *Identification of near-fault velocity and prediction of resulting response spectra*. Proceedingsof Geotechnical Earthquake Engineering and Structural Dynamics IV, Sacramento, CA. [Available at http://www.stanford.edu/~bakerjw/, last accessed 2 August]
Baker R, Rydman S and Talesnick M. 1993. *Slope stability analysis for undrained loading conditions.* Int. Jnl. Num. and Anal. Methods Geomech. 17: 14-43
Bakun W. H., 1984. *Magnitudes and moments of duration.* Bull. seism. Soc. Am., 74, 2335-2356
Baldovin G., Allaria N., Baldovin E., 1991. *The core of Castagnara dam on Metramo river.* XVII International Conference On Large Dams, Wien, vol. IV, pp. 179-205
Bally A.W., Burbi L., Cooper C., Ghelardoni R., 1986. *Balanced sections and seismic reflection profiles across the Central Apennines*. Mem. Soc. Geol. It. 35, 257-310
Bao H., 1998. *Finite element simulation of earthquake ground motion in realistic basins*. Ph.D. Thesis, Carnegie Mellon University, Pittsburgh
Bao H., J. Bielak, O. Ghattas, L. F. Kallivokas, D. R. O'Hallaron, J. R. Shewchuk, and J. Xu, 1998. *Large-scale simulation of elastic wave propagation in heterogeneous media on parallel computers*. Comp. Methods Appl. Mech. Eng. 152, 85-102
Bardet J.F., 1986. *Bounding surface plasticity model for sand*. J. Eng. Mech., Voi 112, 1198- 1217
Battaglia J., Zollo A., Virieux J. and Dello Iacono D., 2008. *Merging active and passive data sets in traveltime tomography: the case study of Campi Flegrei Caldera (Southern Italy).* Geophys. Prospect., 56(4), 555- 573

Bauer E., Wu W., 1993. *A hypoplastic model for granular soils under cyclic loading*. In: Kolymbas D, editor. Modern Approaches to Plasticity. Elsevier; p. 247-58

Bazzurro P., Cornell C.A., 1999: *Disaggregation of seismic hazard*. Bulletin of Seismological Society of America, 89(2), 501-520

Beccaluva L., Brotzu P., Macciotta G., Morbidelli L., Serri G. and Traversa G., 1989. *Cenozoic tecto-magmatic evolution and inferred mantle sources in the Sardo-Tyrrhenian Area. In: Boriani A., Bonafede M., Piccardo G.G. and Vai G.B. (Eds).* The Lithosphere in Italy: Advances in Earth Science Research. Accademia Nazionale dei Lincei, Rome, Italy, 229-248

Becker A.M. and N.A. Abrahamson, 1997. *Stress drops in normal faulting earthquak.* Seismological Research Letters, 68, 322

Been K., and Jefferies M. G., 1985. *A state parameter for sands*. Géotechnique, London;35(2), 99-112

Been K., Jefferies M.G., 1985. *A state parameter for sands*. Géotechnique; 35(2): 99-112

Benjamin J. R. and C. A. Cornell, 1970. *Probability, Statistics, and Decision for Civil Engineers, McGraw-Hill, New York, 684 pp. Berberian, M. and D. Papastamatiou (1978). Khurgu (north Bandar Abbas, Iran) earthquake of 21 March 1977-a preliminary field report and a seismotectonic discussion.* Bull. Seism. Soc. Am. 68, 4ll-428

Benz H., Chouet B., Dawson P., Lahr J., Page R. and Hole, J., 1996. *Three-dimensional P and S wave velocity structure of redoubt volcano, Alaska.* J. geophys. Res., 101(B4), 8111-8128.

Berardi R., Berenzi A., Capozza F., 1981. *Campania-Lucania earthquake on 23 November 1980: accelerometric recordings of the main quake and relating processing*. Technical report, Ente Nazionale per l'Energia Elettrica (ENEL), Rome

Berberian M., Jacks.on, J. A., Ghorashi, M. and Kadjar, M. H., 1984. *Field and teleseismic observations of the 1981 Golbaf-Sirch earthquakes in SE Iran. Geophys. J. R. astr. Soc.,* 77, 809-838

Berge-Thierry C., Bernard P., Herrero A., 2001. *Simulating Strong Ground Motion with the "k^{-2}" Kinematic Source Model: An Application to the Seismic Hazard in the Erzincan basin, Turkey.* J. Seismology 5, 85-101

Bernard P. and Zollo A., 1988. *Inversion of S polarization from near-source accelerograms. Application to the records of 1980 Irpinia earthquake (Italy).* Seismic Hazards in Mediterranean regions, ed. J. Bonnin et al., Kluwer Ac. Publ., pp. 59-69

Bernard P. and Zollo A., 1989. *The Irpinia (Italy) 1980 earthquake: detailed analysis of a complex normal fault*. Journal of Geophysical Research, 94, 1631-1648

Bernard P. and A. Zollo, 1988a. *Analysis of strong ground motion data of the 1980, November 23 Campania-Lucania earthquake (Italy).* Processing of Strasbourg, 1986 Summer School on "Seimic Hazard in Mediterranean Region", edited by J. Bonnin, M. Cara, A. Clatemaa, and R. Frantechi, 69-69

Bernard P. and A. Zollo, 1989. *The Irpinia (Italy) 1980 earthquake: Detailed analysis of a complex normal faulting.* J. Geophys. Res. 94, 1631-1647

Bernard P. and R. Madariaga, 1984. *A new asymptotic method for the modeling of near-field accelerograms.* Bull. Seismol. Soc. Am. 74, 539-558

Bernard P. and Herrero A., 1994. S*lip Heterogeneity, Body-Wave Spectra, and Directivity of Earthquake Ruptures.* Annali di Geofisica, Vol. XXXVII, 1679-1690

Bernard P., Herrero A., Berge C., 1996. *Modeling Directivity of Heterogeneous Earthquake Ruptures.* Bull. Seism. Soc. Am. 86, 1149-1160

Bernard, P. and Madariaga, R., 1984. *A new asymptotic method for the modelling of near-field accelerograms.* Bull. Seism. Soc. Am., 74, 539-557

Beroza G.C. and Spudich P., 1988. Linearized inversion for fault rupture behavior: application to the 1984 Morgan Hill, California, earthquake. J. Geophys. Res., 93: 6275- 6296

Bertero V., S. Mahin and R. Herrera, 1978. *Aseismic design implications of near-fault San Fernando earthquake records.* Earthquake Eng. Struct. Dynam. 6, no. 1, 31-42

Bevc D., 1997. *Flooding the topography: Wave equation datuming of land data with rugged acquisition topography.* Geophysics, 62, 1558-1569

Beyer K. and Bommer J.J., 2006. *Relationships between median values and between aleatory variabilities for different definitions of the horizontal component of motion*. Bulletin of the Seismological Society of America; 96(4A):1512-1522

Bezzeghoud M., 1987. *Inversion et anaiyse spectraie des ondes P. Ph.D.* Thesis, Univ. Paris VII, France. Boschi, E., Muiargia, F., Mantovani, E., Bonafede, M., Dziewonski, A.M. and Woodhouse, J.H., 1981. The Irpinia earthquake of November 23, 1980. EOS Trans. Am. Geophys. Unioun, 62: 330

Bielak J. and P. Christiano, 1984. *On the effective seismic input for non- linear soil-structure interaction systems.* Earthq. Eng. Struct. Dyn. 12, 107-119

Bielak J., K. Loukakis, Y. Hisada and C. Yoshimura, 2003. *Domain reduction method for three-dimensional earthquake modeling in localized regions*. *Part I: theory.* Bull. Seism. Soc. Am. 93, 817-824

Bielak J., R. C. MacCamy, D. S. McGhee and A. Barry, 1991. *Unified symmetric BEM-FEM for site effects on ground motion-SH waves.* J. Eng. Mech.; 117, 2265-2285

Bilotta E., Pagano L. and Sica S., 2008. *Asincronismo del moto sismico di dighe in terra*. Italian Geotechnical Journal; 4(08):54-77. (in Italian)

Bilotta E., Pagano L. and Sica S., 2010. *Effect of ground-motion asynchronism on the equivalent acceleration of earth dams*. Soil Dynamic sand EarthquakeEngineering30(2010)561-579

Bindi D., Luzi L., Pacor F. and Paolucci R., 2011. *Identification of accelerometric stations in ITACA with anomalous seismic response.* Bull. Earthq. Eng, doi: 10.1007/s10518-011-9271-5

Bindi D., L. Luzi, M. Massa, and F. Pacor, 2009. *Horizontal and vertical ground motion prediction equations derived from the Italian Accelero- metric Archive (ITACA).* Bull. Earthquake Eng., doi 10.1007/s10518- 009-9130-9

Bindi D., Parolai S., Cara F., Di Giulio G., Ferretti G., Luzi L., Monachesi G., Pacor F. and Rovelli A., 2009. *Site Amplification observed in the Gubbio basin, Central Italy: Hints for lateral propagation effects*. Bull Seismol Soc Am, Vol. 99 (2A), pp. 741-760

Bindi D., R. R. Castro, G. Franceschina, L. Luzi and F. Pacor, 2004. *The 1997-1998 Umbria-Marche sequence (central Italy): Source, path and site effects estimated from strong motion data recorded in the epicentral area*. J. Geophys. Res. 109, B04312, doi 10.1029/ 2003JB002857

Biondi G., Cascone E. and Maugeri M., 2002. *Flow and deformation failure of sandy slopes.* Soil Dyn Earthquake Eng; 22(9-12):1103-14

Biondi G., Cascone E. and Rampello S., 2007. *Performance-based pseudo-static analysis of slopes*. In: fourth international conference on earthquake geotechnical engineering, Thessaloniki, Greece, June 25-28

Biot M.A., 1941. *General theory of three-dimensional consolidation*. J. Appl. Phys., 12, pp. 155-164

Biot M.A., 1956b. *Theory of Propagation of Elastic Waves in a Fluid-Saturated Porous Solid: II Higher Frequency Range.* Journal of the Acoustical Society of America, 28, pp. 179-191

Biot M.A., 1957. *The elastic coefficients of the theory of consolidation.* Journal of Applied Mechanics, Trans. ASME, 24, 594-601

Biot M.A., 1962. *Mechanics of deformation and acoustic propagation in porous media*. Journal of Applied Physics (33): 1482-1498

Bisio L., Di Giovambattista R., Milano G. and Chiarabba C., 2004. *Three-dimensional earthquake locations and upper crustal structure of the Sannio-Matese region (Southern Italy).* Tectonophysics, 385, 121- 136

Bleistein N., 1984. *Two-and-one-half dimensional in-plane wave propagation.* Research report, Center of Wave Phenomena, Colorado School of Mines, Golden, Colorado

Boatwright J., 1980. *A Spectral Theory for Circular Seismic Source; Simple Estimates of Dimension, Dynamic Stress Drop, and Radiated Energy.* Bull Seismol. Soc. Am. 70, 1 - 27

Boatwright J., 2007. *The persistence of directivity in small earthquakes.* Bulletin of the Seismological Society of America; 97(6):1850-1861

Boatwright J. and Boore D.M., 1982. *Analysis of the ground accelerations radiated by the 1980 Livermore Valley earthquakes for directivity and dynamic source characteristics*. Bull. Seism. Soc. Am.; 72: 1843-1865

Bollettinari G. and Panizza, M., 1981. *Una "faglia di superficie" presso San Gregorio Magno in occasione del sisma del 23-Xl-1980 in Irpinia.* Rend. Soc. geol. It., 4, 135-136 (in Italian)

Boncio P., Mancini T., Lavecchia G. and Selvaggi G., 2007. *Seismotectonics of strike-slip earthquakes within the deep crust of southern Italy: geometry, kinematics, stress field and crustal rheology of the Potenza 1990-1991 seismic sequences (M_{max} 5.7).* Tectonophysics, 445, 281-300

Bonilla M. G., 1988. *Minimum earthquake magnitude associated with coseismic surface faulting.* Bull. Assoc. Eng. Geologists 25, 17-29

Bonilla M. G. and J. M. Buchanon, 1970. *Interim report on worldwide historic surface faulting.* U.S. Geol. Surv. Open-File Rept. 70-34, 32 pp

Bonilla M. G., R. K. Mark and J. J. Lienkaemper, 1984. *Statistical relations among earthquake magnitude, surface rupture length, and surface fault displacement.* Bull. Seism. Soc. Am. 74, 2379- 2411

Boore D.M., Joyner W.B. and Fumal T.E., 1997. *Equations for estimating horizontal response spectra and peak acceleration from Western North American earthquakes: a summary of recent work.* Seismol Res Lett; 68(1):128-53

Boore D. M. and G. M. Atkinson, 2007. *Boore-Atkinson NGA ground motion relations for the geometric mean horizontal component of peak and spectral ground motion parameters.* Technical report, Pacific Earthquake Engineering Research Center, Berkeley, California

Boore D. M. and G. M. Atkinson, 2008. *Ground-motion prediction equations for the average horizontal component of PGA, PGV, and 5%-damped PSA at spectral periods between 0.01 s and 10.0 s*. Earthquake Spectra 24, no. 1, 99-138

Boore D. M., 1983. *Stochastic simulation of high-frequency ground motion based on seismological models of the radiated spectra*. Bull. Seismol. Soc. Am. 73, 1865-1894

Boore D. M., 2003. *Simulation of ground motion using the stochastic method.* Pure Appl. Geophys. 160, 635-676

Boore D.M., 2009. *Comparing stochastic point-source and finite-source ground-motion simulations: SMSIM and EXSIM.* Bull. Seismol. Soc. Am. 99, 3202-3216

Boore D. M. and W. B. Joyner, 1982. *The empirical prediction of ground motion.* Bull. Seism. Soc. Am. 72, S43-S60

Boore D.M. and W. Joyner, 1997. *Site amplification for generic rock sites.* Bull. Seism. Soc. Am., 87, 327-341

Boore D.M. and Atkinson G.M., 2007. *Boore-Atkinson NGA ground motion relations for the geometric mean horizontal component of peak and spectral ground motion parameters.* PEER Report, May

Boore D.M. and Atkinson G.M., 2008. *Ground-motion prediction equations for the average horizontal component of PGA, PGV and 5%-damped PSA at spectral period between 0.01 s and 10.0 s.* Earthquake Spectra; 24(1):99-138

Boore D.M., Joyner W.B. and Fumal T.E., 1997. *Equations for estimating horizontal response spectra and peak acceleration from western North American earthquakes: A summary of recent work*. Seism. Res. Lett; 68: 128-151

Borcherdt R.D., 1970. *Effects of local geology on ground motion near San Francisco Bay*. Bull Seismol Soc Am 60:29-61

Borcherdt R.D., 1994. *Estimates of site-dependent response spectra for design (methodology and justification).* Earthq Spectra 10:617-654

Borja R.I., Lin C.H. and Montans F.J., 2001. *Cam-clay plasticity part IV: implicit integration of anisotropic bounding surface model with nonlinear hyperelasticity and ellipsoidal loading function*. Computer Methods in Applied Mechanics and Engineering; 190:3293-3323

Borja R.I., Sama K.M. and Sanz P.F., 2003. *On the numerical integration of three-invariant elastoplastic constitutive models*. Computer Methods in Applied Mechanics and Engineering; 192:1227-1258

Boschi E., Console R., Di Maro R. and Murru M., 1998. *Contributo alla conoscenza della sismicità nella Basilicata* (online at http://www.consiglio.basilicata.it/basilicata_regione_notizie/la-ricerca_in_basilicata/05199804.pdf, in Italian).

Boschi E., F. Mulargia, E. Mantovani, M. Bonafede, A, M. Dziewonski and J. H. Woodhouse, 1981. *The Irpinia earthquake of November 28, 1980 (abatract)* Eas, Trans, AGU, 62330

Bouchon M., 1981. *A simple method to calculate Green's functions for elastic layered media.* Bull Seismol Soc Am 74:1615-1621

Bouchon M., 2003. *A review of the discrete wavenumber method, in Seismic Motion, Lithospheric Structures, Earthquake and Volcanic Sources: The Keiiti Aki Volume.* Pageoph Topical Volumes 2003, pp. 445-465

Bouchon M., Aki K., 1977. *Discrete wavenumber representation of seismic source wave filed*. Bull Seismol Soc Am; 67:259-77

Bouchon M., and J. S. Barker, 1996. *Seismic response of a hill: The example of Tarzana*. California, Bull. Seism. Soc. Am. 86, 66-72

Bouchon M., Hatzfeld D., Jackson J.A., 2006. *Haghshenas E. Some insight on why Bam (Iran) was destroyed by an earthquake of relatively moderate size.* Geophys Res Lett ;33: L09309

Bouckovalas G.D., Papadimitriou A.G., 2003. *Multi-variable relations for soil effects on seismic ground motion*. Earthquake Eng Struct Dyn; 32:1867-96 (Wiley)

Bouckovalas G.D., Papadimitriou A.G., 2005. *Numerical evaluation of slope topography effects on seismic ground motion*. Soil Dyn Earthquake Eng; 25(7-10): 547-555

Bouckovalas G.D., Papadimitriou A.G., Andrianopoulos K.I., 2009. *Estimation of seismic coefficients for the slope stability of earthdams: phase B*. Research Report to Public Power Corporation; 269 (in Greek)

Bozbey I., Gundogdu O., 2011. *A methodology to select seismic coefficients based on upper bound ''Newmark'' displacements using earthquake records from Turkey*. Soil Dynam Earthq Eng ; 31:440-51

Braga F., Dolce M., Liberatore D., 1982. *A statistical study on damaged buildings and an ensuing review of the msk-76 scale.* In: Proceedings of the Seventh ECEE Athens

Brahma S.P. and Harr M.E. 1962. *Transient development of the free surface in a homogeneous earth dam.* Géotechnique 12: 283-302

Bramerini F., Di Pasquale G., Orsini G., Pugliese A., Romeo R., and Sabetta F., 1995. *Rischio sismico del territorio italiano: proposta di una metodologia e risultati preliminari.* In: Proceedings of the 7 Convegno Nazionale L'Ingegneria Sismica in Italia, Siena September 1995, Vol. 3, p. 1099-108

Bray J.D. and Rathje E.M., 1998. *Earthquake-induced displacements of solid-waste landfills*. Journal of Geotechnical and Geoenvironmental Engineering ASCE;124(3):242-53

Bray J.D. and Rodriguez-Marek A., 2004. *Characterization of forward-directivity ground motions in the near-fault region*. Soil Dynamics and Earthquake Engineering; 24(11):815-828

Bray J.D. and Travasarou T., 2007. *Pseudostatic coefficient for use in simplified slope stability evaluation*. J Geotech Geoenviron Eng, ASCE;135(9):1336-40

Bray J.D. and Travasarou T., 2007. S*implified procedure for estimating earthquake-induced deviatoric slope displacements*. J Geotech Geoenviron Eng, ASCE; 133 (4):381-92

Brigante A., 2010. *Dighe in terra: Previsione e monitoraggio degli effetti sismo indotti*. PhD Thesis, University of Naples, Federico II

Brigante A, Sica S. and Pagano L.. *Effect of the component of the ground-motion on predicting the seismic reponse of earth dams*. (in press)

Brillinger D. R. and H. K. Preisler, 1985. *Further analysis of the Joyner-Boore attenuation data.* Bull. Seismol. Soc. Am. 75, 611-614

Brokĕsova J., 1993. *High-frequency ground motions due to extended seismic sources in complex structures.* PhD. Thesis, Charles University, Prague

Brokĕsova J., 1996. *Construction of ray synthetic seismograms using interpolation of travel times and ray amplitudes.* PAGEOPH 148 (3-4), 503-538

Brubns O.T., Xiao H. and Meyers A., 1999. *Self-consistent Eulerian rate type elastoplasticity models based upon the logarithmic stress rate*. Intenat. J. Plasticity 15(1999) 479-520

Brune J. N. and A. Anooshehpoor, 1999. *Dynamic geometrical effects on strong ground motion in a normal fault model.* J. Geophys. Res., 104, 809-815

Brune J.N., 1970. *Tectonic stress and the spectra of seismic shear waves from earthquakes*. J. Geophys. Res. 75, 4997-5009

Brüstle W. and Miiller G., 1983. *Moment and duration of shallow earthquakes from Love-wave modelling far regional distances.* Phys. Earth planet. Int., 32, 312-324

Bunks C., Saleck F.M., Zaleski S. and Chavent G., 1995. *Multi-scale seismic waveform inversion.* Geophysics, 60, 1457-1473

Burger R.W., P.G. Somerville, J.S. Barker, R.B. Herrmann and D.V. Helmberger, 1987. *The effect of crustal structure on strong ground motion attenuation relations in eastern North America.* Bull. Seism. Soc. Am., 77, 420-439

Buzzeghoud M., 1987. *Inversion et analyse des ondes P.* These de doctorat, Univ. of Paris 7

Byrne P., 1991. *A Cyclic Shear-Volume Coupling and Pore-Pressure Model for Sand.* In Proceedings: Second International Conference on Recent Advances in Geotechnical Earthquake Engineering and Soil Dynamics (St. Louis, Missouri, March, 1991), Paper No. 1.24, 47-55

Byrne P.M., Park S-S., Beaty M., Sharp M., Gonzalez L., Abdoun T., 2004. *Numerical modelling of liquefaction and comparison with centrifuge tests*. Canadian Geotechnical Journal; 41(2):193-211

C. Le Blanc, O. Hededal and L. B. Ibsen, 2008. *A modified critical state two-surface plasticity model for sand - theory and implementation.* ISSN 1901-7278 DCE Technical Memorandum No. 8

C.Truesdell, 1956. *Hypoelastic shear*. J. Appl. Phys. 27, 441-447. Reprinted in: C.Truesdell (ed.), Continuum Mechanics III, Tue International Science Review Series. Gordon and Breach, New York. CrossRef

C.Truesdell, 1963 . *Remarks on hypoelasticity*. J. Rea. Nat Bur. Stand. B 67, 141-143
C.Truesdell, 1965. *Hypo-elasticity. J. Rational Mech. Anal.4 (1955) 83-133.Reprinted in: C. Truesdell (ed.), ContinuumMechanics III.* The lntemational Science Review Series. Gordon and. Breach, New York
C. Truesdell, 1965. *The mechanical foundations of elasticity and fluid dynamics*. J. Rational Mech. Anal. 1(1952) 125-300; Corrections and additions, ibid 2 (1953) 593-616. Reprinted in: C.Truesdell (ed.), *Continuum Mechanics I.* The Intenational Science Review Series. Gordon and Breach, New York
C.Truesdell and W. Noll, 1965. *The non linear field theories of mechanics*. In: S. Fliigge (ed.),Handbuch der Physik,Bd IlJ/3.Springer, Berlin (1965) (2nd edition)
C.Truesdell. *The simplest rate theory of pure elasticity*. Comm. Pure Appl. Math. 8 (1955) 123-132.Reprinted in: C.Truesdell (ed.), Continuum Mechanics III, The International Science Review Series. Gordon and Breach, New York (1965). CrossRef
Cai Z. and Bathurst R.J., 1996. *Deterministic sliding block methods for estimating seismic displacements of earth structures*. Soil Dyn Earthquake Eng; 15:255-68
Calabresi G., Rampello S., Sciatti A. and Amorosi A., 2000. *Diga sulla Marana Capacciotti: Verifica delle condizioni di stabilità e analisi del comportamento in condizioni sismiche*. Res. Rep. Dip. di Ingegneria Strutturale e Geotecnica, Università di Roma La Sapienza
Calvi M. et al. 2004. *VIA-Riduzione della vulnerabilità sismica di sistemi infrastrutturali e ambiente fisico*. /http://gndt.ingv.it/Att_scient/ PE2002_Brief_Reports/brief_reports_con_int.htmS (in italian)
Campbell K. W., 1985. *Strong motion attenuation relations: a ten-year perspective.* Earthquake Spectra,1, 759-804
Campbell K.W., 1997. *Empirical near-source attenuation relationships for horizontal and vertical components of peak ground acceleration, peak ground velocity, and pseudo-absolute acceleration response spectra*. Seismol Res Lett; 68(1):154-79
Cantalamessa G., Dramis F., Pambianchi G., Romano A., Santoni, A. M. and Tonnetti, G., 1981. *Fenomeni franosi connessi con attività sismica nell'area compresa tra S. Giorgio La Molara e Bisaccia.* Rend. Soc. geol. It., 4, 467-469 (in Italian)
Cantore L., 2008. *Determination of site amplification in the Campania-Lucania region (southern Italy) by comparison of different site-response estimation techniques*. Ph.D. thesis, Dip. di Fisica, Università Federico II di Napoli
Cantore L., Convertito V., Zollo A. and Elia L., 2008. *Site-condition map and site amplification corrections for early-warning applications and seismic hazard assessment in the Campania-Lucania Region (southern Apennines), Italy (in preparation)*
Carcione J. M., D. Kosloff and R. Kosloff, 1988. *Wave propagation in a linear viscoacoustic medium.* J. R. Astr. Soc.; 78, 105-118
Carlomagno E., 2009. *Analisi sperimentali e modellazione del comportamento meccanico dei terreni a grana grossa*. PhD Thesis - University of Naples Federico II
Carmignani L., Cella G., Cerrina Ferroni A., Funicella R., Kalin O., Meccheri M., Patacca E., Pertusati P., Plesi G., Salvini F., Scandone P., Tartarici L. and Turco, E., 1981. *Analisi del campo di fratturazione superficiale indotto dal terremoto Campano-Lucano del 23/11/80.* Rend. Soc. geol. It., 4, 451-465 (in Italian)
Carnevalle R. and Elgamal A., 1994. *Experimental results of RPI centrifuge Model No. 12.* In: Proceedings of the international conference on verification of numerical procedures for the analysis of soil liquefaction problems, Davis, CA, 1: p. 1019-1026
Carrozzo M.T., Chirenti A., Luzio D., Margiotta C. and Quarta T., 1981. *Carta gravimetrica d'Italia: tecniche automatiche per la sua realizzazione*. Proc. I Annual Meeting of the National Geophys. Group, Rome, Italy, pp. 132-139
Casadei F. and E. Gabellini, 1997a. *Implementation of a 3D-coupled spectral element/finite element solver for wave propagation and soil- structure interaction simulations. Part I: models*. Technical report of the Joint Research Centre, EC EUR Report 17730 EN. JRC, Ispra
Casadei F., E. Gabellini, G. Fotia, F. Maggio, and A. Quarteroni, 2002. *A mortar spectral/finite element method for complex 2D and 3D elas- todynamic problems. Comp. Meth. App. Mech. Eng. 191, 5119-5148. Casadei, F., and E. Gabellini (1997a). Implementation of a 3D-coupled spectral element/finite element solver for wave propagation and soil- structure interaction simulations. Part I: models*. Technical report of the Joint Research Centre, EC EUR Report 17730 EN. JRC, Ispra
Casagrande A., 1936. *Characteristics of cohesionless soil affecting the stability of slopes and earth fills*. Journal of Boston Society of Civil Engineering*;* 23(1):13-32
Casagrande A., 1937. *Seepage through dams. Contributions to soil mechanics, 1925-1940*. Boston Society of Civil Engineers
Cascone E. and Rampello S., 2003. *Decoupled seismic analysis of an earth dam*. Soil Dynam Earthq Eng; 23:349-65
Casero P., F. Roure, L. Endignoux, L. Moreiti, C. Muller, L. Sage and R. Vially, 1988. *Neogene geodynamic evolution of the Southem Apennines. Mem. Soc. Geol. It., 41, 109-120*
Casero P., Roure F. and Vially L., 1991. *Tectonic framework and petroleum potential of the Southern Apennines, in Generation, Accumulation, and Production of Europe's Hydrocarbon, European Association of Petroleum Geoscientists.* Special Publication, Vol. 1, pp. 381-387, ed. Spencer, A.M., Oxford University Press
Casnadei R., 1988. *Subsurface basin analysis of fault-controlled turbidite system in Bradano Trough, Southern Adriatic foredeep, Italy*. Bull. Am. Assoc. Pet. Geol., 72(11), 1370-1380
Costanzo A., Sica S. and Silvestri F., 2011. *Verifica della sicurezza in condizioni sismiche della diga sul fiume Melito (CZ)*. Rivista italiana di geotecnica.
Castro R. R., A. Rovelli, M. Cocco, M. Di Bona and F. Pacor, 2001. *Stochastic simulation of strong-motion records from the 26 September 1997 (Mw 6), Umbria-Marche (Central Italy) earthquake.* Bull. Seismol. Soc. Am. 91, 27-39
Castro R., R. F. Pacor, G. Franceschina, D. Bindi, C. Zonno and L. Luzi, 2008. *Stochastic strong-motion simulation of the Mw 6 Umbria- Marche earthquake of September 1997: Comparison of different approaches.* Bull. of Seismol. Soc Am. 98, no. 2, 662-670, doi 10.1785/0120070092.

Catchings R.D. and W.D. Mooney, 1991. *Basin and Range crustal and upper mantle structure, northwest to central Nevada.* J. Geophys. Res., 96, 6247-6267

Cattin R., Briole P., Lyon-Caen H., Bernard, P.and Pinettes, P., 1999. E*ffects of superficial layers on coseismic displacements for a dip-slip fault and geophysical implications.* Geophys. J. Int., 137, 149-158

Cavanaugh J.E., 1997. *Unifying the derivation for the Akaike and corrected Akaike Informatioin Criteria*. Stat. Probab. Lett., 33, 201-208

Cedergren H.R., 1967. *Seepage, drainage and flow nets.* New York

CEN, 2004. *prEN 1998-1 Eurocode 8: Design of structures for earthquake resistance - Part 1: General rules, seismic actions and rules for buildings*

Cerny V., 1985. *A thermodynamical approach to the travelling salesman problem.* J. Optimisation Theory Appl., 45, 41-51

Cerveny V., Molotkov I.A. and Psencik I., 1977. *Ray Method in Seismology. University of Karlova, Prague. Chakraborty, K., Agarwal, B.N.P., 1992. Mapping of crustal discontinuities by wavelength filtering of the gravity fields*. Geophys. Prospect. 40, 801-822

Chakraborty T., 2009. *Development of a clay constitutive model and its application to pile boundary value problems*. Ph.D. Thesis, Purdue University, West Lafayette, Indiana, USA

Chan A.H.C., 1995. *User Manual for DIANASWANDYNE II.* School of Engineering, University of Birmingham, UK

Charles J.A., Abiss C.P., Gosschalk E.M. and Hinks J.L., 1991. *An engineering guide to seismic risk to dams in the United Kingdom*. Build Res Establish Rep

Chatelain J.L., 1978. *Etude fine de la sismicité en zone de collision continentaleà l'aide d'un réseau de statios portables: la region Hindu-Kush-Pamir.* Thése de 3 éme cycle, Université Paul Sabatier, Toulouse

Chen Y. C., Ishibashi I. and Jenkins J.T., 1988. *Dynamic shear modulus and fabric: Part I, Depositional and induced anisotropy*. Géotechnique, London; 38(1), 25-32

Cheng Z., Dafalias Y.F. and Manzari M.T., 2013. *Application of SANISAND Dafalias-Manzari model in FLAC3D*. 3rd International-Flac/ DEM- Symposium, HANGZHOU (China)

Chi W-C., Dreger D. and Kaverina A., 2001. *Finite-source modeling of the 1999 Taiwan (Chi-Chi) earthquake derived from a dense strong-motion network*. Bull Seismol Soc Am ; 91(5): 1144-57

Chiarabba C. and Amato A., 1994. *From tomographic images to fault heterogeneities*. Ann. Geofis., 37(6), 1481-1494

Chiarabba C. and Amato A., 1996. *Crustal velocity structure of the Apennines (Italy) from P-wave travel time tomography.* Ann. Geofis., 34, 1133-1148

Chiarabba C., Amato A. and Meghraoui M., 1996. *Imaging seismogenic structures with local earthquake tomography.* Phys. Chem. Earth, 21, 247-251

Chiarabba C. and Amato A., 1997. *Upper crustal structure of the Benevento area (southern Italy): fault heterogeneities and potential for large earthquakes.* Geophys. J. Int. 130, 229-239

Chiarabba C., Amato A., Anselmi M., Baccheschi P., Bianchi I., Cattaneo M., Cecere G., Chiaraluce L., Ciaccio M., Gori P. D., Luca G. D., Bona M. D., Stefano R. D., Faenza L., Govoni A., Improta L., Lucente F., Margheriti A. M. L., Mele F., Michelini A., Monachesi G., Moretti M., Pastori M., Piana Agostinetti N., Piccinini D., Roseilli P., Seccia D. and Valoroso, L., 2009. *The 2009 L'Aquila (central Italy) Mw6.3 earthquake: Main shock and aftershocks.* Geophys. Res. Lett., Vol. 36, No. 8, L18308

Chiarabba C., Jovane L. and Di Stefano R., 2005. *A new view of Italian seismicity using 20 years of instrumental recordings.* Tectonophysics, 395, 251-268

Chinnery M. A., 1969. *Earthquake magnitude and source parameters.* Bull. Seism. Soc. Am. 59, 1969-1982

Chioccarelli E. and I. Iervolino, 2010. *Near-source seismic demand and pulse-like records: A discussion for L'Aquila earthquake.* Earthquake Eng. Struct. Dynam. 39, no. 9, 1039-1062

Chioccarelli E., De Luca F., Iervolino I., 2009. *Preliminary Study of L'Aquila Earthquake Ground Motion Records*. [Available at http://www.reluis.it/doc/pdf/Aquila/Peak Parameters L Aquila Mainshock V5.2.pdf]

Chiou B. et al., 2003. *Validation Guidelines for Numerical Simulation of Ground Motion on Rock Conditions.* July 10, 2003

Chiou B., R. Darragh, N. Gregor and W. Silva, 2008. *NGA project strongmotion database*. Earthquake Spectra 24, no. 1, 23-44

Chopra A.K., 1967. *Earthquake response of earth dams*. ASCE Journal of Soil Mechanics and Foundations Division;93(SM2):65-81

Christensen N.I., 1982. *Seismic velocities.* In: Carmichael, R.S. (Ed.), Handbook of Physical Properties of Rocks, Vol. 2. CRC Press, Boca Raton, FL, pp. 1-228

Cimini G.B. and Amato A., 1993. *P-wave teleseismic tomography: contribution to the delineation of the upper mantle structure of Italy. In: Boschi E., Mantovani E. and Morelli A. (Eds.).* Recent Evolution and Seismicity of the Mediterranean Region. Kluwer Academic Publishers, Dordrecht, The Netherlands, 313-331

Cinque A., E. Patacca, P. Scandone and M. Tozzi, 1993. *Quatemary kinematic evolution of the Southem Apennines*. Relationships between surface geological features and deep lithospheric structures, Ann. Geofis., 36 (2), 249-260

Cinque A., Lambiase S. and Sgrosso I., 1981. S*u due faglie nell'alta valle del Sele legate al terremoto del 23.11.1981.* Rend. Soc. geo. It., 4, 127-129 (in ltalian)

Cinti FR, Faenza L, Marzocchi W and Montone P, 2004. *Probability map of the next M C 5.5 earthquakes in Italy*. Geochem Geophys Geosyst 5: Q1103. doi: 10.1029/2004GC000724

Civetta L., Orsi G., Scandone P. and Pece R., 1978. *Eastwards migration of the Tuscan anatectic magmatism due to anticlokwise rotation of the Apennines*. Nature, 276, 604-606

Cividini A. and Gioda G., 1984. *Approximate F. E. analysis of seepage with a free surface.* International Journal for Numerical and Analytical Methods in Geomechanics 8 (6): 549-566

Clark M. M., 1972. *Surface rupture along the Coyote Creek fault.* In The Borrego Mountain Earthquake of Aprii 9, 1968, U.S. Geol. Surv. Profess. Pap. 787, 55-86

Clayton, R. W., and B. Engquist, 1977. *Absorbing boundary conditions for acoustic and elastic wave equations.* Bull. Seism. Soc. Am.; 67, 1529-1540

Clough R. W., and J. Penzien, 1975. *Dynamics of Structures.* McGraw- Hill, New York, 584

CNR-GNDT., 1966. *L'attività del GNDT nel biennio 1993-1995*, a cura di A. Corsanego, E. Facciali, C. Gavarini, P. Scandone, D. Slejko, M. Stucchi

Cocco M. and F. Pacor, 1993. *The rupture process of the 1980 Irpinia, Italy, earthquake from the inversion of strong motion waveforms.* Tectonophysics 218, 157-177

Cocco M. and Pacer F., 1992. *Space-time evolution of the rupture process from the inversion of strong motion waveforms.* In: E. Boschi (Editor), Proc. Int. Workshop Irpina 10 anni dopo (Napoii, Italy), Editrice Compositori, Bologna (in press)

Cocco M. et al., 1999. *The April 1996 Irpinia seismic sequence: evidence for fault interaction.* J. Seism., 3, 105-117

Cocco M. and Pacor F., 1993. *Space-time evolution of the rupture process from the inversion of strong motion waveforms*. Ann Geofis; XXXVI(1):41-9

Cohee B.P. and Beroza G.C., 1994. *A comparison of two methods for finite-fault inversion using strong-motion data*. Ann Geofis; 37(6):77-101

Convertito V., De Matteis R., Cantore L., Zollo A., Iannaccone G. and Caccavale M., 2009. Rapid estimation of ground-shaking maps for seismic emergency management in the Campania Region of southern Italy. Springer Science+Business Media B.V

Convertito V, De Matteis R, Romeo A, Zollo A and Iannaccone G., 2007. *Strong motion relation for early- warning applications in the Campania Region (southern Apennines), Italy*. In: Gasparini et al (eds) Earthquake early warning systems. Springer-Verlag, Berlino

Convertito V. and Herrero A., 2004. *Influence of focal mechanism in probabilistic seismic hazard analysis*. Bulletin of the Seismological Society of America; 94(6):2124-36

Convertito V., Iervolino I. and Herrero A., 2009. *Design earthquakes' map: an additional tool for engineering seismic risk analysis. Application to southern Apennines (Italy).* XIII Convegno Nazionale ANIDIS L'Ingegneria Sismica in Italia, Bologna, 28 giugno - 2 luglio

Convertito, V., A. Emolo and A. Zollo, 2006. *Seismic-hazard assessment for a characteristic earthquake scenario.* An integrated probabilistic-deterministic method. Bull. Seismol. Soc. Am. 96, 377-391

Cooley R. L., 1971. *A finite difference method for unsteady flor in variable saturated porous media: Application to a single pumping well*. Water Res. Res. 7 (6): 1607-1625

Coppersmith K. J., 1991. *Seismic source characterization for en gineering seismic hazard analysis*. In Proc. 4th lnternational Conference on Seismic Zonation, Voi. I, Earthquake Engineering Research Institute, Oakland, California, 3-60

Corigliano M, Scandella L., Lai Carlo G. and Paolucci R., 2011. *Seismic analysis of deep tunnels in near fault conditions: a case study in Southern Italy.* Springer Science+Business Media B.V., Bull Earthquake Eng. DOI 10.1007/s10518-011-9249-3

Corrado G., Rapolla A., 1981. *The gravity field of Italy: analysis of its spectral composition and delineation of a three dimensional crust model for central-southern Italy*. Boll. Geofis. Teor. App. 23 (89), 17-29

Cosenza E, Manfredi G., 1997. *The improvement of the seismic-resistant design for existing and new structures using damage criteria*. In Seismic Design Methodologies for the Next Generation of Codes, Fajfar P, Krawinkler H. (eds). Balkema: Rotterdam, 119-130

Cosenza E., Manfredi G., Ramasco R., 1993. *The use of damage functionls in earthquake engineering: a comparison between different methods*. Earthquake Engineering and Structural Dynamics; 22(10):855-868

Cotton F. and Coutant O., 1997. *Dynamic stress variations due to shear faults in a plane layered medium.* Geophys. J. Int., 128, 676-688

Courboulex F., Virieux, J. and Gilbert D., 1996. *On the use of cross validation theory and simulated annealing for deconvolution.* Bull. seism. Soc. Am., in press

Coutant O., 1989. *Program de simulation numerique AXITRA*. In Rapport LGIT. Universiteè Joseph Fourier, Grenoble, 1989

Cremonini M. G., P. Christiano and J. Bielak, 1988. *Implementation of effective seismic input for soil-structure interaction systems.* Earthquake Eng. Struct. Dyn; 16, 615-625

Crespellani T., Ghinelli A., Madiai C. and Vannucchi G., 1990. *Analisi di stabilità dei pendii naturali in condizioni sismiche.* Rivista Italiana di Geotecnica, 2, pp. 49-74

Creutz M., 1980. *Monte Carlo study of quantized SU (2) gauge theory.* Phys. Rev., 21, 2308-2315

Crosson R. S., 1976. *Crustal structure modeling of earthquake data, 1, Simultaneous least squares estimation of hypocenter and velocity parameters*. J. Geophys. Res., 81,3036-3046

Crosson R. S., M. Martini, R. Scarpa and S. C. Key. *The southern Italy earthquake of 23rd November 1980: An unusual pattern of faulting.* by R. S Crosson, M. Martini, R. Scarpa and S.C key., Bull. Seismol. Soc Am

Crosson R. S., Martini M., Scarpa R. and Key S. C., 1986. *The Southern Italy earthquake of 23rd November 1980: An unusual pattern of faulting.* Bull. seism. Soc. Am., 76, 381-394

Crosson R. S., M. Martini, R. Scarpa and S. C. Key, 1987. *Reply to comment on " The southern Italy eartbquake of 23rd November 1980*: an unusual *pattern of faulting"* by R. S. Crosson, M. Martini, R. Scarpa and S.C. Key., Bull Seismol. Soc Am., 77,1075-1077

Crouch R.S., Wolf J. and Dafalias Y., 1994. *Unified critical state bounding surface plasticity model for soil.* Journal of Engineering Mechanics; 120(11):2251-2270

Cubrinovski M. and Ishihara K., 1998. *State concept and modified elastoplasticity for sand modelling*. Soils Foundations;38(4):213-25

Cultrera G., A. Cirella, E. Spagnuolo, A. Herrero, E. Tinti and F. Pacor, 2010. *Variability of kinematic source parameters and its implication on the choice of the design scenario.* Bull. Seismol. Soc. Am. 100, 941-953

Cultrera, G., F. Pacor, G. Franceschina, A. Emolo and M. Cocco, 2009. *Directivity effects for moderate-magnitude earthquakes (Mw 5.6- 6.0) during the 1997 Umbria-Marche sequence, central Italy*. Tecto- nophysics 476, 110-120

Cundall P.A., Hansteen H., Lacasse S. and Selnes P.B., 1980. *NESSI - soil structure interaction program for dynamic and static problems*. N.G.I., Report 51508-9

Dafalias Y. F., 1982. *Bounding surface elastoplasticity-viscoplasticity for particulate cohesive media*. International Union of Theoretical and Applied Mechanics Conference on Deformation and Failure of Granular Materials (P. A. Vermeer and H. J. Luger, eds.); 97-107

Dafalias Y. F., September, 1986. *Bounding Surface Plasticity, I.* Mathematical Foundation and the Concept of Hypoplasticity. Joumal of Engineering Mechanics, ASCE, Voi. 112, No. 9

Dafalias Y. F., 1986. *Bounding Surface Plasticity, II Application to Isotropie Cohesive Soils.* Journal of Engineering Mechanics, ASCE, Voi. 112, No

Dafalias Y. F., PapadimitriouA. G. and Li, X. S., 2004. *Sand plasticity model accounting for inherent fabric anisotropy*. Journal of Engineering Mechanics, ASCE; 130(11), 1319-1333

Dafalias Y..F, Popov E.P., 1976. *Plastic internal variable formalism of cyclic plasticity*. Journal of Applied Mechanics; 98(4):645-650

Dafalias Y.F. and Popov E.P., 1975. *A model of nonlinearly hardening materials for complex loadings.* Acta. Mech., Vol 21, 173-192. CrossRef

Dafalias Y.F., 1975. *On cyclic and anisotropic plasticity: (i) a general model including material behavior under stress reversals, (ii) anisotropic hardening for initially orthotropic materials*. Ph.D. Thesis, University of California, Berkeley

Dafalias Y.F. and Popov E.P., 1975. *A model of nonlinearly hardening materials for complex loadings*. Acta Mechanica; 21(3):173-92

Dafalias Y.F. and Manzari M.T., 1999. *Modeling of fabric effect on the cyclic loading response of granular soils.* In: Proceedings, 13th ASCE Engineering Mechanics Specialty Conference, Baltimore (in CD-ROM)

Dafalias Y.F. and Manzari M.T., 2004. *Simple plasticity sand model accounting for fabric change effects*. Journal of Engineering Mechanics, ASCE; 130(6):622-34

Dafalias Y.F., Papadimitriou A.G. and Li X.S., 2004. *Sand plasticity model accounting for inherent fabric anisotropy*. Journal of Engineering Mechanics, ASCE; 130(11):1319-33

Dafalias YF and Popov E.P., 1976. *Plastic internal variable formalism of cyclic plasticity*. Journal of Applied Mechanics; 98(4): 645-650

Dakoulas P. and Gazetas G., 1985. *A class of inhomogeneous shear models for seismic response of dams and embankments*. Soil Dyn Earthquake Eng; 4 (4):166-82

Dakoulas P. and Gazetas G., 2008. *Insight into seismic earth and water pressures against caisson quay walls*. Geotechnique; 58(2):95-111

Darendeli M. B., 2001. *Development of a new family of normalized modulus reduction and materiai damping curves.* Ph.D. thesis, University of Texas at Austin

D'Argenio B. and F. Horvath. *Some remarks on the deformation history of Adria; from the Mesozoic to the Tertiary.* Ann. Geophys., 2(2). 143-146. 984

D'Argenio B., F. Honath and J. E. T. Channell, 1980. *Paleotectonic evolution of Adria, the African promontory.* Geology of the Alpine chains born on the Tethys, 27th Intemational Geological Congress, Paris, Mrn. BRGM, 115,33l

Darragh R. B. and B. A. Bolt, 1987. *A comment on the statistical regression relation between earthquake magnitude and fault rupture length.* Bull. Seism. Soc. Am. 77, 1479-1484

Das S. and K. Aki, 1977. *Fault plane with barriers: A versatile earthquake model.* J. Geophys. Res, 81,5658-5670

Davis J. C., 1986. *Statistics and Data Analysis in Geology*. Second Ed., Wiley, New York, 646 pp

Day R.W. 2002. *Geotechnical earthquake engineering handbook.* New York: McGraw-Hill

Day S. M., 1988. *Efficient simulation of constant Q using coarse-grained memory variables.* Bull. Seism. Soc. Am.; 88, 105-1062

Day S. M., 2002. *The PEER/SCEC collaboration for validation of 3D wave propagation codes.* Presented at the SCEC Annual Meeting, 8-11 September 2002, Oxnard, California

Day S. M. and C. R. Bradley, 2001. *Memory-efficient simulation of anealstic wave propagation.* Bull. Seism. Soc. Am.; 91, 520-531

Day S. M. and J. B. Minster, 1984. *Numerical simulation of attenuated wavefields using a Padé approximant method.* Geophys. J. R. Astr. Soc.; 78, 105-118

Day SM., 1982. *Three-dimensional finite difference simuiation of fault dynamics: rectangular faults with fixed rupture velocity*. Bull. Seismol. Sot. Am., 72: 705-727

De Gori P., Cimini G.B., Chiarabba C., De Natale G., Troise C. and Deschamps A., 2001. *Teleseismic tomography of the Campanian volcanic area and surrounding Apenninic belt. J. Volcanol.* Geotherm. Res., 109, 55-75

De Groot M.B., Bolton M.D., Foray .P, Meijers P., Palmer A.C., Sandven R., Sawicki A., Teh T.C., 2006. *Physics of liquefaction phenomena around marine structures*. Journal of Waterway, Port, Coastal and Ocean Engineering; 132(4):227-243

De Luca S., Milana G., Marcucci G. and Sanò T., 2005. *Evidence of low-frequency amplication in the city of L'Aquila, Central Italy, through a multidisciplinary approach including strong- and weak-motion data, ambient noise, and numerical modeling.* Bull Seismol. Soc. Am., Vol. 95, No. 4, pp. 1469-1481

De Matteis R., Matrullo E., Rivera L., Stabile T.A., Pasquale, G. and Zollo A., 2012. *Fault delineation and regional stress direction from the analysis of background microseismicity in Southern Apennines, Italy.* Bull. seism. Soc. Am., 102(4), doi: 10.1785/0120110225

De Matteis R., Romeo A., Pasquale G., Iannaccone G. and Zollo, A., 2010. *3D tomographic imaging of the southern Apennines (Italy): a statistical approach to estimate the model uncertainty and resolution*. Stud. geophys. Geod., 54, 367-387

De Matteis R., Vanorio T., Zollo A., Ciuffi S., Fiordalisi A. and Spinelli E., 2008. *Three- dimensional tomography and rock properties of the Larderello-Travale geothermal area, Italy*. Phys. Earth Planet. Inter., 168, 37-48, doi: 10.1016/j.pepi.2008.04.019

De Natale G., M. Martini and E. Tersini, 1983. *Il terremoto del 23 Novembre 1980: Spostamento su due faglie ortogonali collegato a movimiento di blocchi verticali.* paper presented at the 2nd Convegno Annuale, Gruppo Nas. di Geofis. della Terra Solida, Rome

Deachamps A. and G. C. P. King, 1983. *The Campania-.Lucania (southerm Italy) earthquake of 23 November 1980.* Earth Planet. Sci Lett., 62,296-304

Deachamps A. and G. C. P. King, 1984. *Aftershocks of the Campania-Lucania (Italy) earthquake of 28 November 1980.* Bull Seism. Soc. Am.,74,2483-2and11517

Deschamps A., Iannacone G. and Scarpa R., 1984. *The Umbrian earthquake (Italy) of 19 September 1979*. Annales Geophys., 2, 29-36

DeAlba P., Seed H.B. and Chan C.K., 1976. *Sand liquefaction in large-scale simple shear tests*. Journal of the Geotechnical Engineering Division;102(9):909-27

Del Gaudio S., 2014. *Strong motion simulations with empirical Green's functions: methodology and application to the 2009 L'Aquila earthquake*. PhD Thesis, University of Naples, Federico II

Del Peuo E., G. Iannacone, M. Martbù, and R. Scarpa, 1983. *The 2Srd Novamber 1980 aouthem Italy earthquab.* BvlL Seimand. Soc.,78,187-200

Del Pezzo E., Iannaccone G., Martini M. and Scarpa. R., 1983. *The 23 November 1980 Southern Italy earthquake*. Bull. Seismol. Sot. Am., 73: 187-200

Del Prete M. and G. T. Liussi, 1981. *Risultati dello studio preliminare della frana di Calitri (AV) mobilitata dal terremoto del 23 novembre 1980.* Geol. Appl. idrogeol.,16,153-164

Dell'Aversana P., 2001. *Integration of seismic, MT, and gravity data in a thrust belt interpretation.* First Break, 19, 335-341

Dell'Aversana P., Ceragioli, E., Morandi, S. and Zollo, A., 2000. *A simultaneous acquisition test of high density "global offset" seismic in complex geologicalal settings.* First Break, 18, 87-96

Dell'Aversana P., Zucconi V. and Colombo, D., 2001. *Improvement in seismic acquisition by 3D Global offset approach.* 71st Ann. Internat. Mtg: Soc. Expl. Geophy. Expanded Abstracts, 29-32

Dello Russo A., Sica S. and Simonelli A. L., 2013. *Effetti della propagazione sismica near-source su grandi rilevati in terra: analisi parametriche*. Incontro Annuale dei Ricercatori di geotecnica, 16-18 settembre 2013 – Perugia, Italia

Dello Russo A., Sica S. and Simonelli A. L., 2014. *Propagazione sismica Near-Source: effetti su grandi rilevati in terra*. XXV Convegno Nazionale di Geotecnica, 4-6 giugno 2014 - Baveno (VB), Italia

Dello Russo A., Sica S. and Simonelli A.L., 2015. *Seismic propagation in near-source conditions: effects on large embankments*. XVI European Conference Soil Mechanics Geotechnical Engineering, 13-17 September 2015 – Edinburgh, Scotland.

Desai C.S. and Shernan W.C., 1971. *Unconfined transient seepage in sloping banks.* Jnl. of the Soil Mech. and Found. Div. ASCE, Nº SM2: 357-373

Desai C.S., 1972. *Seepage analysis of earth banks under drawdown*. Jnl. of the Soil Mech. and Found. Div., ASCE, Nº SM11: 1143-1162

Desai C.S., 1977. *Drawdown analysis of slopes by numerical method.* Jnl. of the Soil Mech. and Found. Div., ASCE, Nº GT7: 667-676

Di Luccio F., Fukuyama E. and Pino N.A., 2005. *The 2002 Molise earth- quake sequence: what can we learn about the tectonics of Southern Italy?*. Tectonophysics, 405, 141-154

Di Stefano R., Chiarabba C., Lucente F. and Amato A., 1999. *Crustal and uppermost mantle structure in Italy from the inversion of P-wave arrival times: geodynamic implications*. Geophys. J. Int., 139, 483-498

Díaz-Rodríguez, J. A., Martínez-Vasquez, J. J. and Santamarina, J. C., 2009. *"Strain-rate effects in Mexico city soil."* Journal of Geotechnical and Geoenvironmental Engineering, ASCE, 135(2), 300-305

Dienes J.K., 1979. *On the analysis of rotation and stress rate in deforming bodies*. Acta Mechanica 32 217-232.CrossRef

Dienes J.K., 1987. *A discussion of material rotation and stress rate*. Acta Mechanica 65, 1-11.CrossRef

Dietz L. D. and W. L. Ellsworth, 1990. *The October 17, 1989, Loma Prieta, California, earthquake and its aftershocks: geometry of the sequence from high-resolution Iocations.* Geophys. Res. Lett. 17, 1417-1420

DISS Working Group, 2010. *Database of Individual Seismogenic Sources (DISS), Version 3.1.1: A compilation of potential sources for earthquakes larger than M 5.5 in Italy and surrounding areas*. Available at: http://diss.rm.ingv.it/diss./INGV, Last accessed June 2012.

Dit-UPC, Codebright, 2002. *A 3-D program for thermo-hydro-mechanical analysis in geological media. USER'S GUIDE.* Centro Internacional de Métodos Numéricos en Ingeniería (CIMNE), Barcelona

Doglioni C., Harabaglia P., Martinelli G., Mongelli F., Zito G., 1996. *A geodynamic model of the Southern Apennines accretionary prism.* Terra Nova 8, 540-547

Donald L. Wells and Kevin J. Coppersmith, 1994. New *Empirical Relationships among Magnitude, Rupture Length, Rupture Width, Rupture Area, and Surface Displacement.* Bulletin of the Seismological Society of America, Vol. 84, No. 4, pp. 974-1002

d'Onofrio A., Silvestri F. and Vinale F., 1999. *Strain-rate dependent behaviour of a natural stiff clay*. Soils and Foundations. Voi. 39, No.2, pp. 69-82

Doroudian M. and Vucetic M., 1999. *Results of Geotechnical Laboratory Tests on Soil Samples from the UC Santa Barbara Campus*. UCLA Research Report No. ENG-99-203

Doser D. I., 1985. *The 1983 Borah Peak, Idaho and 1959 Hebgen Lake, Montana earthquakes: models far norma fault earthquakes in the intermountain seismic belt.* In Proc. of Workshop X XVIII on the Borah Peak, Idaho, Earthquake , pp. 368-384, U.S. geol. Surv. Open File Rep., 85-290

Doser D.I., 1986. *Earthquake processes in the Rainbow Mountain - Fairview Peak - Dixie Valley, Nevada region 1954-1959*. J. Geophys. Res., 91, 12572-12586

Douglas A., 1967. *Joint epicentre determination.* Nature, 215, 47-48
Dowell M. and Jarratt P., 1972. *The Pegasus method for computing the root of an equation*. BIT;12:503-8
Dreger D. and Kaverina A., 2000 *Seismic remote sensing for the earthquake source process and near-source strong shaking: a case study of the October 16, 1999 hector mine earthquake*. Geophys Res Lett 27:1941-1944
Duda S. J., 1965. *Secular seismic energy release in the circum Pacific belt.* Tectonophysics 2, 409-452
Duncan J.M. and Chang C.Y., 1970. *Non-linear analysis of stress and strain in soils*. Journal of Geotechnical Engineering (ASCE). Vol. 96, No. 5, pp. 1629-1653
Dziewonski A. M., Franzen J. E. and Woodhouse J. H., 1985. *Centroid-moment tensor solutions far July-September, 1984.* Phys. Earth planet. Int., 38, 203-213
Dziewonski A. M., T.A. Chow and J. H. Woodhouse, 1981. *Determination of earthquake source parameters from waveform data for studies of global and regional seismicity.* J. Geophys. Res. 86, 2825-2852
Edi K., Urs K. and Hansrudi M., 1995. *Velest user's guide.* European-Mediterranean Seismological Centre (EMSC)
Egglezos D. N. and Bouckovalas G. D., 1999. *Permanent strain and pore pressure relations for cyclic loading of sand.* Proc., 2nd Int. Conf. on Earthquake Geotech. Engrg., Vol. 1; 131-136
Ekstrom G., 1994. *Teleseismic analysis of the 1990 and 1991 earthquakes near Potenza*. Ann. Geofis., XXXVII, 1591-1599
Electric Power Research Institute, 1987. *Seismic hazard methodology for the central and eastern United States-Volume 1: Methodology, Report NP4726,* prepared for Seismicity Owners Group and Electric Power Research Institute under research projects P101- 38, -45, -46, 2256-14
Electric Power Research Institute, 1993. *Guidelines for determining design basis ground motions.* EPRI TR 102293
Elgamal A-WM., 1992. *Three dimensionai seismic analysis of La Villita Dam.* J. Geotech Eng ASCE;118:1937-58
Elgamal A., W., Parra E., Yang Z. and Adalier K., 2002. *Numerical analysis of embankment foundation liquefaction countermeasures*. J. Earth. Engng., 6, 4, pp. 447-471
Elgamal A., Yang Z. and Parra E., 2002. *Computational modelling of cyclic mobility and post-liquefaction site response*. Soil Dynamics and Earthquake Engineering; 22(4):259-271
Elgamal A.M., Scott R.F., Succarieh M.F. and Yan L., 1990. *La Villita Dam response during earthquakes including permanent deformation*. J Geotech Eng ASCE;116(10):1443-62
Elgamal A.W. and Gunturi R.V., 1993. *Dynamic behaviour and seismic response of El Infiernillo Dam*. Earthquake Engineering and Structural Dynamics 22:665-84
Elia G., 2004. *Analisi FEM di problemi al contorno in condizioni statiche e dinamiche con un modello costitutivo avanzato*. Ph. D. Thesis, Technical University of Bari, Italy
Elia G., Amorosi A. and Chan A.H.C., 2004. *Nonlinear ground response: effective stress analyses and parametric studies*. Proc. Japan-Europe Seismic Risk Workshop, Bristol, UK
Elia G., Amorosi A. and Chan A.H.C., 2005. *Fully coupled dynamic analysis of an earth dam using a complex constitutive assumptio*n. Proc. 11th Int. Conf. of IACMAG, Turin, Italy, pp. 257-264
Elia L., Satriano C. and Iannaccone G. 2009. *SeismNet Manager: a web application to manage hardware and data of a seismic network.* Seismol. Res. Lett., 80(3), 420-430
EM 1110-2-2300., 2004. *General design and construction considerations for earth and rock-fill dams*. US Army Corps of Engineers
Emmerich H., and M. Korn 1987. *Incorporation of attenuation into time domain computations of seismic wave fields.* Geophysics 52, 1252- 1264
Emolo A., G. Cultrera, G. Franceschina, F. Pacor, V. Convertito, M. Cocco and A. Zollo, 2008. *Ground motion scenarios for the 1997 Colfiorito, central Italy, earthquake.* Ann. Geophys. 51, 509-525
Emolo A. and Zollo A., 2001. *Accelerometric Radiation Simulation for the September 26, 1997 Umbria-Marche (Central Italy) Main Shocks*. Annali di Geofisica 44, 605-617
EN 1998-1, 2003. *Eurocode No.8: design of structures for earthquake resistance of structures.* CEN European Committee for Standardisation
EN 1998-5. *Eurocode 8: Design of structures for earthquake resistance - Part 5: foundations, retaining structures and geotechnical aspects*. Bruxelles, Belgium: CEN European Committee for Standardization
ENEL, 1977. *Catalago dei terremoti italiani dall'anno 1000 al 1975.* Progetto finalizzado Geodinamica, Conv. Naz. delle Ris., Rome, Italy
Engquist B., Majada A., 1977. *Absorbing boundary conditions for the numerical simulation of waves*. Math Comput; 31(139): 629-55
ER 1110-2-1806., 1995. *Earthquake design and evaluation for civil works projects*. US Army Corps of Engineers
Erdik M., Doyuran V., Gulkan P. and Akkas N., 1983. *Statistical evaluation of earthquake hazard in Turkey.* Middle East Technical University, Department of Civil Engineering. (in Turkish)
Ericksen J.L., 1958. *Hypoelastic potentials*. Quart. Mech. Appl. Math. 11 67-72
Eurocode 8, 2003. *Design of structures for earthquake resistance*. Part 1: general rules, seismic actions and rules for buildings. Draft January 2003
Evans J.R. and Zucca J.J., 1988. *Active high resolution seismic tomography of compressional wave velocity and attenuation at Medicine Lake Volcano, Northern California Cascade Range*. J. Geophys. Res., 93, 15016-15036
Eyidogan H. and Jackson J. A., 1985. *A seismological study of normal faulting in the Demirci, Alasehir and Gediz earthquakes of 1969-1970 in western Turkey: implications for the nature and geometry of deformation in the continental crust.* Geophys. J. R. astr. Soc., 81, 569-607
F. Courboulex, J. Virieux, A. Deschamps, D. Gibert and A. Zollo, 1996. *Source investigation of a small event using empirical Green's functions and simulated annealing.* Geophys. J. Int. 125,768-780
Faccioli, E., F. Maggio, R. Paolucci and A. Quarteroni, 1997. *2D and 3D elastic wave propagation by a pseudo-spectral domain decomposition method*. J. Seism. 1, 237-251

Faccioli E. and Cauzzi C., 2006. *Macroseismic intensities for seismic scenarios, estimated from instrumentally based correlations*. In: 1st European conference on earthquake engineering and seismology, Geneva, 3- 8 Sept 2006, Paper no. 569
Faccioli E., Vanini M., Paolucci R. and Stupazzini M., 2005. *Comment on "Domain Reduction Method for Three-Dimensional Earthquake Modeling in Localized Regions, Part I: Theory," by J. Bielak, K. Loukakis, Y. Hisada, and C. Yoshimura, and "Part II: Verification and Applications," by C. Yoshimura, J. Bielak, Y. Hisada, and A. Fernández*. Bulletin of the Seismological Society of America, Vol. 95, No. 2, pp. 763-769, doi: 10.1785/0120040039
Fäh D., P. Suhadolc and G. Panza, 1990. *Estimation of strong ground motion in laterally heterogeneous media: modal summation-finite differences.* Proc. IX Europ. Conf. Earthq. Eng., Moscow, 100-109
Fäh D., P. Suhadolc, and G. F. Panza, 1993. *Variability of seismic ground motion in complex media: the case of a sedimentary basin in the Friuli (Italy) area.* J. Appl. Geophys.; 30, 131-148
Fäh D., P. Suhadolc, St. Mueller, and G. F. Panza, 1994. *A hybrid method for the estimation of ground motion in sedimentary basins: Quantitative modeling for Mexico City.* Bull. Seism. Soc. Am.; 84, 383-399
Fahey M., 1992. *Shear modulus of cohesionless soil: variati.on with stress and strain level*. Canadian Geotechnical Journal. Voi. 29, No. 1, pp. 157-161
Fahey M. and Carter J.P., 1993. *A finite element study of the pressuremeter test in sand using a non linear elastic plastic model.* Canadian Geotechnical Joumal, Voi. 30, No.2, pp. 348-362
Fajfar P., Vidic T. and Fischinger M., 1992. *On energy demand and supply in SDOF systems*. In: Fajfar P, Krawinkler H, editors. Nonlinear seismic analysis of RC buildings. Amsterdam: Elsevier; p. 41-61
Farrel T. and Kutter B., 1994. *Experimental results of Model No. 12*. In: Proceedings of the international conference on verification of numerical procedures for the analysis of soil liquefaction problems, Davis, CA, 1: p. 1027-1034
Favreau P., Archuleta R.J., 2003. *Direct seismic energy modeling and application to the 1979 Imperial Valley earthquake*. Geophys Res Lett; 30(5):1198.
Fedi M. and A. Rapolla, 1990. *Aeromagnetic anomaly shape analysis in the Italian region for the evaluation of the crustal block rotations.* J. Geodyn., 12 (2-4), 149-161
Feignier B., 1991. *How geology can influence scaling relations.* Tectonophysics, 197, 41-53
Fels A., Pugliese A. and Muzzi F., 1981. *Campano-Lucano earthquake, November 1980, ltaly: Strong motion data related to loca/ site conditions. Contributo alla caratterizzazione della sismicita' del territorio Italiano, 105-124.* Contribution to the annual convention of the Italian National Research Project on ltalian Seismicity, Udine, 12-14 May 1981
Festa G., 2004. *Slip imaging by isochron back projection and source dynamics with spectral element methods.* PhD Thesis in Geophysics. Link: http://people.na.infn.it/~festa/Paper/festa_thesis.pdf.
Finn W.D.L., Lee K.W. and Martin G.R., 1977. *An effective stress model for liquefaction*. Proc. ASCE, Journal of Geothechnical Engineering Division, Vol. 103, N. GT6
Finn W.D.L. and Bathia S.K., 1981. *Prediction of Seismic Porewater pressures.* Proc. in the Tenth Int. Conf. on Soil Mechanics and Foundation Engineering, Vol. 3, A.A. Balkema, Rotterdam, pp. 201-206
Finn W.D.L. and Ledbetter R.H., 1991. *Evaluation of liquefaction effects and remediation strategies by deformation analysis*. Proc. Int. Conf. on Geotechnical Eng. for Costal Development, GEOCOAST 91, pp. 1-20
Finn L.W.D, Yogendrakumar M, Yoshida N and Yoshida H., 1986. *TARA-3: a program to compute the response of 2-D embankments and soil-structure systems to seismic loadings*. Canada: Department of Ovil Engineering, University of British Columbia
Finn L., Ventura C.E. and Schuster N.D. 1995. *Ground motions during the 1994 Northridge earthquake*. Canadian Journal of Civil Engineering, Vol 22, 300-315.
Finn L.W.D., Ledbetter R.H. and Marcusson W.F., 1997. *North American practise for evaluating the seismic safety of embankment dams*. In: Ishihara K. editor. Earthquake Geotechnical Engineering. Rotterdam: Balkema; p. 1227-52
Finn L.W.D., 2000. *State-of-the-art of geotechnical earthquake engineering practice.* Soil Dyn Earthquake Eng 2000; 20:1-15
Frankel A. and Wennerberg L., 1989. *Microearthquake spectra from the Anza, California, seismic network: site response and source scaling.* Bull. Seism. Soc. Am., 79, 581-609
Frankel A., 1993. *Three-dimensional simulations of ground motions in the San Bernardino Valley, California, for hypothetical earthquakes on the San Andreas fault*, Bull. Seism. Soc. Am.; 83, 1024-1041
Frankel A. and J. E. Vidale, 1992. *A three-dimensional simulation of seismic waves in the Santa Clara Valley, California from a Loma Prieta aftershock.* Bull. Seism. Soc. Am.; 82, 2045-2074
Franklin A.G., Chang F.K., 1977. *Permanent displacements of earth embankments by Newmark sliding block analysis*. Report 5, Miscellaneous paper S-71-17, US Army Corps of Engineers, Waterways Experiment Station, Vicksburg, Mississippi
František Gallovič and Johana Brokešová, 2004. *On strong ground motion synthesis with k^{-2} slip distributions.* Submitted to Journal of Seismology Vol 8, p.211-224
Freeze R. S., 1971. *Three dimensional transient saturated- unsaturated flow in a groundwater basin.* Water Res. Res. 7 (2): 347-366
Frepoli A. and Amato A., 2000. *Spatial variation in stress in peninsular Italy and Sicily from background seismicity.* Tectonophysics, 317, 109-124
Frisenda M., Massa M., Spallarossa D., Ferretti G. and Eva C., 2005. *Attenuation relationship for low magnitude earthquakes using standard seismometric records*. J. Earthq Eng 9:23-40
Fu Q. and C. Menun, 2004. *Seismic-environment-based simulation of near-fault ground motions.* In Proc. 13th World Conference on Earthquake Engineering, Vancouver, Canada, 15 pp
Fukao Y., 1979. *Tsunami Earthquakes and Subduction Processes near Deepsea Trenches.* J. Geophys. Res. *84*, 2303 - 2314
Fukuyama E. and Irikura K., 1986. *Rupture process of the 1983 Japan Sea (akita-oki) earthquake using a waveform inversion method.* Bull. Seism. Soc. Am., 76, 1623-1640

Futterman W. I., 1962. *Dispersive body waves.* J. geophys. Res., 67, 5279-5291

Gajo A. and Wood D.M., 1999. *A kinematic hardening constitutive model for sands: the multiaxial formulation*. International Journal for Numerical and Analytical Methods in Geomechanics; 23:925-65

Gallovíc F. 2002. *High frequency strong motion synthesis for k^{-2} rupture models*. Master Thesis, Charles University, Prague, http://geo.mff.cuni.cz/students/gallovic.

Gallovič F. and J. Brokešová, 2004. *The k^{-2} rupture model parametric* study: example of the 1999 Athens earthquake. Studia geoph. et geod. 48, 589-613

Gallovič F. and J. Burjánek, 2007. *High-frequency directivity in strong ground motion modeling methods*. Ann. Geophys. 50, 203-211

Gallovič F. and Brokešhová J., 2004. *On strong ground motion synthesis with k^{-2} slip distributions*. J Seismol 8:211-224

Gallovič F. and J. Brokešová, 2007. *Hybrid k-squared source model for strong ground motion simulations: Introduction.* Phys. Earth Planet. In. 160, 34-50

Gars G., 1983. *Etudes seismotectoniques en Mediterranée centrale et orientale: I. La neotectonique de l'Appenin meridianal et le seisme (23 Nov 80) de l'Irpinia (ltalie). Il. Les failles activées parles seismes (Fev.-Mars 81) de Corinthe (Grèce).* Thesis, Université de Paris Sud, Centre d'Orsay (in French)

Gasparini C., Iannacone G., Scandone P. and Scarpa R., 1982. *Seismotectonics of the Calabrian arc.* Tectonophys., 84, 267-286

Gasparini C., Iannacone G. and Scarpa R., 1985. *Fault piane solutions and seismicity of the ltalian peninsula.* Tectonophys., 117, 59-78

Gasparre A., 2005. *Advanced Laboratory Characterisation of London Clay.* PhD Thesis, Imperial College London

Gasparre A., Nishimura S., Coop M. R. and Jardine R. J., 2007b. *The influence of structure on the behaviour of London clay*. Géotechnique; 57(1), 19-31

Gasparre A., Nishimura S., Minh N. A., Coop M. R. and Jardine R. J., 2007a. *The stiffness of natural London clay*. Géotechnique; 57(1), 33-7

Gazetas G., 1982. *Shear vibration of vertically inhomogeneous earth dams.* Int J Numer Anal Methods Geomech 1982;6:219-41

Gazetas G., 1987. *Seismic response of earth dams: some recent developments*. Soil Dyn Earthquake Eng ; 6(1):3-47

Gazetas G., Dakoulas P., 1992. *Seismic analysis and design ofrockfill dams: state-ofthe-art.* Soll Dyn Earthquake Eng;11: 27-61

Gazetas G., Garini E., Berrill J.B. and Apostolou M., 2012. *Sliding and overturning potential of Christchurch 2011 earthquake records.* Earthquake Eng Struct Dyn; 41 (14):1921-44

Gens A., 1982. *Stress-strain and strength of a low plasticity clay*. Ph.D. Thesis Imperial College, London

Gens A., Sánchez M. and Sheng D., 2006. *On constitutive modeling of unsaturated soils.* Acta Geotechnica, 1, 137-147

Georgiannou V. N., Rampello S. and Silvestri F., 1991. *Static and dynamic measurements of undrained stiffness on natural overconsolidated clays. in Proceedings 10th European Conference on Soil Mechanics and Foundation.* Engineering, Firenze, Voi. I, pp. 91-95

Ghisetti F. and Vezzani L., 1982. *Different styles of deformation in the Calabrian are (Southern Italy): implications for a seismotectonic zoning.* Tectonophys., 85, 149-165

Ghisetti F., Scarpa R. and Vezzani L., 1982. *Seismic activity, deep structures and deformation processes in the Calabrian are, southern Italy.* Earth Evolution Sci., 3, 248-260

Giardini D., 1992. *The November 23, 1980 Irpinia earthquake: teieseismic observations.* In: E. Boschi (Editor), Proc. Workshop Irpinia 10 anni dopo (Napoli, Italy, Nov. 1990), Editrice Compositori, Bologna (in press).

Giardini D., 1993. *Teleseismic observation of the November 23 1980, Irpinia earthquake.* Ann. Geophys. 36, 17-25

Giardini D., Dziewonski A.M., Woodhouse J.H. and Boschi E., 1984. *Systematic analysis of the seismicity of the Mediterranean region using the entroid-moment tensor method.* In: A. Brambati and 13. Siejko (Editors), The Osservatorio Geofisico Sperimentaie Silver Anniversary Volume, O.G.S., Trieste, pp. 121-142

Gibert D. and Virieux J., 1991. *Electromagnctic imaging and simulated annealing.* J. geophys. Res., 96, 8057-8067

Goltz J.D., 2003. *Applications for new real-time seismic information: the TriNet project in southern California.* Seismol Res Lett 74:516-521

Gomberg J.S., Shedlock K.M. and Roecke S.W., 1990. *The effect of S-wave arrival times on the accuracy of hypocenter estimation.* Bull. Seism. Soc. Am., 80, 1605-1628

Gorler K. and Giese P., 1978. *Aspects of the Evolution of the Calabrian are, in Alps, Apennines, Hellenides: Geodynamic lnvestigations along Geotraverses by an international group of geoscientists, lnter-Union Commission of Geodynamics Scientific Rep. 38.* pp. 374-388, eds Closs, H., Roeder, D. and Schmidt, K., E. Schweizerbartische Verlagsbuchhandlung, Stuttgart, West Germany

Graves R. W. and A. Pitarka, 2010. *Broadband ground-motion simulation uUsing a hybrid approach.* Bull. Seismol. Soc. Am. 100,2095-2123

Graves R. W., 1993. *Modeling three-dimensional site response effects in the Marina District Basin, San Francisco, California.* Bull. Seism. Soc. Am.; 83, 1042-1063

Graves R. and Wald D., 2001. *Resolution Analysis of Finite Fault Source Inversion Using One- and Three-dimensional Green's Functions, 1. Strong Motions.* Journal of Geophysical Research, Vol. 106, 8745-8766

Graves R.W. and Pitarka A., 2010. *Broadband Ground-Motion Simulation Using a Hybrid Approach*. Bull. Seismol. Soc. Am., Vol. 99, No. 5A, pp. 2095-2123

Graves R.W., 1996. *Simulating seismic wave propagation in 3D elastic media using staggered-grid finite differences*. Bull. Seismol. Soc. Am. 86 (4), 1091-1106

Green A.E. and Mclnnis B.C., 1967. *Generalized hypoelasticity*. Proc. Roy. Soc. Edinburgh A 57 220-230

Green A.E. and. Naghdi P.M, 1965. *A general theory of an elastic-plastic continuum*. Arch. Rational Mech. Anal. 18 251-281. CrossRef

Green A.E., 1956. *Hypo-elasticity and plasticity*. Proc. Ray. Soc. London A234 46-59

Green A.E., 1956. *Hypo-elasticity and plasticity II*. Arch. Rational Mech. Anal. S 725-734

Green A.E., 1956. *Simple extension of hypoelastic body of grade zero*. J. Rational Mech. Anal. 5 637-642
Greenfield R.J., 1995. *Comments on An efficient method for computing Green's functions for a layered half- space with sources and receivers at close depths by Y. Hisada.* Bull. Seism. Soc. Am., *85*, 1523-1524
Griffiths D.V. and Prevost JH, 1988. *Two- and three dimensionai dynamic finite element analyses ofthe long valley dam.* Géotechnique; 38:367-88
Gruppo di lavoro MPS, 2004. *Redazione della mappa di pericolosità sismica prevista dall'Ordinanza PCM 3274 del 20 marzo 2003.* Rapporto conclusivo per il Dipartimento della Protezione Civile, INGV, Milano - Roma, 65 pp. + 5 appendici
Guan G. S., Rahardjo H. and Choon L. E., 2010. *Shear strength equations for unsaturated soil under drying and wetting.* Journal of Geotechnical and Geoenvironmental Engineering, ASCE, 136(4), 594-606
Guatteri M., P.M. Mai and G.C. Beroza, 2004. *A Pseudo-Dynamic Approximation to Dynamic rupture Models for Strong Ground Motion Prediction.* Bull. Seis.. Soc. Am., Vol. 94, 2051-2063
Guatteri M., P.M. Mai, G.C. Beroza and J. Boatwright, 2003. *Strong ground-motion prediction from stochastic-dynamic source models.* Bull. Seis. Soc. Am, 93, 301-313
Gubbins D., 1990. *Seismology and Plate Tectonics,* Cambridge University Press, Cambridge, England, 339 pp
Gudehus G., 1995. *Attractors for granular sorage and flow*. In 3rd European Symposium - Storage and Flow of Particulate Solids, Paper for the conf. 'Partec 95', pages 333-345
Gudehus G., 1996. *A comprehensive constitutive equation for granular materials*. Soils and Foundations, 36(1):1-12
Gudehus G., 2004. *A visco-hypoplastic constitutive relation for soft soils*. Soils and Foundations, 44(4):11-25
Guidotti R., 2012. Near-field earthquake ground motion rotations and relevance on civil engineering structures. Ph.D, Thesis
Gulkan P., Yucemen S.M., Kocyigit A., Doyuran V. and Basoz N., 1993. *Seismic zoning map of Turkey based on the latest data.* Middle East Technical University, Department of Civil Engineering (in Turkish)
Gutenberg B., 1945. *Amplitudes of surface waves and magnitudes of shallow earthquakes.* Bull. Seism. Soc. Am. 34, 2-12
Gutenberg B. and C. F. Richter, 1954. *Seismicity of the Earth and Associated Phenomena , Second Ed., Princeton University Press, Princeton, New Jersey, 310 pp. Hanks, T. C. and H. Kanamori (1979). A moment-magnitude scale.* J. Geophys. Res. 84, 2348-2350
Hachiguchi K. and Ueno M., 1977. *Elastoplastic constitutive laws of granular materials, Proceedings, Constitutive Equations of Soils*. Ninth International Conference of Soil Mechanics and Foundation Engineering; Sp. Session 9:73-82
Hagiwara T., 1958. *A note on the theory of the electromagnetic seismograph.* Earthquake Res. Inst. Bull.Tokyo University, 36, 139-164
Hájek V., Mašín D. and Boháč J., 2009. *Capability of constitutive models to simulate soils with different OCR using a single set of parameters*. Computers and Geotechnics; 36, 655-664
Hall J. F., T. H. Heaton, M. W. Halling and D. J. Wald, 1995. *Near-source ground motion and its effects on flexible buildings*. Earthquake Spectra 11, no. 4, 569-605
Hancock J. and Bommer J.J., 2006. *A state-of-knowledge review of the influence of strong-motion duration on structural damage.* Earthquake Spectra; 22(3):827-845
Hanks T. C., and H. Kanamori, 1979. *A moment magnitude scale*. J. Geophys. Res., 84, 2348-2350
Hanks T. C., 1982. *Fmax*. Bull. Seism. Soc. Am. 72, 1867-1879
Hanks T. C., and M. Wyss, 1972. *The use of body-wave spectra in the determination of seismic-source parameters.* Bull. Seism. Soc. Am. 62, 561-589
Hanks T. C., J. A. Hileman and W. Thatcher, 1975. *Seismic moments of the larger earthquakes of the southern California region.* Geol. Soc. Am. Bull. 86, 1131-1139
Harder L-F, Bray J.D., Volpe R.L. and Rodda K., 1998. *Performance of earth dams during the Loma Prieta Earthquake.* USGS Professional: 1552 (D)
Hardin B. O., 1978. *The nature of stress-strain behavior for soils*. Proc., ASCE Spec. Conf. on Earthquake Engrg. and Soil Dyn., Stateof- the-art Rep., ASCE, New York; 3-90
Hardin B.O. and Drnevich V.P., 1972. *Shear modulus and damping in soils: design equations and curves*. J Soil Mech Found Division, ASCE; 98(SM7):667-92
Hardin B. O. and Black W., 1968. *Vibration modulus ofnormally consolidated clay*. Journal of the Soil Mechanics and Foundations Division (ASCE). Vol. 94, No. SM2, pp. 353 to 369
Harry Martindale and Dipanjan Bas, 2011. *Constitutive model for rate dependent behavior of clay.* Internal Geotechnical Report 2011-3
Hartzell S., 1978. *Earthquake aftershocks as Green's functions.* Geophys. Res. Lett., 5, 1-4
Hartzell S., 1989. *Comparison of seismic waveform inversion results for a rupture history of a finite fault: application to the 1986 North Palm Springs, California, earthquake.* J. geophys. Res., 94, 7515-7534
Hartzell S. and Heaton T., 1983. *Inversion of strong ground motion and teleseismic waveform data for the fault rupture history of the 1979 Imperial Valley California.* Bull Seism Soc Am; 73(6):1553-83
Hashiguchi K., 1985. *Two and three surface models of plasticity.* Proc.5th Int. Conf Numerical Methods in Geomechanics, Nagoya, 125-134
Hashiguchi K., 1981. *Constitutive equations of elastoplastic materials with anisotropie bardening and elastic-plastic transition.* J. Appl. Mech.,ASME, Vol 48, 297-301
Haskell N.A., 1964. *Total energy and energy spectral density of elastic wave radiation from propagating faults.* Bull Seismol Soc Am; 54(6A):1811-41
Hatzfeld D. et al., 1993. *Subcrustal microearthquake seismicity and fault piane solutions beneath the Helenic are.* J. geophys. Res., 98, 9861-9870
Hau K.W., 2003. *Application of a Three surface kinematic Hardening Model to the Repeated Loading of Thinly Surfaced Pavements.* PhD Thesis, University of Nottingham, UK

Hawkins F.F., R. LaForge and R.A. Hansen, 1986. S*eismotectonic study of the Truckee / Lake Tahoe area, northeastern Sierra Nevada, California for Stampede, Prosser Creek, Boca, and Lake Tahoe dams*. Seismotectonic Rept. No. 85-4, U.S. Bureau of Reclamation, Denver, Colorado, 1-210

Hearn T.M. and Ni J.F., 1994. *Pn velocities beneath continental collision zones.* Geophys. J. Int., 117, 273-283

Heaton T, 1990. *Evidence for and Implications of Self healing Pulses of Slip in Earthquake Rupture.* Phys. Earth and Planet. Int. 8, 25 - 83

Helmberger D. and Wiggins, R., 1971. *Upper mantle structure of the mid-western United States.* J. geophys. Res., 76, 3229-3245

Helmberger D. V., 1983. *Theory and application of synthetic seismograms, in Earthquakes: Observation, Theory and lnterpretation,* LXXXV Corso, pp. 174-222, eds Kanamori, H. and Boschi, E., Soc. Italiana di Fisica, Bologna

Henkel D.J., 1960. *The shear strength of saturated remoulded clays*. Proc. ASCE Research Conference on Shear Strength of Cohesive Soils Boulder: 533-554

Herle I., 1997. *Hypoplastizität und granulometrie of einfacher korngerüste*. PhD thesis, Universit¨at Fridericiana in Karlsruhe

Herle I. and D. Kolymbas, 2004. *Hypoplasticity for soils with low friction angles*. Computers and Geotechnics, 31(5):365-373

Hernandez B., Cocco M., Cotton F., Stramondo S., Scotti O., Courboulex,F. and Campillo, M., 2004. *Rupture history of the 1997 Umbria-Marche (Central Italy) main shocks from the inversion of GPS, DInSAR and near field strong motion data*. Annals of Geophysics, Vol. 47, pp. 1355-1376

Herrera I. and J. Bielak, 1977. *Soil structure interaction as a diffraction problem.* Proc. VI World Conf. Earthq. Eng., New Delhi, 19-24

Herrero A. and P. Bernard, 1994. *A kinematic self-similar rupture process for earthquakes*. Bull. Seismol. Soc. Am. 84, 1216-1228

Herrero A., 1994. *Paramétrisation spatio temporelle et spectrale dessources sismiques: application au risque sismique.* Thèse de doctorat, University of Paris 6, France

Herrero A. and Bernard P., 1994. *A kinematic self-similar rupture process for earthquakes*. Bull Seismol Soc Am 84:1216-1228

Herrero A., Zollo A. and Virieux J., 1999. *2D Non linear first arrival time inversion applied to Mt. Vesuvius active seismic data (TomoVes96).* Eur. Geophys. Soc.,, XXIV, General Assembly, 19-23 April, 1999, The Hague, The Netherlands

Herrin E., 1968. *1968 seismological tables for P phases.* Buil. seism. Soc. Am., 58, 1193-1241

Hight D.W., McMillan F., Powell J. J. M., Jardine R.J. and Allenou C.P., 2003. *Some characteristics of London clay*.Characterization of Engineering Properties of Natural Soils, Balkema; 851-908

Hill R, 1950. *The Mathematical Theory of Plasticity*. Clarendon Press, Oxford

Hinchberger S. D. and Rowe K. R. 1998. *Evaluation of the predictive ability of two elasticviscoplastic constitutive models*. Canada Geotechnical Journal; 35, 769- 789

Hisada Y and Bielak J, 2003. *A Theoretical Method for Computing Near-Fault Strong Motions in Layered Half-Space Considering Static Offset due to Surface Faulting, with a Physical Interpretation of Fling Step and Rupture Directivity*. Bull. Seism. Soc. Am., *93*, 1154-1168

Hisada Y., 1993. *An efficient method for computing Green's functions for a layered half-space with sources and receivers at close depths.* Bull. Seism. Soc. Am., *84*, 1456 -1472

Hisada Y., 1995. *An efficient method for computing Green's function for a layered half-space with sources and receivers at close depths (Part 2).* Bull. Seism. Soc. Am. 85, 1080-1093

Hisada Y., 2000. *A Theoretical Omega-Square Model Considering the Spatial Variation in Slip and Rupture Velocity.* Bull. Seism. Soc. Am. 90, 387-400

Hisada Y., H. Bao, J. Bielak, O. Gattas and D. R. O'Hallaron, 1998. *Simulation of long-period ground motions during the 1995 Hyogo- ken-Nanbu (Kobe) earthquake using 3-D finite element method, in Proc*. 2nd International Symposium on the Effect of Surface Geology on Seismic Motion, 1-3 December 1998, Yokohama, Japan, 1353-1360

Hisada Y., K. Aki and T. L. Teng, 1993. *3-D simulations of surface wave propagation in the Kanto sedimentary basin, Japan. Part 2: Application of the surface wave BEM.* Bull. Seism. Soc. Am. 83, 1700-1720.

Hoger A., 1987. *The stress conjugate to the logarithmic strain*. Internat. J. Solids Structures 23 1645-1656. CrossRef

Honda R. and Yomogida K., 2003. *Effects of a soft surface layer on near-fault static and dynamic displacements.* Geophys. J. Intern., *154*, 441-462

Hongjun SI and Saburoh MIDORIKAWA, 2004. *Evaluation of rupture directivity effects on strong ground motion based on hybrid simulation method.* 13th World Conference on Earthquake Engineering Vancouver, B.C., Canada , Paper No. 455

Horton S.P., D.M. dePolo and W.R. Walter, 1997. *Source parameters and tectonic setting of the 1990 Lee Vining, California, earthquake sequence*. Bull. Seism. Soc. Am. 87, 1035-1045

Hough S., Seeber L., Lerner-Lam A., Armbruster J. and Guo, H., 1991. *Empirical Green's functions analysis of Loma Prieta aftershoc*ks. Bull. Seism. Soc. Am., 81, 1737-1753

Houlsby G.T., 1999. *A model for the variable stiffness of undrained clay*. Proc.lnt. Symp. on Prefailure Deformation of Soils, Torino, Vol 1, 443-450

Houlsby G.T. and Mortara G., 2004. *A Continuous Hyperplasticity Model for Sands under Cyclic Loading*. In: Proceedings of the International Conference on Cyclic Behaviour of Soils and Liquefaction Phenomena, Bochum, Germany, 31 March-2 April; 21-26, Balkema

Howard J. K., C. A. Tracy and R. G. Burns, 2005. *Comparing observed and predicted directivity in Near-Source ground motion.* Earthquake Spectra 21, no. 4, 1063-1092

Hromadka T. V. and Guymon G. L., 1980. *Some effects of lin- earizing the unsaturated soil moisture transfer diffusivity model*. Water Res. Res. 16 (4), 643-650

Huang M., Romeo F. and Sangiovanni-Vincentelli A., 1986. *An efficient general cooling schedule for simulated annealing*. Proc. IEEE Int. Conf. Computer-Aided Design, Santa Clara, 381-384
Hueckel T. and Nova R., 1979. *Some hysteresis effects of the behaviour of geological media*. Int. J. Solids and Struct.; 15, 625-642
Hujeux J.C., 1985. *Une loi de comportement pour le chargem.ent cyclique des sols*. In: Davidovici V, editor. Genie parasismique. Presses ENCP. p. 287-302
Hutchinson J.W. and Neale K.W., 1980. *Finite deformation J 2 defonnation theory*. In: O.E. Carlson and R.T. Shield (eds), Finite Elasticity. Martinus Nijhoff Publishers. The Hague pp.137-147
Hutchinson J.W. and Neale K.W., Sheet necking-II, 1978. *Time-independent behavior*. In: D.P. Koistinen and N.M. Wang (eds.), Mechanics of Sheet Metal Forming. Plenum, New York pp. 127-153
Hwang J-H., Wu C-P. and Wang S-C., 2007. *Seismic record analysis of the Liyutan earth dam*. Can Geotech J; 44:1351-77
Hynes-Griffin M.E. and Franklin A.G., 1984. *Rationalizing the seismic coefficient method*. Miscellaneous Paper GL-84-13, U.S. Army Corps of Engineers Waterways Experiment Station, Vicksburg, Mississippi:21 (pp)
Iai S., Matsunaga Y. and Kameoka T., 1992. *Strain space plasticity model for cyclic mobility*. Soils and Foundations; 32(2):1-15
Iannaccone G., Improta L., Biella G., Castellano M., Deschamps A., De Franco R., Malagnini L., Mirabile L., Romeo R. and Zollo A., 1995. *A study of local effects in the Benevento town (Southern Italy) by the analysis of seismic records of explosion*. Ann. Geofis. 38 (4), 411-427
Iannaccone G., Improta L., Capuano P., Zollo A., Biella G., De Franco R., Deschamps A., Cocco M., Mirabile L. and Romeo R., 1998. *A P-wave velocity model of the upper crust of Sannio region (Southern Apennines), Italy. Ann.* Geofis. 41 (4), 567-582
Ibsen L.B., 1999. *The mechanism controlling static liquefaction and cyclic strength of sand*. Workshop on the physics and mechanics of soil liquefaction. A.A.Balkema
Ibsen L.B. and Lade P.V., 2002. *The role of the characteristic line in static soil behavior*. 4” Workshop on localisation and bifurcation theory for soils and rocks. A.A.Balkema
Ibsen L.B. and Praastrup U., 2002. *The danish rigid boundary true triaxial apparatus for soil testing*. Geotechnical testing journal; 25(3):1-12
Ichinose G., J.G. Anderson, K.D. Smith and Y. Zeng, 2003. *Source parameters of eastern California and western Nevada earthquakes from regional moment tensor inversion*. Bull Seism. Soc. Am, 93, 61-84
Ichinose G., J.G. Anderson, K.D. Smith, D. DiPolo, R. Schweickert and M. Lahren, 1999. *The seismotectonics of the 30 October 1998 Incline Village, Nevada earthquake and its effects*. Seismological Research Letters 70, 297-305
Ichinose G., K.D. Smith and J.G. Anderson, 1997. *Source parameters of the 15 November Border Town, Nevada, earthquake sequence.* Bull Seism. Soc. Am, 87, 652-667
Ichinose G., P.G. Somerville and H.K. Thio, 2005. *Rupture process of the 1948 Fukui earthquake (M 7.1) from the joint inversion of seismic waveform and geodetic data*. J. Geophys. Res. 110, B05301, doi: 10.1029/2004JB003437
Icold, 1980. *Deterioration of dams and reservoirs. Examples and their analysis*. ICOLD, Paris. Balkema, Rotterdam
Icold, 2001. *Design features of dams to resist seismic ground motion.* Bulletin 120
Icold, 2010. *Selecting seismic parameters for large dams: guideline*s. Bulletin; 72
Icold, 2012. *Dam safety and Earthquakes*. Position paper of International Commission on Large Dams, chaired by Dr. Martin Wieland
Idriss I.M., 1985. *Evaluating seismic risk in engineering practice*. In: Proceedings, 11th international conference on soil mechanics and D342D341foundation engineering, San Francisco, vol. 1; p. 255-320
Idriss I.M. and Sun J.I., 1992. S*HAKE91- a computer program for conducting equivalent linear seismic response analysis of horizontally layered soil deposits*. User's Guide. Center for Geotechnical Modeling, Civil Engineering Department, U.C. Davis
Iervolino I. and Cornell C.A., 2005. *Record Selection for nonlinear seismic analysis of structures*. Earthquake Spectra, 21(3), 685-713
Iervolino I. and Cornell C.A., 2008. *Probability of occurrence of velocity pulses in near-source ground motions.* Bulletin of the Seismological Society of America; 98(5):2262-2277
Iervolino I., Giorgio M., Galasso C. and Manfredi G., 2008. *Prediction relationships for a vector valued ground motion intensity measure accounting for cumulative damage potential.* 14th World Conference on Earthquake Engineering, Beijing, China, October 12-17
Iervolino I., Galasso C., Manfredi G. and Giorgio M., 2009. *Analisi di pericolosità sismica vettoriale per parametri di picco e integrali del moto sismico*. ANIDIS, Bologna.
Iervolino I., Manfredi G. and Cosenza E., 2006. *Ground-motion Duration Effects on Non-Linear Structural Response*. Earthquake Engineering and Structural Dynamics 35, 21-38
Iida K., 1959. *Earthquake energy and earthquake fault, Nagoya University.* J. Earth Sci. 7, 98-107
Imam S.M.R., Morgenstern N.R., Robertson P.K. and Chan D.H., 2005. *A critical-state constitutive model for liquefiable sand*. Canadian Geotechnical Journal; 42(3):830-855
Improta L., 1998. *Studio degli effetti delle eterogeneità geologiche a scala crostale e locale sulla propagazione della radiazione sismica: applicazioni alla regione del Sannio.* Tesi di Dottorato di Ricerca in Geofisica e Vulcanologia, Università degli Studi di Napoli «Federico II», Napoli
Improta L., Bonagura, M., Capuano, P. and Iannaccone, G., 2003. *An integrated geophysical investigation of the upper crust in the epicentral area of the 1980, Ms = 6.9, Irpinia earthquake (Southern Italy).* Tectonophysics,361, 139-169
Improta L., Iannaccone G., Capuano P., Zollo A. and Scandone P., 2000. *Inferences on the upper crustal structure of Southern Apennines (Italy) from seismic refraction investigations and subsurface data*. Tectonophysics, 317, 273-297

Improta L., M. Bonagura, P. Capuano and G. Iannaccone, 2003. *An integrated geophysical investigation of the upper crust in the epicentral area of the 1980, Ms = 6:9, Irpinia earthquake (Southern Italy).* Tectonophysics 361, no. 1-2, 139-169

Improta L., Zollo A., Frattini M.R., Virieux J., Herrero A. and Dell'Aversana P., 2000. *Mapping interfaces in an overthrust region by non-linear traveltime inversion of reflection data.* Am. geophys. Un.,Fall Meeting, 15-19 December 2000, San Francisco, USA

Improta L., Zollo A., Herrero A., Frattini R., Virieux J. and Dell'Aversana P., 2002. *Seismic imaging of complex structures by non-linear traveltime inversion of dense wide-angle data: application to a thrust belt.* Geophys. J. Int. 151, 264-278

Ingber L., 1993. *Simulated annealing: Practice versus theory, Math*. Comput. Model., 18, 29-57

Ippolito F., Ortolani F. and di Nocera S., 1974. *Alcune Considerazioni sulla struttura profonda dell'Appenino Irpino: reinterpretazione di ricerche di idrocarburi.* Boll. Soc. geol. It., 93, 861-881 (in Italian)

Ippolito, F., d'Argenio, B., Pescatore, T. and Scandone P., 1975. *Structural-stratigraphic units and the tectonic framework of the Southern Apennines.* In Geology of Italy, pp. 317-328, ed. Squyres, C. H., The Earth Sciences Society of the Libyan Arab Republic, Tripoli, Libya

Irikura K., 1986. *Prediction of strong acceleration motions using Green's function*. Proc. 7th Japan Earthquake Engineering Symp. 151-156

Irikura K. and Kamae K., 1994. *Estimation of strong motion in broad-frequency band based on a seismic source scaling models and an empirical Green's function technique*. ANNALI DI GEOFISICA, XXXVII, 1994; 6: 1721-1743

Irikura K. and Kamae K., 1999. *Strong ground motions during the 1948 Fukui earthquake -Estimation fo broad-band ground motion using a hybrid simulation technique*. Zisin 1999; 52(1): 129-150 (in Japanese, with English abstract)

Irwin G., 1957. *Analysis of stresses and strains near the end of a crack traversing a plate*. Journal of Applied Mechanics 24, 361–364

Ishibashi I. and Zhang X., 1993. *Unified dynamic shear moduli and damping ratios of sand and clay*. Soils and Foundations; 33(1):182-91

Ishihara K. and Okada S., 1982. *Effects of large preshearing on cyclic behaviour ofsand*. Soils Found (22):109-25

Ishihara K., Tatsuoka F. and Yasuda S., 1975. *Undrained deformation and liquefaction of sand under cyclic stresses*. Soils and Found., Tokyo; 15(1), 29-44

Italian Explosion Seismology Group, 1982. *Crustal structure in the Southern Apennines region from DSS data reporter S. Scarascia*. Proc. EGS-EGC Meeting, Leeds

Itasca Consulting Group Inc., 2005. *FLAC - Fast Lagrangian Analysis of Continua*. Version 5.0, User's Manual

Itasca Consulting Group, Inc. 2012a. *FLAC3D - Fast Lagrangian Analysis of Continua in Three-Dimensions, Ver. 5.0, User's Guide Manual.* Minneapolis: Itasca

Itasca Consulting Group, Inc. 2012b. *FLAC3D - Fast Lagrangian Analysis of Continua in Three-Dimensions, Ver. 5.0, Dynamic Analysis Manual*. Minneapolis: Itasca

Ivanson S., 1983. *Remark on an earlier proposed tomographi calgorithm.* Geophys. J.R. Astron. Sot., 75: 855-860

Iwan W. D., 1997. *Drift spectrum: measure of demand for earthquake ground motions.* J. Struct. Eng. 123, no. 4, 397-404

Iwan W.D., 1967. *On a class of models for the yielding behaviour of continuous and composite systems*. J. Appl. Mech., Vol 34, 612-617

Iwan W.D. Corrected Accelerogram, 1992 Landers earthquake, COSMOS Virtual Data Center (http://db.cosmos-eq.org/).

Jackson J., Gagnepain J., Housman G., King G., Papadimitriou P., Soufleris C. and Virieux, J., 1982a. *Seismicity, normal faulting and the geomorphological development of the Gulf of Corinth (Greece): the Corinth earthquakes of February and March 1981. Earth planet. Sci. Lett., 57, 377-397*

Jackson J. and McKenzie D., 1988. *The relationship between plate motions and seismic moment tensors, and the rates of active deformation in the Mediterranean and Middle East.* Geophys. J. Int., 93, 45-73

Jackson J. A. and McKenzie D. P., 1983. *The geometrical evolution of normal fault systems.* J. struct.Geol., 5, 471-487

Jackson J. A., 1987. *Active normal faulting and continental extension.* in Continental Extensional Tectonics, pp. 3-17, eds Coward, M. P., Dewey, J. F. and Hancock, P. L., Spec. Publ. geol. Soc. Lond., Blackwell Scientific Publications, Oxford

Jackson J. A., King G. and Vita-Finzi C., 1982b. *The neotectonics of the Aegean: an alternative view.* Earth planet. Sci. Lett., 61, 303-318

Japanese National Committee on Large Dams., 1988. *Standards for Aseismic Civil Engineering Constructions. Design criteria for dams*. In: Earthquake resistant design regulations, a word list. International Association for Earth- quake Engineering; p. 579-645

Japanese Society of Civil Engineers., 2001. *Dynamic analysis and earthquake resistant design, vol. 3: dams - nuclear power plants - electrical transformers and transmission lines - aboveground storage tanks and piping*. London: Taylor and Francis; 276 p

Jean W.Y., Chang Y.W., Wen K.L. and Loh C.H., 2006. *Early estimation of seismic hazard for strong earthquakes in Taiwan*. Nat Hazards 37:39-53

Jefferies M. G., 1993. *Nor-Sand: A simple critical state model for sand*. Géotechnique, London; 43(1), 91-103

Jefferies M. G. and Been K., 1987. *Use of critical state representations of sand in the method of characteristics*. Can. Geotech. J., Ottawa; 24(3), 441-446.

Jefferies M.G., 1993. *Nor-Sand: a simple critical state model for sand*. Geotechnique; 43(1):91-103

Jeffreys H. and Bullen K. E., 1967. *Seismological Tables,* British Association for the Advancement of Science, London

Jibson R.W., 1993. *Predicting earthquake-induced landslide displacements using Newmark's sliding block analysis*. Transportation Research Record 1411, Transportation Research Board, National Research Coundl, Washington DC; p. 9-17

Jibson R.W., 2007. *Regression models for estimating coseismic landslide displacement*. Eng Geol; 91:209-18

Jin S. and Beydoun W., 2000. *2D multiscale non-linear velocity inversion.* Geophys. Prospect., 48, 163-180

Jin S. and Madariaga R., 1994. *Nonlinear velocity inversion by a two step Monte Carlo method.* Geophysics, 59, 577-590

Johnson C.E., Bittenbinder A., Bogaert B., Dietz L. and Kohler W., 1995. *Earthworm: a flexible approach to seismic network processing.* IRIS Newsl 14:1-4

Johnston A. C., 1991. *Surface rupture in stable continental regions.* EOS 72, 489

Johnston A. C., and L. R. Kanter, 1990. *Earthquakes in stable continental crust.* Scientific American 262, 68-75

Johnston D. E. and Langston C. A., 1984. *The effect of assumed source structure on earthquake source parameters: the eastern Hispaniola earthquake of 14 September 1981.* Bull. Seism. Soc. Am., 74, 2115-2134

Jommi C., 2000. *Remarks on the constitutive modelling of unsaturated soils.* Experimental evidence and theoretical approaches in unsaturated soils, Balkema, Rotterdam, 139-153

Jonathan D. Braya and Adrian Rodriguez-Marek, 2004. *Characterization of forward-directivity ground motions in the near-fault region.* Soil Dynamics and Earthquake Engineering 24 815-828

Joyner W. B. and Boore D. M., 1981. *Peak horizontal acceleration and velocity from strong-motion records including records from the Imperial Valley, California, earthquake.* Bull. Seism. Soc. Am., 71, 2011-2038

Joyner W. B. and D. M. Boore, 1981. *Peak horizontal acceleration and velocity from strong-motion records including records from the 1979 Imperial Valley, California, earthquake.* Bull. Seismol. Soc. Am. 71, 2011-2038

Joyner W.B. and Fumal T.E., 1985. *Predictive mapping of earthquake ground motion. In: Ziony JE (ed) Evaluating earthquake hazard in the Los Angeles region-an earth-science perspective*. U.S. Geological Survey professional paper 1360, pp 203-220

Julian B. R., 1983. *Evidence for dyke intrusion earthquake mechanisms near Long Valley caldera, California*, *Nature,* 303, 323-325

Jung B. C. and Biscontin G., 2006. *Modeling of strain rate effects on clay in simple shear*. Proceedings of GeoCongress; 1-6

K.W. Neale, 1981. *Phenomenological constitutive laws in finite plasticity*. Solid Mech. Arch. 6 79-128

Kagawa T., K. Irikura and P.G. Somerville, 2004. *Differences in ground motion and fault rupture process between the surface and buried rupture earthquakes*. Earth Planets Space, 56, 3-14

Kaliakin V. N. and Dafalias Y. F., 1990a. *Theoretical aspects of the elastoplastic- viscoplastic bounding surface model for cohesive soils.* Soils and Foundations; 30(3), 11-24

Kaliakin V. N. and Dafalias Y. F., 1990b. *Verification of the elastoplastic-viscoplastic bounding surface model for cohesive soils.* Soils and Foundations; 30(3), 25-36

Kamae K., Irikura K. and Fukuchi Y., 1991. P*rediction of strong ground motion based on scaling law of earthquake*. Journal of Struct. Construct. Eng.; 430: 1-9 (in Japanese, with English abstract)

Kanamori H. and Anderson D. L., 1975. *Theoretical basis of some empirical relations in seismology.* Bull. Seismol. Soc. Am. 65, 1073 - 1095

Kanamori H. and G. S. Stewart, 1978. *Seismological aspects of the Guatemala earthquake of february 4, 1976.* J. Geophys. Res., 83,3427-3434

Kanamori H. and J. W. Given, 1982. *Use of long period surface waves for rapid determination of earthquake source parameters, 2.* Preliminary determination of source mechanisms of large earthquakes (M_w 6.5) in 1980, *Phys. Earth Planet. Inter.,* 30260-268

Kanamori H., 1983. *Magnitude scale and quantification of earthquakes.* Tectonophysics 93, 185-199

Kanamori H., Thio H., Dreger D., Hauksson E. and Heaton, T., 1992. *Initial investigation of the Landers California earthquake of the 28 June 1992 using TER Rascope.* Genphys. Res. Lett. 19, 2267 2270

Kanamori H. and Anderson D.L., 1975. *Theorical basis of some empiricalrelations in scismology.* Bull. Seism. Soc. Am., 65, 1073 1095

Kanasewich E. R., 1981. *Time Series Analysis in Geophysics,* 3rd edn, pp. 274-277. University of Alberta Press, Edmonton, Canada

Kasahara K. *Earthquake Mechanics* (Cambridge University Press, Cambridge 1981) 248 pp

Katona M.G., Zienkiewicz O.C., 1985. *A unified set of single step algorithms Part 3: the Betam method, a generalisation of the Newmark scheme*. Int. J. Num. Meth. Engng., 21, pp. 1345-1359

Kausel E., R. V. Whitman, J. P. Morray, and F. Elsabee, 1978. *The spring method for embedded foundations.* Nucl. Eng. Des.; 48, 377-392

Kavazanjian E., and Mitchell J. K., 1980. *Time-dependent deformation behavior of clays*. *J*ournal of Geotechnical and Geoenvironmental Engineering, ASCE; 106(6), 611-630

Kavvadas M., Amorosi A., 2000. *A constitutive model for structured soils.* Géotechnique, 50, n. 3, pp. 263-273

Kawase H., 1996. *The cause of the damage belt in Kobe: "the basin-edge effect", constructive interference of the direct S-wave with the basin- induced diffracted/Rayleigh wave.* Seism. Res. Lett.; 67, 25-34

Kawase H., and K. Aki, 1990. *Topography effect at the critical SV-wave incidence: Possible explanation of damage pattern by the Whittier Narrows, California, earthquake of 1 October 1987.* Bull. Seism. Soc. Am.; 80, 1-22

Key S. C. and Crosson R. S., 1984. *Ground deformation modelling of the southern Italy earthquake of November 23, 1980 (abstr.), Eos, Trans. Am.* Geophys. Un., 65, 1015

Khan A.S. and Huang S.J., 1995. *Continuum Theory of Plasticity*. Wiley, New York

Khong C.D. and Yu H.S., 2002. *Computational aspects of a unified critical state model for clay and sand*. Proc. 8th NUMOG, Rome, 271-277

Khong C.D., 2004. *Development and Numerical Evaluation of Unified Critical State Models*. PhD Thesis,University of Nottingham, UK

Khromovskikh V. S., 1989. *Determination of magnitudes of ancient earthquakes from dimensions of observed seismodislocations*. Tectonophysics 166, 269-280

Kim M-K, Lee S-H, Choo Y-W and Kim D-S., 2011. *Seismic behavior of earth-core and concrete faced rock-fill dams by dynamic centrifuge tests*. Soil Dyn Earthquake Eng; 31:1579-93

Kim T. C. and Novale M., 1981. *Dynamic properties of some cohesive soils of Ontario.* Canadian Geotechnical Journal. Voi. 18, No. 3, pp. 371-389. Konder, R. L. (1963). Hyperbolic stress-strain respoose: cohesive soils. Journal of the Soil Mechanics and Foundations Division (ASCE). Voi. 89, No. SMl, pp. 115-143

King, G.C.P., 1986. S*peculations on the geometry of the initiation and termination of earthquake rupture and its relation to mohoio and geological structure*. Pure Appl. Geophys., 124: 567-585

Kirkpalrick S., Gellat J. and Vecchi. M ., 1983. *Optimization by simulated annealing.* Science, 220, 67 1 680

Kissling E., 1988. *Geotomography with local earthquake data.* Rev. Geophys., 26, 659-698

Kissling E., 1995. *Velest User's Guide. Internal Report, 26 pp.* Institute of Geophysics, ETH Zurich

Kissling E., Ellsworth W.L., Eberhart-Phillips D. and Kradolfer U., 1994. *Initial reference model in local earthquake tomography.* J. Geophys. Res., 99, 19635-19646

Knopoff L. and Randall M. J., 1970. *The compensated linear-vector dipole: a possible mechanism for deep earthquakes.* J. geophys. Res., 75, 4957-4963

Knuepfer P. L. K., 1989. *Implications of the characteristics of end points of historical surface fault ruptures for the nature of fault segmentation.* In Proc. of Conf. XLV, Fault Segmentation and Controls of Rupture Jnitiation and Termination, D. P. Schwartz and R. H. Sibson (Editors), U.S. Geo/. Surv. Open-File Rept. 89-315, 193-228

Kodaira S., Takahashi N., Nakanishi A., Miura S. and Kaneda Y., 2000. *Subducted seamount imaged in the rupture zone of the 1946 Nankaido earthquake.* Science, 289, 104-106

Kokusho T. and Esashi Y., 1981. *Cyclic triaxial test on sands and coarse materials*. In: Proceedings of 10th international conference on soil mechanics and foundation engineering, Stockholm

Kolymbas D., 1991. *An outline of hypoplasticity*. Archive of Applied Mechanics, 61:143-151

Konstantinos I. Andrianopoulos, Achilleas G. Papadimitriou and George D. Bouckovalas, 2010. *Explicit integration of bounding surface model for the analysis of earthquake soil liquefaction.* international journal for numerical and analytical methods in geomechanics Int. J. Numer. Anal. Meth. Geomech. 2010; 34:1586-1614

Konstantinos I. Andrianopoulos, Achilleas G. Papadimitriou, George D. Bouckovalas and Dimitrios K. Karamitros, 2013. *Insight into the seismic response of earth dams with an emphasis on seismic coefficient estimation.* Computers and Geotechnics 55 195-210

Konstantinos I. Andrianopoulos, Achilleas G.Papadimitriou and George D.Bouckovalas, 2010. *Bounding surface plasticity model for the seismic liquefaction analysis of geostructures.* Soil Dynamic sand Earthquake Engineering 30 895-911

Kostrov B.V., 1966. *Self-similar problems of propagation of shear cracks.* J. Appl. Math. Mech., 28: 1077-1087

Kramer S.L., 1996. *Geotechnical earthquake engineering*. New Jersey: Prentice-Hall Inc.

Kramer S.L. and Smith M.W., 1997. *Modified Newmark model for seismic displacements of compliant slopes*. J Geotech Geoenviron Eng ;123(7):635-44

Krawinkler H. and Alavi B., 998. *Development of improved design procedures for near-fault ground motions*. SMIP 98, Seminar on Utilization of Strong Motion Data: Oakland, CA

Krenk S., 1996. *Family of Invariant Stress Surfaces*. Journal of Engineering Mechanics - Proceedings of the ASCE; 122(3):201-208

Krenk S., 2000. *Characteristic state plasticity for granular materials : Part I: Basic theory*. International Journal of Solids and Structures; 37(43):6343-6360

Krieg R.D., 1975. *A practical two-suraface plasticity theory.* J. Appl. Mech.,Vol 42, 641-646

Krieg R.D. and Krieg D.B., 1977. *Accuracies of numerical solution methods for the elastic-perfectly plastic model.* Journal of Pressure Vessel Technology; 99:510-515

Kristek J., P. Moczo, K. Irikura, T. Iwata and H. Sekiguchi, 1999. *The 1995 Kobe mainshock simulated by the 3D finite differences*, in The Effects of Surface Geology on Seismic Motion, K. Irikura, et al. (Ed- itors), Vol. 3, Balkema, Rotterdam, 1361-1368

Krstelj I. and Prevost J.H., 1994. *Experimental results of Model No. 12*. In: Proceedings of the international conference on verification of numerical procedures for the analysis of soil liquefaction problems, Davis, CA, 1: p. 1007-1017

Kuhlemeyer R.L., Lysmer J., 1973. *Finite element method accuracy for wave propagation problems.* GJ Soil Mech Found ASCE;99(5):421-7

Kulhawy F. H. and Mayne, P. W., 1990. *Manual on estimating soil properties for foundation design*. Rep. No. EL-6800, Electric Power Research Institute, Palo Alto, California

Kutner M.H., C. Nachtsheim and J. Neter, 2004. *Applied Linear Regression Models.* McGraw-Hill/Irwin, Boston; New York

Kwok A.O.L., Sstewart J.P., Hashash Y.M.A., Matasovic N., Pyke R., Wang Z. and Yang Z., 2007. *Use of exact solutions of wave propagation problems to guide implementation of nonlinear seismic ground response analysis procedures*. J. Geotech. and Geoenv. Engng. ASCE, 133, 11, pp. 1385-1398

Kwon O. and A. S. Elnashai, 2006. *The effect of material and ground motion uncertainty on the seismic vulnerability curves of a RC structure.* Engineering Structures 28, 289-303

Lacy S.J. and Prevost J.H., 1987. *Constitutive model for geomaterials*. Proc. Ind lnt. Conf on Constitutive Lawsfor Eng. Materials, Elsevier, Vol 1, 149-160

Lacy S.J., 1994. *Numerical prediction for Model No. 1*. In: Proceedings of the international conference on verification of numerical procedures for the analysis of soil liquefaction problems, Davis, CA, 17-20 October, 1: p. 153-168

Ladd C. C., Foott R., Ishihara K., Schlosser F. and Poulos H. G., 1977. *Stress-deformation and strength characteristics*. Proc., 9th Int. Conf. on Soil Mech. and Found. Engrg., State-of-the-art rep., Vol. 2; 421-494

Ladd C.C. and Varallyay J., 1965. *The influence of the stress system on the behavior of saturated clays during undrained shear.*Research Report No R65-11, Department of Civil Engineering, MIT, Cambridge, MA

Lade P.V., 1977. *Elasto-plastic stress-strain theory for cohesionless soil with curved yield surfaces*. International Journal of Solids and Structures: 13:1019-1035

Lade P.V. and Ibsen L.B., 1997. *A study of the phase transformation and the characteristic lines of sand behaviour.* Deformation and progressive failure in Geomechanics. IS-NAGOYA. Pergamon Press; 353-358

Lafond C. F. and Levander A. R., 1990. *Fast and accurate dynamic raytracing in heteregoneous media.* Bull. Seism. Soc. Am. 80, 1284-1296

Lancieri M. and Zollo A., 2009. *Simulated shaking maps for the 1980 Irpinia earthquake, Ms 6.9: Insightson the observed damage distribution*. Soil Dynamic sand Earthquake Engineering 29 1208-1219

Lane P.A. and Griffiths D.V., 2000. *Assessment of stability of slopes under drawdown conditions.* Jnl. Geotech. and Geoenv. Engng. 126(5): 443-450

Langston C. and Helmberger D., 1975. *A procedure for modelling shallow dislocation sources.* Geophys. J.R. astr. Soc., 42, 117-130

Lanier J., Caillerie D., Chambonn R., Viggiani G., Bésuelle P. and Desrues J., 2004. *A general formulation of hypoplasticity*. Int. J. Numer. Anal. Meth. Geomech.,2004; 28:1461-1478 (DOI: 10.1002/nag.394)

Lanzo G., Tallini M., Milana G., Di Capua G., Del Monaco F., Pagliaroli A. and Peppoloni S., 2011. *The Aterno valley strong ground motion array: seismic characterization and determination of subsoil model*. Bull. Earthq. Eng. Accepted for publication.

Larry J. Ruff, 1999. *Dynamic Stress Drop of Recent Earthquakes: Variations within Subduction Zones.* Pure appl. geophys. 154 409-431

Latorre D., Virieux J., Monfret T., Monteiller V., Vanorio T., Got J.L. and Lyon-Caen H., 1997. *A new seismic tomography of Aigion area (Gulf of Corinth-Greece) from a 1991 dataset*. Geophys. J. Int., 159, 1013-1031

Lawrence Von Thun J., 1985. *San Luis Dam upstream slide.* Int. Conf. on Soil Mech. Found. Eng. 11, 2593- 2598

Lawson C.L. and Hanson R., 1974. *Solving Least Sqllares Problems.* Prentice-Hall, Englewood Cliffs, NJ

Le Meur H., 1994. *Tomographie 30 de la croùte dans la région de Pat ras (Grèce).*PhD thesis, University of Paris 7, France

Le Pichon X. and Angelicr J., 1987. *The Hellenic are and trench systcm: a key to the evolution of t he Eastern Mcditcrrancan area.* Tectonophysics, 60, l -42

Lee W. H. K., F. T. Wu, and S. C. Wang, 1978. *A catalog of instrumentally determined earthquakes in China (magnitude >6) compiled from various sources.* Bull. Seism. Soc. Am. 68, 383-398

Lee W.H.K. and Lahr J.C., 1975. *HYPO71 (Revised): A Computer Program for Determining Hypocenter, Magnitude and First Motion Pattern of Local Earthquakes*. U.S. Geol. Surv. Open File Rep. 75-311, 113 pp

Lee W.H.K., Shin T.C., Kuo K.W. and Chen K.C., 1999. *CWB free-field strongmotion data from the 921 Chi-Chi earthquake*. Digital acceleration files on CD-ROM, pre-publication version (December 6; 1999), vol. 1

Lees J.M. and Crosson R.S., 1989. *Tomographic inversion for three dimensional velocity structure at Mount St Helens using earthquake data.* J. Geophys. Res., 94, 5716-5728

Lermo J. and F. J. Chávez-García, 1993. *Site effect evaluation using spectral ratio with only one station*. Bull. Seismol. Soc. Am. 83, 1574-1594

Leroueil S., Kabbaj M., Tavenas F. and Bouchard R., 1985. *Stress-strain rate relation for the compressibility of sensitive natural clays. Géotechnique,* ;35(2), 159-180

Leroueil, S., Tavenas, F., Samson, L. and Morin, P. (1983). *Preconsolidation Pressure of Champlain Clays - Part II: Laboratory Determination.* Canadian Geotechnical Journal, 20(4), 803-816

Levander A.R., 1988. *Fourth-order-finite-difference P-SV seismograms.* Geophysics 53, 1425-1436

Li X.X. and Dafalias Y.F., 2004. *A constitutive framework for anisotropic sand including non-proportional loading*. Geotechnique; 54(1):41-55

Li X. S., 1990. *Free Field Soil Response under Multi-directional Earthquake Loading.*Ph.D. dissertation, University of California, Davis, 1990

Li X. S. and Dafalias Y. F., 2000. *Dilatancy for cohesionless soils.* Géotechnique, London; 50(4), 449-460

Li X. S., Dafalias Y. F. and Wang Z. L. 1999. *State-dependent dilatancy in critical-state constitutive modelling of sand*. Can. Geotech. J., Ottawa; 36(4), 599-611

Li X.S., 2002. *A sand model with state-dependent dilatancy*. Geotechnique; 52(3): 173-86

Li X.S. and Dafalias Y.F., 2000. *Dilatancy for cohesionless soils*. Géotechnique; 50(4):449-460

Li X.S., Wang Z.L. and Shen C.K., 1992. *SUMDES: a nonlinear procedure for response analysis of horizontally-layered sites subjected to multi-directional earthquake loading*. User's Manual, Department of Civil Engineering, UC Davis

Liberatore A., 1992. *Statistical models of damage to buildings and the MSK scale*. In: Proceedings of the Tenth World Conference on Earthquake Engineering

Lienkaemper J.J., 1984. *Comparison of two surface-wave magnitude scales-M of Gutenberg and Richter (1954) and Ms of "preliminary determination of epicenters*". Bull. Seism. Soc. Am. 74, 2357-2378

Lirer S., 2008. *Caratterizzazione meccanica di materiali a grana grossa in condizioni di carico ciclico*. Rapporto di ricerca, Dipartimento di Ingegneria Idraulica, Geotecnica ed Ambientale, Università di Napoli "Federico II"

Lin J-S. and Whitman R.V., 1983. *Decoupling approximation to the evaluation of earthquake induced plastic slip in earth dams*. Earthquake Eng Struct Dynam; 11:667-78

Ling H. I., Yue D., Kaliakin V. and Themelis N.J., 2002. *An anisotropic elasto-plastic bounding surface model for cohesive soils*. Journal of Engineering Mechanics, ASCE; 128(7), 748-758

Ling H. and Liu H., 2003. *Pressure-level dependency and densification behaviour of sand through generalized plasticity model.* Journal of Engineering Mechanics; 129(8):851-860

Ling H.I. and Yang S., 2006. *Unified sand model based on the critical state and generalized plasticity*. Journal of Engineering Mechanics;132(12): 1380-91

Liping J., Haian L., Yongqiang L. and Chunhui L., 2011. *Characteristics and factors that influenced damage to dams in the Ms 8.0 Wenchuan earthquake*. Earthq Eng and Eng Vib; 10:349-58

Liu P., Archuleta R. J. and Hartzell, S. H., 2006. *Prediction of Broadband Ground Motion Time Histories: Hybrid Low/High-Frequency Method with Correlated Random Source Parameters*. Bull. Seismol. Soc. Am., Vol. 96, No. 6, pp. 2118-2130

Lo Presti D. C. F., Jamiolkowski M., Pallara O., Cavallaro A. and Pedroni S., 1997. *Shear modulus and damping of soils.* Géotechnique. Voi. 47, No.3, pp. 603-617

Lohman R.B., M. Simons and B. Savage, 2002. *Location and mechanism of the Little Skull Mountain earthquake as constrained by satellite radar interferometry and seismic waveform modeling.* J. Geophys. Res. 107

Lomax A., Michelini A. and Curtis A., 2009. *Earthquake location, direct, global-search methods, in Encyclopedia of Complexity and System Science.* Part 5, pp. 2449-2473, ed. Meyers, R.A., Springer, New York

Lomax A., Virieux J., Volant P. and Thierry B.C., 2000. *Probabilistic earthquake location in 3D and layered models.* In: Thurber C.H. and Rabinowitz N. (Eds.), Advances in Seismic Event Location. Modern Approaches in Geophysics, 18, Kluwer Academic Publishers, Dordrecht, The Netherlands, 101-134

Lopez-Querol S. and Blazquez R., 2006. *Liquefaction and cyclic mobility model for saturated granular media*. International Journal for Numerical and Analytical Methods in Geomechanics; 30:413-39

Loukakis K. and J. Bielak, 1995. *Seismic response of 2D-valleys: Local site effects, in Third International Conference on Recent Advances in Geotechnical Earthquake* Engineering and Soil Dynamics, St. Louis, Missouri, 2-7 April 1995, 2, 595-598

Loukakis K. E., 1988. T*ransient response of shallow layered valleys for inclined incident SV waves calculated by the finite element method.* M.Sc. Thesis, Carnegie Mellon University, Pittsburgh

Loukakis, K. and J. Bielak, 1994a. *Seismic response of two-dimensional sediment-filled valleys to oblique incident SV-waves calculated by the finite element method*, in Proceeding of the Fifth U.S. National Conference on Earthquake Engineering, 10-14 July 1994, Chicago, Vol. III, 25-34

Loukakis K. and J. Bielak 1994b. *Layering and damping effects on seismic response of sedimentary valleys to oblique excitation*, in Proceedings of the Second International Conference on Earthquake Resistant Construction and Design, 15-17 June 1994, Berlin, Germany, 93-100

Loukidis D. and Salgado R., 2008. *Modeling sand response using two-surface plasticity*. Computers and Geotechnics; 36, 166-186

Lowe J. and Karafiath L. 1980. *Effect of anisotropic consolida-tion on the undrained shear strength of compacted clays.* Proc. Research Conf. on Shear Strength of Cohesive Soils. Boulder: 237-258

Lu N. and Likos W. J., 2004. *Unsaturated soil mechanics*. John Wiley and Sons, Inc., New Jersey

Luco N. and C. A. Cornell, 2007. *Structure-specific scalar intensity measures for near-source and ordinary earthquake ground motions.* Earthquake Spectra 23, no. 2, 357-392

Luong M.P., 1982. *Stress-strain aspects of cohesionless soils under cyclic and transient loading*. International symposium on soil under cyclic and transient loading. A.A.Balkema

Lutter W.J. and Nowack R.L., 1990. *Inversion of crustal structure using reflections from the PASSCAL Ouachita experiment*. J. Geophys. Res., 95, 4633-4646

Lutter W.J., Nowack R.L. and Braile L.W., 1990. *Seismic imaging of the upper crustal structure using travel times from the PASSCAL Ouachita Experiment.* J. geophys. Res., 95, 4621-4631

Luzi, L., S. Hailemikael, D. Bindi, F. Pacor, F. Mele and F. Sabetta (2008). ITACA (ITalian ACcelerometric Archive): A web portal for the dissemination of Italian strong-motion data, *Seismol. Res. Lett.* 79, 716-722

Lynn W.S. and Claerbout J.F., 1982. V*elocity estimation in laterally varying media.* Geophysics, 47, 884-897

Lyon-Caen H. *et al.,* 1994. S*eismotectonics and deformation of the Gulf of Corinth, EOS.* Trans. Am . geophys . Un., 75, 116

Lysmer J. and R. L. Kuhlemeyer, 1969. *Finite dynamic model for infinite media.* J. Eng. Mech. Div. ASCE, 95 (EM4), 859-877

Lysmer, J. and L. A. Drake, 1971. *The propagation of Love waves across nonhorizontally layered structures*. Bull. Seism. Soc. Am. 61, 1233- 1252

M. Scheidler, 1994. *The tensor equation $AX + XA=\Phi(A, H)$, with applications to kinematics of continua*. J. Elasticity 36 117-153. CrossRef

M.E. Gurtin, 1972. *The linear theory of elasticity*. In: S. Flugge (ed.), Handbuch der Physik, Bd VIB/2. Springer, Berlin

M.E. Gurtin, 1983. *On the hypoelastic formulation of plasticity usllig the past maximum of stress*. ASME J. Appl. Mech. 50, 894- 896.CrossRef

Madariaga R., 1976. *Dynamics of an expanding circular fault.* Bull. Seismol. Sot. Am., 66: 639-666

Madariaga R., 1983. *High frequency radiation from dynamic fault models, Annls.* Geophys., 1, 17-23

Madariaga R. and Boschi E., 1983. *Earthquake Source theory: a review.* Bull., Polar Proj. OP-O3A4, Earthquakes: Observation, Theory and Interpretation, vol. 65 - no. 4, 1-44 Amsterdam.

Maggi C., Frepoli A., Cimini G.B., Console, R. and Chiappini, M., 2009. *Recent seismicity and crustal stress field in the Lucanian Apennines and surroundings areas (Southern Italy): seismotectonic implications.* Tectonophysics, 463, 130-144

Magistrale H., S. Day, R. W. Clayton and R. Graves, 2000. *The SCEC southern California reference three-dimensional seismic velocity model version 2.* Bull. Seism. Soc. Am. 90 (6B), 65-76

Magri, G. and Molin, D., 1979. *Attività macrosismica in Basilicata, Campania e Puglia dal 1847 al 1861*. Comitate Nazionale Energia Nucleare rep. no. RT/ AMB(79)5 (in Italian)

Mai M. and Beroza C., 2000. *Source Scaling Properties from Finite-Fault Rupture Models.* Bull. Seism. Soc. Am. 90, 604-615

Mai P. and Beroza G., 2002. *A spatial random model to characterize complexity in earthquake slip.* Journal of Geophysical Research, Vol. 107(B11), 2308-2329

Mai P. M. and G. C. Beroza, 2003. *A hybrid method for calculating near-source, broadband seismograms: Application to strong motion prediction.* Phys. Earth Planet. Int. 137, 183-199

Mai P. M., P. Spudich and J. Boatwright 2005. *Hypocenter locations in finite-source rupture models.* Bull. Seis. Soc. Am, 95, 965-980

Mai P.M. and Beroza G.C., 2001. *A Spatial Random-Field Model to Characterize Complexity in Earthquake Slip.* J. Geophys. Res., in review

Mai P.M., Imperatori W. and Olsen K.B., 2010. *Hybrid Broadband Ground-Motion Simulations: Combining Long-Period Deterministic Synthetics with High-Frequency Multiple S-to-S Backscattering.* Bull. Seismol. Soc. Am., Vol. 100, No. 5A, pp. 2124-2142

Makdisi F.H. and Seed H.B., 1978. *Simplified procedure for estimating dam and embankment earthquake-induced deformations*. J. Geotech Eng Division, ASCE;104(7):849-67

Makdisi F.I., Kagawa T. and Seed H.B., 1982. *Seismic response of earth dams in triangular canyons*. J Geotech Eng ASCE; 108(10):1328-37

Makris N. and C. J. Black, 2004. *Dimensional analysis of bilinear oscillators under pulse-type excitations*.J. Eng. Mech. 130, no. 9, 1019-1031

Makris N., 1997. *Rigidity-plasticity-viscosity: can electrorheological dampers protect base-isolated structures from near-source ground motions.* Earthquake Eng Struct Dyn; 26:571-91

Makris N. and C. Black, 2003. *Dimensional analysis of inelastic structures subjected to near fault ground motions.* Earthquake Engineering Research Center, EERC 2003-05, Berkeley, California, 96 pp

Malagnini L., Hermann R.B. and Di Bona M., 2000. *Ground-motion scaling in the Apennines (Italy).* Bull Seismol Soc Am; 90(4):1062-81

Malinverno A. and Ryan W.B.F., 1986. *Extension in the Tyrrhenian Sea and shortening in the Apennines as result of arc migration driven by sinking of the lithosphere*. Tectonics, 5, 227-245

Mallat S. G., 1999. *A Wavelet Tour of Signal Processing, Academic Press, San Diego, 637 pp. Mavroeidis, G. P., and A. S. Papageorgiou (2002). Near-source strong ground motion: characterizations and design issues.* On *Proc. 7th U.S. National Conference on Earthquake Engineering*, Boston, Massachusetts, CD-ROM

Mallet R., 1862. *The Great Neopolitan Earthquake of 1857,* 2 vol, Chapman and Hall, London. Mantovani, E. and Boschi, E., 1983. Tectonics and seismicity in the Italian region, in *Earthquakes: Observation, Theory and Interpretation , LXXXV Corso, pp. 519-529, eds Kanamori, H. and Boschi, E., Soc. Italiana di fisica, Bologna*

Manfredi G., 2001. *Evaluation of Seismic Energy Demand*. Earthquake Engineering and Structural Dynamics 30, 485-499

Manzari M. T. and Dafalias Y. F., 1997. *A critical state two-surface plasticity model for sands.* Géotechnique, London; 47(2), 255-272

Manzari M.T. and Arulanandan K., 1994. *Numerical predictions for Model No. 1*. In: Proceedings of the international conference on verification of numerical procedures for the analysis of soil liquefaction problems, Davis, CA, 17-20 October, 1: p. 179-185

Manzari M.T. and Prachathananukit R., 2001. *On integration of a cyclic soil plasticity model.* International Journal for Numerical and Analytical Methods in Geomechanics; 25(6):525-549

Marcellini A., Bard P.Y., Iannaccone G., Meneroud J.P., Mouroux P., Romeo R., Silvestri F., Duval A., Martin C. and Tento A., 1995b. *Benevento seismic risk project: The microzonation. Proc. 5th Int*. Conf. Seismic Zonation, Nice, France

Marcusson W.F. III., 1981. *Moderator's report for session on 'Earth dams and stability of slopes under dynamic loads*'. Proceedings, international conference on recent advances in geotechnical earthquake engineering and soil dynamics, vol. 3; p. 1175

Mardia K.V., 1985. *Mardia's Test of Multinormality*. In Encyclopedia of Statistical Sciences, S. Kotz and N.L. Johnson, (eds.) 5, 217-221

Margaris B. N. and D. M. Boore, 1998. *Determination of Δσ and κ0 from response spectra of large earthquakes in Greece.* Bull. Seismol. Soc. Am. 88, 170-182

Mariotti G. and Doglioni C., 2000. *The dip of the foreland monocline in the Alps and Apennines*. Earth Planet. Sci. Lett., 181, 191-202

Marone C. and Schoiz C.H., 1988. *The depth of seismic faulting and the upper transition from stable to unstable slip regimes*. Geophys. Res. Lett., 15: 621-624

Marsal R. and Ramirez L., 1972. *Performance of El Infiernillo Dam, 1963-1966*. Journal of the Soil Mechanics and Foundation Division ASCE. 93(SM4);265-98

Marsal R.J., Ramirez De Arellano L., Guzman M.A. and Adame Z.H., 1976. *El Infiernillo-Comision Federal de Electricitad. Chapter of Behaviour of dams built in Mexic.* In: Contribution to the XII international congress on large dams, Mexico, Secreteria de Recursos Hidraulicos, Comision Federal de Electricitad, Instituto de Ingenieria UNAM; p. 240-312

Marsella E., Bally A.W., Cippitelli G., D'Argenio B. and Pappone G., 1995. *Tectonic history of the Lagonegro domain and Southern Apennines thrust belt evolution*. Tectonophy-sics 252, 307-330

Marsella E., Patella D., Petrillo Z. and Siniscalchi A., 1998. *Magnetotelluric profiles in Southern Apennines*. Proc. XXIII Gen. Ass. EGS, 20-24 April 1998, Nice, France

Martin G.R., Finn W.D.L. and Seed H.B., 1975. *Fundamentals of liquefaction under cyclic loading.* Proc. ASCE, Journal of Geothechnical Engineering Division, Vol. 101, N. GT5

Martin J. and Cundall P.A., 1982. *Mixed discretisation procedure for accurate solution of plasticity problems*. International Journal for Numerical and Analytical Methods in Geomechanics; 6:129-39

Martindale H., 2011. *Rate-Dependent Behavior of Clay.* M.S. Thesis, University of Connecticut, Storrs, Connecticut, USA

Martini M. and Scarpa, R., 1983. *Earthquakes in Italy in the last century.* In Earthquakes, Observation, Theory and lnterpretation , LXXXV Corso, pp. 479-492, eds Kanamori, H. and Boschi, E., Soc. Italiana di Fisica, Bologna

Martini M. and R. Scarpa, 1986. *Earthquakes in Italy in the last century, in Mostardini, M. et al*. Agenzia Italiana dei Petroli , Soc. Geol. Ltal

Mašín D., 2005. *A hypoplastic constitutive model for clays*. International Journal for Numerical and Analytical Methods in Geomechanics, 29(4):311-336

Mašín D. and Herle I., 2005. *State boundary surface of a hypoplastic model for clays.* Computers and Geotechnics (submitted for publication)

Mašín D., Tamagnini C., Viggiani G. and Costanzo D., 2005. *Directional response of a reconstituted fine granied soil. part II: Performance of different constitutive models*. International Journal for Numerical and Analytical Methods in Geomechanics (submitted for publication)
Mašín D. and Herle I., 2005. *Development and applications of hypoplastic constitutive models*. In dissertation submitted for habilitation
Mašín D. and Gudehus G., 2006. *Graphical representation of rate independent constitutive relations for saturated clay*s. Soils and Foundations (in preparation)
Masing G., 1926. *Eignespannungen und verfestigung beim messing*. Second International Congress on Applied Mechanics, Zurich, Switzerland, pp. 332–335
Massachusetts Institute of Technology (MIT), 1979. *Cyclic triaxial tests on Oosterschelde sands*. Res. Rep. R79-24, Soils Publ. No. 646, Department of Civil Engineering, Cambridge, Mass
Matešić L. and Vucetic M., 2003. *Strain-Rate Effect on Soil Secant Modulus at Small Cyclic Strains*. Journal of Geotechnical and Geoenvironmental Engineering, ASCE; 129(6), 536-549
Matrullo E., De Matteis R., Satriano C., Amoroso O. and Zollo A., 2013. *An improved 1-D seismic velocity model for seismological studies in the Campania–Lucania region (Southern Italy)*. Geophys. J. Int., 195, pp. 460–473
Matsumoto N., 2002. *Evaluation of permanent displacement in seismic analysis of fill dams*. In Proc third US-Japan workshop on advanced research on earthquake engineering for dams, San Diego, 22-23 June 2002
Matsuoka H. and Nakai T., 1985. *Relationship among Tresca, Mohr-Coulomb and Matsuoka-Nakai failure criteria*. Soils and Foundations; 25:123-128
Mavroeidis G. P. and A. S. Papageorgiou, 2003. *A mathematical representation of near-fault ground motions*. Bull. Seism. Soc. Am. 93, no. 3, 1099-1131
Mavroeidis G. P., G. Dong and A. S. Papageorgiou, 2004. *Near-fault ground motions, and the response of elastic and inelastic singledegree- of-freedom (SDOF) systems*. Earthquake Eng. Struct. Dyn. 33, no. 9, 1023-1049
Mayeda K and W.R. Walter, 1996. *Moment, energy, stress drop, and source spectra of western United States earthquakes from regional coda envelopes*. J. Geophys. Res. 101,11,195-11,208
Mazzotti A.P., Stucchi E., Fradelizio G.L., Zanzi L. and Scandone P., 2000. *Seismic exploration in complex terrains: a processing experience in the Southern Apennines*. Geophysics, 65, 1402-1417
McDowell G.R., 2002. *A simple non-associated flow model for sand*. Granular Matter, Vol 4, 65-69. CrossRef
McGill University, 1987. *Rayamp-pc-documentation, 2D Raytracing-Synthetic Seismograms*. Version 2.11, September 1987, Geophysics Laboratory
McGuire R. K., 2004. *Seismic Hazard and Risk Analysis*. Earthquake Engineering Research Institute, Berkeley, California
McKenzie D. P., 1972. *Active tectonics of the Mediterranean region*. Geophys. J. R. astr. Soc., 30, 109-185
McVay M. and Taesiri Y., 1985. *Cyclic behaviour of pavement base materials*. J. Geotech. Eng., ASCE, Vol 111, 1-17. CrossRef
Meletti C., F. Galadini, G. Valensise, M. Stucchi, R. Basili, S. Barba, G. Vannucci and E.Boschi, 2008. *A seismic source zone model for the seismic hazard assessment of the Italian territory*. Tectonophysics 450(2008) 85-108
Mena B., Mai P.M., Olsen K.B., Purvance M.D. and Brune J.N., 2010. *Hybrid Broadband Ground-Motion Simulation Using Scattering Green's Functions: Application to Large-Magnitude Events*. Bull. Seismol. Soc. Am., Vol. 100, No. 5A, pp. 2143-2162
Mena, B., E. Durukal and M. Erdik, 2006. *Effectiveness of hybrid Green's function method in the simulation of near field strong motion: An application to the 2004 Parkfield earthquake*. Bull. Seismol. Soc. Am. 96, S183-S205
Menardi A. and Rea G., 2000. *Deep structure of the Campania-Lucania arc (Southern Apennine, Italy)*. Tectonophysics, 324, 239-265
Mendoza C. and S. H. Hartzell, 1988. *Aftershock patterns and main shock faulting*. Bull. Seism. Soc. Am. 78, 1438-1449
Menke W., 1989. *Geophysical Data Analysis: Discrete Inverse Theory*. Revised edn, Academic Press
Menun C. and Q. Fu, 2002. *An analytical model for near-fault ground motions and the response of SDOF systems* In Proc. 7th U.S. National Conference on Earthquake Engineering, Boston, Massachusetts, 10 pp
Metropolis N., Rosenbluth A., Rosenbluth M., Teller, A. and Teller, E., 1953. *Equation of state calculation by fast computing machines*. J. Chem. Phys.. 21, 1087-1092
Michel Bouchon, 2003. *A Review of the Discrete Wavenumber Method*. Pure appl. geophys. 160 445-465
Michelini A. and Lomax A., 2004. *The effect of velocity structure errors on double-difference earthquake location*. Geophys. Res. Lett., 31, L09602, doi: 10.1029/2004GL019682
Midorikawa S., 1991. *Attenuation of the peak ground acceleration and velocity during the 1985 Chile and Nihonkai-chubu earthquakes*. Journal of Struct. Construct. Eng.; 422: 37-44 (in Japanese, with English abstract)
Milana G., Azzara R. M., Bertrand E., Bordoni P., Cara F., Cogliano R., Cultrera G., Di Giulio G., Duval A.M., Fodarella A., Marcucci S., Pucillo S., Régnier J. and Riccio G., 2011. T*he contribution of seismic data in microzonation studies for downtown L'Aquila*. Bull. Earthq. Eng., Vol. 9, No. 3, pp. 741-759, DOI: 10.1007/s10518-011-9246-6
Ministero dei lavori pubblici, D. M. 24/03/82. *Norme tecniche per la progettazione e la costruzione delle dighe di sbarramento*. Supplemento alla Gazzetta Ufficiale 04/08/82, n. 212
Mishra D.C. and Pedersen L.B., 1982. *Statistical analysis of potential fields from subsurface reliefs*. Geoexploration 19, 247-265
Mita A. and J. E. Luco, 1987. *Dynamic response of embedded foundations: a hybrid approach*. Comput. Methods Appl. Mech. Eng. 63, 233- 259
Miyake H., Iwata T. and Irikura K., 2003. *Source Characterization for Broadband Ground-Motion Simulation: Kinematic Heterogeneous Source Model and Strong Motion Generation Area*. Bull. Seismol. Soc. Am., Vol. 93, No. 6, pp. 2531-2545
Moczo P., E. Bystricky´, J. Kristek, J. M. Carcione and M. Bouchon, 1997. *Hybrid modeling of P-SV seismic motion at inhomogeneous viscoelastic topographic structures*. Bull. Seism. Soc. Am. 87, 1305-1323.

Moczo P., J. Kristek and E. Bystrické, 2001. *Efficiency and optimization of the 3D finite-difference modeling of seismic ground motion*. J. Comput. Acoust. 9, 593-609

Moczo P., M. Lucká, J. Kristek and M. Kristeková, 1999. *3D displacement finite differences and a combined memory optimization.* Bull. Seism. Soc. Am.; 89, 69-79

Montone P., Mariucci M.T., Pondrelli S. and Amato A., 2004. *An improved stress map for Italy and surrounding regions (central Mediterranean).* J. geophys. Res., 88, 6415-6429

Morelli C., Gantar T., Honkasalo T., McConnell P.K., Tanner J.B., Szabo B., Uotila U. and Whalen C.T., 1974. In: The International Gravity Standardization Net 1971 (IGSN71), IUGG, AIG, Publ. spec. n. 4, Paris, 165-179

Morgenstern, 1963. *Stability charts for earth slopes during rapid drawdown*. Géotechnique 13(1):121-131

Mori J., 1993. *Fault piane determination for three snall earthquakes along the San Jacinto fault, California: search for cross faulta.* J. geop hys. Res.. 98, 7 1 1-723

Mori, J. and Hartzell, S., 1990. *Source inversion of the 1988 Upland, California earthquakes determination of a fault plane for a small event*. Bull. Seism. Soc. Am.. 80, 507-518

Mossessian T. and M. Dravinski, 1987. *Application of a hybrid method for scattering of P, SV, and Rayleigh waves by near-surface irregularities.* Bull. Seism. Soc. Am.; 77, 1784-1803

Mostardini F. and Merlini S., 1986. *Appennino centro-meridionale. Sezioni geologiche e proposta di modello strutturale*. Mem. Soc. Geol. Ital., 35, 177-202 (in Italian)

Motazedian D. and G. M. Atkinson, 2005. *Stochastic finite-fault modelling based on a dynamic corner frequency.* Bull. Seismol. Soc. Am. 95, 995-1010

Mroz Z., 1967. *On the description of anisotropie hardening*. J. Mech. Phys. Solids, Vol 15, 163-175. CrossRef

Mroz Z., Norris V.A. and Zienkiewicz O.C., 1979. *Application of an anisotropie hardening model in the analysis of elasto-plastic deformation of soils.* Geotechnique, Vol 29, 1-34

Mroz Z., Norris V.A. and Zienkiewicz O.C., 1981. *An anisotropie criticai state model for soils subject to cyclic loading.* GeotechniqueVol 31, 451-469

Mucciarelli I M. and Gallipoli M.R., 2006. *Comparison between Vs30 and other estimates of site amplification in Italy*. Proc. 1st European Conf. on Earth. Engng. and Seism., Geneva, Switzerland

Mueller C., 1985. *Souree pulse enhancement by deconvolution of an empirical Green's function.* Geophys. Res. Lett. 12, 33-36

Mukabi J.N. and Tatsuoka F., 1999. *Influence of reconsolidation stress history and strain rate on the behaviour of kaolin over a wide range of strain.* 12th ARC: Geotechnics for Developing Africa, Durban, South Africa;365-377

Muraleetharan K.K., Deshpande S. and Adalier K., 2004. *Dynamic deformations in sand embankments: centrifuge modelling and blind, fully coupled analyses.* Can. Geotech. J., 41, 1, pp. 48-69

Murphy JR and O'Brien LJ., 1997. *The correlation of peak ground acceleration amplitude with seismic intensity and other physical parameters*. Bull Seism Soc Am ;67(3):877-915

Mylonakis G. and Reinhorn A.M., 2001. *Yielding oscillator under triangular ground acceleration pulse*. Journal of Earthquake Engineering; 5: 225-51

Collins N., Graves R., Ichinose G.and P. Somerville, 2006. G*round motion attenuation relations for the intermounta in west.* Research supported by the U.S. Geological Survey (USGS), Department of the Interior, under award number 05HQGR0031

Nabelek J. L., 1984. *Determination of earthquake souree parameters from inversion of body waves.* PhD thesis, Massachusetts Institute of Technology

Nafe J. and Drake C.L., 1963. *In: Physical Properties of Marine Sediments. The Sea, 3, M.N.* Interscience Publ, 74-815

Nakanishi I. and Kanamori H., 1984. *Source mechanisms of twenty-six large shallow earthquakes (M, > 6.5) during 1980 from P-wave first motion and long-period Rayieigh wave data.* Bull. Seismoi. Sot. Am., 74: 805-818

National Earthquake Hazards Reduction Program, 1994. FEMA report 222A/223A, *Recommended provisions for seismic regulations for new buildings, Provision 1 and Commentary 2.* Federal Emergency Management Agency, Washington, D.C.

Naylor D.J., 1985. *A continuous plasticity version of the critical state model*. International Journal for Numerical Methods in Engineering; 21:1187-1204

Needleman A. and Tvergaard V., 1977. *Necking of biaxially stretched elastoplastic circular plates*. J. Mech. Phys. Solids 25 159-183. CrossRef

Nelder J.A. and Mead R., 1965. *A simplex method for function minimization.* Comput J., 7, 308-313.

Nemat-Nasser S. and Tobita Y., 1982. *Influence of fabric on liquefaction and densification potential of cohesionless sand*. Mechanics of Materials; 1: 43-62

Nercessian A., Hirn A. and Tarantola A., 1984. *Three dimensional seismic transmission prospecting of the Mont Dore volcano, France*. Geophys. J. R. Astr. Soc., 76, 307-315

Neumann S.P., 1973. *Saturated-unsaturated seepage by finite elements*. Jnl. Hydraul. Div., ASCE, 99, HY12: 2233-2250

Newmark N.M., 1965. *Effect of earthquakes on dams and embankments*. Géotechnique;15(2):139-60

Ng C. W. W. and Menzies B., 2007. *Advanced unsaturated soil mechanics and engineering*. Taylor and Francis, London

Niazi M., 1982. *Source dynamics of the 1979 Imperial Valley earthquake from near-source observations of ground acceleration and velocity.* Bull. Seism. Soc. Am., 72, 1969-2002

Nicolai C. and Gambini R., 2007. *Structural architecture of the Adria platform and basin system*. Boll. Soc. Geol. Ital., 7, 21-37

Niemunis A., 1996. *A visco-hypoplastic model for clay and its FE implementation. In Resultats recents en mechanique des sols et des roches*. XI Colloque Franco-Polonais. Gdańsk

Nishimura S., 2005. *Laboratory study on anisotropy of natural London Clay.* PhD Thesis, Imperial College London

Nolet G., 2008. *A Breviary of Seismic Tomography: Imaging the Interior of the Earth and Sun*. Cambridge University Press, Cambridge, U.K.

Novotńy O., Zahradńık J. and Tselentis G. A., 2001. *Northwestern Turkey Earthquakes and the Crustal Structure Inferred from Surface Waves Observed in Western Greece.* Bull. Seism. Soc. Am. 91, 875-879

Nowroozi A.A., 1985. *Empirical relations between magnitudes and fault parameters for earthquakes in Iran.* Bull. Seism. Soc. Am. 75, 1327-1338

Nuth M. and Laloui L., 2008. *Effective stress concept in unsaturated soils: clarification and validation of a unified framework*. International Journal for Numerical and Analytical Methods in Geomechanics, 32, 771-801

Oda M., Nemat-Nasser S. and Konishi J., 1985. *Stress-induced anisotropy in granular materials*. Soils and Found., Tokyo; 25(3), 85- 97

Oglesby D.D., R.J. Archuleta and S.B. Neilson, 2000. *The three-dimensional dynamics of dipping faults.* Bull. Seis. Soc. Am. 90, 616-628

Ogniben L. and Vezzani L., 1975. *Mappe structure of Sicily, Calabria and Lucania, ltaly.* In Geology of Italy , pp. 83-104, ed. Squyres, C. H., The Earth Sciences Society of the Libyan Arab Republic, Tripoli, Libya

Ohnaka M., 1978. *Earthquake-source parameters related to magnitude.* Geophys. J. R. Astr. Soc. 55, 45-66

Ohno S., Ohta T., Ikeura T. and Takemura M., 1993. *Revision of the attenuation formula considering the effect of fault size to evaluate strong ground motion spectra in near field*. Tectonophysics 218:69-81

Ohtsuka H., P.G. Somerville and T. Sato, 1998. *Estimation of broadband strong ground motions considering uncertainty of fault parameters.* J. Struct. Mech. Earthq. Eng., JSCE, No.584/I-42, 185-200

Oka F., Yashima A., Shibata T., Kato M. and Uzuoka R., 1994. *FEM-FDM coupled liquefaction analysis of a porous soil using an elasto-plastic model*. Applied Scientific Research; 52:209-245

Okada Y., 1985. *Surface deformation due to shear and tensile faults in a half-space.* Bull. Seism. Soc. Am., 75, 1135-1154

Olivares L. and F. Silvestri, 2001. *Analisi della risposta sismica e della subsidenza post-sismica del colle di Bisaccia a seguito del terremoto irpino-lucano del 1980.* Proc. X National Conference of ANIDIS (in Italian)

Olsen E.T. and Bernstein B., 1984. *A class of hypo-elasticnon-elastic materials and their thermodynamic*s. Arch. RationaJ Mech. A.naL 86 291-303.CrossRef

Olsen K. B., J. C. Pechmann and G. T. Schuster, 1995. *Simulation of 3D elastic wave propagation in the Salt Lake basin.* Bull. Seism. Soc. Am. 85, 1688-1710

Olsen K. B. and Archuleta, 1996 R. J. *3D simulation of earthquakes on the Los Angeles fault system.* Bull. Seism. Soc. Am.; 86, 575-596

Olson A. H., 1987. *A Chebyshev condition for accelerating convergence of iterative tomographic method-solving large least square problems*. Phys. Earth Planet. Inter., 47: 333-345

Olson A.H., Orcutt J.A. and Frazier G.A., 1984. *The discrete wave number/finite element method for synthetic seismograms*. Geophys. J. R. Astr. Soc.; 77: 421-460

Oprsal I. and J. Zahradník, 1999. *Elastic finite-difference method for irregular grids.* Geophysics; 64, 240-250

Opřsal I., Brokěsova J., Faeh D. and Giardini D., 2002. *3D Hybrid Ray-FD and DWN-FD Seismic Modeling For Simple Models Containing Complex Local Structures.* Stud. Geophys. Geod., in press

Oprsal, I. and J. Zahradník, 2002. *Three-dimensional finite difference method and hybrid modeling of earthquake ground motion.* J. Geophys. Res. 107 (B8), 2161, doi: 10.1029/2000JB000082

Ori G., 1989. *Geologica history of the extensional basin of the Gulf of Corinth.* Greece, *Geology,* 17, 918-921

Ornthammrath T., 2007. *Artificial neutral networks applied to the seismic design of deep tunnels.* A Dissertation Submitted for the Master Degree in earthquake engineering, Rose School, Pavia-Italy

Orsini G. A., 1999. *Model for buildings' vulnerability assessment using the parameterless scale of seismic intensity (PSI).* Earthquake Spectra; 15(3): 463-83

Ortiz M. and Simo J. C., 1986. *An Analysis of a New Class of Integration Algorithms for Elastoplastic Constitutive Relations*. 23, 353-366

Ortiz M. and Popov E.P., 1985. *Accuracy and stability of integration algorithms for elastoplastic constitutive equations*. International Journal for Numerical Methods in Engineering; 21:1561-1576

Ortolani F., 1981. *Principali effetti geologici di superficie del terremoto del 23.11.1980.* Rend. Soc.Geol. It., 4, 71 (in Italian)

Ortolani F. and Torre M., 1981. *Guida all'Escursione nell'area interessata dal terremoto del 23 Novembre 1980.* Rend. Soc. Geol. It., 4, 173-214 (in ltalian)

Ortolani F., 1975. *Assetto strutturale dei Monti Piccntini, della valle del Sele e del gruppo di Monte Marzano-Monte Ogna (Appennino meridionale): implicazioni idrogeologiche.* Boll. Soc. Geol. Ital., 94, 209-230 (in Italian)

Ozkan M.Y., Erdik M., Tunçer M.A. and Yilmaz Ç, 1996. *An evaluation of Siirgii Dam response during 5 May 1986 earthquake.* Soil Dyn Earthquake Eng 1996; 15:1-10

Ozkan M.Y., Ozyazicioglou M. and Aksar U.D., 2006. *An evaluation of Guldurcek dam response during 6 June 2000 Orta earthquake*. Soil Dynam Earthq Eng; 26:405-19

Martin Mai P., 2008. *Calculation of Near-Field Ground-Motions General Setup and Modelling Strategy.* Swiss Federal Institute of Technology in Zurich (ETHZ)

Somerville P., Collins N., Abrahamson N., Graves R. and Saikia C., 2001. *Ground motion attenuation relations for the central and eastern united states.* Research supported by the U.S. Geological Survey (USGS), Department of the Interior

Pacor, F., G. Cultrera, A. Mendez and M. Cocco, 2005. *Finite fault mod- eling of strong ground motions using a hybrid deterministic-stochastic approach.* Bull. Seismol. Soc. Am. 95, 225-240

Pagano L., 1998. *Steady state and transient unconfined seepage analysis for earthfill dams.* In: Proceedings ofVIII ABAQUS Users' Conference. Milano; pp. 577-585

Pagano L., Desideri A. and Vinale F., 1998. *Interpreting the settlement profiles of earth dams*. J Geotechn Geoenviron Eng, ASCE; 124(10): 923-32

Pagano L., Mancuso C. and Sica S., 2008. *Prove in sito sulla diga del Camastra: tecniche sperimentali e risultati*. Italian Geotechnical Journal; 3(08):11-28. (in Italian)

Pagano L., Sica S. and Desideri A., 2006. *Representativeness of measurements in the interpretation of earth dam behavior*. Canadian Geotech J 2006;43(1):87-99

Pagano L., Sica S. andFenelli G.B., 2003. *Interpreting the Camastra Dam behaviour in 40 years of operation*. In: Proceedings of the third international symposium on deformation characteristics of geomaterials ISLyon03; p. 1389-94

Paige C. and Sanders M.A., 1982. *LSQR: an algorithm for sparse linear equation and sparse least squares.* Trans. Math. Software, 8, 43-71

Pakiser L.C., 1989. *Geophysics of the Intermontaine system*. In Geophysical Framework of the Continental United States, Geological Society of America Memoir 172, p. 235-247

Pantosti D. and G. Valensise, 1990. *Faulting mechanism and complexity of the 23 November 1980, Campania-Lucania earthquake, inferred from surface observations.* J. Geophys. Res. 95, 15319-15341

Pantosti D. and Valensise G., 1993. *Source geometry and long-term behavior of the 1980, Irpinia earthquake fault based on field geologic observations*. Ann Geofis; XXXVI(1):41-9

Panza G. F., S. J. Duda, L. Cernobori, and M. Herak, 1989. *Gutenberg's surface-wave magnitude calibrating function: theoretical basis from synthetic seismograms.* Tectonophysics 166, 35-43

Paolucci R., 2009. *Long-period earthquake ground motion: recent advances and observations from the April 6 2009, Mw 6.3 L'Aquila Earthquake, Italy.* Proceedings of Aces Workshop on Performance-Based Earthquake Engineering Corfu, Greece

Paolucci R. and Smerzini C., 2010. *Strong ground motion in the epicentral region of the MW 6.3 Apr 6 2009, L'Aquila earthquake, Italy*. In Proceedings of the 5th International conference on Recent advances in Geotechnical Earthquake Engineering and Soil Dynamics, Paper EQ4, 11 pp., May 24-29, 2010, San Diego, California

Paolucci R. and Smerzini C., 2011. *3D numerical simulations of earthquake ground motion in sedimentary basinis: the cases of Gubbio and l'Aquila, Central Italy*. 4th IASPEI/IAEE International Symposium: Effects of Surface Geology on Seismic Motion August 23-26, 2011 · University of California Santa Barbara

Papadimitriou A.G., Bouckovalas G.D. and Andrianopoulos K.I., 2014. *Methodology for estimating seismic coefficients for performance-based design of earthdams and tall embankments*. Soil Dynam Earthq Eng; submitted for publication

Papadimitriou A. G., 1999. *Elastoplastic modeling of monotonic and dynamic behavior of soils*. Doctorate thesis, Geotech. Div., National Technical University of Athens, Athens, Greece (in Greek)

Papadimitriou A.G., 2011. *Topographic aggravation of the peak seismic acceleration near two dimensional hills and slopes*. In: Proceedings, 5th international conference on earthquake geotechnical engineering, Santiago, Chile; January 10-13

Papadimitriou A.G., Andrianopoulos K.I., Bouckovalas G.D. and Anastasopoulos K., 2010. *Improved methodology for the estimation of seismic coefficients for the pseudo-static stability analysis of earthdams*. In: Proceedings, 5th international conference on recent advances in geotechnical earthquake engineering and soil, dynamics; p. 24-9

Papadimitriou A.G., Bouckovalas G.D. and Dafalias Y.F., 1999. *Use of elasto-plasticity to simulate cyclic sand behavir*. In: Proceedings of the second international conference on earthquake geotechnical engineering, Lisbon, 1: p. 125-130

Papadimitriou A.G., Bouckovalas G.D. and Dafalias Y.F., 2001. *Plasticity model for sand under small and large cyclic strains*. Journal of Geotechnical and Geoenviron- mental Engineering ASCE; 127(11):973-83

Papadimitriou A.G. and Bouckovalas G.D., 2002. *Plasticity model for sand under small and large cyclic strains: a multiaxial formulation*. Soil Dynamics and Earthquake Engineering; 22:191-204

Papadimitriou A.G., Manzari M.T. and Dafalias Y.F., 2005. *Calibration of A Simple Anisotropic Plasticity Model for Soft Clays*. Proceedings, GeoFrontiers Conference of ASCE, January 24-26, Austin, TX, Geotechnical Special Publication No; 128, 415-424

Paquin G., 1983. *Contribution á l'étude de la Déstructuration et Restructuration des Argiles Sensible*. M.S. Thesis, Université Laval, Quebec, P.Q.

Park I-J., Desai CS., 2000. *Cyclic behavior and liquefaction of sand using disturbed state concept*. Journal of Geotechnical and Geoenvironmental Engineering, ASCE; 126(9):834-46

Park S. and Elrick S., 1998. *Predictions of shear wave velocities in southern California using surface geology.* Bull Seismol Soc Am 88:677-685

Park S-S. and Byrne P.M., 2004. *Practical constitutive model for soil liquefaction*. In: Proceedings of the ninth international symposium on numerical models in geomechanics (NUMOG IX), p. 181-186

Pascal Bernard and Aldo Zollo, 1989. *The Irpinia (Italy) 1980 Earthquake Detailed Analysis of a Complex Normal Faulting.* Journal of Geophysical, Vol. 94, NO. B2, Pages 1631-1647

Pasquale G., De Matteis R., Romeo A. and Maresca R., 2009. *Earthquake focal mechanisms and stressinversion in the Irpinia Region (southern Italy)*. J. Seismol., 13,107-124, doi: 10.1007/s10950-008-9119-x

Pastor M., Zienkiewicz O.C. and Chan A.H.C., 1990. *Generalized plasticity and the modelling of soil behaviour*. International Journal for Numerical and Analytical Methods in Geomechanics; 14:151-190

Patacca E., R. Sartori and P. Scandone, 1990. *Tyrrhenian basin and Apenninic arcs: kinematic relations since Late Tortonian timeS.* Mem. Soc. Geol. It., 45, 425-451

Patacca E. and Scandone P., 1989. *Post-Tortonian mountain building in the Apennines: the role of the passive sinking of a relic lithospheric slab*. In The Lithosphere in Italy: Advances in Earth Science Research, Vol. 80, pp. 157-176, ed. Boriani, A., Accademia Nazionale dei

Patacca E. and Scandone P., 2001. *Late thrust propagation and sedimentary response in the thrust belt: foredeep system of the Southern Apennines (Pliocene-Pleistocene)*. In Anatomy of an Orogen: The Apennines and Adjacent Mediterranean Basins, pp. 401-440, ed. Vai, G.M., Kluwer Academic Publishers

Patacca E. and Scandone P., 2007. *Constraints on the interpretation of the CROP-04 seismic line derived from Plio-Pleistocene foredeep and thrust- sheet-top deposits (Southern Apennines, Italy), in Results of the CROP Project, Sub-Project CROP-04, Southern Appeinnes (Italy).* Bollettino della Societa` Geologica Italiana (*Italian Journal of Geoscience*), Special Issue no. 7, pp. 241-256, eds Mazzotti A., Patacca E. and Scandone P.

Patacca E. and Scandone P., 1987. *Tectonic evolution of the outer margin of the Apennines and related foredeep system.* In: Boriani A., Bonafede M., Piccardo G.G. and Vai G.B. (Eds), The Lithosphere in Italy: Advances in Earth Science Research. Accademia Nazionale dei Lincei, Rome, Italy, 139-142

Patacca E. and Scandone P., 1989. *Post-Tortonian mountain building in the Apennines: the role of the passive sinking of a relic lithospheric slab.* In: Boriani A., Bonafede M., Piccardo G.G. and Vai G.B. (Eds), The Lithosphere in Italy: Advances in Earth Science Research. Accademia Nazionale dei Lincei, Rome, Italy, 157-176

Patacca E., P. Scandone, M. Bellatalia, N. Perilli and U. Santini, 1992. *La zona di giunzione tra l'arco appenninico settentrionale e l'arco appenninico meridionale nell'Abruzzo e nel Molise.* Studi Geologici Camerti Voi. Spec. (1991-92), 417-441

Patacca E., Sartori R. and Scandone P., 1990. *Tyrrhenian Basin and Apenninic arcs: kinematic relations since Late Tortonian times*. Mem. Soc. Geol. Ital., 45, 425-451

Patacca E. and Scandone P., 1992. *The Numidian-sand event in the Southern Apennines. Mem.* Soc. Geol. Padova 43, 297-337

Paton J. and Semple N.G., 1961. *Investigation of the stability of an earth dam subjected to rapid drawdown including details of pore pressure recorded during a controlled drawdown test*. Pore pressure and suction in soils: 85-90. Butterworths, London

Paul A., Cattaneo M., Thouvenot F., Spallarossa D., Béthoux N. and Fréchet J., 2001. *A three- dimensional crustal velocity model of the southwestern Alps from local earthquakes tomography*. J. Geophys. Res., 106(B9), 19367-19389

Pavlis G.L. and Booker J.R., 1980. *The mixed discrete-continuous inverse problem: Application to the simultaneous determination of earthquake hypocenters and velocity structure.* J. Geophys. Res., 85(B9), 4801-4810

Pavlis G.L., 1986. *Appraising earthquake hypocenter location errors: a complete, practical approach for single event locations.* Bull. Seism. Soc. Am., 76, 1699-1717

Pereira C., 2011. *Study of the Barcelona Basic Model.* Influence of suction on shear strength. Master Thesis, IST, Lisbon (in Portuguese)

Perzyna P., 1963. *The Constitutive Equations for Rate Sensitive Plastic Materials*. Quarterly of Applied Mathematics; 20, 321-332

Perzyna P., 1966. *Fundamental Problems in Viscoplasticity*. Advances in Applied Mechanics; 9, 244-377

Pestana J. M., Whittle A. J. and Gens A., 2002. *Evaluation of a Constitutive Model for Clays and Sands: Part II - Clay Behavior.* International Journal for Numerical and Analytical Methods in Geomechanics; 26, 1123-1146

Pestana J.M., 2000. *A unified constitutive model for clays and sands*. Ph.D. Thesis MIT, Cambridge, Mass

Pingue F., De Natale G. and Briole P., 1993. *Modeling of the 1980 Irpinia earthquake source: constraints from geodetic data.* Ann Geofis; XXXVI(1):27-40

Pinos S. F., 2000. *Instrumentación de presas de tierra, aplicaciones para evaluar la respuesta sísmica de presas chilenas*. University of Chile (Universidad de Chile). Unpublished thesis presented to obtain the degree of Civil Engineer in Construction and Structures (Ingeniero Civil en Construcción y Estructuras)

Pitarka A., 1999. *3D elastic finite-difference modeling of seismic motion using staggered grids with non-uniform spacing.* Bull. Seism. Soc. Am.; 89, 54-68

Pitarka, A., K. Irikura, T. Iwata and H. Sekiguchi, 1998. *Three-dimensional simulation of the near-fault ground motion for the 1995 Hyogoken Nanbu (Kobe), Japan, earthquake.* Bull. Seism. Soc. Am. 88, 428- 440

Plicka V. and Zahradńık J., 2002. *Inversion of Rupture Nucleation from Regional Records by EGF Method for Unequal Focal Mechanisms of the Mainshock and Aftershock*: The Athens 1999 Earthquake, Tectonophysics, in press

Podvin P. and Lecomte I., 1991. *Finite difference computation of traveltimes in very contrasted velocity model: A massively parallel approach and its associated tools.* Geophys. J. Int., 105, 271-284

Pollitz F.F., 1992. *Postseismic relaxation theory on the spherical earth.* Bull. Seism. Soc. Am., 82, 422-453

Pollitz F.F., 1996. *Coseismic deformation from earthquake faulting on a layered spherical Earth.* Geophys. J. Int., 125, 1-14

Poorooshasb H.B. and Pietruszczak S., 1986. *A generalized flow theory for sand*. Soils and Foundations; 26(2):1-15

Popescu R. and Prevost J. H., 1995. *Comparison between VELACS numerical 'Class A' simulations and centrifuge experimental soil test results*. Soil Dyn. and Earthquake Engrg.; 14(2), 79-92

Popescu R., Prevost J.H., 1994. *Numerical class ''A'' predictions for Model Nos 1, 2, 3, 4a, 4b, 6, 7, 11 and 12.* Proceedings, International Conference on Verification of Numerical Procedures for the Analysis of Soil Liquefaction Problems, Davis, CA, 2: 1105-1207

Potts D. M. and Zdravković L., 1999. *Finite element analysis in geotechnical engineering.* Theory. Thomas Telford Limited

Potts D.M. and Ganedra D., 1994. *An evaluation of substepping and implicit point algorithms*. Computer Methods in Applied Mechanics and Engineering; 119:341-354

Poulos H.G., Booker J.R. and Ring G.J., 1972. *Simplified calculation of embankment deformations.* Soils Found; 12(4):1-17

Praastrup U., 2000. *Three dimentional stress-strain behavior of soils tested in the danish rigid boundary true triaxial apparatus*. Ph.D. Thesis, Geotechnical engineering group, Aalborg University. Aalborg University

Prager W., 1955. *The theory of plasticity-a survey of recent achievements.* Proc./nst. Mech. Eng., London, 3-19

Prashant A., 2004. *Three-Dimensional Mechanical Behavior of Kaolin Clay with Controlled Microfabric Using True Triaxial Testing.* PhD. Dissertation, University of Tennessee, Knoxville, USA

Prato C.A. and Delmastro E., 1987. *1-D seismic analysis of embankment dams*. J. Geotech Eng ASCE; 113(8):904-9

Prevost J.H., 1977. *Mathematical modelling of monotonic and cyclic undrained clay behaviour*. Int. J. Num. Anal. Meth. Geomech., Vol I, 195-216. CrossRef

Prevost J.H., 1978. *Plasticity theory for soil stress-strain behaviour*. Journal of Engineering Mechanics, ASCE;104(5):1177-94

Prevost J.H., 1985. *A simple plasticity theory for frictional cohesionless soils.* Soil Dynamics Earthquake Eng., Vol 4, 9-17. CrossRef

Prevost J.H., 1985. *Wave propagation in fluid-saturated porous media: an efficient finite element procedure.* Soil Dyn. Earth. Eng., Vol. 4, N°4, pp. 183-202

Prevost JH., 2002. *Dynaflow. A non linear transient finite element analysis program*. Version 0.2 Technical Report, Department of Civil and Environmental Engineering, Princeton University, Princeton, NJ

Prevost J.H., Abdel-Ghaffar A.M. and Lacy S.J., 1985. *Nonlinear dynamic analyses of an earth dam*. J Geotech Eng ; 111(7):882-97

Prevost J.H., Cunny B., Hughes T.J.R. and Scott R.F., 1981. *Offshore gravity structures: analysis*. J. Geotech. Eng. Div., Vol 107, 143-165

Prevost J.H., Krstelj I. and Popescu R., 1994. *Overview of experimental results for centrifuge model No. 12.* In: Proceedings of the international conference on verification of numerical procedures for the analysis of soil liquefaction problems, Davis, CA, 2: p. 1619-1634

Priestley K.F., K.D. Smith and R.S. Cockerham, 1988. *The 1984 Round Valley, California earthquake sequence*. Geophys. J. 95, 215-235

Pujol J., 1988. *Comments on the joint determination of hypocenter and station corrections.* Bull. Seism. Soc. Am., 78, 1179-1189

Purcaru G. and H. Berckhemer, 1982. *Quantitative relations of seismic source parameters and a classification of earthquakes, in Quantification of Earthquakes, S. J. Duda and K. Aki (Editors).* Tectonophysics 84, 57-128

Pyke R., 1991. *Selection of seismic coefficients for use in pseudo-static slopestability analyses*.

R. Butterfield. 1979. *A natural compression law for soils.* Géotechnique, 29(4):469- 480

R. Hill, 1978. *Aspects of invariance in solid mechanics.* Ad. Appl. Mech. 18 1-75

R.M. Brannon, 1998. *Caveats concerning conjugate stress and strain measures for frame indifferent anisotropic elasticity*. Acta Mech. 129 107-116. CrossRef

R.W. Ogden, 1984. *Non-Linear Elastic Deformations.* Ellis Horwood, Chichester

Ramberg W. and Osgood W. R., 1943. *Description of stress-strain curve by three parameters*. Technical Note 902, National Advisory Committee for Aeronautics, Washington, D.C.

Rampello S. and Silvestri F., 1993. *The stress-strain behaviour of natural and reconstituted samples of two overconsolidated clays*. In Geotechnical Engineering of Hord Soils-Soft Rocks, Anagnostopoulos et al. (eds), Balkema, Rotterdam

Rampello S., Callisto L. and Fargnoli P., 2008. *Evaluation of seismic coefficients for slope stability analysis using a displacement-based approach. Panel Paper*. In: Seismic Engineering International Conference commemorating the 1908 Messina and Reggio Calabria Earthquake (MERCEA), in press

Rampello S., Callisto L. and Fargnoli P., 2009. *Two-dimensional seismic response analysis to evaluate permanent slope displacements*. In: Kokusho A, Tsukamoto A, Yoshimine A, editors. Performance-based design in earthquake geotechnical engineering. London: Taylor and Francis Group; p. 929-36

S. Rampello, E. Cascone and N. Grosso, 2009. *Evaluation of the seismic response of a homogeneous earth dam*. Soil Dynamics and F.arthquake Engineering 29 782-798

Rampello S. and Viggiani G.M.B., 2001. *Prefailure deformation characteristics of geomaterials. Discussion leader report on session la: laboratory tests.* In: Proceedings of the second international symposium on “prefailure deformation characteristics of geomaterials”, vol. 2, Torino. p. 1279-89

Rathje E.M. and Antonakos G., 2011. *A unified model for predicting earthquake-induced sliding displacements of rigid and flexible slopes*. Eng Geol; 122:51-60

Rathje E.M. and Bray J.D., 1999. *An examination of simplified earthquake-induced displacement procedures for earth structures*. Can Geotechj; 36:72-87

Rathje E.M. and Bray J.D., 2000. *Nonlinear coupled seismic sliding analysis of earth structures*. J Geotech Geoenviron Eng, ASCE; 126(11):1002-14

Rathje E.M. and Bray J.D., 2001. *One- and two-dimensional seismic analysis of solid-waste landfills*. Can Geotech J; 38(4):850-62

Rayleigh L., 1945. *Theory of Sound, vol. I.* Dover Publication, New York

Regan J. and D. G. Harkrider, 1989. *Numerical modelling of SH Lg waves in and near continental margins.* Geophys. J. Int.; 98, 107-130

Reinius E., 1954. *The stability of the slopes of earth dams.* Géotechnique 5: 181-189

Reiter L., 1990. *Earthquake hazard analysis-issues and insight*s. Columbia University Press, New York, 254 pp

Resendiz D., Romo M.P. and Moreno E., 1982. *El Infiernillo and La Villita Dams: seismic behaviour*. Journal of Geotechnical Engineering Division ASCE; 108(GT1): 109-31

Reutter K. J., Giese P. and Closs H., 1980. *Lithospheric split in the descending plate: observations from the northern Apennines*. Tectonophys., 64, Tl -T9

Reutter K.J., 1981. *A trench-forearc model for the Northern Apennines. Sedimentary basins of Mediterranean Margins.* In: Wezel F.C. (Ed.), Sedimentary Basins of Mediterranean Margins. C.N.R. Italian Project of Oceanography, Tecnoprint, Bologna, 433-443

Richards B.G. and Chan C.Y., 1969. *Prediction of pore pressures in earthdams*. Proc. 7th Int. Conf. S.M.F.E., 2: 355-362. Mexico

Richards R. and Elms D.G., 1979. *Seismic behaviour of gravity retaining walls*. J Geotech Eng Div, ASCE; 105(4):449-64

Richardson A. M. and Whitman R. V., 1963. *Effect of strain-rate upon undrained shear resistance of a saturated remoulded fat clay.* Géotechnique. Voi. 13, No.4, pp. 310-324

Richter C. F.,1958. *Elementary Seismology.* W. Il. Freeman, San Francisco, 768 pp

Rigo A., 1994. *Etude sismot ectoniq ue et géodésiq ue du golfe de Corinthe (Grèce).* PhD Thesis. University of Paris, France

Ripperger J., P. M. Mai and J. P. Ampuero, 2008. *Variability of near-field ground motion from dynamic earthquake rupture simulations*. Bull. Seismol. Soc. Am. 92, 2217-2232

Ritsema A. R., 1971. *Notes on plate tectonics and are movements in the Mediterranean region, Commuus*. Obs. r. Belg. Geophys. Ser., 101, 22

Rodriguez-Marek A., 2000. *Near fault seismic site response.* Ph.D. Thesis, Civil Engineering, University of California, Berkeley, 451 pp

Rodríguez-Marek A., EERI M., Bray Jonathan D. and Abrahamson N., 2001. *An Empirical Geotechnical Seismic Site Response Procedure*. Earthquake Spectra, Volume 17, No. 1

Rollins K.M., Evans M.D., Diehl N.B. and Daily W.D., 1998. *Shear modulus and damping relationships for Gravels*. Journal of Geotechnical and Geoenvironmental Engineering ASCE; 124(5):396-405

Roscoe K.H. and Burland J.B., 1968. *On the generalized stress-strain behaviour of ''wet'' clay.* In: Engineering plasticity, Cambridge University Press, pp. 535-609

Roscoe K.H., Schofield A.N. and Wroth C.P., 1958. *On yielding of soils.* Géotechnique; 8(1):22-53

Rossetto T. and Elnashai A., 2003. *Derivation of vulnerability functions for European type RC structures based on observational data*. Eng Struct; 25:1241-63

Rothe J. P., 1969. *The Seismicity of the Earth, 1953-1965.* UNESCO, Paris

Rothman D., 1986. *Automatic estima tion of large residual statics corrections.* Geophysics. 51, 332-346

Rotili F., 2010. *Risposta sismica locale nel territorio di Castelnuovo (AQ)*. Master degree thesis (in Italian), University of Sannio, Benevento - Italy

Rouainia M. and Wood D.M., 2001. *Implicit numerical integration for a kinematic hardening soil plasticity model*. International Journal for Numerical and Analytical Methods in Geomechanics; 25:1305-1325

Roure F., Casero P. and Vially R., 1991. *Growth processes and melange formation in the Southern Apennines accretionary wedge*. Earth Planet. Sci. Lett. 102, 395-412

Rovelii, A., Bonamassa, O., Cocco, M., Di Bona, M. and Mazza, S., 1988. Scaling laws and spectral parameters of the ground motion in active extensional areas in Italy. Bull. Seismol. Sot. Am., 78: 530-560

Rowe P. W., 1962. *Tue stress-dilatancy relation for statie equilibrium of an assembly of particles in contact*. Proc. R. Soc. A., Vol 267, 500-527

Royden L., Patacca E. and Scandone R., 1987. *Segmentation and configuration of subducted lithosphere in Italy: an important control on thrust-belt and foredeep-basin evolution*. Geology, 15, 714-717

Rubin J., 1968. *Theoretical analysis of two-dimensional transsient flow of water in unsaturated and partly saturated soils*. Soil Sci. Soc. Am. Proc. 32 (5): 607-615

Rudnicki J. W. and B. Kanamori, 1981. *Effects of fault interaction on moment stress drop and stress energy release.* J, Geophys Res., 86,1785-1793

Rudnicki J.W. and Rice J.R., 1975. *Conditions for the localization of defonnation in pressure-sensitive dilatant materials*. J. Mech. Phys. Solids 23, 371-394. CrossRef

Ruff L. J. and Kanamori *H.,* 1983. *The Rupture Process and Asperity Distribution of Three GreatEarthquakes from Long-period Diffracted P Waves.* Phys. Earth Planet. Int. 31, 202 - 230

S. Nemat-Nasser, 1983. *On finite plastic flow of crystalline solids and geomaterials.* ASME J. Appl. Mech. 50 1114-1126. CrossRef

S. Nemat-Nasser, 1992. *Phenomenological theories of elastoplasticity and strain localization at high strain rates*. Appl. Mech. Rev. 45 S19-S45

S. Storen and J.R. Rice, 1975. *Localized necking in thin sheets*. J. Mech. Phys. Solids 23 421-441. CrossRef

S.N. Atluri, 1984. *On constitutive relations at finite strain: Hypoelasticity and elstoplasticity with isotropic or kinematic hardening.* Comp. Methods Appl. Mech. Engrg. 43 137-171. CrossR.ef

S3 Project Deliverable D0, 2007. S*cenari di scuotimento in aree di interesse prioritario e/o strategico, Deliverable D0: Tecniche di simulazione*. (in Italian). Last accessed January 2011.

Sabetta F. and Pugliese A., 1987. *Attenuation of peak horizontal acceleration and velocity from Italian strong-motion records*. Bullettin of the Seismological Society of America 77, 1491-1513

Sabetta F., Goretti A. and Lucantoni A., 1998. *Empirical fragility curves from damage survey and estimated strong ground motion*. In: 11th European Conference on Earthquake Engineering

Sabetta F. and Pugliese A., 1996. *Estimation of response spectra and simulation of nonstationarity earthquake ground-motion*. Bullettin of the Seismological Society of America 86, 337-352

Sadigh K., C.Y. Chang, J.A. Egan, F. Makdisi and R.R. Youngs, 1997. *Attenuation relationships or shallow crustal earthquakes based on California strong motion data.* Seismological Research Letters 68, 180-189

Salgado F., September 11 2011. *Re-evaluation of the slope stability pseudo-static method of analysis*. In: Proceedings, ERTC-12 workshop on evaluation of EC8, Athens

Sallarès V., Charvis P., Flueh E.R. and Bialas J., 2003. S*eismic structure of Cocos and malpelo Volcanic Ridges and implications for hot spot-ridge interaction.* J. Geophys. Res., 108(B12), 2564, doi: 10.1029/2003JB002431

Samson C., Barton P.J. and Karwatowski J., 1995. *Imaging beneath an opaque basaltic layer using densely sampled wide-angle OBS.* Geophys. Prospect., 43, 509-527

Samuelli-Ferreti A. and L. Siro, 1983. *Indagini preliminary sugli insediamenti più colpiti dal terremoto del 23-11-1980 per fornire indicazioni urgenti sull'uso del territorio dal punto di vieta geologico e sismico: Comune di Calitri, in Indagni di Microzonizzazione Sismica.* Progetto finalizzato geodinamica, Consiglio Nazionale delle Ricerche, Rome, Italy

Sánchez-Sesma F. J. and F. Luzón, 1995. *Seismic response of three-dimensional valleys for incident P, S, and Rayleigh waves.* Bull. Seism. Soc. Am.; 85, 269-284

Sarma S.K., 1975. *Seismic stability of earth dams and embankments*. Geotechnique; 25(4):743-61

Sasani M and Bertero VV. 2000. *Importance of severe pulse-type ground motions in performance-based engineering: Historical and critical review.* Proceedings of the 12th World Conference on Earthquake Engineering (12WCEE), Auckland, New Zealand

Satake K., 1995. *Linear and Nonlinear Computations of the 1992 Nicaragua Earthquake Tsunami.* Pure appl. geophys. 144, 455 - 470

Sato T. and Hirasawa T., 1973. *Body Wave Spectra from Propagating Shear Cracks.* J. Phys. Earth 23, 323 - 331

Sato T., R. W. Graves and P. G. Somerville, 1999. *Three-dimensional finite-difference simulations of long-period strong motions in the Tokyo metropolitan area during the 1990 Odawara earthquake (MJ 5.1) and the great 1923 Kanto earthquake (MS 8.2) in Japan*. Bull. Seism. Soc. Am. 89, 579-607

Savage J.C., 1998. *Displacement field for an edge dislocation in a layered half-space.* J. geophys. Res., 103, 2439-2446

Savy J., 1997. *Ground motion attenuation in eastern North America.* Section 4.3 of Report on Trial SHAC Methodology Implementation Project, Lawrence Livermore National Laboratory

Saygili G. and Rathje E.M., 2008. *Empirical predictive models for earthquake-induced sliding displacements of slopes*. J Geotech Geoenviron Eng, ASCE; 134 (6):790-803

Scandella L., 2007. *Numerical eavaluation of transient ground strains for the seismic analysis of underground structures*. PhD Thesis. Politecnico di Milano

Scandarella L. and Vanini M., 2007. *The Spectral Element Method enanched by the Domain Reduction Method (DRM).* Dipartimento di Ingegneria Strutturale, Politecnico di Milano

Scandone P. and E. Patacca, 1984. *Tectonic evolution of the Central Mediterranean area.* Ann. Geophys, 2(2),139-142

Scandone P., 1979. *Origin of the Tyrrhenian Sea and Calabrian Arc*. *Boll. Soc. Geol. It*., 98, 27-34. Scarpa R., Tronca F., Bianco F. and Del Pezzo E., 2002. High resolution velocity structure beneath Mount Vesuvius from seismic array data. Geophys. Res. Lett., 29, 2040

Scarpa R., 1982. *Travel-time residuals and three-dimensional velocity structure of Italy*. Pure Appl. Geophys., 120, 583-606

Schanz T., 1998. *Zur modellierung des mechanischen verhaltens von reibungsma terialen*. Habilitation, Stuttgart Universitat

Schanz T. and Vermeer P.A., 1999. *Bonnier PG. Formulation and verification of the hardening-soil model.* In: Brinkgreve RBJ, editor. Beyond 2000 in computational geotechnics. Rotterdam: Balkema. p. 281-90

Schmedes J., Archuleta R. and Lavallee D., 2010. C*orrelation of earthquake source parameters inferred from dynamic rupture simulations*. J. Geophys. Res. 115, B03304

Schneider W.A., Phillip L.D. and Paal E.F., 1995. *Wave-equation velocity replacement of the low velocity layer for overthrust-belt data.* Geophysics, 60, 573-579

Schofield A. N. and Wroth C. P., 1968. *Critical state soil mechanics*, McGraw-Hill, London

Scholz C. H., 1990. *The Mechanics of Earthquakes and Faulting* (Cambridge University Press, Cambridge) 439 pp

Scholz C., 1982. *Scaling laws for Jarge earthquakes: consequences for physical models.* Bull. Seism. Soc. Am. 72, l-14

Schwartz S. Y. and Ruff L. J., 1987. *Asperity Distribution and Earthquake Occurrence in the Southern Kuril Islands Arc*, Phys. Earth Planet. Int. *49*, 54 - 77

Schwartz D. P. and Coppersmith, K. J., 1984. *Fault behaviour and characteristic earthquakes: examples from the Wasatch and San Andreas fault zones.* J. geophys. Res., 89, 5681-5698

Schwartz D. P., 1988. *Geology and seismic hazards: moving into the 1990's, in Earthquake Engineering Soil Dynamics II-Recent Advances in Ground Motion Evaluation.* Vol. 20, J. L. Van Thun (Editor), American Society of Civil Engineers Geotechnical Special Publication, New York, 1-42

Schwartz D. P. and K. J. Coppersmith, 1986. S*eismic hazardsnew trends in analysis using geologie data, in Active Tectonics.* National Academy Press, Washington, D.C., 215-230

Scrocca D., Carminati E. and Doglioni C., 2005. *Deep structure of the southern Apennines, Italy: thin-skinned or thick-skinned?* Tectonics, 24, 1-20

Scrocca D., Sciamanna S., Di Luzio E., Tozzi M., Nicolai C. and Gambini R., 2007. *Structural setting along the CROP-04 deep seismic profile (Southern Apennines - Italy).* Boll. Soc. Geol. Ital., 7, 283-296

Seed H.B., 1979. *Considerations in the earthquake-resistant design of earth and rockfill dams*. Geotechnique; 29(3):215-63

Seed H.B. and Booker J.R., 1977. *Stabilization of potentially liquefiable sand deposits using gravel drains*. Journal of the Geotechnical Engineering Division, ASCE; 103(7):755-68

Seed H.B., Idriss I.M. and Kiefer F.W., 1969. *Characteristics of rock motions during earthquakes*. J Soil Mech Found Div, ASCE; 95(SM5):1199-218

Seed H.B., Lee K.L., Idriss I.M. and Makdisi R., 1973. *Analysis of the slides in the San Fernando dams during the earthquake of Feb. 9 1971*. Report No. EERC 73-2, Earthquake Engineering Research Center, University of California, Berkeley, p. 150

Seed H.B., Lee K.L. and Idriss I.M., 1969. *Analysis of Sheffield Dam failure*. J. Soil Mech. Found. Div. ASCE, 95, SM6, pp. 1453-1490

Seed H.B., Makdisi F.I. and DeAlba P. 1978. *The performance of earthfill dams during earthquakes.* Journal of the Geotechnical Engineering Division, ASCE, Volume 104, No. GT7, pp. 967-994

Seed H.B. and Martin G.R., 1966. *The seismic coefficient in earth dam design*. Journal of Soil Mechanics Foundations Division ASCE; 92(SM3):105-34

Seed H.B., Murauka J., Lysmer J. and Idriss I.M., 1976. *Relationships between maximum acceleration, maximum velocity, distance from source and local site conditions for moderately strong earthquakes.* Bull. Seism. Soc. of America, 66, 4, pp. 1323-134

Seed H.B., Seed R.B., Lai S.S. and Khamenehpour B., 1985. *Seismic design of concrete faced rockfi.ll dams*. In: Concrete face rockfill dams-design, construction and performance. ASCE; 1985. p. 459-78

Seed H. B., Tokimatsu K., Harder L. F. and Chung R. M., 1985. *Influence of SPT Procedures in Soil Liquefaction Resistance Evaluations.* Journal of Geotechnical Engineering, ASCE, Vol. 111, No. 12, pp. 1425 - 1445

Seed H.B., Wong R.T., Idriss I.M. and Tokimatsu K., 1986. *Moduli and damping factors for dynamic analyses of cohesionless soils*. Journal of Geotechnical and Geoenvironmental Engineering ASCE; 112(11):1016-32

Seidalinov Gaziz, 2012. *A simple anisotropic bounding surface plasticity model for cyclic response of clays.* Master of applied science in The Faculty of Graduate Studies (Civil Engineering) the university of British Columbia

Seid-Karbasi M. and Byrne P.M., 2004. *Embankment dams and earthquakes*. Int J Hydropower Dams; 11(2):96-102

Sellari E., 2007. *Modellazione matematica e numerica del comportamento dinamico dei terreni argillosi con riferimento alla risposta sismica delle dighe in terra*. PhD Thesis, Università degli Studi di Roma "La Sapienza"

Serpelloni, E., Anderlini, L., Anzidei, M., Devoti, R., Esposito, A., Galvani, A., Pietrantonio, G., Riguzzi, F., Sepe, E. and Belardinelli M., 2010. *Fault Geometry, Co-Seismic and Post-Seismic Slip Distribution of the April 6, L'Aquila Earthquake Imaged From Inversion of GPS Data*. EGU General Assembly, Vol. 12, EGU2010-10934

Serva, L., 1981. *Il terremoto del 1694 in Irpinia e Basilicata, in Contributo alla caratterizzazione della sismicita' del territorio Italiano*. pp. 183-208. Contribution to the Annual Convention of the ltalian National Research Project on Italian Seismicity, Udine, 12-14 May 1981 (in ltalian)

Shapiro S.S. and Wilk M.B., 1965. *An analysis of variance test for normality (complete samples)*. Biometrika 52, 591-611

Sheahan T.C., 1991. *An Experimental Study of the Time-Dependent Undrained Shear Behavior of Resedimented Clay Using Automated Stress Path Equipment*. Doctoral Dissertation, MIT, Cambridge, MA

Sheahan T.C., 2005. *A Soil Structure Index to Predict Rate Dependence of Stress-Strain Behavior.* Testing, Modeling and Simulation in Geomechanics, ASCE, Geotechnical Special Publication, no; 143, 81-97

Sheahan T.C., Ladd C.C., and Germaine J.T. 1996. *Rate Dependent Undrained Shear Behaviour of Saturated Clay*. Journal of Geotechnical and Geoenvironmental Engineering, ASCE; 122(2), 99-108

Shearer P.M., 1997. *Improving local earthquake locations using the L1 norm and waveform correlation application to the Whittier Narrows, California, aftershock sequence*. J. geophys. Res. 102(B4), 8269-8283

Sheng D., Fredlund D. G. and Gens A., 2008a. *A new modelling approach for unsaturated soils using independent stress variables.* Canadian Geotechnical Journal, 45, 511-534

Sheng D., Gens A., Fredlund, D. G. and Sloan S. W., 2008b. *Unsaturated soils: From constitutive modelling to numerical algorithms*. Computers and Geotechnics, 35, 810-824

Sheng D., Sloan, S. W. and Gens A., 2004. *A constitutive model for unsaturated soils: ther-momechanical and computational aspects.* Computational Mechanics, 33, 453-465

Sherard J.L., Woodward R.J., Gizienski S.F. and Clevenger W.A., 1963. *Earth and earth-rock dams.* John Wiley and Sons, New York

Shewchuk J. R. and D. R. O'Hallaron, 199*8. Archimedes, www.cs. cmu.edu/quake/archimedes.html (last accessed 4 March 2003)*

Shi B., J.N. Brune, Y. Zeng and A. Anooshehpoor, 2003. *Dynamics of earthquake normal faulting: two-dimensional lattice particle model.* Bull Seism. Soc. Am., 93, 1179-1197

Shibuya S. and Mitachi T., 1994. *Small strain modulus of clay sedimentation in a state of normal consolidation*. Soils and Foundations. Vol. 34, No.4, pp. 67-77

Shrey K., Shahi and Jack W. Baker, 2011. *An Empirically Calibrated Framework for Including the Effects of Near-Fault Directivity in Probabilistic Seismic Hazard Analysis.* Bulletin of the Seismological Society of America, Vol. 101, No. 2, pp. 742-755, doi: 10.1785/0120100090

SI H., Midorikawa S., 2001. *Evaluation of rupture directivity effects on peak ground motion using stochastic Green's function method.* Journal of Struct. Construct. Eng.; 546: 47-53 (in Japanese, with English abstract)

Sibson R.H., 1987. *Effects of fault heterogeneity on rupture propagation.* In Proc. of Conf. XXXIX, Directions in Paleoseismology, A. J. Crone and E. M. Omdahl (Editors), V.S. Geol. Surv. Open-File Rept. 87-673, 362-373

Sibson R., 1982. *Fault zone models, heat flow and the depth distribution of earthquakes in th e conti nental crust of the United States.* Bull. Seism. Soc. Am.. 72, 151- I 63

Sica S., 2001. *Analisi del comportamento dinamico di dighe in terr*a. Tesi di Dottorato, Consorzio delle Università di Napoli e Roma [in ltalian]

Sica S., Dello Russo A., Rotili F. and Simonelli A. L., 2014. *Ground motion amplification due to shallow cavities in nonlinear soils.* Natural Hazards, 71 (3), pp 1913-1935

Sica S., Pagano L., Modaressi A., 2008. *Influence of past loading history on the seismic response of earth dams.* Computers and Geotechnics, 35 (1), pp. 61-85

Sica S. and Pagano L., 2009. *Performance-based analyses of earth dams: procedures and applications to a sample case.* Soils Found; 49(6):921-39

Sica S., Pagano L. and Modaressi A., 2008. *Influence of past loading history on the seismic response of earth dams*. Computers and Geotechnics; 35:61-85

Sica S., Pagano L. and Vinale F., 2008. *Interpretazione dei segnali sismici registrati sulla diga di Camastra*. Italian Geotechnical Journal; 4(08):97-111

Sica S., Rotili F., Simonelli A. L. and Dello Russo A., 2012. *The role of underground cavities on ground motion amplification*. 15th Word Conference Earthquake Engineering, 24-28 September 2012 – Lisbon, Portugal.

Siddiqqi J. and G. Atkinson, 2002. *Ground motion amplification at rock sites across Canada, as determined from the horizontal-to-vertical component ratio.* Bull. Seismol. Soc. Am. 92, 877-884

Simo J.C. and Hughes T.J.R., 2000. *Computational Inelasticity*. Springer: New York; 392

Simo J.C. and Ortiz M., 1985. *A unified approach to finite deformation elastoplasticity based on the use of hyperelastic constitutive equations*. Computer Methods in Applied Mechanics and Engineering; 49:221-245

Simo J.C. and Taylor RL., 1986. *Return mapping algorithm for plane stress elastoplasticity*. International Journal for Numerical Methods in Engineering; 22:649-670

Simò J.C. and Pister K..S., 1984. *Remarks on rate constitutive equations for finite deformation problems: Computational implications*. Comp. Methods Appl. Mech. Engrg. 46 201-215

Simpson B., 1992. *Retaining structure: displacement and design*. Geotechnique, Vol 42, 539-576

Singh P.J., 1985. *Earthquake ground motions: implications for designing structures and reconciling structural damage.* Earthquake Spectra; 1(2):239-270

Singh R., Roy D. and Das D., 2007. *A correlation for permanent earthquake-induced deformation of earth embankments*. Eng Geol; 90:174-85
Singh R., Roy D. and Jain S.K., 2003. *Investigation of liquefaction failure in earthen dams during the Bhuj earthquake*. Kharagpur, India: Indian Institute of Technology
Singh S. K., E. Bazan and L. Esteva, 1980. *Expected earthquake magnitude from a fault.* Bull. Seism. Soc. Am. 70, 903-914
Siro, L. and Chiaruttini C., 1989. *Source complexity of the 1980 southern Italian earthquake from the analysis of strong motion S-wave polarization*. Bull. Seismol. Sot. Am., 79: 1810-1832
Skempton A.W., 1954. *The pore pressure coefficients A and B.* Géotechnique 4(4), 143-147
Slemmons D.B., 1977. *Faults and earthquake magnitude, U.S. Army Corps of Engineers.* Waterways Experimental Station, Miscellaneous Papers S-73-1, Report 6, 1-129
Slemmons D.B., 1982. *Determination of design earthquake magnitudes for microzonation.* Proc. of the Third International Earthquake Microzonation Corif. VoL 1, U.S. National Science Foundation, Washington, D.C., 119-130
Slemmons D.B., P. Bodin and X. Zang, 1989. *Determination of earthquake size from surface faulting events.* Proc. of the International Seminar on Seismic Zonation, Guangzhou, China, State Seismological Bureau, Beijing, 13
Sloan S.W., 1987. *Substepping schemes for the numerical integration of elastoplastic stress-strain relations*. International Journal of Numerical Methods on Engineering; 24:893-911
Sloan S.W., Abbo A.J. and Sheng D., 2001. *Refined explicit integration of elastoplastic models with automatic error control.* Engineering Computations; 18(1/2):121-54
Smerzini C., 2010. *The earthquake source in numerical modelling of seismic wave propagation in heterogeneous earth media.* Ph.D. Thesis, ROSE School, IUSS, Pavia
Smerzini C., Paolucci R. and Stupazzini M., 2011. C*omparison of 3D, 2D and 1D numerical approaches to predict long period earthquake ground motion in the Gubbio plain, Central Italy.* Bull. Earthq. Eng, DOI: 10.1007/s10518-011-9289-8
Smith K.D. and K.F. Priestley, 2000. *Faulting in the 1986 Chalfant, California, sequence: local tectonics and earthquake source parameters*. Bull. Seis. Soc. Am. 90, 813-831
Smith R. B. and Bruhn R. L., 1984. *Intraplate extensional tectonics of the eastern Basin-Range: inferences on structural style from seismic reflection data, regional tectonics and thermal-mechanical models of brittle-ductile deformation.* J. geophys. Res., 89, 5733-5762
Smith R.B., W.C. Nagy, K.A. Julander, J.J. Vivieros, C.A. Barker and D.G. Dants, 1989. *Geophysics and tectonic framework of the eastern Basin and Range - Colorado Plateau - Rocky Mountain transition.* In Geophysical Framework of the Continental United States, Geological Society of America Memoir 172, p. 205-234
Soga K., 1994. *Mechanical behaviour* and *constitutive modellng of natural structured soils.* Ph.D. thesis, University of California at Berkeley
Somerville P.G., 1998. *Development of an improved representation of near fault ground motions*. Proc. SMIP98 Seminar on Utilization of Strong Ground Motion Data, p. 1-20
Somerville P.G., 2000. *New developments in seismic hazard estimation*. Proceedings of the 6th International Conference on Seismic Zonation (6ICSZ), Palm Springs, CA, November 12-15
Somerville P.G., 2001. *Ground motion attenuation relations for the central and eastern United States*. Proceedings of the second ATC-35 National Earthquake Ground Motion Mapping Workshop, San Francisco, May 10-11
Somerville P.G., 2003. *Magnitude scaling of the near fault rupture directivity pulse*. Physics of the Earth and Planetary Interiors; 137:201-212
Somerville P.G., 2005. *Engineering characterization of near fault ground motion.* 2005 New Zealand Society for Earthquake Engineering Conference (NZSEE), Taupo, New Zealand, 8 pp
Somerville P.G., N.F. Smith and R.W. Graves, 1994. *The effect of critical Moho reflections on the attenuation of strong motion from the 1989 Loma Prieta earthquake, in "The Loma Prieta, California, Earthquake of October 17, 1989 - Strong Ground Motion"*. U.S. Geological Survey Professional Paper 1551-A, A67-A75
Somerville, P.G., J.P. McLaren, C.K. Saikia and D.V. Helmberger, 1990. *The November 25, 1988 Saguenay, Quebec earthquake: source parameters and the attenuation of strong ground motion*. Bull. Seism. Soc. Am., 80, 1118-1143
Somerville P., C.K. Saikia, D. Wald and R. Graves, 1996. *Implications of the Northridge earthquake for strong ground motions from thrust faults*. Bull. Seism. Soc. Am., 86, S115 - S125
Somerville P.G., N. F. Smith, R.W. Graves and N. A. Abrahamson, 1997. *Modification of empirical strong ground motion attenuation relations to include the amplitude and duration effects of rupture directivity.* Seismol. Res. Lett. 68, no. 1, 199-222
Somerville P.G., Irikura K., Graves R., Sawada S., Wald D., Abrahamson N., Iwasaki Y., Kagawa T., Smith N. and Kowada A., 1999. *Characterizing crustal earthquake slip models for the prediction of strong ground motion*. Seismol Res Lett; 70(1):59-80
Somerville P.G., H. Krawinkler and B. Alavi, 2000. *Development of improved ground motion representation and design procedures for near-fault ground motions*. Final Report to CSMIP Data Utilization Program, Contract No. 1097-601.
Somerville P.G., N. Collins, N. Abrahamson, R. Graves and C. Saikia, 2001. *Earthquake source scaling and ground motion attenuation relations for the central and eastern United States*. Final Report to the U.S. Geological Survey, Contract No. 99HQGR0098
Somerville P.G., R. Graves, A. Pitarka and N. Collins, 2003. *Strong Motion Simulations for Phase NGA-E of the Next Generation Attenuation (NGA)*. Program. Report to SCEC
Somerville P.G. and A. Pitarka, 2006. *Differences in earthquake source and ground motion characteristics between surface and buried earthquakes*. Proceedings of the Eighth National Conference on Earthquake Engineering, San Francisco, California
Sorensen K.K., Baudet B. A. and Simpson B., 2007. *Influence of Structure on the Time-Dependent Behaviour of a Stiff Sedimentary Clay.*Géotechnique; 57(1), 113-124

Sorensen, M. B., N. Pulido, and K. Atakan, 2007. *Sensitivity of ground-motion simulations to earthquake source parameters: A case study for Istanbul, Turkey.* Bull. Seismol. Soc. Am. 97, 881-900

Soufleris C. and Stewart G. S., 1981. *A source study of the Thessaloniki (north Greece) earthquake sequence.* Geophys. J. R. astr. Soc., 67, 343-358

Spector A. and Grant F.S., 1970. *Statistical models for interpreting aeromagnetic data. Geophysics 35, 293-302. Talwani, M., Worzel, L., Landisman, M., 1959. Rapid gravity computation for two-dimensional bodies with application to Mendocino submarine fracture zone*. J. Geophys. Res. 64, 49-59

Spencer C. and Gubbins D., 1980. *Travel-time inversion for simultaneous earthquake location and velocity structure determination in laterally varying media*. Geophys. J. R. Astron. Soc., 63, 95-116

Spudich P. and B. S. J. Chiou, 2008. *Directivity in NGA earthquake ground motions: Analysis using isochrone theory.* Earthquake Spectra 24, no. 1, 279-298

Spudich P. and L. N. Frazer, 1984. *Use of ray theory to calculate high-frequency radiation from earthquake sources having spatially variable rupture velocity and stress drop.* Bull. Seismol. Soc. Am. 74, 2061-2082

Spudich P. and L. Xu, 2002. *Software for calculating earthquake ground motions from finite faults in vertically varying media.* In International Handbook of Earthquake and Engineering Seismology, edited by W. H. K. Lee, Kanamori, H., Jennings, P., Kisslinger, C., Academic Press, Orlando

Spudich P. and Archuleta R., 1987. *Techniques for earthquake ground motion calculation with applications to source parameterization of finite faults.* Bolt BA editor. Seismic strong motion synthetics: Orlando, Florida: Academic Press: 205-265

Spudich P., W.B. Joyner, A.G. Lindh, D.M. Boore, B.M. Margaris and J.B. Fletcher, 1999. *SEA99: A revised ground motion prediction relation for use in extensional tectonic regimes.* Bull. Seis. Soc. Am. 89, 70, 1156-1170

Spudich,P., B. S. Chiou, R. W. Graves, K. R. Collins and P. G. Somerville, 2004. *A formulation of directivity for earthquake sources using isochrone theory, U.S. Geol. Surv. Open-File Rept. 2004-1268, 54 pp. Tothong, P., C. A. Cornell, and J. W. Baker (2007).* Explicit-directivitypulse inclusion in probabilistic seismic hazard analysis, Earthquake Spectra (in press)

Stabile T.A., Satriano C., Orefice A., Festa G. and Zollo A., 2012. *Anatomy of a microearthquake sequence on an active normal fault.* Sci. Rep., 2, 410, doi: 10.1038/srep00410

Stacey R., 1988. *Improved transparent boundary formulations for the elastic-wave equation, Short Note.* Bull. Seism. Soc. Am.; 78, 2089- 2097

Stallebrass S.E. and Taylor R.N., 1997. *Tue development and evaluation of a constitutive model for the prediction of ground movements in overconsolidated clay.* Geotechnique, Vol 47, 235-253. CrossRef

Stallebrass S.E., 1990. *The Effect of Recent Stress History on the Deformation of Overconsolidated Soils.* PhD Thesis, City University, UK

Stein R. S. and Barrientos S. E., 1985. *Planar high-angle faulting in the Basin and Range: geodetic analysis of the 1983 Borah Peak, Idaho, earthquake.* J. geophys. Res., 90, 11 355-11 366

Stephenson D., 1978. *Drawdown in embankments*. Géotechnique 28(3): 273-280

Stepp J.C., I. Wong, J. Whitney, R. Quittmeyer, N. Abrahamson, G. Toro, R. Youngs, K. Coppersmith, J. Savy, T. Sullivan and Yucca Mountain PSHA Project Members, 2001. *Probabilistic seismic hazard analyses for ground motions and fault displacement at Yucca Mountain*. Nevada. Earthquake Spectra 17, 113-151

Stewart J.P., Blake T.F. and Hollingsworth R.A., 2003. *A screen analysis procedure for seismic slope stability*. Earthquake Spectra; 19(3):697-712

Stidham C., M. Antolik, D. Dreger, S. Larsen and B. Romanowicz, 1999. *Three-dimensional structure influences on the strong motion wave- field of the 1989 Loma Prieta earthquake.* Bull. Seism. Soc. Am.; 89, 1184-1202

Stokoe K.H., Darendeli M.B., Menq F. Y. and Choi W.K., 2004. *Comparison of the linear and nonlinear dynamic properties of gravels, sands, silts and clays*. Proc. XI ICSDEE/III ICEGE, San Francisco, 1, pp. 1-4

Strasser F. O., N. A. Abrahamson and J. J. Bommer, 2009. *Sigma: Issues, insights, and challenges.* Seismol. Res. Lett. 80, 41-56

Stupazzini M., 2004. *A spectral approach for 3D dynamic soil-structure interaction problems*. Ph.D. Thesis, Department of Structural Engineering, Politecnico di Milano, Italy

Stupazzini M., 2004. *A spectral element approach for 3d dynamic soil-structure interaction problems.* PhD Thesis in Earthquake Engineering - XVI cycle. Disponibile sul sito http://geoelse.stru.polimi.it

Stupazzini M., Paolucci R. and Igel H., 2009. *Near-Fault Earthquake Ground Motion Simulation in the Grenoble Valley by a High-Performance Spectral Element Code.* Bull. Seismol. Soc. Am., Vol. 99, No. 1, pp. 286-301

Suhadole P., 1988. *Synthetic accelerograms: Caae axamples from Irpinia and Friuli, Proceedings of Strasbourg, 1986 Summer School on "Seismic Hazard in Mediterranean Regions*", edited by J. Bonnin, M. Cara, A. Cisternas, and R. Frantechi, 105-128

Swaisgood J. R., 1998. *Seismically-induced deformation of embankment dams*. In proceedings of sixth national conference on earthquake engineering. Seattle, Washington, U. S. A. May 31 - June 4 1998

Swaisgood J.R. and Au-Yeung Y., 1991. *Behavior of dams during the 1990 Philippines earthquake*. Presented at the ASDSO 1991 annual conference, San Diego, 29 Sep- 2 Oct 1991

Swaisgood J. R., P.E. and C.P.G., 2003. *Embankment dam deformations caused by earthquakes.* Consulting, Conifer, Colorado, U.S.A.

T. Tokuoka, 1971. *Yield conditions and flow rules derived from hypo-elasticity.* Arch. Rational Mech. Anal. 42 239-252.CrossRef

T. Tokuoka, 1973. *Thermo-hypo-elasticity and derived fracture and yield conditions.* Arch. Rational Mech. Anal. 46 114-130

T.Y. Thomas, 1955. *Combined elastic and Prantl-Reuss stress-strain relations.* Proc. National. Acad. Sci. U.S.A. 41 720-726. CrossRef

T.Y. Thomas, 1955. *On the structure of stress-strain relation.* Proc. Nat. Acad. Sci. U.S.A. U 716-720. CrossRef

Taiebat M., Shahir H. and Pak A., 2006. *Study of pore pressure variation during liquefaction using two constitutive models for sand*. Soil Dynamics and Earthquake Engineering; 27(1):60-72
Tamagnini C., Castellanza R. and Nova R., 2002. *A generalized backward Euler algorithm for the numerical integration of an isotropic hardening elastoplastic model for mechanical and chemical degradation of bonded geomaterials*. *I*nternational Journal for Numerical and Analytical Methods in Geomechanics; 26:963-1004
Tanioka Y. and Ruff L. J. and SATAKE K. 1997. W*hat Controls the Lateral Variation of Large Earthquake Occurrence along the Japan Trench?* The Island Arc 6, 261 - 266
Tanioka Y. and Ruff L. J., 1997. *Source-time Functions*. Seismol. Res. Lett. *68*, 386 - 400
Tarantola A. and Valette B., 1982. *Generalized nonlinear inverse problems solved using the least squares criterion, Rev*. Geophys. Space Phys., 20, 219-232
Tarantola A. and Valette B., 1982. *Inverse problems = quest for information.* J. geophys. Res., 50, 159-170
Tarantola, A., 1987. *Inverse problem theory: methods for data filling and model parameter estimation.* Elsevier. Amsterdam
Tatsuoka F. and Shibuya S., 1992. *Defonnation charactetistics of soils and rocks from field and laboratory tests, Keynote Lecture, in Proceedings 9th Asian Regional Coriference on Soil Mechanics and Foundation Engineering.* Bangkok, 1991, Voi. 2, pp. 101-170
Tatsuoka F. and Ishihara K., 1974. *Drained deformation under cyclic stresses reversing direction.* Soils and Found., Tokyo; 14(3), 51-65
Tatsuoka F., Jardine R. J., Lo Presti D., Di Benedetto H. and Kodaka T., 1997. C*haractetising the prefailure deformation properties of geomaterials, Theme lecture for the plenary session No. 1, in Proceedings of XIV lnternational.* Conference on Soil Mechanics and Foundation Engineering, Hamburg, September 1997, Voi. 4, pp. 2129-2164
Teachavorasinskun S., Thongchim P. and Lukkunaprasit P., 2002. *Shear modulus and damping of soft Bangkok clays (Technical Note)*. Canadian Geotechnical Journal. Voi. 39, No. 5, pp. 1201-1208
Tepel, R.E.; Nelson, J.L. and Hosokawa, A.M. 1996. *Seismic response of eleven embankment dams, Santa Clara County, California, as measured by crest monument surveys.* In Seismic design and performance of dams; Sixth annual USCOLD lecture, Los Angeles, 22 -26 July 1996
Terzaghi K., 1943. *Theoretical Soil Mechanics, John Wiley and Sons*. New York
Terzaghi K. and Peck R.B. 1948. *Soil mechanics in engineering practice*. Wiley, New York
Terzaghi K., 1952. *Mechanisms of landslides*. The geological survey of America. Berkeley: Engineering Geology
Th. Lehmann, 1991. *Z.H. Guo and H.Y. Liang, The conjugacy between Cauchy stress and logarithm of the left stretch tensor*. European J. Mech. A 10. 395-404
Thatcher W. and Hanks T., 1973. S*ource paramcter s of southern California earthquakes*. J. geophy s. Res., 78, 8547-8576
Thompson G.A., R. Catchings, E. Goodwin, S. Hollbrook, C. Jarchow, C. Mann, J. McCarthy and D. Okaya, 1989. *Geophysics of the western Basin and Range province*. In Geophysical Framework of the Continental United States, Geological Society of America Memoir 172, p. 177-204
Thurber C.H., 1983. *Earthquake locations and three-dimensional crustal structure in the Coyote Lake Area, Central California.* J. geophys. Res., 88(B10), 8226-8236
Thurber C.H., 1984. *Seismic detection of the summit magma complex of Kilauea volcano*. Hawaii. Science, 223, 165-167
Thurber C.H., 1992. *Hypocenter -velocity structure coupling in local earthquake tomography*. Phys. Earth Planet. Inter., 75, 55-62
Tiberti M.M., Orlando L., Di Bucci D., Bernabini M. and Parotto M., 2005. *Regional gravity anomaly map and crustal model of the Central-Southern Apennines (Italy).* J. Geodyn., 40, 73-91
Tichelaar B. and Ruff L. J., 1993. *Depth of Seismic Coupling along Subduction Zones.* J. Geophys. Res. *98*, 2017 - 2037
Tocher D., 1958. *Earthquake energy and ground breakage.* Bull. Seism. Soc. Am. 48, 147-153
Tokimatsu K. and Seed H.B., 1987. *Evaluation of settlements in sands due to earthquake shaking*. J Geotech Eng, ASCE; 113(8):861-78
Toro G. R., N. A. Abrahamson and J. F. Schneider, 1997. *Model of strong ground motions from earthquakes in Central and Eastern North America: Best estimates and uncertainties.* Seismol. Res. Lett. 68, no. 1, 41-57
Toshinawa T. and T. Ohmachi, 1992. *Love wave propagation in a three-dimensional sedimentary basin.* Bull. Seism. Soc. Am. 82, 1661-1667. Wald, D. J., and T. H. Heaton (1994). Spatial and temporal distribution of slip for the 1992 Landers, California, earthquake, Bull. Seism. Soc. Am. 84, 668-691
Tothong P., C. A. Cornell and J.W. Baker, 2007. *Explicit-directivity-pulse inclusion in probabilistic seismic hazard analysis.* Earthquake Spectra 23, no. 4, 867-891
Tothong P. and Cornell C.A., 2006. *Probabilistic seismic demand analysis using advanced ground motion intensity measures, attenuation relationships, and near fault effect*. PEER Report 2006/11, Pacific Earthquake Engineering Research Center, Berkeley, CA
Tresca H., 1864. *Mémoire sur l'écoulement des corps solides soumis à de fortes pressions*. C.R. Acad. Sci. Paris, vol. 59, p. 754
Trisee, 1997-1999. *3D site effects and soil-foundation interaction in earthquake and vibration risk evaluation.* In Environment and Climate Programme of the European Commission, E. Faccioli, R. Paolucci, and M. Vanini (Editors.), contract n. ENV4-CT96-0254, Politecnico di Milano, 92 pp
Troncoso J.H., 1990. *Failure risks of abandoned tailing dams.* In: Proceedings of the international symposium on safety and rehabilitation of tailing dams, ICOLD, Paris, p. 82-89
Troncoso J.H., Krause A.J. and Corser P.G., 1999. *Seismic design oflined face earth dams*. In: Proceedings of the second international conference on earthquake geotechnical engineering, Usbon; p. 703-9
Troutman B. M. and G. P. Williams, 1987. *Fitting straight lines in the earth sciences.* In Use and Abuse of Statistica[Methods in the Earth Sciences, W. B. Size (Editor), Oxford University Press, New York, 107-128
Tryggvason A. and Bergman B., 2006. *A traveltime reciprocity discrepancy in the Podvin and Lecomte time3d finite difference algorithm.* Geophys. J. Int., 165, 432-435

Tselentis G. A. and Zahradńık J., 2000. *The Athens Earthquake of 7 September 1999.* Bull. Seism. Soc. Am. 90, 1143-1160

Uscold., 1985. *Guidelines for selecting seismic parameters for dam projects*. Report of Committee on Earthquakes. U.S. Committee on Large Dams; 1985

Utsu T., 1969. *Aftershocks and earthquake statistics (I), some parameters which characterize an aftershock sequence and their interrelations.* J. Faculty Sci., Series VII, Vol. III, Hokkaido University, Japan, 129-195

Utsu T. and A. Seki, 1954. *A relation between the area of aftershock region and the energy of main-shock.* 1. Seism. Soc. Japan 7, 233-240

Vanorio T., Virieux J., Capuano, P. and Russo, G., 2005. *Three-dimensional seismic tomography from P wave and S wave microearthquake travel times and rock physics characterization of the Campi Flegrei Caldera.* J. geophys. Res., 110, B0320, doi:10.1029/2004JB003102

Vardanega P. I. and Bolton. MD., 2011. *Practical methods to estimate the non-linear shear stiffness of fine grained soils.* International Symposium on Deformation Characteristics of Geomaterials, Seoul, Korea

Velasco A., Ammon C. and Lay T., 1994. *Empirical Green function deconvol ution of broùadband surface waves: ru pt ure directi vity of the 1992 Landers, California (M w = 7.3), earthquake.* Bull. Seism. Soc. Am. 84, 735 750

Verderame G.M., Iervolino I. and Ricci P., 2009. *Report on the Damages on Buildings Followings the Seismic Event of 6th of April.* [Available at http://www.reluis.it/doc/pdf/Aquila/Rapporto fotografico V1.2.pdf]

Vermeer P. and Brinkgreve R.B.J., 1998. *Plaxis V7, Material models manual*. Rotterdam: Balkema

Viggiani G., 1992. *Small strain stiffness of fine grained soils*. PhD thesis, City University, London

Villani M., 2010. *High resolution SHA in the vicinity of earthquake sources.* Ph.D. thesis, ROSE School, IUSS Pavia

Virieux J. and Farra V., 1991. *Ray tracing in 3D complex isotropic media: An analysis of the problem.* Geophysics, 56, 2057-2069

Virieux J. and Madariaga R., 1982. *Dynamic faulting studied by finite difference method*. Bulletin of the Seismological Society of America 72, 345-369

Von Estorff O. and E. Kausel, 1989. *Coupling of boundary and finite elements for soil-structure interaction problem*. Earthq. Eng. Struct. Dyn. 18, 1065-1075

Vucetic M. and Dobry R., 1991. *Effect of soil plasticity on cyclic response*. Journal of Geotechnical Engineering (ASCE). Vol. 117, No. 1,pp. 89-117

Vucetic M. and Tabata K., 2003. *Influence of soil type on the effect of stra.in rate on small-strain cyclic shear modulus.* Soils and Foundations. Vol. 43, No. 5, pp. 161-173

Vucetic M., 1994. *Cyclic threshold shear strains in soils*. Journal of Geotechnical and Geoenvironmental Engineering (ASCE); 120(12):2208-2228

Vuoetic M., Dobry R., 1991. *Effect of soil plasticity on cyclic response*. J Geotech Eng 1991;117(1):89-107

W. Noll, 1965. *On the continuity of the solid and fluid state.* J. Rational Mech. Anal. 4 (1955) 3-81. Reprintedin: C.Truesdell (ed.), Continuum Mechanics II, The International Science Review Series. Gordon and Breach, New York

W.D. Reinhardt and R. N. Dubey, 1996. *Coordinate-independent representations of spins in continuum mechanics*. J. Elasticity 42, 133-144

W.D. Reinhardt and R.N. Dubey, 1995. *Eulerian strain-rate as a rate of logarithmic strain.* Mech. Res. Commun. 22 165-170. CrossRef

W.F. Chen and A.F. Saleeb, 1994. *Constitutive Equationsfor Engineering Materials*. Voi. 1:Elasticity and Modeling, revised Elsevier, New York

Wajeman C., Bard P., Hatzfeld D., Diagourtas, D., Mak ropulos K. and Gariel J.C., 1995. *Experim ental tests on the empirical Green's Functi on methods.* Proc. 5 th Int. Conf in S eismic Zonation, Nice, France

Wald D. and Graves R., 2001. *Resolution Analysis of Finite Fault Source Inversion Using One- and Three-dimensional Green's Functions, 2.* Combining Seismic and Geodetic Data, Journal of Geophysical Research, Vol. 106, 8767-8788

Wald D.J. and Heaton T.H., 1994. *Spatial and temporal distribution of slip for the 1992 Landers, California earthquake*. Bull. Seism. Soc. Am., *84*, 668-691

Wald D.J., Quitoriano V., Heaton T.H. and Kanamori H., 1999b. *Relationship between peak ground acceleration, peak ground velocity, and modified Mercalli intensity for earthquakes in California*. Earthq Spectra 15:557-564

Wald D.J., Quitoriano V., Heaton T.H., Kanamori H., Scrivner C.W. and Worden C.B., 1999a. *TriNet shakemaps: rapid generation of instrumental ground motion and intensity maps for earthquakes in southern California*. Earthq Spectra 15:537-555

Wald et al., 2006. *ShakeMap manual*

Waldhauser F. and Ellsworth W.L., 2000. *A double-difference earthquake location algorithm: method and application to the northern Hayward Fault, California.* Bull. Seism. Soc. Am, 90, 1353-1368

Waldhauser F., 2001. *HypoDD: A computer program to compute double- difference hypocenter locations*. Open File Rep, U.S. Geol. Surv., 01-113

Wan R.G. and Guo P.J., 1998. *A simple constitutive model for granular soils: modified stress-dilatancy approach*. Computers and Geotechnics; 22(2):109-133

Wang J., 2005. *The Stress-Strain and Strength Characteristics of Portaway Sand.* PhD Thesis, University of Nottingham, UK

Wang R., 1999. *A simple orthonormalization method for the stable and efficient computation of Green's functions.* Bull. Seism. Soc. Am., 89, 733-741

Wang R., Martin, F.L. and Roth F., 2003. *Computation of deformation induced by earthquakes in a multi-layered elastic crust FORTRAN programs EDGRN/EDCMP.* Computers and Geosciences, 29, 195-207

Wang Z-L., Dafalias Y.F. and Shen C.K., 1990. *Bounding surface hypoplasticity model for sand*. Journal of Engineering Mechanics, ASCE;116 (5):983-1001

Wang Z-L., Makdisi F.I. and Egan J., 2006. *Practical applications of a nonlinear approach to analysis of earthquake-induced liquefaction and deformation of earth structures*. Soil Dynamics and Earthquake Engineering; 26:231-252

Wang, Z. L., 1990. *Bounding Surface Hypoplasticity Model for Granular Soils and lts Applications*. Ph.D. dissertation, University of California, Davis, U·M·I Dessertation lnformation Service, Order Number 9110679
Wartman J., Bray J.D. and Seed R.B., 2003. *Inclined plane studies of the Newmark sliding block procedure*. J Geotech Geoenviron Eng, ASCE; 129(8):673-84
Weber E. et al., 2007. *An advances seismic network in Southern Apennines (Italy) for seismicity investigations and experimentation with earthquake early warning.* Seismol. Res. Lett., 78(6), 622-634
Weber E., Convertito V., Iannaccone G., Zollo A., Bobbio A., Cantore L., Corciulo M., Di Crosta M., Elia L., Martino C., Romeo A. and Satriano C., 2007. *An advanced seismic network in southern Apennines (Italy) for seismicity investigations and experimentation with earthquake early warning*. Seismol Res Lett 78:622-634
Wells D.L., Coppersmith KJ., 1994. *New empirical relationships among magnitude, rupture length, rupture width, rupture area, and surface displacement*. Bull Seism Soc Am; 84(4):974-1002
Wesnousky S. G., 1986. *Earthquakes, Quaternary faults, and seis mic hazards in California.* J. Geophys. Res. 91, 12587-12631. Wesnousky, S. G., C. H. Scholz, K. Shimazaki, and T. Matsuda (1983). Earthquake frequency distribution and mechanics of faulting, J. Geophys. Res. 88, 9331-9340
Wessel P. and W. H. F. Smith, 1998. *New, improved version of the Generic Mapping Tools released.* Eos Trans. AGU 79, 579
Wessel P., Smith, W.H.F., 1991. *Free Software Helps Map and Display Data.* EOS Trans. AGU 72, 441, 445-446
Westaway R. W. C., 1985. *Active tectonics of Campania, southern Italy*. Ph. D. thesis, Univ. of Cambrig.
Westaway R. W. C., 1987a. *The Campania, southern Italy, earthquakes of 1962 August 21*. Geophys. J.R. astr. Soc., 88, 1-24
Westaway R. W. C., 1987b. *Comment on "The Southern Italy earthquake of 23rd November 1980: An unusual of faulting" by R. S. Crosson, M. Martini, R. Scarpa and S. C. Key.* Bull. Seismol. Soc. Am., 77, 1071-1074
Westaway R. W. C., 1993. *Fault rupture geometry for the 1980 Irpinia earthquake: a working hypothesis.* Ann. Geofis., 36, 51-69
Westaway R. W. C. and J. Jacksaon, 1984. *Surface faulting In the southern Italian Campania-Basilitica earthquake of 23 November 1980*. Nature,312, 436-438
Westaway R. and Jackson J., 1987. *The earthquake of 1980 November 23 in Campania-Basilicata (Southern Italy).* Geophy. J. R. astr. Soc., 90, 375-443
Wheeler S. J. and Sivakumar V., 1995. *An elasto-plastic critical state framework for unsatu-rated soil*. Géotechnique, 45(1), 35-53
Wheeler S. J., Gallipoli D. and Karstunen M., 2002. *Comments on use of the Barcelona Ba-sic Model for unsaturated soils.* International Journal for Numerical and Analytical Methods in Geome-chanics, 26, 1561-1571
Whitcomb J. H., Allen C. R., Garmany, J. D. and Hileman, J. A., 1973. *San Fernando earthquake sequence, 1971: focal mechanisms and tectonics*. Rev. Geophys. Space Phys., 11, 693-730
Whitman R.W. and Liao S., 1984. *Seismic design of retaining walls*. In: Proceeding of the eighth world conference on earthquake engineering, San Francisco; p. 533-40
Whittle A.J., 1993. *Evaluation of a constitutive model for overconsolidated clays.* Geotechnique, Vol 43, 289-313
Won I.L. and Bevis M., 1987. *Computing the gravitational and magnetic anomalies due to a polygon. Algorithms and fortan subroutines.* Geophysics 53, 232-238
Wood D.M., Belkheir K. and Liu D.F., 1994. *Strain softening and state parameters for sand modelling.* Géotechnique; 44(2):335-339
Woodward P.K. and Griffiths D.V., 1996. *Influence of viscous damping in the dynamic analysis of an earth dam using simple constitutive models.* Computers and Geotechnics, 19, 3, pp. 245-263
Wroth C.P. and Houlsby M.F., 1985. *Soil mechanics: property characterisation and analysis procedures*. Proc. 11th Int. Conf. Soil Mech. Found. Engng., San Francisco; pp. 1-50
Wroth C.P., Randolph M.F., Houlsby G.T. and Fahey M., 1979. *A review of the engineering properties of soils woth particular reference to the shear modulus*. Tech. Report CUED/D-SOILS TR75, University of Cambridge
Wu F. T., 1968. *Parkfield earthquake of 28 June 1966-magnitude and source mechanism.* Bull. Seism. Soc. Am. 58, 689-709
Wu H. and Lees J.M., 1999. *Three-dimensional P- and S-wave velocity structures of the Coso Geothermal Area, California, from microseismic travel time data.* J. Geophys. Res., 104, 13217-13233
Wyss M., 1979. *Estimating maximum expectable magnitude of earthquakes from fault dimensions.* Geology 7, 336-340
Xiao H., 1995a. *General irreducible representations for constitutive equations of elastic crystals and transversely isotropie elastic solid*s. J. Elasticity 39 47-73
Xiao H., 1995b. *Invariant chamcteristic representations for classical and mìcropolar anisotropie elastìcity tensors*. J. Elasticity 40 239-265. CrossReff
Xiao H., 1995c. *Unified explicit basis-free expressions for time rate and conjugate stress of an arbitrary Hill's strain*. Internal. J. Solids Structures 32, 3327-3340. CrossRef
Xiao H., 1996a. *On anisotropie scalar functions of a single symmetric tensor*. Proc. Roy. Soc. London A 452, 1545-1561.CrossRef
Xiao H., 1996b. *On minimal representations for constitutive equations of anisotropie elastic materials*. J. Elasticity 45 13-32
Xiao H., Bruhns O.T. and Meyers A., 1996. *A new aspect in kinematics of large deformations*. In: N.K. Gupta (ed.), Plasticity and Impact Mechanics. New Age Intern. Pubi., New Delhi pp. 100-109
Xiao H.. Bruhns O.T. and Meyers A., 1997a. *Hypoelasticity model base upon the logarithmic stress rate*. J. Elasticity 41 51-68. CrossRef
Xiao H.. Bruhns O.T. and Meyers A., 1997b, *Logarithmic strain, logarithmic spin and logarithmic rate.* Acta Mechanica 124, 89-105. CrossRef
Xiao H.. Bruhns O.T. and Meyers A., 1998a. *Objective corotational rates and unified work-conjugacy relation between Eulerian and Lagrangean strain and stress measures*. Arch. Mech. 50 1015-1045

Xiao H.. Bruhns O.T. and Meyers A., 1998b. *On objective corotational rates and their defining spin tensors.* Int. J. Solids Structures 35, 4001-4014. CrossRef

Xiao H.. Bruhns O.T. and Meyers A., 1999. *A Natural Generalization of Hypoelasticity and Eulerian Rate Type Forrnulation of Hyperelasticity*. Journal of Elastlcity 56: 59-93

Xiao H.. Bruhns O.T. and Meyers A., 1999. *Existence and uniqueness of the integrable-exactly hypoelastic equation i* =λ(trD)+2μD and its significance to finite inelasticity*. Acta Mech. 138 31-50

Yamada M. and Heaton T., 2007. *Real-time Estimation of Fault Rupture Extent using Envelopes of Acceleration*

Yamada Y. and lshihara,K., 1983. *Undrained Deformation Characteristics of Sand in Multi-directional Shear.* Soils and Foundations, Voi. 23, No. 1

Yang Y., Muraleetharan K.K. and Yu H.S., 2006. *A middle surface concept (MSC) model for saturated sands in general stress space*. International Journal for Numerical and Analytical Methods in Geomechanics; 30:389-412

Yang Z. and Elgamal A., 2008. *Multi-surface cyclic plasticity sand model with Lode angle effect*. Geotechnical and Geological Engineering; 26: 335-48

Yang Z., Elgamal A. and Parra E., 2003. *Computational model for cyclic mobility and associated shear deformation*. Journal of Geotechnical and Geoenvironmental Engineering, ASCE;129(12):1119-27

Yang Z., Lu J. and Elgamal A., 2004. *A web-based platform for computer simulation of seismic ground response*. Advances in Engineering Software; 35(5):249-259

Yano T., Shao G., Liu Q., Ji C. and Archuleta R., 2010. *Finite Fault Co-Seismic Kinematic and Post-Seismic Slip Distribution Model of the 2009 MW 6.3 Aquila Earthquake from Joint-Inversion of Strong Motion, GPS, and InSAR Data.* SCEC Annual Meeting, poster 2-063

Yegian M.K., Marciano E.A. and Gharaman V.G., 1991. *Earthquake-induced permanent deformations: probabilistic approach*. ASCE, J Geotech Eng; 117(1):35-50

Yielding G., Jackson J, King G., Sinvhal H., Vita-Finzi C. and Wood R., 1981. *Relations between surface deformation, fault geometry, seismicity and rupture characteristics during the El Asnam (Algeria) earthquake of 10 October 1980.* Earth planet. Sci. Lett., 56, 287-304

Yimsiri S., 2001. *Prefailure deformation characteristics ofsoils: anisotropy and soil fabric.* Ph.D. thesis, University of Cambridge, U.K

Yoder P.J. and Iwan W.D., 1981. *On the formulation of strain-space plasticity with multiple loading surfaces.* J. Appl. Mech., Vol 48, 773-778.CrossRef

Yoshiaki Hisada and Jacobo Bielak, 2004. *Effects of sedimentary layers on directivity pulse and fling step.*13th World Conference on Earthquake Engineering Vancouver, B.C., Canada, Paper No. 1736

Yoshimura C., J. Bielak, Y. Hisada and A. Fernández, 2003. *Domain reduction method for three-dimensional earthquake modeling in localized regions. Part II: verification and applications.* Bull. Seism. Soc. Am. 93, 825-840

Youd T.L. and Idriss I.M., 2001. *Liquefaction resistance of soils: summary report from the 1996 NCEER and 1998 NCEER/NSF Workshops on Evaluation of Liquefaction Resistance of Soils*. J Geotech Geoenvirn Eng, ASCE; 127(4):297-313

Yu H.S, 2006. *Multi-Surface and Bounding Surface Plasticity.* Advances in Mechanics and Mathematics Volume 13, pp 153-196

Yu H.S. and Khong C.D., 2003. *Bounding surface fonnul.ation of a unitied critical state model for clay and sand.* Proc. 3rd lnt. Conf.Deformation Characteristics of Geomaterials, Lyon, 1111- 1118

Yu H.S., 1995. *A unified criticai state model for clay and sand.* Civil Engineering Research Report No 112.08.1995, University of Newcastle, NSW

Yu H.S., 1998. *CASM: A unified state parameter model for clay and sand Int.J. Num.* Analy. Meth. Geomech., Vol 22, 621-653.CrossRef

Yu H.S., Khong C.D. and Wang J., 2006. *A unified plasticity model for cyclicbehaviour of clay and sand.* Mech. Res. Commun. (in press)

Yu H.S., Khong C.D., Wang J. and Zhang G., 2005. *Experimental evaluation and extension of a simple critical state model for sand.* Granular Matter,Vol 7, 213-225.CrossRef

Vilardo G., Nappi R., Petti P. and Ventura G., 2003. *Fault geometries from the space distribution of the 1990–1997 Sannio–Benevento earthquakes: inferences on the active deformation in Southern Apennines*. Tectonophysics 363, 259– 271

Zahradník J. and P. Moczo, 1996. *Hybrid seismic modeling based on discrete-wavenumber and finite-difference methods.* Pure Appl. Geophys. 148, 21-38

Zahradník J., 1995. *Simple elastic finite-difference scheme.* Bull. Seism. Soc. Am.; 85, 1879-887

Zahradńık J., 2002. *Focal Mechanism of the Athens 1999 Earthquake by ASPO Method, Res*. Report, Dept. of Geophysics, Faculty of Math. and Phys., Charles University, Prague, http://seis30.karlov.mff.cuni.cz

Zahradńık J. and Tselentis G. A., 2002. *Modeling Strong-Motion Accelerograms By "PEXT" Method, Application To The Athens 1999 Earthquake.* Proc., European Seismological Commission (ESC), XXVIII General assembly, Genoa, Italy, September 1-6, CD-ROM

Zahradńik J. and Sokos E., 2011. *Multiple-point source solution of the Mw 7.2 Van earthquake, October 23, 2011, Eastern Turkey*. Report submitted to EMSC

Zangar C. *Hydrodynamic pressures on dams due to horizontal earthquake effects*. Monograph, http://www.usbr.gov/pmts/hydraulics_lab/pubs/EM/ EM11.pdf

Zania V., Tsompanakis Y. and Psarropoulos P.N., 2011. *Seismic slope stability of embankments: a comparative study on EC8 provisions*. In: Maugeri M, editor. Proceedings, ERTC-12 workshop on evaluation of geotechnical aspects of EC8, Athens, Sept. 11. Patron Editore-Quarto Inferione- Bologna

Zelt B.C., Talwani M. and Zelt C.A., 1998. *Prestack depth migration of dense wide-angle seismic data.* Tectonophysics, 286, 193-208

Zelt C.A. and Barton P.J., 1998. *Three-dimensional seismic refraction tomography: a comparison of two methods applied to data from the Faeroe Basin.* J. geophys. Res., 103, 7187-7210.

Zelt, C.A., 1998. *Lateral velocity resolution from three-dimensional seismic refraction data.* Geophys. J. Int.,135, 1101-1112
Zeng Y., J. G. Anderson and G. Y. Anderson, 1994. *A composite source model for computing realistic synthetic strong ground motions.* Geophys. Res. Lett. 21, 725-728
Zhan Z., Wei S., Ni S. and Helmberger, D., 2011. *Earthquake centroid locations using calibration from ambient seismic noise.* Bull. Seism. Soc. Am., 101(3), 1438-1445
Zhang J., Andrus R.D. and Juang, C.H., 2005. *Normalized shear modulus and mstetial damping ratio relationships*. Journal of Geotechnical and Geoenvironmental Engineering (ASCE). Voi. 131, No. 4, pp. 453-464
Zhang J. and McMechan G.A., 1994. *3D transmission tomography using wide aperture data for velocity estimation for irregular salt bodies.* Geophysics, 59, 1620-1630
Zhang Y. and Iwan W.D., 2002. *Active interaction control of tall buildings subjected to near-field ground motions*. Journal of Structural Engineering, ASCE; 128:69-79
Zhao D., Hasegawa A. and Horiuchi S., 1992. *Tomographic imaging of P- and S-wave velocity structure beneath Northeastern Japan.* J. Geophys. Res, 97, 19909-19928
Zhao J., Sheng D., Rouainia M. and Sloan S.W., 2005. *Explicit stress integration of complex soil models.* International Journal for Numerical and Analytical Methods in Geomechanics; 29:1209-1229
Zheng Z. and Rice J. R., 1998, *Conditions under which Velocity Weakening Friction Allows a Salf-healing Versus a Crack-like Mode of Rupture.* Bull. Seismol. Soc. Am. *88*, 1466 - 1483
Zheng Y., Chu J. and Xu Z., 1986. *Strain space formulation of the elasto-plastic theory and its finite element implementation*. Comput. Geotech. Vol 2, 373-388. CrossRef
Zhou H. and Randolph M.F., 2007. *Computational Techniques and Shear Band Development for Cylindrical and Spherical Penetrometers in Strain-Softening Clay*. International Journal of Geomechanics; 7(4), 287-295
Zhu T. J., A. C. Heidebrecht and W. K. Tso, 1988. *Effect of peak ground acceleration to velocity ratio on ductility demand of inelastic systems.* Earthq. Eng. Struct. Dyn. 16, 63-79
Zhu X., Angstmon B.G. and Sixta D.P., 1998. *Overthrust imaging with tomo-datuming: A case study.* Geophysics, 63, 25-38
Zhu X., Sixta D.P. and Angstman B.G., 1992. *Tomo-statics: Turning-ray tomography + static corrections*. The Leading Edge, 11, 15-3
Ziegler H., 1959. *A modification of Prager's hardening rule.* Quart.Appl. Math. Vol 17, 55
Zienkiewicz O. C. and Cormeau I. C., 1974. *Viscoplasticity, Plasticity and Creep in Elastic Solids: A Unified Numerical Solution Approach.International* Journal of Numerical Methods in Engineering; 8, 821-828
Zienkiewicz O.C., Chan A.H.C., Pastor M., Schrefler B.A. and Shiomi T., 1999. *Computational Geomechanics (with special reference to earthquake engineering)*. Wiley and Sons, Chichester
Zienkiewicz O.C. and Shiomi T., 1984. *Dynamic behaviour of saturated porous media; the generalised Biot formulation and its numerical solution.* Int J Numer Ana1 Meth Geomech; 8:71-96
Zollo A. and Bernard P., 1991a. *Fault mechanisms from near source data: joint inversion of S polarizations and P polaritics.* Geophys. J. Int., 104, 441 -451
Zollo A., D'Auria L., De Matteis R., Herrero A., Virieux J. and Gasparini P., 2002. *Bayesian estimation of 2-D P-velocity models from active seismic arrival time data: imaging of the shallow structure of Mt Vesuvius (Southern Italy).* Geophys. J. Int., 151, 566-582
Zollo A., Emolo A., Herrero A. and Improta L., 1999. *High frequency strong ground motion modelling in the Catania area associated with the ibleo-maltese fault system*. J Seism; 3(3)
Zollo, A. and Bernard, P., 1991 b. *How does an asperity brcak? New elemen ts from the waveform inversion of accelerograms for the 23 19 UT, October 15, 1979, Imperia. Valley aftershock.* J. geophys. R es., 96, 549-573
Zollo A., Bobbio A., Emolo A., Herrero A. and De Natale G., 1997. *Modeling of Ground Acceleration in the Near Source Range: the Case of 1976, Friuli Earthquake (M=6.5), Northern Italy.* J. Seismology 1, 305-319
Zollo A., Capuano P. and Singh S., 1995. *Use of small earthquake records to determine the source function of a larger earthquake: an alternative method and an application.* Bull. Seism. Soc. Am., 85, 1249-1256
Zollo A. and Emolo A. 2011. *Terremoti ed onde.* Liguori Editore - Italian